Translating Stem Cell-Based Regenerative Approaches into Clinical Therapies for Musculoskeletal Tissue Repair

Lead Guest Editor: Arianna B. Lovati
Guest Editors: Bruna Corradetti and Roberto Narcisi

Translating Stem Cell-Based Regenerative Approaches into Clinical Therapies for Musculoskeletal Tissue Repair

Translating Stem Cell-Based Regenerative Approaches into Clinical Therapies for Musculoskeletal Tissue Repair

Lead Guest Editor: Arianna B. Lovati
Guest Editors: Bruna Corradetti and Roberto Narcisi

Antonio Salgado, Portugal
Fermin Sanchez-Guijo, Spain
Heinrich Sauer, Germany
Coralie Sengenes, France
Dario Siniscalco, Italy
Shimon Slavin, Israel
Sieghart Sopper, Austria
Valeria Sorrenti, Italy
Ann Steele, USA
Alexander Storch, Germany
Bodo Eckehard Strauer, Germany
Hirotaka Suga, Japan
Gareth Sullivan, Norway
Masatoshi Suzuki, USA
Kenichi Tamama, USA
Daniele Torella, Italy
Marc L. Turner, United Kingdom
Aijun Wang, USA
Darius Widera, United Kingdom
Bettina Wilm, United Kingdom
Wasco Wruck, Germany
Qingzhong Xiao, United Kingdom
Takao Yasuhara, Japan
Zhaohui Ye, USA
Shuiqiao Yuan, China
Quan Yuan, China
Holm Zaehres, Germany
Elias T. Zambidis, USA
Dunfang Zhang, China
Ludovic Zimmerlin, USA
Ewa K. Zuba-Surma, Poland
Eder Zucconi, Brazil
Maurizio Zuccotti, Italy
Nicole Isolde zur Nieden, USA

Contents

Editorial

Translating Stem Cell-Based Regenerative Approaches into Clinical Therapies for Musculoskeletal Tissue Repair

Arianna B. Lovati [ID],[1] **Bruna Corradetti** [ID],[2,3] **and Roberto Narcisi** [ID][4]

[1]*Cell and Tissue Engineering Laboratory, IRCCS Istituto Ortopedico Galeazzi, Milan, Italy*
[2]*Department of Nanomedicine, Houston Methodist Research Institute, Houston, TX, USA*
[3]*Swansea University Medical School, Swansea, Wales, UK*
[4]*Department of Orthopaedics and Sports Medicine, Erasmus MC, University Medical Center, Rotterdam, Netherlands*

Correspondence should be addressed to Arianna B. Lovati; arianna.lovati@grupposandonato.it

Musculoskeletal tissue repair still represents a challenge in orthopaedics. Stem cell-based regenerative therapies have been widely explored using a variety of approaches, from targeted delivery of stem cells and their derivatives to advanced manufacturing of tissue grafts. Although several studies support the potential of stem cells in musculoskeletal tissue repair, few approaches have been successfully translated into clinics, attributable in part to a lack of well-defined standards of care in preclinical and clinical studies. This translational delay also depends on the intrinsic variability and complexity of the regulatory and legal frameworks worldwide. Stem cell therapy-based strategies vary significantly depending on the nature of the musculoskeletal damage to be restored. While tissue engineering approaches localize stem cells at the site of injury through biomaterials able to create a proregenerative environment, the use of free cells or their derivatives (e.g., secretome, microvesicles, and exosomes) requires limited manipulation and lower processing costs compared to tissue engineering.

This special issue presents the recent advances in the preclinical and clinical use of mesenchymal stem cells (MSCs) or their derivatives (e.g., bone marrow aspirate concentrate, known as BMAC, secretome) for a better understanding of their therapeutic impact.

In this special issue, the manuscript by C. Centeno et al. reports the results of a randomized controlled trial on 25 patients of the treatment of partial to full-thickness supraspinatus tendon tears by BMAC and platelet products as injectable regenerative therapies. Patients reported a mean 89% improvement at 24 months, with sustained functional gains, pain reduction, and a size decrease of most tears post-BMAC treatment, suggesting that BMAC injections are a safe and useful alternative to conservative exercise therapy in rotator cuff tears. In their systematic meta-analysis, S. Palombella et al. assessed the current clinical evidence for the efficacy of bone marrow-derived cell-based approaches associated or not with bone scaffolds to treat bone nonunions. Specifically, in the review, the authors indicate that BMAC or BMAC/scaffold is the primary choice versus bone marrow-derived stromal cells (BMSCs) to treat nonunions with a successful healing at a midterm follow-up (6-12 months). For the clinical translation of cell-based products, rigid protocols need to be established. In their work, R. B. Dias et al. described the manufacture of GMP-grade BMSC in compliance with Brazilian regulatory guidelines for cells intended for use in humans. Indeed, *in vitro*-expanded BMSCs have long been proposed for the treatment of complex bone injuries due to their inherent potential to differentiate into multiple skeletal cell types, modulate inflammatory responses, and support angiogenesis.

In the field of musculoskeletal tissue repair, nerve injuries represent a prominent clinical issue. Damaging the connection between muscle and neural fibers, for example, leads to muscle atrophy, with also a known negative impact on the differentiation capacity of the resident tissue-specific progenitor cells. In their review, Y. Wang et al. focused on the mechanism of

action, the role and the possible regenerative medicine applications of Adipose Stem Cells (ASCs) for diseases affecting the nervous system, overall indicating how these cells can become one of the most important cell-based tools for the treatment of neural pathologies in the future.

This special issue also introduces the reader to basic research aiming at identifying an alternative source of stem cells with improved differentiative potential into musculoskeletal tissues. The study conducted by H. E. Owston et al. assesses the migration and differentiation properties of multipotent stromal cells from clinically accessible human periosteum compared to BMSCs, demonstrating that periosteum represents a consistently rich source of highly proliferative multipotent stromal cells compared to donor-matched BMSCs with similar osteochondral capacity and lower adipogenic potential. In the same line, in their *in vivo* study, E. R. Moore et al. highlighted the importance of periosteal Prx1-expressing cells in contributing to the mechanically induced bone formation. Interestingly, the authors were able to show how primary cilia are necessary for a complete mechanical response of the Prx1-expressing cells, contributing to increase the knowledge around the role of this, still poorly understood, cellular organelle during bone (re)generation.

The relevance of the immunomodulatory potential of stem cells in the treatment of musculoskeletal diseases has been investigated by M. Viganò et al. The authors proposed the microfragmented adipose tissue (μFAT) as a convenient autologous product for the application of MSC-based therapies in clinical settings. In particular, they demonstrated its efficacy to favor tissue healing in the context of tendon inflammation, highlighting its capability to counteract the catabolic and fibrotic response elicited by the proinflammatory interleukin-1 beta (IL-1b) on tendon cells and providing insights on the mechanism of action of this therapeutic approach for the treatment of tendon disorders.

The special issue widely reports preclinical studies testing the efficacy of stem cell-based therapies in animal models and their relevance with respect to the human pathology in orthopaedics. In their study, M. Bottagisio et al. demonstrated the beneficial role of undifferentiated BMSCs loaded within decellularized xenografts undergoing a stretch-perfusion culture as an immunomodulatory weapon reducing the inflammatory process in tendon ruptures. This study associates the advantages of *in vitro* expanded and dynamically cultured BMSCs with new biologically relevant biomaterials with the potential to promote tendon reconstruction. In particular, J. Zhang et al. address an important clinical problem for the restoration of injured musculoskeletal tissues, which is related to the poor intrinsic healing potential of tendon and ligament tissue. The authors investigated the influence of Fibroblast Growth Factor-2- (FGF-2-) transfected human amniotic MSCs (hAMSCs) seeded on a human acellular amniotic membrane scaffold on tendon-to-bone healing process, using *in vitro* tests and a rabbit *in vivo* model. Their data demonstrate a significantly better healing of a tendon-to-bone junction, compared to the previously used biological materials.

Animal models are also a useful tool to investigate the cell fate/engraftment by tracking imaging in orthopaedics. The original article by C. Horstmeier et al. investigated *in vivo* the magic angle imaging technique to track ASCs labelled with superparamagnetic iron oxide particles (SPIO) and to discriminate SPIO-induced artefacts from the surrounding tendon tissue in equine digital flexor tendons.

Overall, in this research topic, we wanted to underline the importance of verifying the safety and efficacy of stem cell-based approaches, as well as the development of relevant preclinical studies, both *in vitro* and *in vivo*. Moreover, a multidisciplinary approach is required to better elucidate the mechanisms of stem cell differentiation, function, and tissue healing. Even more importantly, a good design of clinical trials should be implemented for the final validation of stem cell-based therapies in orthopaedics.

Conflicts of Interest

The editors declare that they have no conflicts of interest regarding the publication of this special issue.

Acknowledgments

Arianna B. Lovati
Bruna Corradetti
Roberto Narcisi

Research Article

A Randomized Controlled Trial of the Treatment of Rotator Cuff Tears with Bone Marrow Concentrate and Platelet Products Compared to Exercise Therapy: A Midterm Analysis

Christopher Centeno,[1,2] **Zachary Fausel,**[1] **Ian Stemper,**[2] **Ugochi Azuike,**[1] **and Ehren Dodson** [ID][2]

[1]*Centeno-Schultz Clinic, 403 Summit Blvd 201, Broomfield, Colorado 80021, USA*
[2]*Regenexx, LLC, 6151 Thornton Ave #200, Des Moines, Iowa 50321, USA*

Correspondence should be addressed to Ehren Dodson; edodson@regenexx.com

Injectable regenerative therapies such as bone marrow concentrate (BMC) and platelet-rich plasma (PRP) may represent a safe alternative in the treatment of rotator cuff tears. This is a midterm review of a randomized, crossover trial comparing autologous BMC and platelet product injections versus exercise therapy in the treatment of partial and full-thickness supraspinatus tears. Patients enrolled into the study were between 18 and 65 years of age presenting to an outpatient orthopedic clinic with partial to full thickness, nonretracted supraspinatus tendon tears. Enrolled patients were randomized to either ultrasound-guided autologous BMC with PRP and platelet lysate (PL) percutaneous injection treatment or exercise therapy. Patients could cross over to BMC treatment after at least 3 months of exercise therapy. Patients completed the Disability of the Arm, Shoulder and Hand (DASH) scores as the primary outcome measure. Secondary outcomes included the numeric pain scale (NPS), a modified Single Assessment Numeric Evaluation (SANE), and a blinded MRI review. At this midterm review, results from 25 enrolled patients who have reached at least 12-month follow-up are presented. No serious adverse events were reported. Significant differences were seen in patient reported outcomes for the BMC treatment compared to exercise therapy at 3 and 6 months for pain, and for function and reported improvement (SANE) at 3 months ($p < .05$). Patients reported a mean 89% improvement at 24 months, with sustained functional gains and pain reduction. MRI review showed a size decrease of most tears post-BMC treatment. These findings suggest that ultrasound-guided BMC and platelet product injections are a safe and useful alternative to conservative exercise therapy of torn, nonretracted supraspinatus tendons. This trial is registered with NCT01788683.

1. Introduction

The rotator cuff is a structure formed by the tendinous attachments of a group of muscles that work to stabilize the glenohumeral joint. Tears of these crucial active shoulder joint stabilizers are commonly associated with trauma and age-related degeneration [1]. Rotator cuff disorders (RCD), which can be found in 30%-50% of the population aged over 50, account for over 4.5 million physician visits per year, with over 250,000 repairs performed annually in the United States [1, 2].

Traditional management of RCD includes conservative treatment which involves analgesia, anti-inflammatory drugs, corticosteroid injections, and physical therapy [3]. The rate of success with conservative treatment for rotator cuff tears varies widely from 15 to 85% [4–10]. When conservative therapy is ineffective, open or arthroscopic surgery using suture anchors in a variety of configurations is used

with the goal of reducing pain and increasing function [11]. Despite traditional management with surgery to repair partial and full-thickness rotator cuff tears, several studies have shown high failure rates of tendon to bone rotator cuff repairs ranging from 30% to 94% [1, 2, 11, 12]. It can be difficult to determine which types and sizes of tears will benefit from surgical management as tear size and morphology have been shown to be poor predictors for pain and functional scores [13]. There is also evidence that surgical management does not result in superior outcomes compared to nonoperative treatment [14–16]. A recent meta-analysis of 57 randomized controlled trials found no difference between surgical outcomes compared to conservative management for treatment of full-thickness rotator cuff tears [17].

One of the difficulties with surgically repairing the rotator cuff may be on a cellular level. Animal models have demonstrated that the tendon-bone interface does not regenerate well after surgical repair with a resultant poorly formed fibro-osseous interface [18]. Research has also demonstrated that tears are prone to heal with scar tissue formation at the tendon-bone interface resulting in tissue that is weaker than the original, predisposing the rotator cuff to failure [1, 19]. As a result, practitioners have been investigating repair techniques that focus on improving the biologic healing environment of tears as well as the integrity of the tendon itself.

As an alternative treatment, early research on regenerative therapies such as platelet-rich plasma (PRP) and bone marrow concentrate (BMC) has shown promise in enhancing the healing properties of torn rotator cuff tendons, reducing retear rates over time, and improving symptoms and function [20–22]. BMC contains mesenchymal stem cells (MSCs) which are multipotent, readily available, and immune-privileged that contribute to tissue healing. When appropriately stimulated, MSCs can differentiate into bone, cartilage, fat, and tendon cells. This provides a promising mechanism to promote the healing of injured tissues [2, 23, 24]. They likely promote tendon healing through paracrine effects by secreting exosomes, growth factors, chemokines, and cytokines [25]. Several animal models have demonstrated cell-based approaches using MSCs can improve tendon repair, and when these studies are taken together, they improved histological and biomechanical properties of the tendons, indicating an increased rate of tendon healing and maturation [25, 26]. BMC and autologous-derived stem cells have also been used in the surgical management of rotator cuff repair to augment healing [22, 27–29].

In this present study, we describe a midterm analysis for a randomized controlled, crossover trial investigating a treatment for partial or complete, nonretracted rotator cuff tears using a specific protocol of BMC and platelet product injection. The primary objective of this study is to compare the patient-reported clinical outcomes for BMC versus exercise therapy.

2. Methods

2.1. Study Design. This was a prospective, randomized controlled, crossover study of symptomatic patients with chronic partial or full thickness nonretracted rotator cuff tears. Review and approval of the study protocol were obtained through the International Cellular Medicine Society IRB (OHRP Registration #IRB00002637). All patients provided informed consent prior to study enrollment.

Sample size determination was targeted at an enrollment of 50 patients with 25 in the exercise therapy group and 25 in the treatment group. This distribution was determined to have an 80% power to detect a 10-point difference in the mean change from baseline to 3-month DASH scores between treatment groups at $\alpha = 0.05$. This estimate was based on DASH outcomes reported previously for the treatment of rotator cuff impingement with exercise therapy by Camargo et al. and the surgical treatment of rotator cuff repair along with exercise therapy by Duzgun et al. [30, 31]. Enrolled patients were randomized at a 1 : 1 ratio between the two groups. Study condition allocation was revealed by opening sequentially numbered envelopes that contained study condition based on a computer-based randomization program.

Recruitment for the study occurred throughout the local community at gyms, sports clubs/leagues, physical therapy clinics, clinic website, online research study listings, and online advertisements. Eligible patients were identified from those presenting to an outpatient orthopedic clinic with a primary complaint of shoulder pain from June 2013 to July 2017. Patients were informed of the study protocol, and those meeting the inclusion and exclusion criteria were enrolled after obtaining informed consent. Inclusion criteria included patients aged 18-65 with unremitting pain in the affected shoulder having failed conservative treatment for at least three months, significant functional disability related to symptoms, and physician exam consistent with rotator cuff tear confirmed with positive diagnostic imaging confirming partial nonretracted tear of supraspinatus tendon. Patients were excluded if they had a massive tear demonstrated by ≥grade 3 muscle strength, previous surgery to affected shoulder, prior injection-based therapies within the last 3 months, concomitant tears of multiple rotator cuff or bicep tendons, SLAP tear ≥ grade 2, type 3 acromion, significant bone spurs in subacromial space, inflammatory or autoimmune-based joint diseases, KL grade ≥ 2 glenohumeral osteoarthritis, adhesive capsulitis, symptomatic cervical spine pathology, or testing positive for malignancies. Once enrolled, patients underwent randomization into one of the two study conditions. Using a computer-generated randomization method, allocations of study condition were placed in concealed numbered envelopes and opened in order of study enrollment. Patients in the treatment group received an injection of autologous BMC and platelet products. The home exercise program was prepared by a licensed physical therapist and included stretches in all planes along with nonweighted exercises incorporating strengthening of scapular stabilizing muscles as well as the triceps and the rotator cuff muscles (Supplement 1). Upon randomization into the exercise group, patients all met with the same physical therapist to obtain the instructions for the home exercise program, including proper technique and provided a n instructional handout to take home. Compliance with the exercises and

check-in was completed at 6 weeks. Exercise therapy patients completed the stretching, strengthening, and stability exercises at home, with the opportunity to cross over to the treatment group after at least 3 months of the home exercise program if desired improvement was lacking. The duration of three months of exercise therapy is in line with other published research using exercise therapy for torn rotator cuffs [4, 21, 32, 33]. Patients were followed for 24 months after receiving BMC treatment.

2.2. Initial Evaluation.

All patients were evaluated by a physician prior to study enrollment. Coronal, axial, and sagittal MRI images of the affected shoulder were reviewed for evaluation of study criteria. Supraspinatus tears were identified in multiple planes as hyperintense signal within the supraspinatus tendon.

At initial evaluation, ultrasound examination was performed in both long and short axis to the supraspinatus tendon with a Sonosite Edge II system (SonoSite Micromaxx SonoSite, Inc. 21919 30th Drive SE Bothell, WA) and a 13-6 MHz linear phased array transducer in the modified Crass position to assess the supraspinatus. Tears were identified as hypoechoic areas within the tendon that were bursal-sided, articular-sided, or intrasubstance. Retractions were identified as a loss of tendon attachment at the expected footprint of the supraspinatus.

2.3. Procedure Description.

Patients randomized to the treatment group, and patients after crossover, received ultrasound-guided injections of BMC and platelet products to the targeted rotator cuff tear area. All patients completed a bone marrow aspiration (BMA). The BMA procedure and processing protocols utilized for this study have been previously described [20]. In brief, bone marrow aspirate of 5-15 mL from six-nine sites was collected from the bilateral posterior superior iliac crests for a total volume of 60-90 mL into heparinized syringes. This was serially centrifuged with a resultant 1-3 mL of buffy coat collected. In addition, 60 mL of intravenous blood was drawn to isolate PRP and platelet lysate (PL). PRP was prepared by centrifugation and stored at -20°C, and PL was isolated via recentrifugation of the PRP. Total nucleated cell count (TNCC) of BMC was obtained using the TC20™ Automated Cell Counter (Bio-Rad, 2000 Alfred Nobel Dr. Hercules, CA). A $10 \mu L$ sample of BMC was pipetted into $450 \mu L$ of sterile water which was then mixed with $450 \mu L$ of sodium chloride for a total dilution of $1:100$. $10 \mu L$ of this mixture was then placed into a microcentrifuge tube and gently mixed with $10 \mu L$ of trypan blue and pipetted onto a cell counting slide. The slide was loaded into the slot of the TC20™ Automated Cell Counter which gave a total cell count per mL, as well as a live cell count per mL. This number was multiplied by the inverse of the dilution of the BMC sample (100) and then multiplied by the total volume of the BMC sample to obtain the TNCC. For the treatment procedure, under sterile conditions, ultrasound was used to localize the patient's supraspinatus tendon deficit. Under ultrasound guidance, 1-2 cc injectate consisting of 60% by volume of BMC, 20% by volume of PRP, and

20% by volume of PL was then percutaneously injected into the area of the tear.

Postprocedure, all patients were encouraged to follow a standard rehabilitation and return to activity protocol. No bracing was utilized postprocedurally. Patients were instructed to avoid any activities that caused more than a 2/10 pain throughout their rehabilitation course. Patients on days 0-3 were instructed to limit lifting/pushing and perform passive range of motion exercises 3x daily after applying heat. From 3 days postprocedure until week 4, patients were encouraged to continue 3x daily range of motion exercises with the addition of pendulum and pulley exercises and other exercises focusing on strengthening the shoulder girdle. From weeks 5 to 11, patients were encouraged to begin resistance training by starting light and progressing slowly without using resistance bands. After week 12 restrictions were lifted, patients were encouraged to perform eccentric and concentric exercises with gradual progression back to preinjury activity levels.

2.4. Outcome Measures.

Patients completed clinical outcome questionnaires before treatment and at each follow-up visit at 1 month, 3 months, 6 months, 12 months, and 24 months. Patients completed three self-administered outcome measures in this study. The primary outcome was the Disabilities of the Arm, Shoulder and Hand (DASH), which evaluates disability, function, and symptoms for upper limb musculoskeletal conditions on a 0-100-point scale where 0 is no disability and 100 is severe disability [34, 35]. This is derived from answers to 30 questions assessing various aspects of daily and recreational activities, in addition to specific symptoms, including pain, tingling, stiffness, and weakness. Secondary outcomes included a numeric pain scale (NPS) and a modified version of the Single Assessment Numeric Evaluation (SANE). NPS directs a patient to select a whole number (ranging from 0 to 10) indicating the intensity of their pain, where 0 is no pain and 10 is the worst possible pain [36]. The modified SANE asks patients to indicate to what extent they have seen a change in their condition compared to before treatment on a scale of -100% worsened to 100% improved [37, 38]. Any scores below 0% were truncated at 0% to match the widely reported SANE scale (0%-100%). Minimal clinically important difference (MCID) was defined by a 2-point reduction in the NPS score and a 10-point reduction in the DASH score [39, 40]. Pain medications and adverse events were also recorded.

An MRI assessment of supraspinatus tears on pre- and posttreatment MRIs was performed for patients with available posttreatment imaging after at least 12 months. Pre- and posttreatment coronal and sagittal sequences of the shoulder were presented side-by-side using a computer-based randomization sequence, with physician blinded to which side represented the pre- and posttreatment MRI. Blinded to patient and image order, three grading physicians independently compared the two image sequences and identified which demonstrated the healthier tendon based on overall appearance. An additional blinded MRI assessment was also performed to measure tears by a single physician to prevent interrater variability. Tear width was measured

at the widest point seen on a fluid-sensitive coronal sequence on both pre- and posttreatment MRIs. The evaluating physician was blinded to all patient data and to whether the sequences were taken before or after treatment.

2.5. Statistical Analysis. Linear mixed-effects models with post hoc Tukey were used to assess if outcome scores changed after BMC treatment. The effect of exercise was assessed using a Wilcoxon signed-rank test between baseline and the 1- and 3-month time points. BMC treatment was compared to exercise via Wilcoxon rank-sum tests for 1- and 3-month SANE scores, and NPS and DASH differential scores. The percent of those meeting the MCID for NPS and DASH was calculated. Linear mixed-effects models were used to determine if outcomes differed significantly between the crossover and the BMC treatment groups. MRI interrater reliability was calculated using Fleiss' kappa. All analyses were performed using R version 3.5.1, and RStudio version 1.1.456.

3. Results

During the period of June 2013 to July 2017, 25 patients were enrolled with supraspinatus tears for this study ($N = 14$ in the BMC group; $N = 11$ in exercise therapy). The study continues to enroll new participants, but only patients who had reached at least 12 months posttreatment at the time of analysis were included in this midterm review. 24 patients have reached the 12-month follow-up time point, 17 have reached the 24-month mark, and all but 1 exercise therapy patient crossed over to the BMC treatment (Figure 1). Of the 25 total patients, 11 were diagnosed with full thickness tears of the supraspinatus and 13 were diagnosed with partial thickness tears encompassing greater than 50% of the tendon thickness. Of the partial thickness tears, 6 were considered articular-sided, 6 were at the bursal surface, and 2 were intrasubstance.

Baseline demographic characteristics were obtained revealing an average age of 47 years, average BMI of 26.4, and a male majority of 56% to 44% (Table 1). No patients in either the exercise therapy group or the treatment group have been lost to follow-up. TNCC of BMC was obtained on each study participant who received BMC treatment ranging from 271 to 2334 million, with an average of 810 million. Viability data was not recorded initially, thus data presented is for the most recent 11 study patients.

No serious adverse events were identified in any study patients during follow-up. Participants could report AEs anytime and were asked about complications at each follow-up visit. In total, there were 5 adverse events reported after receiving BMC treatment and no adverse events in the exercise group. Postprocedural pain at the shoulder and bone marrow aspiration sites were reported by two patients. One patient reported a new onset of pain and numbness in the hands and fingers starting at the 12-month time point. Two patients reported pathology in the contralateral shoulder. One patient sustained a new injury to the treated shoulder and was withdrawn from the study after 12-month posttreat-
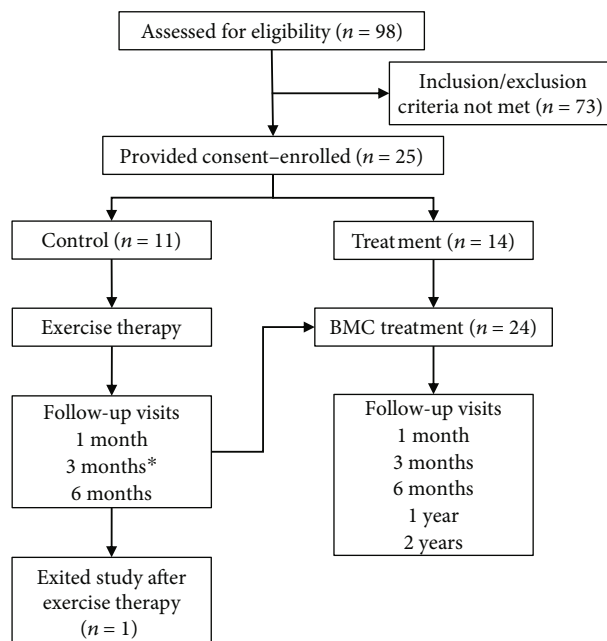
Figure 1: Flow diagram of study. *Exercise therapy patients were given option to cross over to BMC treatment group any time after 3 months of therapy; therefore, some 6-month outcome data was not available.

Table 1: Demographic characteristics.

Variable	N	Exercise Mean ± SD/%	N	BMC treatment Mean ± SD/%
Age (years)	11	49 ± 11		46 ± 11
BMI (kg/m^2)	11	25.9 ± 5.3		26.8 ± 3.7
TNCC (million)	10	690 ± 338	14	896 ± 517
Viability (percent)	4	92 ± 3	7	94 ± 4
Gender	11		14	
Male	5	45.5%	9	64%
Female	6	54.5%	5	36%

ment. No patient had surgical repair of their rotator cuff during the 24-month follow-up.

The study's primary outcome of DASH scores demonstrated statistically significant improvement after BMC treatment in comparison to the exercise therapy at 3 months ($p < .05$) and trended towards significance at 6 months ($p = .06$). DASH improvements met statistical significance compared to baseline starting at 3 months through the 24-month time point for all patients receiving BMC treatment ($p < .01$) (Figure 2). MCID for DASH was met by 61% of the BMC treatment group at the 3-month time point, improved to 91% at the 12-month time point, and was maintained through 24 months (94%). In contrast, the MCID for DASH scores in the exercise therapy group was met by 40% at the 3-month time point and 20% at 6 months (Figure 3).

The secondary outcome of NPS was significantly better at 3 and 6 months for the BMC group compared to the exercise
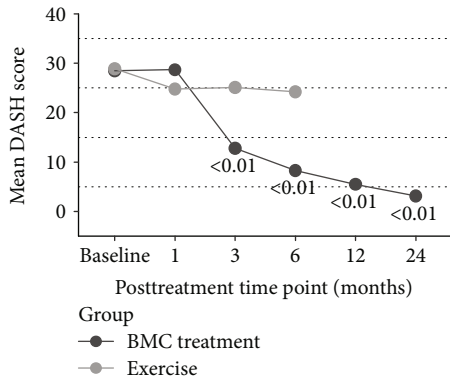
FIGURE 2: DASH scores at baseline and follow-up time points. Displayed *p* values reflect comparison to baseline. Exercise *N*: 9, 10, 5; treatment *N*: 23, 22, 24, 24, 23, 17.
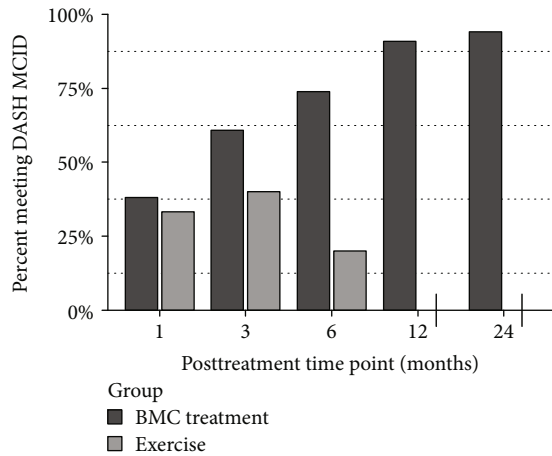
FIGURE 3: Percentage of patients who met MCID for DASH. Exercise *N*: 9, 10, 5; treatment *N*: 21, 23, 23, 22, 19, 17.
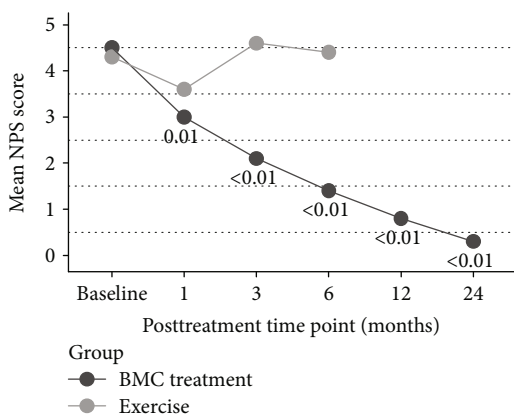
FIGURE 4: NPS scores before and after BMC treatment. Displayed *p* values reflect comparison to baseline. Exercise *N*: 9, 10, 5; BMC treatment *N*: 23, 22, 24, 23, 23, 17.

therapy group ($p < .05$). NPS also reached statistically significant improvements at all posttreatment time points starting as early as 1 month ($p < .05$) in the BMC treatment group
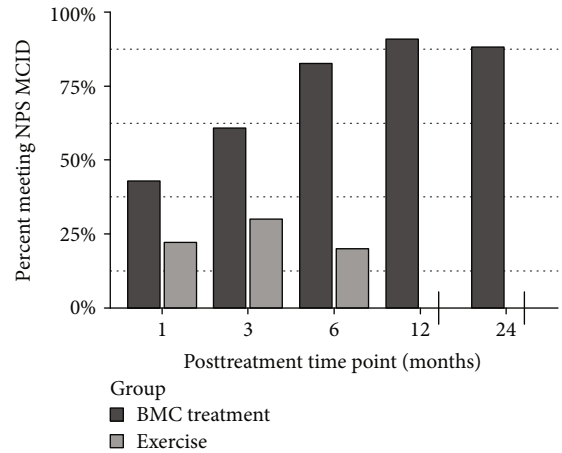
FIGURE 5: Percentage of patients who met MCID for NPS. Exercise *N*: 9, 10, 5; treatment *N*: 21, 23, 23, 22, 17.

and were maintained for the remaining follow-up time points ($p < .01$) (Figure 4). Our exercise group did not meet statistically significant improvement in either NPS or DASH group before crossover ($p < .01$) compared to baseline. MCID for NPS was reached by 43% of the BMC treatment group at 1 month, which improved to 91% at 12 months and was maintained to the 24-month time point (88%). MCID for NPS in the exercise therapy group was met by 22% of patients at 1 month, improved slightly to 30% at the 3-month time point, before dropping to 20% at 6 months, for those who had not yet crossed over (Figure 5). Modified SANE scores differed significantly between groups at 3 months ($p < .01$) and exhibited significant improvements compared to 1 month in the BMC group at all later time points ($p < .01$), with a mean SANE at 12 months of 80% and 24 months of 89% (Figure 6). TNCC did not correlate to any outcome parameter at any posttreatment time point. Outcomes compared at 24 months between the crossover treatment group and the BMC treatment only group were not statistically different for DASH, NPS, or SANE ($p > .05$).

A blinded comparison of pre- and postprocedural MRIs by three physicians was performed as an additional secondary outcome. This demonstrated a consensus pick of the posttreatment MRI as the MRI demonstrating the healthier supraspinatus tendon in 14 of 15 images available for review. The interreader reliability (IRR) for this was 0.64 ($p < .01$), indicating substantial agreement [41]. The tear size assessment showed a mean decrease of 26% after BMC treatment ($p > .05$).

An additional treatment injection of autologous PRP was allowed at the physician's discretion if the patient continued to experience pain and functional impairments. Such injections were administered to 12 patients (2 patients received 2 PRP injections) at a mean of 7 months after the BMC treatment.

4. Discussion

This is a midterm review of data from a single-site, prospective, randomized controlled, crossover trial assessing the

Figure 6: Modified SANE scores after BMC treatment at all time points.

treatment efficacy of supraspinatus tears with BMC and platelet products in comparison to conservative exercise therapy. The BMC treatment group demonstrated significant reductions in pain and increases in function when compared to baseline and when compared to the exercise therapy group at 3 and 6 months. Those improvements continued out to the 24-month follow-up for patients receiving the BMC treatment. All but 3 patients treated with BMC reached MCID at 12 and 24 months for pain and function. Improvement in tendon pathology shown near the 3-month time point is consistent with other studies evaluating tendon healing with treatment of biologics [42, 43].

The exact mechanisms pertinent to the ability of BMC to produce these clinical results are unclear, but it is believed that MCS in the BMC provide therapeutic effects via paracrine signaling that includes immunomodulation, antiapoptosis, angiogenesis, and support progenitor cells through stimulating mitosis, proliferation, and differentiation [44]. Animal studies have demonstrated that MSC transplantations restore function and improve tissue healing [45]. Clinical studies of BMC transplantation have shown augmentation of surgical repair of the rotator cuff with subsequent decrease in retear rates [22]. Other clinical studies have revealed improvements in pain and function with simple injections in the setting of rotator cuff pathology [20, 22].

Exercise therapy in our study did not demonstrate statistically significant improvement over baseline. It should be noted that response to exercise therapy varied across patients in the exercise group, with 40% of patients meeting the MCID for DASH at 3 months, even though the overall mean does not show significant improvements. There are multiple explanations for these results. It is possible that patients were not given enough time to demonstrate clinical improvement as 10/11 patients randomized to the exercise group crossed over by the 6-month mark to the BMC treatment group, though per the study protocol all patients were required to have 3 months of conservative treatment prior to enrollment, thus extending the time of conservative therapy prior to BMC treatment. These inclusion criteria may have also led to the unintended consequence that any major improvements resulting from an exercise therapy program may have occurred prior to enrollment into the study. It is also possible that the exercise group was too small to show a statistically significant difference since this is an early review; however, significant differences were found despite the small sample in the BMC group. Finally, the patients randomized to the

exercise group were given a self-guided home exercise program to be performed without the supervision of a trained practitioner which may have negatively affected compliance. The results from our home-based exercise therapy program may not be generalizable to a more rigorous physical therapy program monitored by a physiotherapist.

A comparison by three physicians was conducted for blinded pretreatment MRIs to posttreatment MRIs as a secondary outcome measure in the study. These physicians demonstrated substantial agreement that the posttreatment MRI demonstrated the healthier and less pathologic supraspinatus tendon fibers with a high interrater reliability. This finding, coupled with the tear measurements, lends evidence that there are demonstrable MRI improvements with BMC treatment to a torn supraspinatus tendon. Although the mean of tear length improvement was only 26% at a minimum of 12 months after BMC treatment, symptomatically patients were reporting feeling 80% better on average at 12 months and 89% better on average at 24 months. One possible explanation is that the BMC plus platelet product treatment decreases the concentrations of certain inflammatory cytokines, such as interleukin-8 levels in the shoulder joint fluid, which have been positively correlated to pain levels in patients with rotator cuff tears [46].

The expected natural course of a symptomatic substantial or full-thickness rotator cuff tear is to enlarge over time with an estimated 50%-82.4% of full-thickness tears and 26.1% of partial thickness tears enlarging in 12-18 months [47, 48]. There were no differences in the percentage of patients with recurrent tears after repair and patients with a tear size increase after conservative treatment, suggestive that repair does not necessarily change the natural progression of the tear [49]. Yoo et al. demonstrated no significant differences in pain and clinical outcome function scores between those with surgical repair and those who declined surgery in patients with symptomatic full thickness rotator cuff tears in which surgery was recommended [50]. The 24-month clinical outcomes after BMC injection in the current study have demonstrated encouraging data regarding improvement of pain and functional scores as well as radiographic improvement in tendon appearance.

Of the numerous components in the complex milieu of a BMC injection, the number of MSCs likely has a high impact on healing potential based on their innate healing properties. TNCC has previously been used as a proxy for the number of

MSCs in an injection as it is more readily available prior to treatment than colony-forming units. While a minimum TNCC has been postulated for other areas of treatment [51], no TNCC threshold has been established in treatment of supraspinatus tears. TNCC was obtained for each BMC sample processed and varied greatly, but individual outcomes in this investigation had no correlation to the TNCC measured of each patient's BMC.

There are several potential study limitations. First, our sample size is currently small with a total of 25 subjects for this analysis. Enrollment is ongoing. We also currently have incomplete data collection at this midterm review, with a few missing data points and only 17 patients having reached the full 24-month follow-up; however, we feel it is important to present the current data since enrollment is taking longer than originally anticipated. Second, posttreatment MRI images were only available for 19 patients in the study. Three independent physician reviewers demonstrated significant interrater reliability by usually choosing the posttreatment MRI sequences as the healthier supraspinatus tendon, but the lack of complete data may limit our ability to draw conclusions on radiographic improvement. Third, a longer duration of conservative management and restricting crossover of the patients enrolled in the exercise group may have provided a more accurate comparison to conservative treatment. However, patients already had completed at least 3 months of conservative therapy prior to enrollment in the study, and almost half did not crossover until closer to 6 months after starting exercise therapy. Additionally, it has previously been showed that 3-month outcomes after an exercise rehabilitation program predicted outcomes at 2 years after commencing treatment [52]. The shorter-term conservative management and the ability to cross over was designed in part to aide subject recruitment and retention. Compliance to the home exercise program was not measured and may have been an issue, although this did not appear to be an issue noted at any follow-ups during the exercise treatment.

Fourth, both PRP and PL were combined with the BMC injection which may have influenced outcomes over a BMC injection alone. We added PRP and PL into the BMC injectate as the combination may encourage more musculoskeletal healing than any would individually [53, 54]. The growth factor, cytokine, and chemokine profiles seen in PRP, PL, and BMC are different and likely work synergistically in encouraging healing [55–58]. Multiple studies have evaluated utilizing PRP in arthroscopic repair of full-thickness supraspinatus tears without clear benefit based on clinical outcome scores but with decreased rates of failure-to-heal [59, 60]. There is only one case report on treatment of a full-thickness supraspinatus tear with percutaneous PRP injection. This demonstrated neotendon infilling and improvements in pain and function at 1 year but did not report on longer term functional or pain outcomes [61]. There is little evidence to support the use of PRP only in the percutaneous treatment of full-thickness supraspinatus tears.

Future research opportunities include directly comparing long-term exercise outcomes to rotator cuff BMC injection without a crossover group or looking at chronicity of tear prior to treatment in relationship to the outcomes of treatment with BMC. Utilization of exercise diaries would help track compliance to the home exercise program. There also needs to be research performed to see if there are different outcomes associated with different locations, types, and severities of tears.

In conclusion, according to the midterm review data from our randomized controlled, crossover trial, injections of BMC with platelet products provide significant functional gains and reductions in pain compared to a guided home exercise program in the treatment of partial and full-thickness, nonretracted supraspinatus tears. This is the first randomized controlled trial, to our knowledge, of the injection of BMC for the treatment of partial and full-thickness supraspinatus tears in a nonsurgical setting. Our findings suggest that ultrasound-guided injection of BMC and platelet product may be a safe and useful alternative to conservative management nonretracted supraspinatus tendons.

Data Availability

The data used to support the findings of this study are restricted in order to protect patient privacy. Data are available from corresponding author upon request for researchers who meet the criteria for access to confidential data.

Conflicts of Interest

CC is a shareholder and CMO of Regenexx, LLC and president and owner of the Centeno-Schultz Clinic. ZF, IS, UA, and ED have declared no competing interests.

Acknowledgments

Supplementary Materials

Instructional handouts provided to all patients in the home exercise group. (*Supplementary Materials*)

References

[1] M. Valencia Mora, M. A. Ruiz Ibán, J. Díaz Heredia, R. Barco Laakso, R. Cuéllar, and M. García Arranz, "Stem cell therapy in the management of shoulder rotator cuff disorders," *World Journal of Stem Cells*, vol. 7, no. 4, pp. 691–699, 2015.

[2] I. R. Murray, R. LaPrade, V. Musahl et al., "Biologic treatments for sports injuries II think tank-current concepts, future research, and barriers to advancement, part 2: rotator cuff," *Orthopaedic Journal of Sports Medicine*, vol. 4, no. 3, p. 2325967116636586, 2016.

[3] U. G. Longo, F. Franceschi, A. Berton, N. Maffulli, and V. Droena, "Conservative treatment and rotator cuff tear progression," *Medicine and Sport Science*, vol. 57, pp. 90–99, 2012.

[4] J. E. Kuhn, W. R. Dunn, R. Sanders et al., "Effectiveness of physical therapy in treating atraumatic full-thickness rotator

cuff tears: a multicenter prospective cohort study," *Journal of Shoulder and Elbow Surgery*, vol. 22, no. 10, pp. 1371–1379, 2013.

[5] D. J. Bokor, R. J. Hawkins, G. H. Huckell, R. L. Angelo, and M. S. Schickendantz, "Results of nonoperative management of full-thickness tears of the rotator cuff," *Clinical Orthopaedics and Related Research*, vol. 294, pp. 103–110, 1993.

[6] B. A. Goldberg, R. J. Nowinski, and F. A. Matsen III, "Outcome of nonoperative management of full-thickness rotator cuff tears," *Clinical Orthopaedics and Related Research*, vol. 382, pp. 99–107, 2001.

[7] R. H. Hawkins and R. Dunlop, "Nonoperative treatment of rotator cuff tears," *Clinical Orthopaedics and Related Research*, vol. 321, pp. 178–188, 1995.

[8] S. Moosmayer, G. Lund, U. Seljom et al., "Comparison between surgery and physiotherapy in the treatment of small and medium-sized tears of the rotator cuff," *Journal of Bone and Joint Surgery. British Volume (London)*, vol. 92-B, no. 1, pp. 83–91, 2010.

[9] S. Koubâa, F. Z. Ben Salah, S. Lebib, I. Miri, S. Ghorbel, and C. Dziri, "Conservative management of full-thickness rotator cuff tears. A prospective study of 24 patients," *Annales de Réadaptation et de Médecine Physique*, vol. 49, no. 2, pp. 62–67, 2006.

[10] M. Jeanfavre, S. Husted, and G. Leff, "Exercise therapy in the non-operative treatment of full-thickness rotator cuff tears: a systematic review," *International Journal of Sports Physical Therapy*, vol. 13, no. 3, pp. 335–378, 2018.

[11] D. Giotis, A. Aryaei, T. Vasilakakos, and N. K. Paschos, "Effectiveness of biologic factors in shoulder disorders," *The Open Orthopaedics Journal*, vol. 11, pp. 163–182, 2017.

[12] P. S. Randelli, A. Menon, E. Nocerino et al., "Long-term results of arthroscopic rotator cuff repair: initial tear size matters: a prospective study on clinical and radiological results at a minimum follow-up of 10 years," *The American Journal of Sports Medicine*, vol. 47, no. 11, pp. 2659–2669, 2019.

[13] E. J. Curry, E. E. Matzkin, Y. Dong, L. D. Higgins, J. N. Katz, and N. B. Jain, "Structural characteristics are not associated with pain and function in rotator cuff tears: the ROW cohort study," *Orthopaedic Journal of Sports Medicine*, vol. 3, no. 5, 2015.

[14] J. Kukkonen, A. Joukainen, J. Lehtinen et al., "Treatment of non-traumatic rotator cuff tears: a randomised controlled trial with one-year clinical results," *The Bone & Joint Journal*, vol. 96-b, no. 1, pp. 75–81, 2014.

[15] S. Moosmayer, G. Lund, U. S. Seljom et al., "Tendon repair compared with physiotherapy in the treatment of rotator cuff tears: a randomized controlled study in 103 cases with a five-year follow-up," *The Journal of Bone and Joint Surgery. American Volume*, vol. 96, no. 18, pp. 1504–1514, 2014.

[16] J. C. Seida, C. LeBlanc, J. R. Schouten et al., "Systematic review: nonoperative and operative treatments for rotator cuff tears," *Annals of Internal Medicine*, vol. 153, no. 4, pp. 246–255, 2010.

[17] C. Khatri, I. Ahmed, H. Parsons et al., "The natural history of full-thickness rotator cuff tears in randomized controlled trials: a systematic review and meta-analysis," *The American Journal of Sports Medicine*, vol. 47, no. 7, pp. 1734–1743, 2019.

[18] S. Thomopoulos, G. Hattersley, V. Rosen et al., "The localized expression of extracellular matrix components in healing tendon insertion sites: an in situ hybridization study," *Journal of Orthopaedic Research*, vol. 20, no. 3, pp. 454–463, 2002.

[19] S. Chaudhury, "Mesenchymal stem cell applications to tendon healing," *Muscles, Ligaments and Tendons Journal*, vol. 2, no. 3, pp. 222–229, 2012.

[20] C. J. Centeno, H. al-Sayegh, J. Bashir, S. Goodyear, and M. D. Freeman, "A prospective multi-site registry study of a specific protocol of autologous bone marrow concentrate for the treatment of shoulder rotator cuff tears and osteoarthritis," *Journal of Pain Research*, vol. 8, pp. 269–276, 2015.

[21] S. J. Kim, E. K. Kim, S. J. Kim, and D. H. Song, "Effects of bone marrow aspirate concentrate and platelet-rich plasma on patients with partial tear of the rotator cuff tendon," *Journal of Orthopaedic Surgery and Research*, vol. 13, no. 1, p. 1, 2018.

[22] P. Hernigou, C. H. Flouzat Lachaniette, J. Delambre et al., "Biologic augmentation of rotator cuff repair with mesenchymal stem cells during arthroscopy improves healing and prevents further tears: a case-controlled study," *International Orthopaedics*, vol. 38, no. 9, pp. 1811–1818, 2014.

[23] K. Gopal, H. A. Amirhamed, and T. Kamarul, "Advances of human bone marrow-derived mesenchymal stem cells in the treatment of cartilage defects: a systematic review," *Experimental Biology and Medicine (Maywood, N.J.)*, vol. 239, no. 6, pp. 663–669, 2014.

[24] A. I. Caplan, "The mesengenic process," *Clinics in Plastic Surgery*, vol. 21, no. 3, pp. 429–435, 1994.

[25] D. Docheva, S. A. Müller, M. Majewski, and C. H. Evans, "Biologics for tendon repair," *Advanced Drug Delivery Reviews*, vol. 84, pp. 222–239, 2015.

[26] L. Liu, J. Hindieh, D. J. Leong, and H. B. Sun, "Advances of stem cell based-therapeutic approaches for tendon repair," *Journal of Orthopaedic Translation*, vol. 9, pp. 69–75, 2017.

[27] J. L. Ellera Gomes, R. C. da Silva, L. M. R. Silla, M. R. Abreu, and R. Pellanda, "Conventional rotator cuff repair complemented by the aid of mononuclear autologous stem cells," *Knee Surgery, Sports Traumatology, Arthroscopy*, vol. 20, no. 2, pp. 373–377, 2012.

[28] V. Havlas, J. Kotaška, P. Koníček et al., "Use of cultured human autologous bone marrow stem cells in repair of a rotator cuff tear: preliminary results of a safety study," *Acta Chirurgiae Orthopaedicae et Traumatologiae Cechoslovaca*, vol. 82, no. 3, pp. 229–234, 2015.

[29] Y. Kaizawa, A. Franklin, J. Leyden et al., "Augmentation of chronic rotator cuff healing using adipose-derived stem cell-seeded human tendon-derived hydrogel," *Journal of Orthopaedic Research*, vol. 37, no. 4, pp. 877–886, 2019.

[30] P. R. Camargo, M. A. Avila, F. Alburquerque-Sendín, N. A. Asso, L. H. Hashimoto, and T. F. Salvini, "Eccentric training for shoulder abductors improves pain, function and isokinetic performance in subjects with shoulder impingement syndrome: a case series," *Revista Brasileira de Fisioterapia*, vol. 16, no. 1, pp. 74–83, 2012.

[31] I. Duzgun, G. Baltaci, and O. A. Atay, "Comparison of slow and accelerated rehabilitation protocol after arthroscopic rotator cuff repair: pain and functional activity," *Acta Orthopaedica et Traumatologica Turcica*, vol. 45, no. 1, pp. 23–33, 2011.

[32] T. G. Baumer, D. Chan, V. Mende et al., "Effects of rotator cuff pathology and physical therapy on in vivo shoulder motion and clinical outcomes in patients with a symptomatic full-thickness rotator cuff tear," *Orthopaedic Journal of Sports Medicine*, vol. 4, no. 9, 2016.

[33] R. M. Miller, A. Popchak, D. Vyas et al., "Effects of exercise therapy for the treatment of symptomatic full-thickness supraspinatus tears on in vivo glenohumeral kinematics," *Journal of Shoulder and Elbow Surgery*, vol. 25, no. 4, pp. 641–649, 2016.

[34] D. E. Beaton, J. N. Katz, A. H. Fossel, J. G. Wright, V. Tarasuk, and C. Bombardier, "Measuring the whole or the parts? Validity, reliability, and responsiveness of the Disabilities of the Arm, Shoulder and Hand outcome measure in different regions of the upper extremity," *Journal of Hand Therapy*, vol. 14, no. 2, pp. 128–146, 2001.

[35] P. L. Hudak, P. C. Amadio, and C. Bombardier, "Development of an upper extremity outcome measure: the DASH (disabilities of the arm, shoulder and hand) [corrected]. The Upper Extremity Collaborative Group (UECG)," *American Journal of Industrial Medicine*, vol. 29, no. 6, pp. 602–608, 1996.

[36] S. Hawker, S. Payne, C. Kerr, M. Hardey, and J. Powell, "Appraising the evidence: reviewing disparate data systematically," *Qualitative Health Research*, vol. 12, no. 9, pp. 1284–1299, 2002.

[37] K. D. Shelbourne, A. F. Barnes, and T. Gray, "Correlation of a single assessment numeric evaluation (SANE) rating with modified Cincinnati knee rating system and IKDC subjective total scores for patients after ACL reconstruction or knee arthroscopy," *The American Journal of Sports Medicine*, vol. 40, no. 11, pp. 2487–2491, 2012.

[38] G. N. Williams, T. J. Gangel, R. A. Arciero, J. M. Uhorchak, and D. C. Taylor, "Comparison of the Single Assessment Numeric Evaluation method and two shoulder rating Scales," *The American Journal of Sports Medicine*, vol. 27, no. 2, pp. 214–221, 1999.

[39] A. A. Sorensen, D. Howard, W. H. Tan, J. Ketchersid, and R. P. Calfee, "Minimal clinically important differences of 3 patient-rated outcomes instruments," *The Journal of Hand Surgery*, vol. 38, no. 4, pp. 641–649, 2013.

[40] L. A. Michener, A. R. Snyder, and B. G. Leggin, "Responsiveness of the numeric pain rating scale in patients with shoulder pain and the effect of surgical status," *Journal of Sport Rehabilitation*, vol. 20, no. 1, pp. 115–128, 2011.

[41] J. R. Landis and G. G. Koch, "The measurement of observer agreement for categorical data," *Biometrics*, vol. 33, no. 1, pp. 159–174, 1977.

[42] R. Yadav, S. Y. Kothari, and D. Borah, "Comparison of local injection of platelet rich plasma and corticosteroids in the treatment of lateral epicondylitis of humerus," *Journal of Clinical and Diagnostic Research*, vol. 9, no. 7, pp. RC05–RC07, 2015.

[43] S. J. Kim, D. H. Song, J. W. Park, S. Park, and S. J. Kim, "Effect of bone marrow aspirate concentrate-platelet-rich plasma on tendon-derived stem cells and rotator cuff tendon tear," *Cell Transplantation*, vol. 26, no. 5, pp. 867–878, 2017.

[44] S. Meirelles Lda, A. M. Fontes, D. T. Covas, and A. I. Caplan, "Mechanisms involved in the therapeutic properties of mesenchymal stem cells," *Cytokine & Growth Factor Reviews*, vol. 20, no. 5-6, pp. 419–427, 2009.

[45] S. Yokoya, Y. Mochizuki, K. Natsu, H. Omae, Y. Nagata, and M. Ochi, "Rotator cuff regeneration using a bioabsorbable material with bone marrow-derived mesenchymal stem cells in a rabbit model," *The American Journal of Sports Medicine*, vol. 40, no. 6, pp. 1259–1268, 2012.

[46] K. Okamura, T. Kobayashi, A. Yamamoto et al., "Shoulder pain and intra-articular interleukin-8 levels in patients with rotator cuff tears," *International Journal of Rheumatic Diseases*, vol. 20, no. 2, pp. 177–181, 2017.

[47] R. Z. Tashjian, "Epidemiology, natural history, and indications for treatment of rotator cuff tears," *Clinics in Sports Medicine*, vol. 31, no. 4, pp. 589–604, 2012.

[48] Y. S. Kim, S. E. Kim, S. H. Bae, H. J. Lee, W. H. Jee, and C. K. Park, "Tear progression of symptomatic full-thickness and partial-thickness rotator cuff tears as measured by repeated MRI," *Knee Surgery, Sports Traumatology, Arthroscopy*, vol. 25, no. 7, pp. 2073–2080, 2017.

[49] P. N. Chalmers, H. Ross, E. Granger, A. P. Presson, C. Zhang, and R. Z. Tashjian, "The effect of rotator cuff repair on natural history: a systematic review of intermediate to long-term outcomes," *JBJS Open Access*, vol. 3, no. 1, article e0043, 2018.

[50] J. C. Yoo, T. K. Lim, D. H. Kim, and K. H. Koh, "Comparison between the patients with surgery and without surgery after recommendation of surgical repair for symptomatic rotator cuff tear," *Journal of Orthopaedic Science*, vol. 23, no. 1, pp. 64–69, 2018.

[51] C. J. Centeno, H. al-Sayegh, J. Bashir, S. Goodyear, and M. D. Freeman, "A dose response analysis of a specific bone marrow concentrate treatment protocol for knee osteoarthritis," *BMC Musculoskeletal Disorders*, vol. 16, no. 1, p. 258, 2015.

[52] R. S. Boorman, K. D. More, R. M. Hollinshead et al., "The rotator cuff quality-of-life index predicts the outcome of nonoperative treatment of patients with a chronic rotator cuff tear," *The Journal of Bone and Joint Surgery. American Volume*, vol. 96, no. 22, pp. 1883–1888, 2014.

[53] J. Bolte, C. Vater, A. C. Culla et al., "Two-step stem cell therapy improves bone regeneration compared to concentrated bone marrow therapy," *Journal of Orthopaedic Research*, vol. 37, no. 6, pp. 1318–1328, 2019.

[54] P. Kasten, M. Beverungen, H. Lorenz, J. Wieland, M. Fehr, and F. Geiger, "Comparison of platelet-rich plasma and VEGF-transfected mesenchymal stem cells on vascularization and bone formation in a critical-size bone defect," *Cells, Tissues, Organs*, vol. 196, no. 6, pp. 523–533, 2012.

[55] M. Baria, W. K. Vasileff, M. Miller, J. Borchers, D. C. Flanigan, and S. S. Durgam, "Cellular components and growth factor content of platelet-rich plasma with a customizable commercial system," *The American Journal of Sports Medicine*, vol. 47, no. 5, pp. 1216–1222, 2019.

[56] S. T. Hsiao, A. Asgari, Z. Lokmic et al., "Comparative analysis of paracrine factor expression in human adult mesenchymal stem cells derived from bone marrow, adipose, and dermal tissue," *Stem Cells and Development*, vol. 21, no. 12, pp. 2189–2203, 2012.

[57] F. Mussano, T. Genova, L. Munaron, S. Petrillo, F. Erovigni, and S. Carossa, "Cytokine, chemokine, and growth factor profile of platelet-rich plasma," *Platelets*, vol. 27, no. 5, pp. 467–471, 2016.

[58] A. J. Villatoro, C. Alcoholado, M. C. Martín-Astorga, V. Fernández, M. Cifuentes, and J. Becerra, "Comparative analysis and characterization of soluble factors and exosomes from cultured adipose tissue and bone marrow mesenchymal stem cells in canine species," *Veterinary Immunology and Immunopathology*, vol. 208, pp. 6–15, 2019.

[59] Y. Z. Cai, C. Zhang, and X. J. Lin, "Efficacy of platelet-rich plasma in arthroscopic repair of full-thickness rotator cuff

tears: a meta-analysis," *Journal of Shoulder and Elbow Surgery*, vol. 24, no. 12, pp. 1852–1859, 2015.

[60] E. A. Malavolta, M. E. C. Gracitelli, J. H. Assunção, A. A. Ferreira Neto, M. Bordalo-Rodrigues, and O. P. de Camargo, "Clinical and structural evaluations of rotator cuff repair with and without added platelet-rich plasma at 5-year follow-up: a prospective randomized study," *The American Journal of Sports Medicine*, vol. 46, no. 13, pp. 3134–3141, 2018.

[61] A. Doss, "Neotendon infilling of a full thickness rotator cuff foot print tear following ultrasound guided liquid platelet rich plasma injection and percutaneous tenotomy: favourable outcome up to one year," *F1000Research*, vol. 2, p. 23, 2013.

Research Article

FGF-2-Induced Human Amniotic Mesenchymal Stem Cells Seeded on a Human Acellular Amniotic Membrane Scaffold Accelerated Tendon-to-Bone Healing in a Rabbit Extra-Articular Model

Jun Zhang,[1] **Ziming Liu,**[2] **Yuwan Li** [iD](ORCID),[3] **Qi You,**[1] **Jibin Yang,**[1] **Ying Jin,**[1] **Gang Zou,**[1]
Jingfeng Tang,[1] **Zhen Ge,**[1] **and Yi Liu** [iD](ORCID)[1]

[1]*Department of Orthopaedic Surgery, Affiliated Hospital of Zunyi Medical University, China*
[2]*Institute of Sports Medicine, Beijing Key Laboratory of Sports Injuries, Peking University Third Hospital, China*
[3]*Department of Orthopaedic Surgery, The First Affiliated Hospital of Chongqing Medical University, Chongqing, China*

Correspondence should be addressed to Yi Liu; 13308529536@163.com

Background. FGF-2 (basic fibroblast growth factor) has a positive effect on the proliferation and differentiation of many kinds of MSCs. Therefore, it represents an ideal molecule to facilitate tendon-to-bone healing. Nonetheless, no studies have investigated the application of FGF-2-induced human amniotic mesenchymal stem cells (hAMSCs) to accelerate tendon-to-bone healing in vivo. *Objective.* The purpose of this study was to explore the effect of FGF-2 on chondrogenic differentiation of hAMSCs in vitro and the effect of FGF-2-induced hAMSCs combined with a human acellular amniotic membrane (HAAM) scaffold on tendon-to-bone healing in vivo. *Methods.* In vitro, hAMSCs were transfected with a lentivirus carrying the *FGF-2* gene, and the potential for chondrogenic differentiation of hAMSCs induced by the *FGF-2* gene was assessed using immunofluorescence and toluidine blue (TB) staining. HAAM scaffold was prepared, and hematoxylin and eosin (HE) staining and scanning electron microscopy (SEM) were used to observe the microstructure of the HAAM scaffold. hAMSCs transfected with and without *FGF-2* were seeded on the HAAM scaffold at a density of 3×10^5 cells/well. Immunofluorescence staining of vimentin and phalloidin staining were used to confirm cell adherence and growth on the HAAM scaffold. In vivo, the rabbit extra-articular tendon-to-bone healing model was created using the right hind limb of 40 New Zealand White rabbits. Grafts mimicking tendon-to-bone interface (TBI) injury were created and subjected to treatment with the HAAM scaffold loaded with FGF-2-induced hAMSCs, HAAM scaffold loaded with hAMSCs only, HAAM scaffold, and no special treatment. Macroscopic observation, imageological analysis, histological assessment, and biomechanical analysis were conducted to evaluate tendon-to-bone healing after 3 months. *Results.* In vitro, cartilage-specific marker staining was positive for the *FGF-2* overexpression group. The HAAM scaffold displayed a netted structure and mass extracellular matrix structure. hAMSCs or hAMSCs transfected with *FGF-2* survived on the HAAM scaffold and grew well. In vivo, the group treated with HAAM scaffold loaded with *FGF-2*-induced hAMSCs had the narrowest bone tunnel after three months as compared with other groups. In addition, macroscopic and histological scores were higher for this group than for the other groups, along with the best mechanical strength. *Conclusion.* hAMSCs transfected with *FGF-2* combined with the HAAM scaffold could accelerate tendon-to-bone healing in a rabbit extra-articular model.

1. Introduction

Tendon-to-bone interface (TBI)—a key anchor that attaches ligaments/tendons to bones—plays a significant role in relieving the high stress transmitted from the ligament/-tendon to the bone [1]. TBI is a special structure between the ligament/tendon and the bone, consisting of four transitional layers: ligament/tendon, uncalcified fibrocartilage, calcified fibrocartilage, and bone tissue [2, 3]. Fibrocartilage is a mechanical load-bearing tissue, and TBI injuries frequently

occur in the fibrocartilage area. Upon injury, TBI heals slowly and does not regain its original structure and mechanical property due to the poor healing ability of the fibrocartilage [4]. The regenerative capacity of fibrocartilage is poor and fairly limited owing to its relative avascularity, resulting in very slow recovery of the injured TBI [5]. Recently, many strategies to augment TBI healing have been devised in basic-science researches and clinical treatments, including the use of biomimetic scaffolds, growth factors, and stem cells [6, 7].

The development of tissue engineering technology, involving three pivotal elements—seed cells, growth factors, and scaffold materials—has enhanced the treatment of several diseases [8]. Mesenchymal stem cells (MSCs) are the most commonly used seed cells in tissue engineering technology and include adipose-derived MSCs [9–11], peripheral blood-derived MSCs [12, 13], and bone marrow MSCs (BMSCs) [14, 15]. Owing to their unique advantages, BMSCs have become the most popular seed cells and are now widely used in many fields. However, there are also some disadvantages of BMSCs, such as potential risks of hemorrhage, infection, and immunological rejection response during the harvesting process [16, 17].

Therefore, it is necessary to explore new seed cells that can be applied to tissue engineering technology. Human amniotic mesenchymal stem cells (hAMSCs), harvested from the discarded placenta of healthy puerperant women, have been successfully isolated and used in many studies [18, 19]. Compared with other MSCs, hAMSCs have many advantages, including consistent and wide availability, simple operation, and no ethical controversies [18, 19]. Du et al. reported that hAMSCs had a greater proliferative ability than BMSCs [20], enabling their potential use as seed cells. However, there is limited research about using hAMSCs to accelerate TBI healing [21].

Scaffold materials are the other crucial factors in tissue engineering technology. They not only promote adhesion and proliferation of cells but also have the potential to facilitate cells to differentiate in the desired direction. Human amnion membrane (HAM), the innermost layer of the fetal membrane, is a translucent membrane that has abundant extracellular matrix (ECM), including hyaluronan, fibronectin, and collagens I, III, IV, V, and VII [22–26]. Human acellular amniotic membrane (HAAM) scaffold is a biological scaffold made by decellularizing HAM organization. HAAM scaffold has been widely used as a scaffold to construct engineered tissues and organs owing to its superior characteristics, such as antimicrobial, anti-inflammatory, and nonantigenic properties [22–26].

Many growth factors have been discovered and applied to tissue engineering technology, including transforming growth factor-β (TGF-β) [27], epidermal growth factor (EGF) [28], vascular endothelial growth factor (VEGF) [29], and fibroblast growth factor (FGF) [30]. Among them, FGF-2 (basic fibroblast growth factor) has been widely used in tissue engineering technology due to its unique advantages [31]. FGF-2 is an effective mitogen for many kinds of cells and has the ability to promote cell proliferation and differentiation [32]. Recently, many studies have found FGF-2 capable of accelerating tendon-to-bone healing [33, 34].

Therefore, in the current study, we hypothesized that (a) FGF-2 could promote chondrogenic differentiation of hAMSCs in vitro and (b) hAMSCs loaded onto the HAAM scaffold and induced by FGF-2 have the potential ability to augment tendon-to-bone healing in vivo.

2. Materials and Methods

2.1. Isolation, Culture, and Characterization of hAMSCs. For this study, placentas were obtained from the Obstetrics Department of the Affiliated Hospital of Zunyi Medical University with informed consent from each patient before operation. In line with a previous research [35], hAMSCs used in this study were isolated from the human placental amniotic membrane of 5 healthy full-term puerperant women by subjecting to enzymatic (Solarbio, China) digestion twice, followed by collagenase type II (Gibco, USA) digestion once. In brief, the isolated amniotic membrane was minced into pieces and digested twice with 0.05% trypsin/0.01% ethylenediaminetetraacetic acid (EDTA) for 30 mins at 37°C, followed by washing the tissue with phosphate buffer solution (PBS) and digestion with 0.75% collagenase type II for 1 h at 37°C. Third-generation (P3) hAMSCs of good condition obtained by this method were used for subsequent experiments. According to the established protocol [35], the stemness of the hAMSCs isolated from placental amniotic membrane was tested via immunostaining with a stem cell marker and a human amniotic epithelial cell marker, vimentin (1 : 300, ab92547, Abcam) and cytokeratin 19 (CK-19, 1 : 200, ab52625, Abcam), respectively.

2.2. Transfection of hAMSCs by Lentivirus Carrying the FGF-2 Gene. Lentivirus containing the *FGF-2* gene was obtained from the Shanghai Jikai Gene Chemical Technology Co. Ltd. According to the manufacturer's instructions, P3 hAMSCs were seeded in a 96-well plate and infected by multiplicity of infection (MOI) of 0, 25, 50, 75,100, and 150. These cells were then classified into three groups: the FGF-2 transfection group, untransfected group, and empty virus group. All three groups were cultured in L-DMEM/F12 culture medium containing 10% (v/v) fetal bovine serum (FBS, Gibco, USA), 1% (v/v) penicillin/streptomycin (P/S, Solarbio, China), 1% (v/v) glutamine (Solarbio, China), and 1% (v/v) nonessential amino acids (Solarbio, China). The culture medium was changed after 12 h, and hAMSCs were observed under an inverted fluorescence microscope. The optimal MOI value was established by observing the expression of green fluorescent protein (GFP) in the live infected hAMSCs, after which the formal experiment was performed according to the aforementioned method, using the optimal MOI. After 72 h, the expression of GFP was observed under an inverted fluorescence microscope to measure the transfection efficiency. Further, the transfection efficiency was detected using quantitative real-time reverse transcriptase-polymerase chain reaction (qRT-PCR). In brief, total RNA extraction was performed using the RNAiso plus reagent kit (Takara Bio Inc., Shiga, Japan), and cDNA was synthesized

TABLE 1: Primer sequences for quantitative RT-PCR analysis.

Gene name	Gene symbol	Primer sequence	Accession number
Basic fibroblast growth factor	FGF-2	F: TTCAAGCAGAAGAGAGAGGAG R: TCCGTAACACATTTAGAAGCC	NM_002006.5
Glyceraldehyde-3-phosphate dehydrogenase	GAPDH	F: GCCTTCCGTGTCCCCACTGC R: CAATGCCAGCCCCAGCGTCA	NM_002006.4
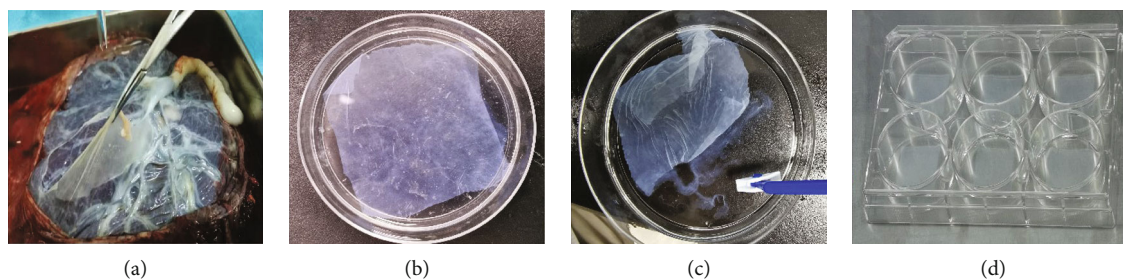
FIGURE 1: The preparation process of the HAAM scaffold. (a) The HAM was isolated from the placenta. (b) The HAM was decellularized using trypsin. (c) The epithelial cells were removed using a scraper. (d) The HAAM scaffold was put into 6-well culture plates carefully for sterilization.

using the PrimeScript RT reagent kit (Takara Bio Inc.). The expression of FGF-2 was detected via quantitative real-time PCR using the TB Green Premix Ex Taq kit (Takara Bio Inc.). Human FGF-2 gene was used. The primers used in qRT-PCR are provided in Table 1. Relative gene expression levels were normalized to human glyceraldehyde-3-phosphate dehydrogenase (GAPDH) and calculated using the $2^{-\Delta\Delta Ct}$ method.

2.3. Immunofluorescence Examination and Toluidine Blue (TB) Staining.

Immunofluorescence was used to detect the expression of collagen II in each group transfected with and without the *FGF-2* gene. P3 hAMSCs were seeded onto sterile cover slips of 6-well plates at a density of 10^5 cells/ml (3 wells per group), followed by addition of lentivirus at the optimal MOI. Fourteen days later, after observing intense fluorescence under an inverted fluorescence microscope, the hAMSCs were fixed with 4% paraformaldehyde for 15 min at room temperature. Wells were blocked with 5% goat serum for 60 mins, and the hAMSCs were incubated overnight at 4°C with the primary antibodies against collagen type II (1 : 200, ab34712, Abcam). The next day, hAMSCs were incubated with Alexa Fluor® 594 conjugated anti-rabbit (Abcam, USA) secondary antibodies for 1 hour at room temperature, and cell nuclei were stained using 2-(4-amidinophenyl)-6-indolecarbamidine dihydrochloride (DAPI). The results were observed using an inverted fluorescence microscope. Fourteen days after transfection of the FGF-2 gene, hAMSCs of each group were fixed with 4% paraformaldehyde for 15 mins at room temperature followed by washing thrice with PBS. TB (Sigma, USA) staining was performed, and results were observed under an inverted microscope.

2.4. Preparation of HAAM Scaffold.
HAM was isolated under sterile conditions from the placentas to prepare the HAAM

scaffold (Figure 1(a)). The isolated HAM was washed with sterile PBS containing P/S solution to separate blood clots, debris, dead cells, and mucus. The HAM was then cut into proper pieces and placed in dishes with the amniotic epithelial layer facing up. Thereafter, the pieces were incubated in 0.25% trypsin with EDTA for 30 mins at 37°C in an incubator (Figure 1(b)). Next, the deciduous epithelial cells were removed carefully with a scraper and were washed thrice with PBS to eliminate the residual epithelial cells and debris thoroughly (Figure 1(c)). The pieces were then recut into smaller sections of approximately 2×2 cm size and put into 6-well culture plates carefully (Figure 1(d)). The pieces were then sterilized using ultraviolet radiation and a mixture of P/S and amphotericin for about 30 mins.

2.5. Hematoxylin and Eosin (HE) Staining and Scanning Electron Microscopy (SEM) Analysis.
HE staining was performed to verify the efficiency of the decellularization process. Fresh HAM and prepared HAAM scaffold were fixed using 4% paraformaldehyde solution for 24 hours, dehydrated, embedded in paraffin wax, and sectioned for HE staining. For SEM analysis, the HAAM scaffold was fixed using 3% glutaraldehyde in 0.1 M PBS for 2 h at 4°C, followed by fixing in 1% osmium tetroxide for 60 mins at room temperature and dehydration using 70%, 80%, 90%, and 100% ethanol for 10 mins. The HAAM scaffold was then air dried, mounted, sputter coated with gold, and tested using the Hitachi SU8100 SEM (Hitachi, Tokyo, Japan).

2.6. Cultured hAMSCs and FGF-2-Induced hAMSCs on HAAM Scaffold.
hAMSCs and hAMSCs transfected with *FGF-2* were seeded on the completed and sterilized HAAM scaffold at a density of 3×10^5 cells/well. Growth status of the cells was observed daily under an inverted microscope. Additionally, adhesion and growth of the hAMSCs were
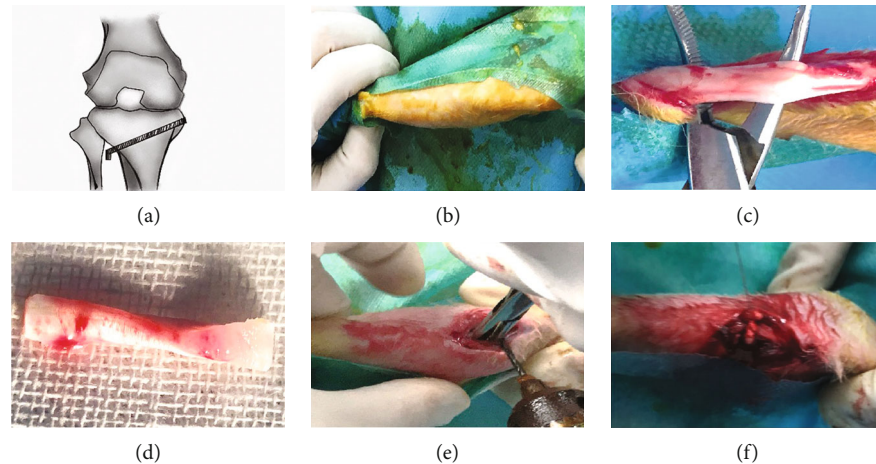
FIGURE 2: Animal surgical procedure. (a) Brief schematic diagram of the surgery. (b) The skin was sterilized. (c, d) Partial-thickness Achilles tendon of the left hind limb was harvested. (e) Bone tunnel was made in the proximal tibia of the right hind limb. (f) The Achilles tendon graft with four different treatments was passed through the bone tunnel.

TABLE 2: Experimental grouping in vivo.

Groups	Treatment methods
Group 1: control	Achilles tendon with no special treatment
Group 2: HAAM	Achilles tendon wrapped with HAAM
Group 3: HAAM+hAMSCs	Achilles tendon wrapped with HAAM-loaded hAMSCs
Group 4: HAAM+FGF-2-induced hAMSCs	Achilles tendon wrapped with HAAM-loaded FGF-2-induced hAMSCs

monitored after the 1st and 7th days via immunofluorescence staining by vimentin. Next, hAMSCs on the HAAM scaffold were fixed with 4% paraformaldehyde and washed with PBS. hAMSCs were blocked using 5% goat serum for one hour and incubated overnight at 4°C with primary antibodies against vimentin, followed by incubation with fluorescent secondary antibodies for 1 h at room temperature. The cell nuclei were stained using DAPI, and the results were observed under a fluorescence microscope. hAMSCs transfected with the FGF-2 gene were stained with phalloidin to observe cell adhesion and growth after the 1st and 7th days. Subsequently, the cells were washed with PBS and fixed with 4% paraformaldehyde. After permeabilizing the cell membrane with 0.5% polyethylene glycol octylphenol ether (Triton X-100) for 5 mins, TRITC-labeled phalloidin solution (Solarbio, China) was added and incubated for 30 mins. DAPI was used to stain cell nuclei, and the results were observed under a fluorescence microscope.

2.7. Surgical Procedure and Creation of Extra-Articular Tendon-to-Bone Healing Model. A total of 48 healthy New Zealand White rabbits (age 5-6 months; weight 2.5–2.7 kg) were purchased from Chongqing, China. The animal provision license was Animals for Medical Use (Word) No. 2017-0010. The animal study was approved by the Ethics Committee of the Affiliated Hospital of Zunyi Medical College, and all procedures were carried out in accordance with institutional guidelines for the care of animals. Preoperation X-ray examination was performed to exclude rele-

vant diseases that may influence experiment results. Eight rabbits (out of 48) were excluded: two rabbits had fractures during transportation, three had dearticulation, and three had joint deformities. With 5 rabbits in each group, 20 rabbits were used for histological assessment and 20 rabbits were used for radiographic analysis and biomechanical testing. The extra-articular tendon-bone healing model was created according to the established protocol [36, 37] (Figure 2). Briefly, 0.75 ml/kg of 3% sodium pentobarbital was administered intravenously to anesthetize the animals, followed by a middle incision along the Achilles tendon of the left hind limb. A partial-thickness tendon of 2 cm length was harvested as a graft. A bone tunnel of 2.5 mm diameter was made in the proximal tibia of the right hind limb, and the Achilles tendon with four different treatments was passed through the bone tunnel (Table 2).

Next, the ends of the implanted tendons were sutured to the surrounding soft tissue, and 0.5 cm of one end was retained for biomechanical tests to be carried out later. Thereafter, the wounds were sutured layer by layer, and the animals were allowed to move freely without any impediment in their cages after surgery. Penicillin (100,000 U/kg) was injected intramuscularly to prevent wound infection, for three consecutive days postoperation. The rabbits were sacrificed at 3 months after surgery, and graft-tibia complexes (GTCs) were prepared for subsequent tests.

2.8. Macroscopic Observation, Morphological Grading, and Imageological Analysis. Three months after the surgery, no

(a)

(b)
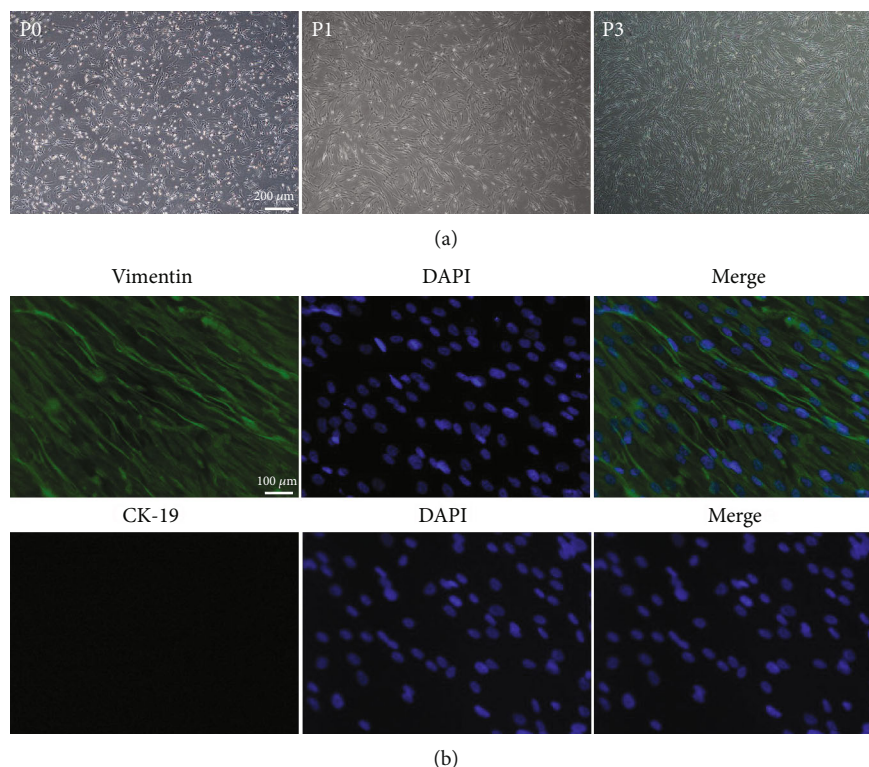
FIGURE 3: (a) Microscopic observations of P0, P1, and P3 hAMSCs; scale bar = 200 μm. (b) P3 hAMSCs were positive for vimentin. P3 hAMSCs hardly expressed CK-19. Scale bar = 100 μm.

infections or other complications were observed in any of the animals. Macroscopic images of the GTC specimens were taken to evaluate the tendon-to-bone healing. Healing status of the tendon-bone interface was assessed using the Yamakado interface morphological grade, which comprised direct type of insertion, collagen fiber continuity, interface without collagen fiber continuity, and separation between the bone and tendon [37]. Each group had five specimens. Additionally, X-ray examination was used to evaluate the bone tunnel area; the GTC samples were scanned perpendicular to the long-bone axis covering the entry and exit of the bone tunnel at the Department of Radiology, Affiliated Hospital of Zunyi Medical University.

2.9. Histological Assessment. The GTC samples were fixed in 4% paraformaldehyde solution for 24 h, decalcified using EDTA decalcifying solution (Solarbio, China) for about 2 weeks, and embedded in paraffin for routine histological sectioning. Five-micrometer-thick sections were cut perpendicular to the longitudinal axis of the tibial tunnel and stained with HE, TB, Safranin O/Fast Green, and Masson's trichrome staining.

2.10. Biomechanical Analysis. Biomechanical analysis was carried out at the Nanjing BiaoPu Testing Technical Service Co. Ltd. Samples of the GTCs were prepared for biomechanical analysis immediately after sacrifice in accordance with a previously reported protocol [33]. Briefly, all remnant soft tissues, except the transplanted tendon around the bone tunnel, were carefully removed. The transplanted tendon end

outside the bone tunnel was sutured for traction, and the tibia was firmly fixed. After a preload with a stationary load of 1 N for 5 min, the biomechanical analysis was performed. The ultimate failure load was carried out with an elongation rate of 2 mm/min. The stiffness and ultimate failure load were measured using the load-deformation curve. For each specimen, the testing was terminated when the graft ruptured or was pulled out of the bone tunnel.

2.11. Statistical Analyses. Data were expressed as mean ± standard deviation. Analysis of variance (ANOVA) and Tukey's multiple comparisons were used to determine significant differences. $P < 0.05$ was considered to have statistically significant difference. SPSS software (version 18.0; IBM) was used for data analysis.

3. Results

3.1. Culture and Characterization of hAMSCs. After 48 h in primary culture (P0), the morphology of the hAMSCs exhibited a spindle-shaped exterior under an inverted microscope. After multiple subcultures, the morphology of the hAMSCs gradually became vortex-like and long fusiform (Figure 3(a)). The "stemness" of the hAMSCs was verified via immunostaining to ascertain whether the cells used in this study were indeed stem cells. Immunofluorescence results showed that P3 hAMSCs highly expressed vimentin (MSCs marker) but hardly expressed cytokeratin 19 (a typical phenotype molecule of human amniotic epithelial

LV-FGF-2-OE   LV-FGF-2-NC   Control

(a)   (b)
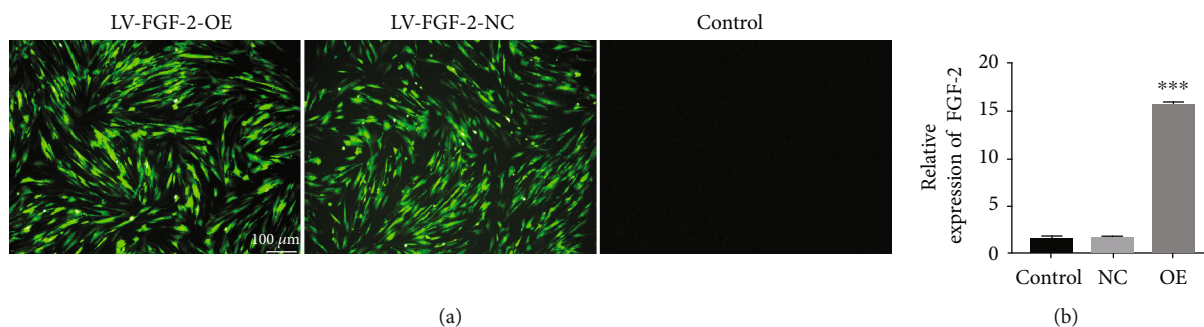
Figure 4: (a) The expression of GFP in each group with lentivirus transfection. MOI = 50. 72 h later, the expression of GFP was observed using a fluorescence microscope. Scale bar = 100 μm. (b) The relative mRNA expression of FGF-2 in each group. $^{***}P < 0.001$. Note: OE: overexpression; NC: negative control.

cells), confirming that the cells used in this experiment were hAMSCs indeed (Figure 3(b)).

3.2. Successful Transfection of the FGF-2 Gene into hAMSCs. After transfection of *FGF-2* using the optimal MOI value (MOI = 50), cellular morphology and fluorescence expression were observed under an inverted microscope and fluorescence microscope, respectively. The cellular morphology of hAMSCs infected with lentivirus did not change greatly, and insignificant fluorescence expression was observed under fluorescence microscopy after 12 h. With passing time, the expression of fluorescence increased and the strongest fluorescence was observed at 72 h (Figure 4(a)). Next, qRT-PCR was used to assess the transfection efficiency, and its results showed that the mRNA expression of *FGF-2* was statistically higher in the transfected group than in the empty virus group and the untransfected group ($P = 0.0001$). There was no significant difference between the empty virus group and the untransfected group ($P = 0.06$, Figure 4(b)).

3.3. Immunofluorescence Examination. After transfection with lentivirus containing the *FGF-2* gene, immunofluorescence test was used to detect the expression of collagen II in each group, and TB staining was further used to detect chondrogenesis. Immunofluorescence results showed that in the transfected group, collagen II was distributed around the cell nucleus while hardly expressed inside the cell nucleus. However, no fluorescent expression of collagen II was observed in the empty virus group and the untransfected group (Figure 5(a)). These results indicated that FGF-2 could promote and induce hAMSCs into cartilage differentiation. TB staining results showed that there were mass blue-dyed areas; whereas, tiny blue-dyed areas were observed in the empty virus and untransfected groups. These results suggested that FGF-2 had the potential capacity to induce hAMSCs to differentiate into chondrocytes (Figure 5(b)).

3.4. HE Staining and SEM. HE staining revealed that the epidermal layer of the fresh HAM was complete and the nucleus was clearly visible (Figure 6(a), i). However, there were no nuclei in the HAAM scaffold and the epidermal layer disappeared after the trypsin treatment (Figure 6(a), ii). Additionally, the basement membrane of the HAAM scaffold was still intact despite undergoing decellularization treat-

ment, suggesting that the HAAM scaffold maintained the ECM structure favorable for cell adherence and growth. SEM results showed that the HAAM scaffold had a network of spatial structures and there were mass ECM components and collagen components (Figures 6(b) and 6(c)).

3.5. Seeding hAMSCs and hAMSCs Transfected with FGF-2 Gene on HAAM Scaffold. One day after the hAMSCs were seeded on the HAAM scaffold, there were only a few hAMSCs on the surface of the HAAM scaffold. After continuously culturing for seven days, the hAMSCs fused into patches covering the surface of the HAAM scaffold. This suggested that the HAAM scaffold had no unfavorable influence on cell proliferation (Figure 7(a)). Similarly, hAMSCs transfected with the *FGF-2* gene showed good adhesion and growth on the HAAM scaffold, evidenced by phalloidin staining (Figure 7(b)).

3.6. Macroscopic Observation, Morphological Grading, and Imageological Examination. Three months postoperation, there were no tears or pullouts from the bone tunnels of the grafts. Poor healing of the tendon-bone interface was observed in Group 1, which was evidenced by obvious gaps between the graft and the bone. In contrast, Group 2 and Group 3 exhibited better healing with marginally narrower gaps. Group 4 displayed the best healing after operation compared with other groups, as there were barely any gaps and the color and luster of the surface were similar to those of normal tissue (Figure 8(a)). Additionally, morphological grading results of the interface showed that direct type of insertion was observed only in Group 4 and Group 4 showed the best healing compared with other groups (Table 3). X-ray examination results showed there was new bone formation observed at the TBI in all the groups. Group 4 demonstrated the highest amount of new bone formation. Additionally, the average bone tunnel area of Group 4 was significantly smaller than that of the other groups. Although, as compared to Group 1, higher new bone formation and smaller average bone tunnel area were observed in Group 2 and Group 3 (Figure 8(b)).

3.7. Histological Assessment. HE staining of Group 1 GTCs revealed many inflammatory cells in the tendon-to-bone interface and wide gaps between the grafts and the bone,

(a)

(b)
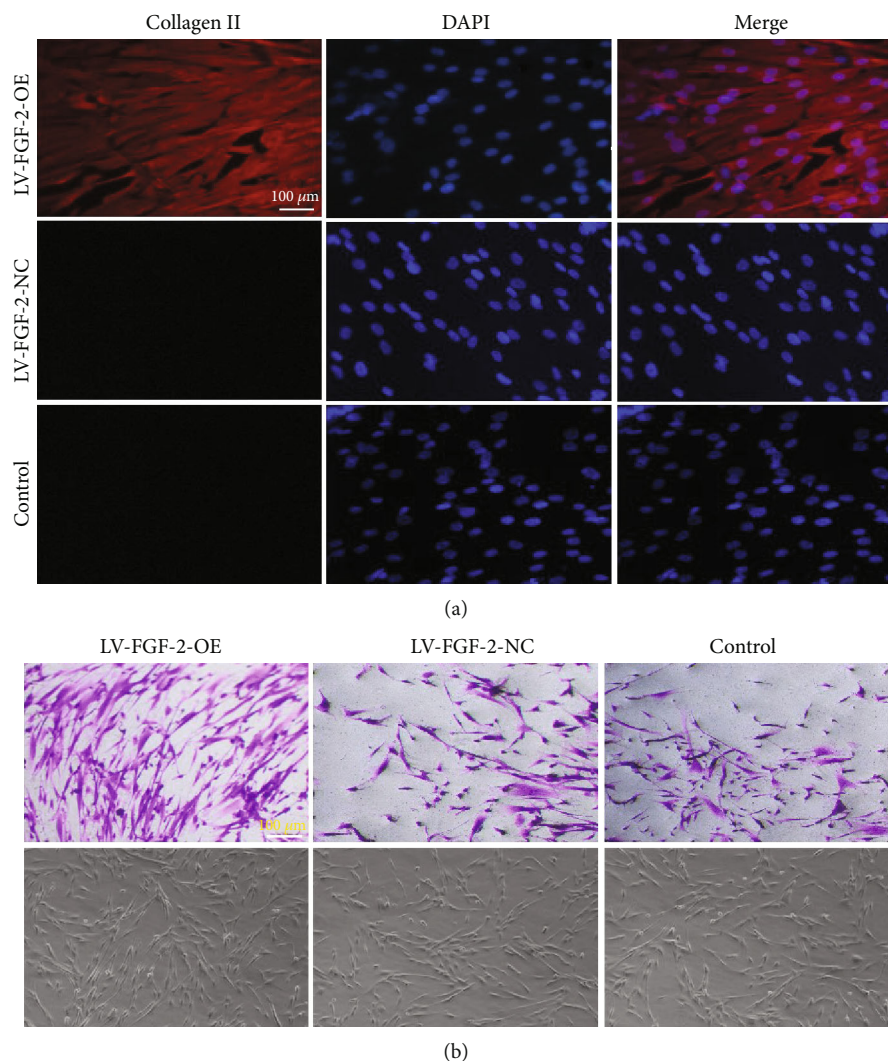
FIGURE 5: (a) Fluorescence expression of collagen II in each group; scale bar = 100 μm. (b) TB staining of each group; scale bar = 100 μm.

suggesting that the healing of the tendon-to-bone interface was poor. In contrast, Group 2 and Group 3 exhibited better healing outcomes as compared with Group 1 but lacked any fibrocartilage-like structure. Group 4 showed the best healing, which was evidenced by lack of inflammatory cells, inconspicuous gaps, and mass fibrocartilage-like structures (Figure 9(a)). Further histochemical staining was performed using TB staining. In Group 1, there were some inflammatory cells and evident gaps, consistent with the results of HE staining. Although fewer inflammatory cells and narrower gaps were found in Group 2 and Group 3, no chondrocyte-like cells were observed. In contrast, large areas were stained positively with TB in Group 4, indicating that there was fibrocartilage formation (Figure 9(b)). Safranin O/Fast Green staining was used to further detect fibrocartilage formation in the TBI. These results also showed mass fibrocartilage formation in Group 4 while no fibrocartilage formation in the other groups, evidenced by positive Safranin O/Fast Green staining results (Figure 9(c)). Masson's trichrome staining results revealed vast collagen fibers distributed in the implanted Achilles tendons of Group 4, while only few or no collagen fibers were observed in the other groups, suggesting increased collagen fiber formation in Group 4 (Figure 9(d)).

3.8. Biomechanical Analysis. Biomechanical analysis was used to investigate the mechanical properties of the grafts three months after surgery (Figure 10(a)). Group 4 showed the highest ultimate failure load. Although the ultimate failure loads of Group 2 and Group 3 were higher than those of Group 1, no statistical difference was found between the two groups (Figure 10(b)). In accordance with the ultimate failure load outcomes, the results of the stiffness test of Group 4 were significantly higher than those of other groups. Similarly, Group 2 and Group 3 showed higher stiffness than Group 1, but there was no statistically significant difference between Group 2 and Group 3 (Figure 10(c)).

4. Discussion

TBI is the key attachment site of ligaments/tendons to bones; it not only allows musculoskeletal movements but also has
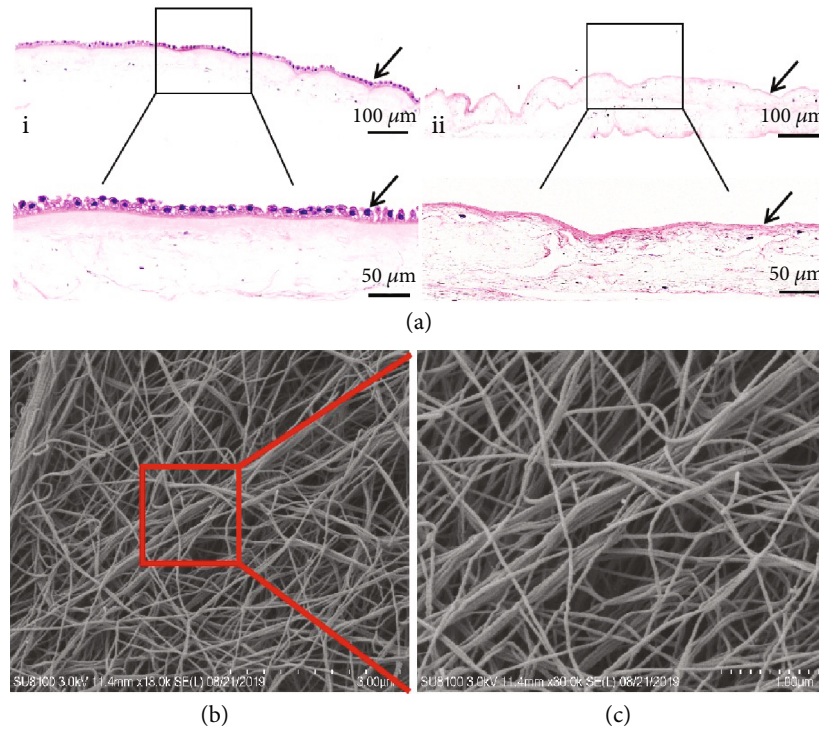
FIGURE 6: (a) Histological examination of fresh HAM (i) and HAAM scaffold (ii). Magnification of the black rectangular area is displayed at the bottom; scale bars = 100 μm and 50 μm. (b) SEM observations of the HAAM scaffold. Magnification of the red rectangular area is displayed in (c); scale bars = 3 μm and 1 μm.

the significant ability to resist high-stress contractions arising from the muscles [38]. However, it is vulnerable to injury due to trauma, overuse, and chronic inflammatory diseases. After injuries, it heals slowly, and the original structure does not restore entirely because of the specialized fibrocartilage zone, which is poor in regenerative ability [39]. Fibrocartilage is the special structure of a normal TBI which plays a crucial role in protecting the TBI from injuries by enabling a gradual transition of mechanical force from the tendon/ligament. The regenerative ability of fibrocartilage is limited owing to its relative avascularity. Although surgical treatments have been used to assist fibrocartilage formation and accelerate tendon-to-bone healing, outcomes have been dissatisfactory. Therefore, the key lies in finding ways to promote fibrocartilage formation by all means available in fundamental researches and clinical settings.

FGF-2 is a potent mitogen for various types of cells and can promote migration, proliferation, and differentiation of MSCs [40]. Owing to its significant role in various types of cell lines, it has been widely applied to restore damaged tissues by promoting cell proliferation, stimulating the release of other growth factors as well as facilitating collagen production. Some studies have found that FGF-2 promotes tendon-to-bone reparation processes, such as healing of ligaments and reconstruction of the rotator cuff, although the exact mechanism is unclear [41, 42]. Additionally, it has been reported that FGF-2 had a positive effect on chondrogenesis and promoting repair of cartilaginous injuries [43].

The HAAM scaffold is a natural biological scaffold, which has been widely used as an extracellular matrix to load cells

for the construction of engineered tissues and organs [44]. Compared with other scaffolds, the HAAM scaffold has the following advantages: extensive availability, low cost, low immunogenicity, and no ethical controversies. So far, the HAAM scaffold has been used in many fields, especially in repairing skin defects [45]. In recent years, an increasing number of studies have found that the HAAM scaffold had a positive effect on orthopedic diseases, such as promoting bone regeneration and repairing articular cartilage defects [46, 47].

In this study, we successfully isolated hAMSCs and properties of the MSCs were verified using immunofluorescence staining. The results showed that hAMSCs expressed vimentin—a marker for MSCs—greatly but hardly expressed cytokeratin 19 (a typical phenotype molecule of human amniotic epithelial cells). Although vimentin was used as the only hAMSC marker, other properties of hAMSCs were confirmed in our previous experiment [35], such as plastic adherence, specific surface antigen (Ag) expression, and multipotent ability to differentiate into osteoblasts, adipocytes, and chondrocytes. After confirming MSC properties in our P3 hAMSC culture lines, we used a lentivirus containing the human FGF-2 gene to transfect the hAMSCs wherein the transfection efficiency was determined via the expression of fluorescence and qRT-PCR. After the FGF-2 gene was successfully transfected into the hAMSCs, its effect on cartilage differentiation was detected using immunofluorescence staining of collagen II and TB staining. The results demonstrated that FGF-2 could promote the formation of chondrocytes, suggesting that FGF-2 had the potential to induce

(a)

(b)
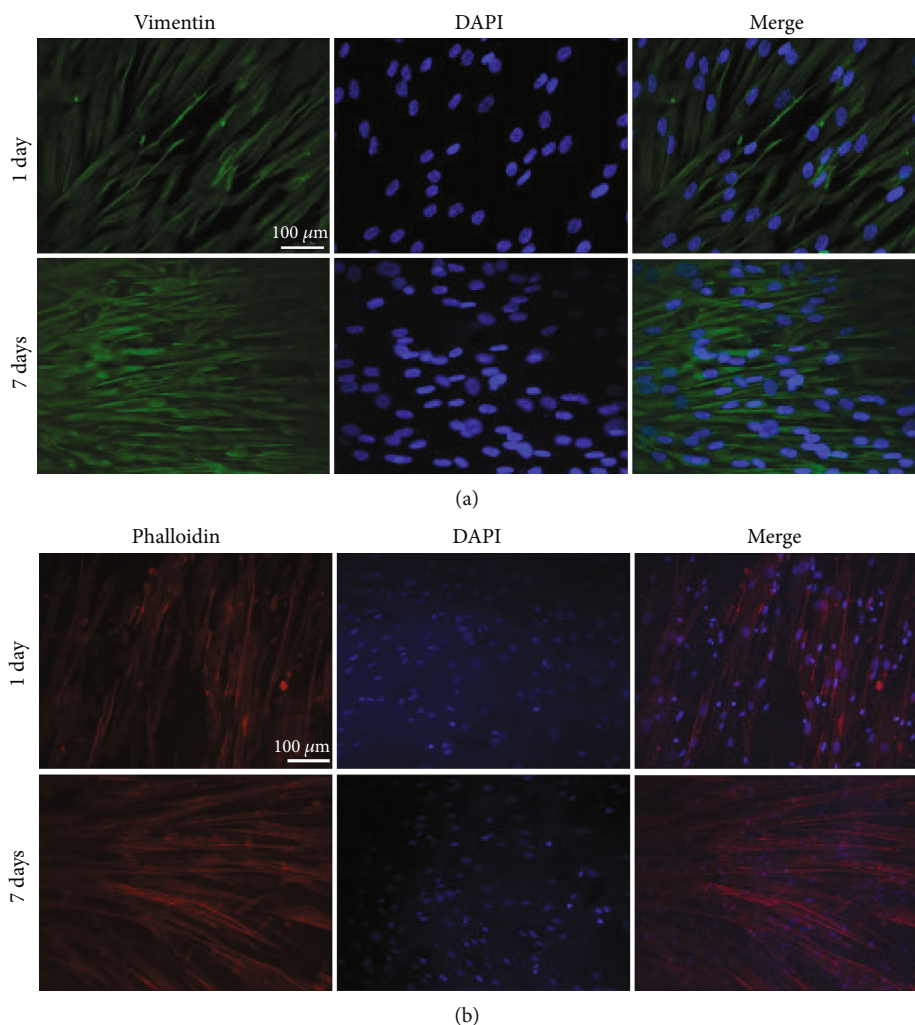
FIGURE 7: hAMSCs and hAMSCs transfected with the *FGF-2* gene cultured on HAAM scaffold. (a) Immunofluorescence examination using vimentin to observe the adhesion and growth of hAMSCs on the HAAM scaffold; scale bars = 100 μm. (b) Phalloidin staining to test the adhesion and growth of hAMSCs transfected with *FGF-2* gene on HAAM scaffold, scale bars = 100 μm.

differentiation of hAMSCs into chondrocytes. Our results are consistent with previous findings that FGF-2 could promote MSCs to differentiate into chondrocytes [48, 49].

We used a simple and inexpensive method to create an HAAM scaffold using enzymatic digestion. In comparison with other methods, this method offered many advantages, such as quicker results, simpler process, and lower cost. Although this method to prepare the HAAM scaffold has been used in other studies [47, 50], we reduced the duration taken for enzymatic digestion, improving the integrity of the extracellular matrix and reducing time and cost. HE staining was performed on fresh HAM and HAAM scaffolds in order to confirm thorough decellularization of HAM. The results showed that epithelial cells existed in the epithelial layer of fresh HAM while no such cells were found in the HAAM scaffold. Additionally, the extracellular matrix remained intact in both the fresh HAM and HAAM scaffolds. These results demonstrated that the decellularization was complete, which was in line with previous studies [44, 50]. The microstructure of the HAAM scaffold was observed

using an SEM, revealing that it was porous and suitable for the growth of cells. Next, hAMSCs and hAMSCs transfected with the *FGF-2* gene were seeded on the HAAM scaffold. The adherence and growth of cells on the HAAM scaffold were detected via immunofluorescence staining and phalloidin staining, respectively. The results suggested that hAMSCs and hAMSCs transfected with the *FGF-2* gene could survive and proliferate on the HAAM scaffold, implying that the HAAM scaffold had nontoxic properties.

For in vivo examination, we used a rabbit extra-articular model to explore the effect of the HAAM scaffold combined with hAMSCs transfected with the *FGF-2* gene on tendon-to-bone healing. Three months after surgery, the GTC specimens were harvested and examined. Histological examination showed that Group 4 exhibited better tendon-to-bone healing. We speculate that the following reasons might explain the results. First, FGF-2 transfected into the hAMSCs might have promoted fibrocartilage formation in the TBI in vivo, which could have assisted tendon-to-bone healing. We can surmise this since we had detected that FGF-2 had
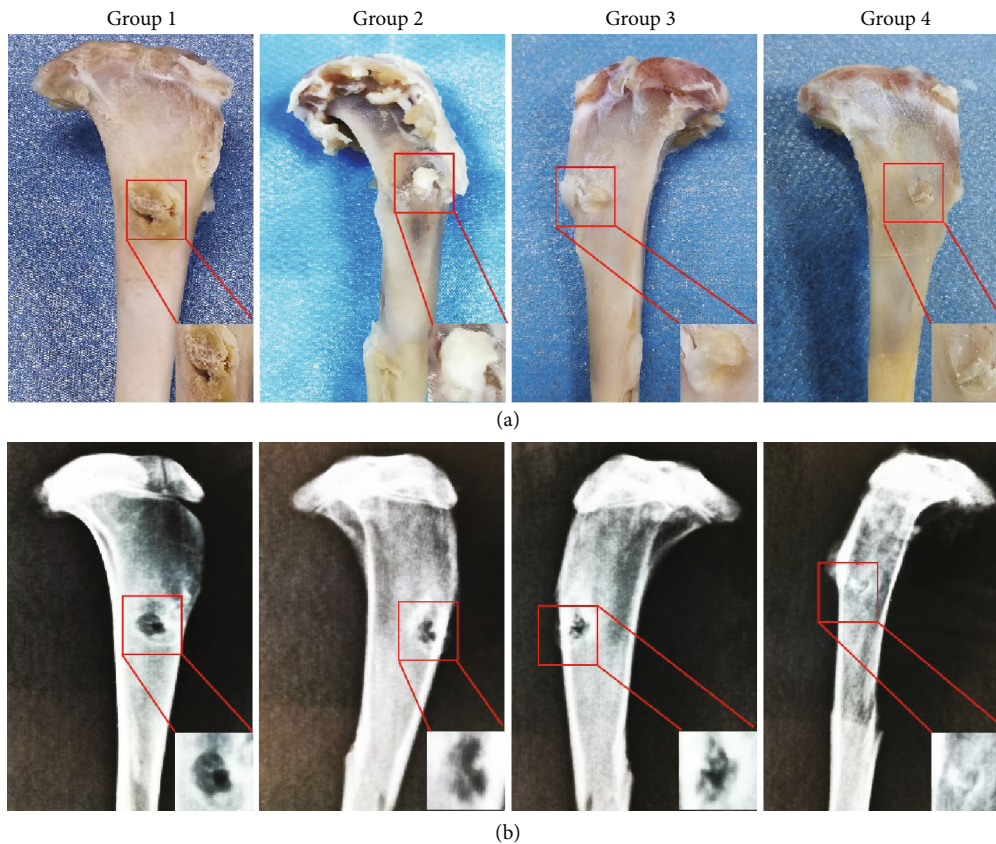
FIGURE 8: (a) Macroscopic observation of the specimens. (b) Imageological evaluation of bone tunnel in all groups at 3 months postoperation. The magnification of the red rectangular area is displayed in the bottom right corner. Note: Group 1: control; Group 2: HAAM; Group 3: HAAM+hAMSCs; Group 4: HAAM+FGF-2-induced hAMSCs.

TABLE 3: Yamakado interface morphological grade ($n = 7$).

	Group 1	Group 2	Group 3	Group 4
Direct type of insertion	0	0	0	4
Collagen fiber continuity	2	3	3	5
Interface without collagen fiber continuity	3	2	2	0
Separation between the bone and tendon	3	1	1	0

Note: Group 1: control; Group 2: HAAM; Group 3: HAAM+hAMSCs; Group 4: HAAM+FGF-2-induced hAMSCs.

the ability to promote cartilage differentiation of hAMSCs in vitro. Fibrocartilage is a critical component of TBI [51, 52]; therefore, fibrocartilage formation had a significant role in promoting tendon-to-bone healing. Second, FGF-2 might have acted as a recruiter or stimulant to activate the release of additional significant factors and consequently accelerated tendon-to-bone healing. This speculation was proven by the conclusion that FGF-2 was a vital growth factor in the healing process of injured tissues and was observed in increased quantities after ligament/tendon injuries [52]. Third, the HAAM scaffold might have the potential ability to promote tendon-to-bone healing. Some studies have found that the HAAM scaffold had a positive effect on bone regeneration and bone mineralization [46, 50]. New bone formation is the one of the most important factors of

tendon-to-bone healing. Thus, the HAAM scaffold might accelerate tendon-to-bone healing by promoting new bone formation. In practice, the greatest measure of tendon-to-bone healing is the restoration of the original mechanical strength with normal load-bearing capacity. In this study, the highest ultimate failure load and stiffness were detected in Group 4, which demonstrated enhanced mechanical strength and better tendon-to-bone healing.

This study had some limitations. First, the model used in this study was different from clinical tendon-to-bone healing cases, although this animal model had been used in many previous researches [36, 37]. Although this was a not a clinically relevant injury model and had no loading environment that played a significant role in the tendon-to-bone healing, we used this simple model to simulate tendon-to-bone
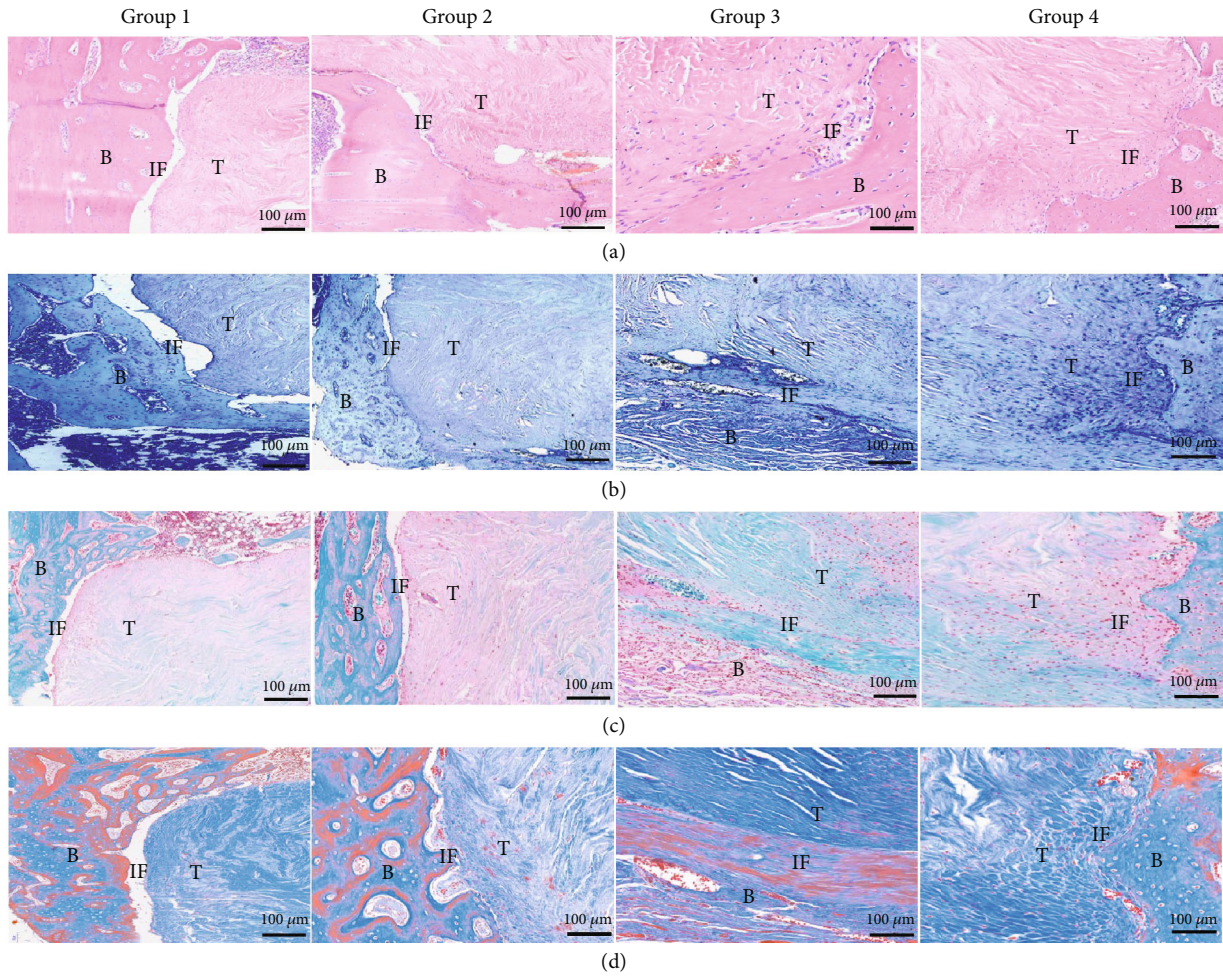
FIGURE 9: Histological evaluation of TBI in all groups at 3 months postoperation: (a) HE staining; (b) TB staining; (c) Safranin O/Fast Green staining; (d) Masson's trichrome staining. Note: Group 1: control; Group 2: HAAM; Group 3: HAAM+hAMSCs; Group 4: HAAM+FGF-2-induced hAMSCs; B: bone; T: tendon; IF: interface.
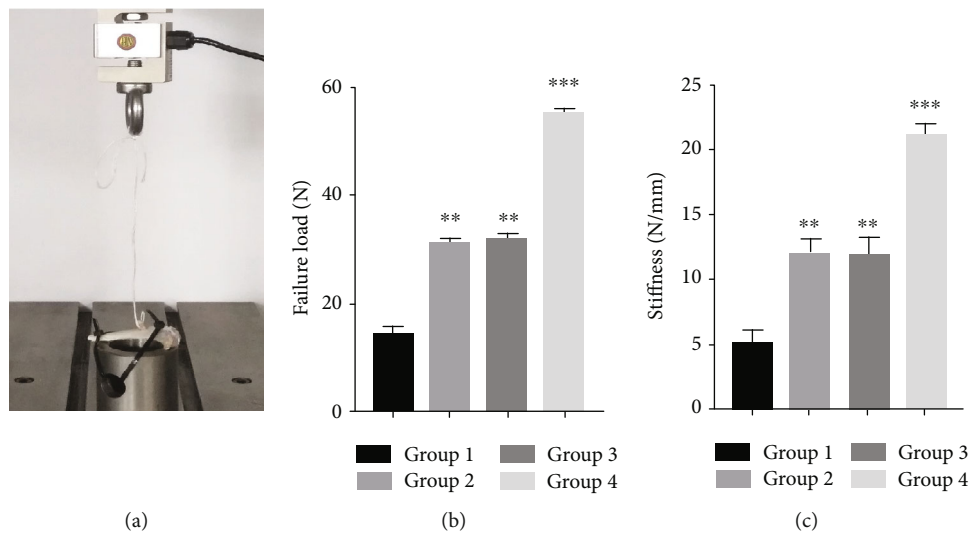
FIGURE 10: Biomechanical testing. (a) The implementation process of biomechanical testing. (b) Comparison of the ultimate failure load in each group. (c) Comparison of the stiffness in each group. Note: Group 1: control; Group 2: HAAM; Group 3: HAAM+hAMSCs; Group 4: HAAM+FGF-2-induced hAMSCs. $^{**}P < 0.01$ and $^{***}P < 0.001$.

healing and explore the effect of FGF-2-induced hAMSCs combined with the HAAM scaffold on tendon-to-bone healing. Further anterior cruciate ligament reconstruction (ACLR) and rotator cuff (RC) tear models are necessary to further investigate tendon-to-bone healing. Second, only one time interval (three months) was set to evaluate the tendon-to-bone healing in this study, although some researchers also chose only one time point to explore the tendon-to-bone healing [51, 52]. The tendon-to-bone healing is a gradual process, and hence, different time points should be chosen to explore the healing process in further studies. Third, this study was conducted exclusively on an animal model. Considerable efforts will be required to implement this approach in clinical practices. Fourth, we did not use mic-CT to quantitatively evaluate the bone tunnel and the healing status of TBI. In the future, mic-CT and other types of quantitative detection will be used to further assess tendon-to-bone healing.

Data Availability

The data used to support the findings of this study are available from the corresponding author upon request.

Disclosure

Jun Zhang and Ziming Liu are co-first authors.

Conflicts of Interest

All contributing authors declare no conflicts of interest.

Acknowledgments

References

[1] S. L. Sherman, P. N. Chalmers, A. B. Yanke et al., "Graft tensioning during knee ligament reconstruction: principles and practice," *The Journal of the American Academy of Orthopaedic Surgeons*, vol. 20, no. 10, pp. 633–645, 2012.

[2] H. H. Lu and S. Thomopoulos, "Functional attachment of soft tissues to bone: development, healing, and tissue engineering," *Annual Review of Biomedical Engineering*, vol. 15, no. 1, pp. 201–226, 2013.

[3] B. B. Rothrauff and R. S. Tuan, "Cellular therapy in bone-tendon interface regeneration," *Organogenesis*, vol. 10, no. 1, pp. 13–28, 2014.

[4] M. W. N. Wong, L. Qin, J. K. O. Tai, S. K. M. Lee, K. S. Leung, and K. M. Chan, "Engineered allogeneic chondrocyte pellet for reconstruction of fibrocartilage zone at bone-tendon junction-a preliminary histological observation," *Journal of Biomedical Materials Research*, vol. 70B, no. 2, pp. 362–367, 2004.

[5] Y. Zhou, J. Zhang, J. Yang et al., "Kartogenin with PRP promotes the formation of fibrocartilage zone in the tendon-bone interface," *Journal of Tissue Engineering and Regenerative Medicine*, vol. 11, no. 12, pp. 3445–3456, 2017.

[6] L. Smith, Y. Xia, L. M. Galatz, G. M. Genin, and S. Thomopoulos, "Tissue-engineering strategies for the tendon/ligament-to-bone insertion," *Connective Tissue Research*, vol. 53, no. 2, pp. 95–105, 2012.

[7] K. Atesok, F. H. Fu, M. R. Wolf et al., "Augmentation of tendon-to-bone healing," *The Journal of Bone and Joint Surgery*, vol. 96, no. 6, pp. 513–521, 2014.

[8] S. Liguo, Q. Ling, Z. Rui et al., "Effects of mechanical stretch on cell proliferation and matrix formation of mesenchymal stem cell and anterior cruciate ligament fibroblast," *Stem Cells International*, vol. 2016, Article ID 9842075, 10 pages, 2016.

[9] N. Rbia, L. F. Bulstra, E. A. Lewallen, S. E. R. Hovius, A. J. van Wijnen, and A. Y. Shin, "Seeding decellularized nerve allografts with adipose-derived mesenchymal stromal cells: an in vitro analysis of the gene expression and growth factors produced," *Journal of Plastic, Reconstructive & Aesthetic Surgery*, vol. 72, no. 8, pp. 1316–1325, 2019.

[10] J. A. Wood, D. J. Chung, S. A. Park et al., "Periocular and intra-articular injection of canine adipose-derived mesenchymal stem cells: an in vivo imaging and migration study," *Journal of Ocular Pharmacology and Therapeutics*, vol. 28, no. 3, pp. 307–317, 2012.

[11] X. Cui, Z. He, Z. Liang, Z. Chen, H. Wang, and J. Zhang, "Exosomes from adipose-derived mesenchymal stem cells protect the myocardium against ischemia/reperfusion injury through Wnt/β-catenin signaling pathway," *Journal of Cardiovascular Pharmacology*, vol. 70, no. 4, pp. 225–231, 2017.

[12] S. Bjelica, M. Diklić, D. Đikić et al., "Hydroxyurea-induced senescent peripheral blood mesenchymal stromal cells inhibit bystander cell proliferation of JAK2V617F-positive human erythroleukemia cells," *The FEBS Journal*, vol. 286, no. 18, pp. 3647–3663, 2019.

[13] M. Yang, H. Liu, Y. Wang et al., "Hypoxia reduces the osteogenic differentiation of peripheral blood mesenchymal stem cells by upregulating Notch-1 expression," *Connective Tissue Research*, vol. 60, no. 6, pp. 583–596, 2019.

[14] T. Kanazawa, T. Soejima, K. Noguchi et al., "Tendon-to-bone healing using autologous bone marrow-derived mesenchymal stem cells in ACL reconstruction without a tibial bone tunnel-a histological study-," *Muscle Ligaments and Tendons Journal*, vol. 04, no. 02, pp. 201–206, 2014.

[15] C. G. Williams, T. K. Kim, A. Taboas, A. Malik, P. Manson, and J. Elisseeff, "In vitro chondrogenesis of bone marrow-derived mesenchymal stem cells in a photopolymerizing hydrogel," *Tissue Engineering*, vol. 9, no. 4, pp. 679–688, 2003.

[16] Y. L. Si, Y. L. Zhao, H. J. Hao, X. B. Fu, and W. D. Han, "MSCs: biological characteristics, clinical applications and their outstanding concerns," *Ageing Research Reviews*, vol. 10, no. 1, pp. 93–103, 2011.

[17] D. García-Sánchez, D. Fernández, J. C. Rodríguez-Rey, and F. M. Pérez-Campo, "Enhancing survival, engraftment, and osteogenic potential of mesenchymal stem cells," *World Journal of Stem Cells*, vol. 11, no. 10, pp. 748–763, 2019.

[18] Y. Qiang, G. Liang, and L. Yu, "Human amniotic mesenchymal stem cells alleviate lung injury induced by ischemia and reperfusion after cardiopulmonary bypass in dogs," *Laboratory Investigation*, vol. 96, no. 5, pp. 537–546, 2016.

[19] Y. Wang, F. Jiang, Y. Liang, M. Shen, and N. Chen, "Human amnion-derived mesenchymal stem cells promote osteogenic differentiation in human bone marrow mesenchymal stem cells by influencing the ERK1/2 signaling pathway," *Stem Cells International*, vol. 2016, 12 pages, 2016.

[20] W. J. Du, Y. Chi, Z. X. Yang et al., "Heterogeneity of proangiogenic features in mesenchymal stem cells derived from bone marrow, adipose tissue, umbilical cord, and placenta," *Stem Cell Research & Therapy*, vol. 7, no. 1, p. 163, 2016.

[21] X. Zhu, L. Ziming, L. Yi et al., "Hypoxia-inducible factor 1α combined with scleraxis modified human amniotic mesenchymal stem cells to promote tibia healing in vitro," *Chinese Journal of Tissue Engineering Research*, vol. 1, pp. 113–118, 2018.

[22] M. Litwiniuk, T. Grzela, A. Ilhan, U. Yolcu, and F. C. Gundogan, "Amniotic membrane: new concepts for an old dressing," *Wound Repair and Regeneration*, vol. 23, no. 1, pp. 145–145, 2015.

[23] M. Fernandes, M. S. Sridhar, V. S. Sangwan, and G. N. Rao, "Amniotic membrane transplantation for ocular surface reconstruction," *Cornea*, vol. 24, no. 6, pp. 643–653, 2005.

[24] S. P. Wilshaw, J. N. Kearney, J. Fisher, and E. Ingham, "Production of an acellular amniotic membrane matrix for use in tissue engineering," *Tissue Engineering*, vol. 12, no. 8, pp. 2117–2129, 2006.

[25] L. Karalashvili, A. Kakabadze, G. Vyshnevska, and Z. Kakabadze, "Acellular human amniotic membrane as a three-dimensional scaffold for the treatment of mucogingival defects," *Georgian Medical News*, vol. 244-245, pp. 84–89, 2015.

[26] C. M. Zelen, R. J. Snyder, T. E. Serena, and W. W. Li, "The use of human amnion/chorion membrane in the clinical setting for lower extremity repair: a review," *Clinics in Podiatric Medicine and Surgery*, vol. 32, no. 1, pp. 135–146, 2015.

[27] R. Wang, B. Xu, and H. G. Xu, "Up-regulation of TGF-β promotes tendon-to-bone healing after anterior cruciate ligament reconstruction using bone marrow-derived mesenchymal stem cells through the TGF-β/MAPK signaling pathway in a New Zealand White rabbit model," *Cellular Physiology and Biochemistry*, vol. 41, no. 1, pp. 213–226, 2017.

[28] S. Cui and L. Jiang, "Factors associated with efficacy of first-generation epidermal growth factor receptor tyrosine kinase inhibitors in non-small-cell lung cancer," *Tumor Biology*, vol. 39, no. 5, article 101042831770534, 10 pages, 2017.

[29] X. Wan, P. Li, X. Jin, F. Su, J. Shen, and J. Yuan, "Poly(ε-caprolactone)/keratin/heparin/VEGF biocomposite mats for vascular tissue engineering," *Journal of Biomedical Materials Research Part A*, vol. 108, no. 2, pp. 292–300, 2019.

[30] X. Wang, Q. Liu, W. Chen, and L. Liu, "FGF adsorbed mesoporous bioactive glass with larger pores in enhancing bone tissue engineering," *Journal of Materials Science*, vol. 30, no. 4, pp. 1–10, 2019.

[31] C. J. Powers, S. W. Mcleskey, and A. Wellstein, "Fibroblast growth factors, their receptors and signaling," *Endocrine-Related Cancer*, vol. 7, no. 3, pp. 165–197, 2000.

[32] S. Barrientos, O. Stojadinovic, M. S. Golinko, H. Brem, and M. Tomic-Canic, "Growth factors and cytokines in wound healing," *Wound repair and regeneration : official publication of the Wound Healing Society [and] the European Tissue Repair Society*, vol. 16, no. 5, pp. 585–601, 2010.

[33] T. Tokunaga, C. Shukunami, N. Okamoto et al., "FGF-2 stimulates the growth of tenogenic progenitor cells to facilitate the generation of tenomodulin-positive tenocytes in a rat rotator cuff healing model," *The American Journal of Sports Medicine*, vol. 43, no. 10, pp. 2411–2422, 2015.

[34] C. Zhang, Q. Li, S. Deng et al., "bFGF- and CaPP-loaded fibrin clots enhance the bioactivity of the tendon-bone Interface to

augment healing," *The American Journal of Sports Medicine*, vol. 44, no. 8, pp. 1972–1982, 2016.

[35] Y. Li, Z. Liu, Y. Jin et al., "Differentiation of human amniotic mesenchymal stem cells into human anterior cruciate ligament fibroblast cells by in vitro coculture," *BioMed Research International*, vol. 2017, Article ID 7360354, 15 pages, 2017.

[36] P. Zhang, Y. Zhi, H. Fang et al., "Effects of polyvinylpyrrolidone-iodine on tendon-bone healing in a rabbit extra-articular model," *Experimental and Therapeutic Medicine*, vol. 13, no. 6, pp. 2751–2756, 2017.

[37] C. Jiangyu, W. Juan, Y. Kaiqiang et al., "Dual-layer aligned-random nanofibrous scaffolds for improving gradient microstructure of tendon-to-bone healing in a rabbit extra-articular model," *International Journal of Nanomedicine*, vol. 13, pp. 3481–3492, 2018.

[38] S. Font Tellado, E. Rosado Balmayor, and M. Van Griensven, "Strategies to engineer tendon/ligament-to-bone interface: biomaterials, cells and growth factors," *Advanced Drug Delivery Reviews*, vol. 94, pp. 126–140, 2015.

[39] J. H. Wang, Q. Guo, and B. Li, "Tendon biomechanics and mechanobiology–a minireview of basic concepts and recent advancements," *Journal of Hand Therapy*, vol. 25, no. 2, pp. 133–40; quiz 141, 2012.

[40] T. Tokunaga, Y. Hiraki, C. Shukunami et al., "Fibroblast growth factor-2 improves the tendon-to-bone healing by stimulating the growth of tenogenic progenitors in a rat rotator cuff repair model," *Journal of Orthopaedic Translation*, vol. 7, pp. 125–128, 2016.

[41] B. Chen, B. Li, Y. J. Qi et al., "Enhancement of tendon-to-bone healing after anterior cruciate ligament reconstruction using bone marrow-derived mesenchymal stem cells genetically modified with bFGF/BMP2," *Scientific Reports*, vol. 6, no. 1, pp. 1–9, 2016.

[42] S. S. Buchmann, G. H. G. Sandmann, L. L. Walz et al., "Refixation of the supraspinatus tendon in a rat model–influence of continuous growth factor application on tendon structure," *Journal of Orthopaedic Research*, vol. 31, no. 2, pp. 300–305, 2013.

[43] J. Frisch, J. K. Venkatesan, A. Rey-Rico et al., "Effects of rAAV-mediated FGF-2 gene transfer and overexpression upon the chondrogenic differentiation processes in human bone marrow aspirates," *Journal of Experimental Orthopaedics*, vol. 3, no. 1, pp. 1–6, 2016.

[44] M. Wu, J. Xiong, S. Shao et al., "Hair follicle morphogenesis in the treatment of mouse full-thickness skin defects using composite human acellular amniotic membrane and adipose derived mesenchymal stem cells," *Stem Cells International*, vol. 2016, Article ID 8281235, 7 pages, 2016.

[45] S. L. Xue, K. Liu, O. Parolini, Y. Wang, L. Deng, and Y.-C. Huang, "Human acellular amniotic membrane implantation for lower third nasal reconstruction: a promising therapy to promote wound healing," *Burns & Trauma*, vol. 6, no. 1, pp. 1–8, 2018.

[46] K. Tang, J. Wu, Z. Xiong, Y. Ji, T. Sun, and X. Guo, "Human acellular amniotic membrane: a potential osteoinductive biomaterial for bone regeneration," *Journal of Biomaterials Applications*, vol. 32, no. 6, pp. 754–764, 2017.

[47] P.-F. Liu, L. Guo, D.-W. Zhao et al., "Study of human acellular amniotic membrane loading bone marrow mesenchymal stem cells in repair of articular cartilage defect in rabbits," *Genetics and Molecular Research*, vol. 13, no. 3, pp. 7992–8001, 2014.

[48] S. Tsutsumi, A. Shimazu, K. Miyazaki et al., "Retention of multilineage differentiation potential of mesenchymal cells during proliferation in response to FGF," *Biochemical and Biophysical Research Communications*, vol. 288, no. 2, pp. 413–419, 2001.

[49] L. A. Solchaga, K. Penick, V. M. Goldberg, A. I. Caplan, and J. F. Welter, "Fibroblast growth factor-2 enhances proliferation and delays loss of chondrogenic potential in human adult bone-marrow-derived mesenchymal stem cells," *Tissue Engineering Part A*, vol. 16, no. 3, pp. 1009–1019, 2010.

[50] Y. J. Chen, M. C. Chung, C. C. J. Yao et al., "The effects of acellular amniotic membrane matrix on osteogenic differentiation and ERK1/2 signaling in human dental apical papilla cells," *Biomaterials*, vol. 33, no. 2, pp. 455–463, 2012.

[51] Y. Zhang, J. Yu, J. Zhang, and Y. Hua, "Simvastatin with PRP promotes chondrogenesis of bone marrow stem cells in vitro and wounded rat Achilles tendon–bone interface healing in vivo," *American Journal of Sports Medicine*, vol. 47, no. 3, pp. 729–739, 2019.

[52] J. Zhang, T. Yuan, N. Zheng, Y. Zhou, M. V. Hogan, and J. H. Wang, "The combined use of kartogenin and platelet-rich plasma promotes fibrocartilage formation in the wounded rat Achilles tendon entheses," *Bone & Joint Research*, vol. 6, no. 4, pp. 231–244, 2017.

Review Article

Bone Marrow-Derived Cell Therapies to Heal Long-Bone Nonunions: A Systematic Review and Meta-Analysis—Which Is the Best Available Treatment?

Silvia Palombella,[1] Silvia Lopa [iD],[1] Silvia Gianola,[2] Luigi Zagra,[3] Matteo Moretti [iD],[1,4] and Arianna B. Lovati [iD][1]

[1]Cell and Tissue Engineering Laboratory, IRCCS Istituto Ortopedico Galeazzi, Milan 20161, Italy
[2]Unit of Clinical Epidemiology, IRCCS Istituto Ortopedico Galeazzi, Milan 20161, Italy
[3]Hip Department, IRCCS Istituto Ortopedico Galeazzi, Milan 20161, Italy
[4]Regenerative Medicine Technologies Lab, Ente Ospedaliero Cantonale, Lugano 6900, Switzerland

Correspondence should be addressed to Silvia Lopa; silvia.lopa@grupposandonato.it

Nonunions represent one of the major indications for clinical settings with stem cell-based therapies. The objective of this research was to systematically assess the current evidence for the efficacy of bone marrow-derived cell-based approaches associated or not with bone scaffolds for the treatment of nonunions. We searched MEDLINE (PubMed) and CENTRAL up to July 2019 for clinical studies focused on the use of cell-based therapies and bone marrow derivatives to treat bone nonunions. Three investigators independently extracted the data and appraised the risk of bias. We analysed 27 studies including a total number of 347 participants exposed to four interventions: bone marrow concentrate (BMAC), BMAC combined with scaffold (BMAC/Scaffold), bone marrow-derived mesenchymal stromal cells (BMSCs), and BMSC combined with scaffold (BMSC/Scaffold). Two controlled studies showed a positive trend in bone healing in favour of BMAC/Scaffold or BMSC/Scaffold treatment against bone autograft, although the difference was not statistically significant (RR 0.11, 95% CI -0.05; 0.28). Among single cohort studies, the highest mean pooled proportion of healing rate was reported for BMAC (77%; 95% CI 63%-89%; 107 cases, $n = 8$) and BMAC/Scaffold treatments with (71%; 95% CI 50%-89%; 117 cases, $n = 8$) at 6 months of follow-up. At 12 months of follow-up, an increasing proportion of bone healing was observed in all the treatment groups, ranging from 81% to 100%. These results indicate that BMAC or BMAC/Scaffold might be considered as the primary choice to treat nonunions with a successful healing rate at a midterm follow-up. Moreover, this meta-analysis highlighted that the presence of a scaffold positively influences the healing rate at a long-term follow-up. More case-control studies are still needed to support the clinical improvement of cell-based therapies against autografts, up to now considered as the gold standard for the treatment of nonunions.

1. Introduction

Nonunions and delayed unions are a frequent occurrence in fracture healing, with an incidence of 5-10% over the total amount of fractures only in the US [1]. Per definition, if a fracture does not heal within 4 months, it can be considered as a delayed union. Fractures of long bones—mainly the femur, tibia, and humerus—are defined as nonunions after 6 months postinjury in the absence of any radiographic progression persisting for at least 3 months [2, 3]. The poor healing of bone fractures is due to multiple factors, including patient-independent factors specifically related to the fracture site, severity of the injury (large gap), impaired vascularization, surgical osteosynthesis, infections, fracture stability,

and biomechanics, and patient-dependent factors, such as age, nutrition, drug therapies, and comorbidities or congenital bone disorders [4, 5]. The diagnosis of nonunions is based mainly on clinical evaluation and radiographic imaging. The physical examination assesses the mobilization of the fracture site, deformity, interpolation of soft tissues, and signs of infection [6, 7]. X-rays are used to determine the progress of fracture healing (i.e., persistent fracture lines, absence of bony bridging, and sclerotic tissue) and the presence or absence of deformity [6]. Radiologically, nonunions can be distinguished as hypertrophic and atrophic. Hypertrophic nonunions are characterized by a large, broad callus towards the fracture gap, with a radiolucent area instead of bone bridging. On the other hand, in most cases, atrophic nonunions are the expression of an impaired biological support to bone healing, which may depend on a damaged vascular supply, and on the destruction of the periosteum and endosteum. Subsequently, the healing process is impaired due to the lack of important biological mediators and/or appropriate blood supply. Mechanical reasons can also be involved. For instance, excessively rigid fixation, insufficient compressive forces, and a wide fracture gap that does not allow bony bridging are major determinants in the development of atrophic nonunions. In radiological images, atrophic nonunions show the absence of callus tissue, the narrowing of bone ends, and a large radiolucent zone in the fracture gap [3]. For all these reasons, atrophic nonunions represent the most challenging occurrence. In fact, atrophic nonunions always require a surgical approach to reduce abnormal mechanical factors and repair the fracture gap by means of bone grafting, which represents the therapeutic gold standard [8].

Since both autograft and allograft have intrinsic limitations, such as the volume of collectable autologous bone and patient morbidity, or immunogenic rejection and risk of disease transmission, respectively, the use of orthobiologics is on the rise in translational medicine for bone repair [8]. Indeed, orthobiologics for bone healing implement the "diamond concept" combining osteoconduction, osteoinduction, and osteogenesis and, hence, appear as a promising strategy to treat nonhealing fractures, in particular atrophic nonunions [9]. Among orthobiologic approaches for bone healing, cell-based therapies, and bone marrow derivatives combined or not with bone grafts and biomaterials have been widely investigated in the recent years [10].

In orthopaedics, iliac crest aspiration is a standard procedure associated with limited morbidity for the harvesting of bone marrow, the most used source of adult mesenchymal stromal cells. Bone marrow can be used either directly as bone marrow aspirate concentrate (BMAC) or as bone marrow-derived mesenchymal stromal cells (BMSCs) after in vitro processing. Advantages of BMAC are the intraoperative preparation using CE-marked kits and centrifuges and compliance with a one-step surgery with limited costs [3]. Despite these benefits, BMAC accounts only for a small population of progenitor cells (0.001% to 0.01%), as compared to expanded BMSCs that are a pure cell population with well-defined features. However, in the clinical setting, the translatability of BMSC is still limited by some drawbacks, such as the need to use GMP-compliant growth factors and reagents and the extensive timeframe required for in vitro expansion in specialized facilities, which imply higher operational complexity and superior costs compared to BMAC.

This systematic review focuses on clinical studies regarding the use of bone marrow derivatives to treat nonunions. Specifically, we aimed to assess the efficacy of cell-based therapies with respect to bone autograft. In addition, we analysed the proportion of the healing rate at 6 and 12 months after treatment with BMAC or BMSC alone or combined with scaffolds. The aim of this meta-analysis is to increase the knowledge in the options available to promote bone healing and represent a tool for clinicians who plan to use cell-based strategies to improve the clinical outcomes of patients with nonunions.

2. Materials and Methods

2.1. Search Strategy. The literature search was focused on the clinical use of bone marrow-derived cell therapies to treat bone nonunions. The literature search was carried out consulting MEDLINE (PubMed) and Cochrane Central Register of Controlled Trials-CENTRAL databases, analysing articles published in English up to July 2019. We also checked the reference lists of all the systematic reviews and included studies identified during the search process. The full search strategy is reported in Appendix S1 in the Supplementary Materials.

2.2. Eligibility Criteria for Meta-Analysis. Inclusion criteria were defined for this meta-analysis. Specifically, we included observational studies such as case reports/studies and prospective and retrospective clinical studies with or without a control group (bone autograft). From these studies, we extrapolated the data relative to patients with long-bone nonunions treated with BMAC or BMSC alone or combined with scaffolds, having more than 18 years and no relevant comorbidities (i.e., congenital bone disorders, tumours, diabetes, and bone infections). Data relative to patients satisfying the inclusion criteria and presenting infected nonunions that were successfully treated before applying the cell-based therapy were included in this meta-analysis.

2.3. Study Selection. Three investigators (SL, SP, and ABL) independently reviewed the literature and classified the references based on the title and abstract. The eligible articles were further screened through the available full text, and the studies matching the inclusion criteria were selected. When a duplicate of published data was retrieved, we only considered the dataset reporting the complete dataset. Any disagreement was solved by discussion. In case a clinical study included both patients satisfying the eligibility criteria and patients that did not satisfy one or more inclusion criteria, the outcome data relative to the latter were excluded from the analysis. Studies reporting outcome data regarding eligible and noneligible patients with aggregated results were completely excluded. For instance, studies including patients with delayed unions and patients with bone nonunions that did not report the healing rate/time for each specific patient were

excluded, since it was not possible to determine the healing rate only for patients with bone nonunions.

2.4. *Data Extraction.* Data extraction was performed by three investigators. Any disagreement was solved by discussion. The following data were extracted: type of treatment, number of included patients, age of patients, site and type of fracture, type and duration of bone nonunion, frequency of radiographic follow-up, healing rate at 6 and 12 months, failure rate at the last follow-up (i.e., variable time point depending on the study design) and reason, type of study, quality assessment, and reference. Treatments were classified into four categories: BMAC, BMAC combined with scaffold (BMAC/Scaffold), BMSC, and BMSC combined with scaffold (BMSC/Scaffold). Outcome data of different treatments included in the same article were individually considered and analysed according to the corresponding treatment category. The same approach was applied for studies reporting data from eligible and noneligible patients. For instance, in case a study that included data relative to patients with and without comorbidities, only the data relative to the latter were included in the meta-analysis.

2.5. *Outcome(s)*

(1) The primary outcome was the bone healing rate investigating cell-based therapies (BMAC/Scaffold, BMSC/Scaffold) versus bone autograft as well as assessing the bone healing rate associated with four different types of cell-based therapies (BMAC, BMAC/Scaffold, BMSC, and BMSC/Scaffold) over a follow-up of 6 and 12 months

(2) The secondary outcome was the correlation between the type and site of nonunion and the efficacy of the aforementioned treatments

2.6. *Quality Assessment.* As a measure of study quality, we selected and evaluated the following biases: (1) retrospective or prospective analysis and source of data (record bias), (2) relevance and definition of nonunion (i.e., lack of data regarding the duration, type, and site of nonunion) (reporting bias), (3) presence in the study of relevant confounding variables that could affect the clinical outcome (i.e., different types of nonunion, different sites of nonunion, different types of fixation, and different number of treatments) (relevant confounding factors bias), and (4) any missing outcome data (outcome reporting bias). Three investigators performed the quality assessment. Disagreements were resolved by consensus.

2.7. *Statistical Analysis.* For controlled studies, we evaluated the treatment effects based on the healing rate at 6 and 12 months as dichotomized outcomes, using the Risk Difference (RD) expressed as 95% confidence intervals (95% CIs). The outcome measures reported in the individual studies were combined by meta-analysis using random effect models, as described by DerSimonian and Laird [11], because a certain degree of heterogeneity of population and treatments would be expected among interventions.

Since the majority of the identified studies did not include any control group, we used the proportional meta-analysis to indirectly compare the different treatments along their CIs. The Effect Size (ES) represented the percentage of healing rate at 6 and 12 months with respect to the total number of patients included in each study per treatment group (BMAC, BMAC/Scaffold, BMSC, and BMSC/Scaffold). The forest plot presents specific proportions with 95% exact CIs for each study, the subgroup and overall pooled estimate with 95% Wald CIs, and the I^2 statistic, which describes the percentage of total variation due to interstudy heterogeneity.

Statistical heterogeneity was assessed using the I^2 statistic and assumed to be influential when the I^2 was greater than 50% and $p < 0.05$ as statistically significant for the calculation of heterogeneity.

All the analyses were done with RevMan 5.3 [12] and STATA software version 15 using the metaprop command [13] as an adaptation of the metan programme developed by Harris et al. [14].

3. Results

3.1. *Study Selection.* Based on the literature search strategy, 340 studies were found (307 in PubMed and 33 in Cochrane). Among them, 15 articles were excluded because they were doubly reported in the literature search. Of the remaining 325 records, 33 records were excluded because they were non-English articles. Other articles were also excluded for different reasons: 4 not available full text, 41 review articles, 1 overlapping study, and 191 articles not satisfying the inclusion criteria. Of the remaining 55 articles, after reading the full text, 29 were excluded for the following reasons: 10 papers describing a preventive therapy in the case of bone fracture, 12 not pertinent with the field of study, and 7 because only a part of patients satisfied all the inclusion criteria and it was not possible to extrapolate the healing rate of single patients. One study was retrieved from the bibliography of a review article. Overall, we finally included 27 studies meeting our eligibility criteria for the subsequent meta-analysis (Figure 1).

3.2. *Features of the Studies and Quality Assessment.* The studies included in the meta-analysis are reported in Table 1. About 70% of the analysed articles (19/27) concerned BMAC-based treatments; the remaining articles (8/27) investigated the efficacy of BMSC-based therapies. About half of the studies (13/27) combined BMAC or BMSC with a scaffold. Bone-derived (i.e., decellularized bone and bone chips) and ceramic scaffolds were the most used types of scaffolds. In total, the analysed studies included 347 patients treated for bone nonunions. Considering the different interventions, 163 patients were treated with BMAC, 153 with BMAC/Scaffold, 22 with BMSC, and 9 with BMSC/Scaffold. Patients' age ranged between 18 and 92 years. Almost half of the treated nonunions concerned the treatment of the tibia/fibula (52.9%), followed by the femur (32.3%), humerus/ulna (11.1%), and radius (3.7%). Only one study, including 50 patients, omitted to specify the number of treated femoral or tibial nonunions. For this reason, this study was not
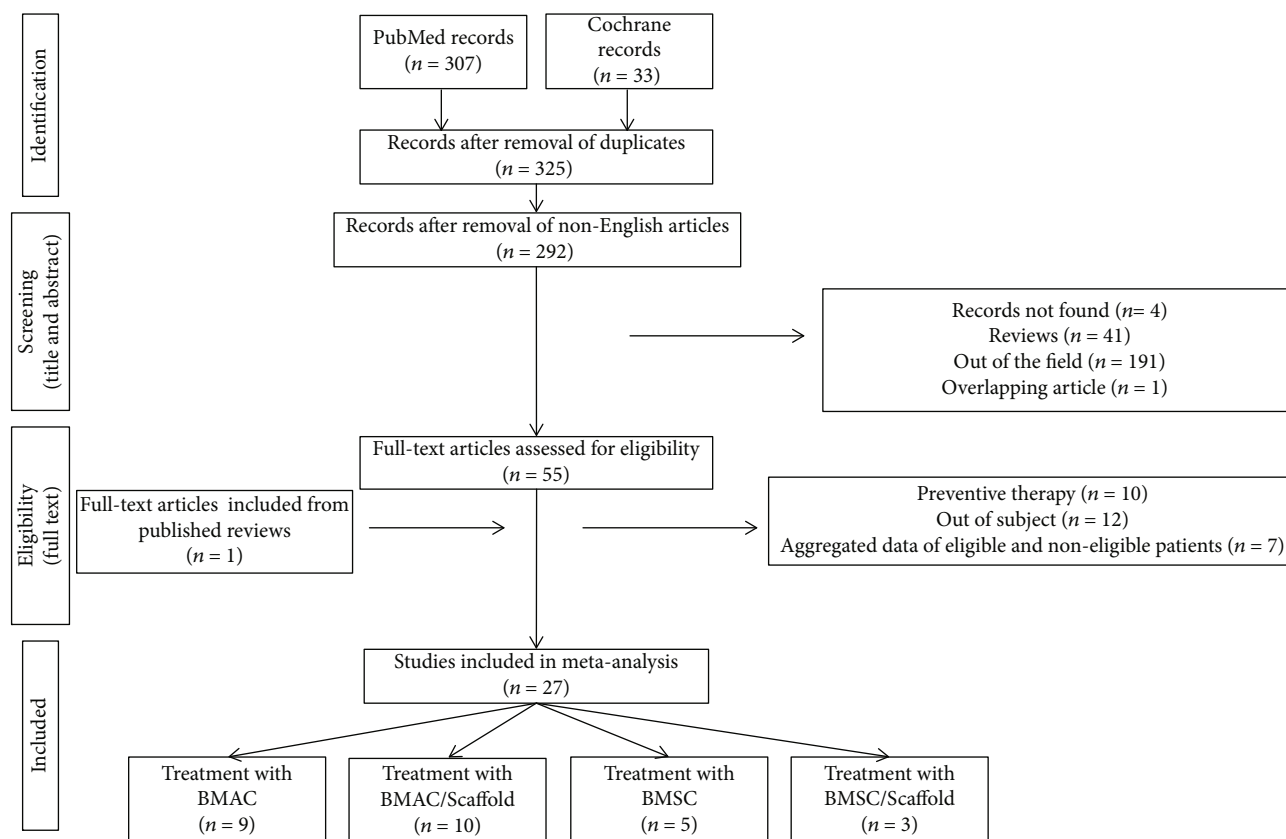
Figure 1: Flow diagram of the study selection process.

included in the calculation of the above described percentages. The type of fracture was described in 16 out of 27 studies (59.3%), with 76.6% of patients treated for closed fractures. Among the studies describing the treatment of open fractures, 3 reported the AO-OTA classification and the remaining reported the Gustilo and Anderson classification. None of the studies reported the defect size. The type of treated nonunion, i.e., atrophic or hypertrophic, was indicated in 14 articles (51.9%) and showed that most of the patients were treated for an atrophic nonunion (86.3%). The duration of nonunion ranged between 6 months and 9 years. Timing and frequency of radiographic follow-ups were very variable among studies. In 4 out of 27 studies, the latest follow-up was 6 months after treatment. Healing rate at 6 and 12 months was reported in 21 and 18 studies, respectively. Among the 15 articles reporting treatment failures at the last analysed follow-up (55.6%), only 6 provided a possible explanation, such as alcoholism, improper osteosynthesis, or bone loss. Adverse events were evaluated in most of the articles, but no side effects directly linked to the delivery of BMAC or BMSC were reported, suggesting that these treatments can be considered safe also in elders. Almost half of the studies were prospective (14/27). The remaining articles included 9 retrospective studies, 3 case studies, and 1 case report. Only 2 studies were controlled and included bone autograft as the control group. However, none of these studies was randomized.

The recorded bias was considered positive for retrospective and case studies/reports. Almost half of the articles presented this bias (15/27). This bias was attributed also to 2 prospective studies since it appeared that they gathered together a series of patients rather than pursuing a systematic and rational patient enrolment. We defined the reporting bias as an omission of relevant information regarding the characteristics of the treated nonunion, such as the type and the site of nonunion. This bias was attributed to 14 out of 27 articles (51.9%). Considering the high variability in the duration of nonunion, even within the same study, and other influencing factors, such as the type and site of nonunion and the type of fixation, almost all the studies were classified as biased by relevant confounding factors. Among the analysed studies, 2 out of 27 (7.4%) did not report the healing rate at the time points defined in the "materials and methods" of the study. Hence, these were classified as affected by outcome reporting bias. The frequency of the radiographic follow-up was not clearly defined in 11 articles (40.7%). Due to the lack of a clear follow-up plan, it was not possible to define if these records were biased or not by outcome reporting.

3.3. Bone Healing Rate at 6 Months of Follow-Up. Two controlled studies investigating cell-based therapies (BMAC/Scaffold or BMSC/Scaffold interventions) did not show any significant difference in bone healing rate versus the control intervention (bone autograft) (2 studies, 100 patients, RD 0.11 95% CI -0.05 to 0.28, $I^2 = 0\%$; $p = 0.18$, Figure 2).

Looking at the cohort studies lacking the control group, 5 studies did not report the outcome data as planned in their

TABLE 1: Studies selected based on inclusion and exclusion criteria. Fracture grading is reporting based either on Gustilo and Anderson (G) or on AO-OTA (OTA) classification scale.

Treatment	n subjects / Age range (years)	Site of fracture	Type of fracture	Type of nonunion	Duration of nonunion	Frequency of radiographic follow-up	Healing rate at 6 months (healed/total)	Healing rate at 12 months (healed/total)	Failure rate at last follow-up / Failure reason(s)	Type of study	Record bias	Reporting bias	Relevant confounding factor bias	Outcome reporting bias	Ref.
BMAC	10 subjects 18-82	10 tibias	1 closed 6 GII 3 GIII	n.d.	7-36 months	n.d.	7/10	9/10	10% n.d.	Prospective	No	Yes	Yes	—	[15]
BMAC	20 subjects 18-65	15 tibias 3 humeri 2 ulnae	10 closed 6 GI 2 GII 2 GIII	n.d.	6-18 months	Monthly	15/20	17/20	15% Fractures with bone loss and ulnar fracture	Prospective	No	Yes	Yes	No	[16]
BMAC	1 subject 44	1 tibia	1 GIII	n.d.	6 months	Every 6 weeks (until 6 months)	1/1	n.d.	0%	Case study	Yes	Yes	No	No	[17]
BMAC	19 subjects 24-60	19 tibias	n.d.	9 atrophic 10 hypertrophic	6-36 months	Every 4-6 weeks (until 6 months)	15/19	n.d.	21% n.d.	Prospective	No	No	Yes	No	[18]
BMAC	17 subjects 25-66	5 femurs 10 tibias 2 ulnae	17 closed	n.d.	6-24 months	Monthly (until 6 months)	16/17	n.d.	6% Improper osteosynthesis	Prospective	No	Yes	Yes	No	[19]
BMAC	7 subjects 25-66	2 femurs 2 humeri 5 ulnae	7 closed	7 atrophic	7-53 months	n.d. (until 6 months)	6/7	n.d.	10% Alcoholism	Retrospective	Yes	No	Yes	—	[20]
BMAC	16 subjects 19-59	16 femurs	12 closed 3 GI 1 GII	7 atrophic 9 oligotrophic	9-97 months	1.5, 4, 6, and 12 months	7/16	8/16	10% Alcoholism	Prospective	No	No	Yes	No	[21]
BMAC	17 subjects 22-80	10 femurs 5 tibias 1 ulna 1 humerus	12 closed 5 open	17 atrophic	9-79 months	1, 2, 3, 6, 9, and 12 months	11/17	13/17	23.5% n.d.	Retrospective	Yes	No	Yes	No	[22]
BMAC	54 subjects 22-64	54 tibias	54 closed	n.d.	n.d.	n.d.	n.d.	49/54	9.25% n.d.	Retrospective	Yes	Yes	Yes	—	[23]
BMAC/Scaffold (porous ceramic mixed with collagen)	3 subjects 26-60	1 femur 1 tibia 1 ulna	n.d.	n.d.	7-12 months	1.5, 3, 6, and 12 months	1/3	2/3.	0%	Prospective	Yes	Yes	Yes	Yes	[24]
BMAC/Scaffold (DBM)	15 subjects 22-87	3 femurs 10 tibias 2 humeri	n.d.	n.d.	n.d.	n.d.	n.d.	n.d.	40% n.d.	Prospective	Yes	Yes	Yes	—	[25]
BMAC/Scaffold (allogeneic bone graft)	12 subjects 19-68	12 tibias	2 closed 1 GI 3 GII 6 GIII	n.d.	>6 months	n.d.	10/12	11/12	8.33% n.d.	Prospective	No	Yes	Yes	—	[26]
BMAC/Scaffold (frozen cancellous bone)	2 subjects 22 and 38	2 humeri	n.d.	n.d.	>6 months	n.d.	1/2	2/2	0%	Retrospective	Yes	Yes	Yes	—	[27]
BMAC/Scaffold (cancellous bone)	7 subjects 26-70	3 femurs 3 tibias 1 ulna	n.d.	n.d.	>6 months	Monthly up to 12 months Yearly afterwards	5/7	7/7	0%	Prospective	No	Yes	Yes	—	[28]
BMAC/Scaffold (autologous bone chips)	14 subjects 33-92	14 femurs	9 OTA32-A2-1 3 OTA32-B3-1 2 OTA31-A2-3	14 atrophic	16-48 months	1.5, 3, 4, 5, 6, 8, 12, and 18 months or until union	7/14	14/14	0%	Retrospective	Yes	No	Yes	No	[29]

TABLE 1: Continued.

Treatment	n subjects / Age range (years)	Site of fracture	Type of fracture	Type of nonunion	Duration of nonunion	Frequency of radiographic follow-up	Healing rate at 6 months (healed/total)	Healing rate at 12 months (healed/total)	Failure rate at last follow-up / Failure reason(s)	Type of study	Record bias	Reporting bias	Relevant confounding factor bias	Outcome reporting bias	Ref.
BMAC/Scaffold (DBM)	19 subjects 20-73	1 femur 8 tibias 3 humeri 3 radii 2 ulnae 2 metatarsi	n.d.	19 atrophic	>9 months	n.d.	n.d.	n.d.	21% n.d.	Prospective	No	No	Yes	—	[30]
BMAC/Scaffold (autologous bone chips+PRP)	50 subjects 18-76.7	n.d. femur n.d. tibia	n.d.	39 atrophic 11 hypertrophic	>6-9 months	1.5, 3,6, 12, and 24 months	23/50	42/50	4.88% Bone loss and failure of fixation device	Retrospective Controlled	Yes	Yes	Yes	No	[31]
BMAC/Scaffold (allogeneic cancellous bone)	18 subjects 19-81	18 femurs	17 closed 1 GIII	n.d.	6 months	Monthly	15/18	15/18	16.7% Impaired bone vascularity	Prospective	No	Yes	Yes	No	[32]
BMAC/Scaffold (DBM)	11 subjects 55-79	11 femurs	n.d.	n.d.	>6 months	0.5, 1.5, 3, 6, 9, and 12 months	11/11	11/11	0%	Retrospective	Yes	Yes	Yes	No	[33]
BMSC	6 subjects 18-73	3 humeri 1 ulna 1 radius 1 ulna and radius	1 OTA12-A1 1 OTA12-B3 1 OTA12-C1 1 OTA22-A1 1 OTA22-A2 1 OTA22-C3	6 atrophic	n.d.	n.d.	6/6	6/6	0%	Retrospective	Yes	No	Yes	—	[34]
BMSC	3 subjects 19-44	1 femur 1 humerus 1 forearm	n.d.	n.d.	19-39 months	3, 6, and 12 months	n.d.	3/3	0%	Retrospective	Yes	Yes	Yes	Yes	[35]
BMSC	1 subject 47	1 ulna	1 OTA22-A1-1	1 atrophic	6 months	n.d.	0/1	1/1	0%	Case study	Yes	No	No	—	[36]
BMSC	7 subjects 26-61	4 femurs 3 tibias	3 closed 4 open	7 atrophic	8-96 months	1, 3, 6, and 12 months	3/7	4/7	42.8% n.d.	Prospective	No	No	Yes	No	[37]
BMSC	5 subjects 23-55	3 femurs 2 tibias	5 closed	5 atrophic	7-72 months	1, 3, 6, and 12 months	2/5	3/5	40% n.d.	Prospective	No	No	Yes	No	[38]
BMSC/Scaffold (CaSO₄ pellets)	1 subject 34	1 tibia	1 closed	1 hypertrophic	9 years	n.d.	1/1	1/1	0%	Case study	Yes	No	No	—	[39]
BMSC/Scaffold (collagen microspheres)	3 subjects 27-81	1 femur 2 tibias	n.d.	3 atrophic	12-24 months	n.d.	n.d.	3/3	0%	Case reports	Yes	No	Yes	—	[40]
BMSC/Scaffold (HA granules)	5 subjects 18-37	3 femurs 1 tibia 1 humerus	n.d.	5 atrophic	37.2 months	Monthly up to 12 months	0/5	5/5	0%	Prospective Controlled	No	No	Yes	No	[41]

n.d.: nondescribed.

Study or subgroup	BMAC/BMSC scaffold		Bone autograft		Weight	Risk difference IV, random, 95% CI	Risk difference IV, Random, 95% CI
	Events	Total	Events	Total			
Dallari, 2016	23	50	12	40	71.4%	0.16 [−0.04, 0.36]	
Ismail, 2016	0	5	0	5	28.6%	0.00 [−0.31, 0.31]	
Total (95% CI)		55		45	100.0%	0.11 [−0.05, 0.28]	
Total events	23		12				

Heterogeneity: tau^2 = 0.00; chi^2 = 0.72, df = 1 (p = 0.40); I^2 = 0%
Test for overall effect: Z = 1.34 (p = 0.18)

FIGURE 2: Bone healing rate at 6 months posttreatment for cell-based therapies vs. bone autograft.
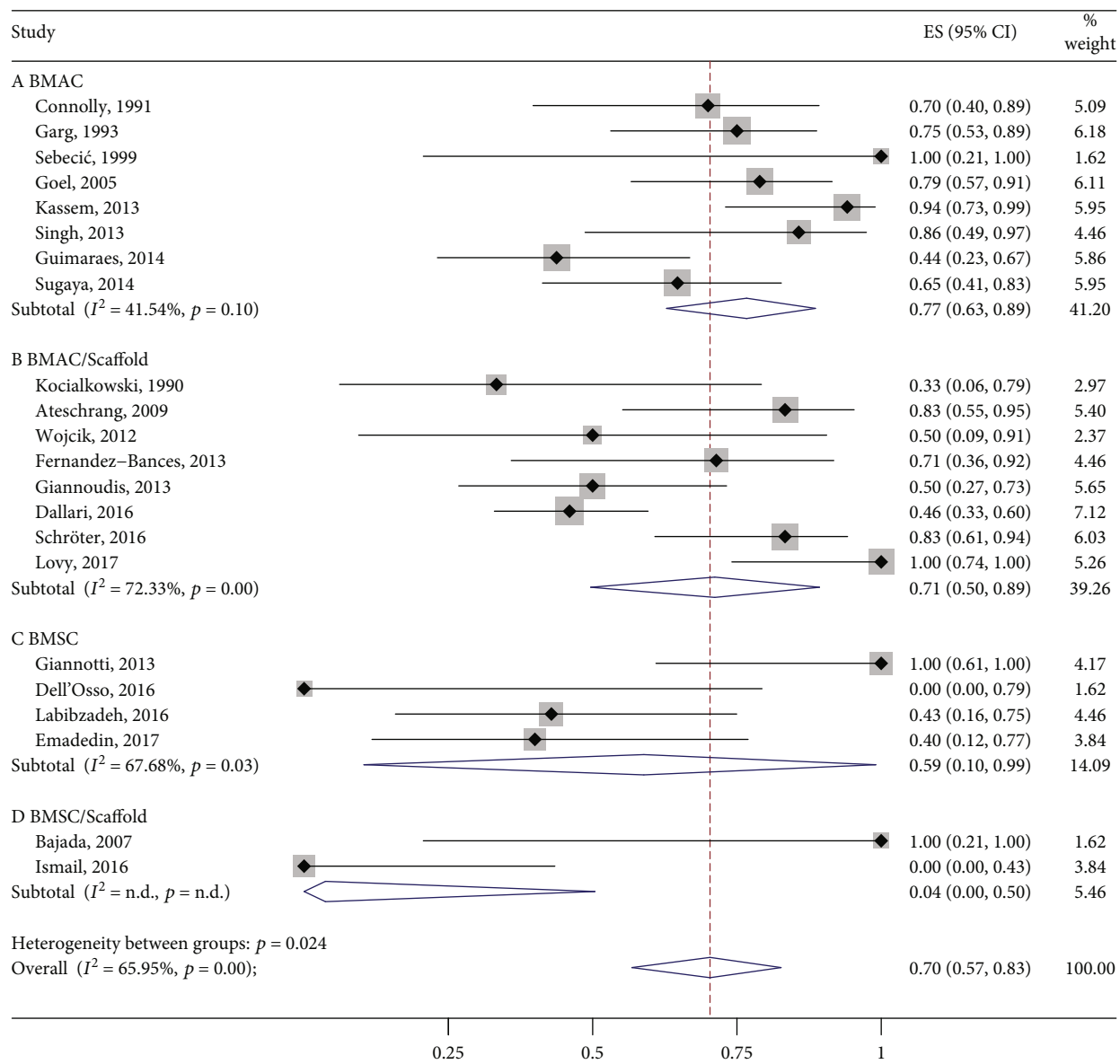
FIGURE 3: Bone healing rate at 6 months posttreatment.

"materials and methods" section (18.5%). Of the remainder, the mean pooled proportion of bone healing rate in the BMAC group was 77% (95% CI 63%-89%, 107 cases, $n = 8$ studies) followed by BMAC/Scaffold with 71% (95% CI 50%-89%, 117 cases, $n = 8$), BMSC with 59% (95% CI 10%-99%, 19 cases, $n = 4$), and BMSC/Scaffold with 4% (95% CI 0%-50%, 6 cases, $n = 2$). The combined overlapped 95% CIs suggested a similar effect among the interventions, with the exception of the BMSC/Scaffold group that, however, was unrepresentative. Data are reported in Figure 3.

| Study or subgroup | BMAC/BMSC scaffold | | Bone autograft | | Weight | Risk difference | Risk difference |
	Events	Total	Events	Total		IV, random, 95% CI	IV, Random, 95% CI
Dallari, 2016	42	50	27	40	75.7%	0.16 [−0.01, 0.34]	
Ismail, 2016	5	5	5	5	24.3%	0.00 [−0.31, 0.31]	
Total (95% CI)		55		45	100.0%	0.12 [−0.03, 0.28]	
Total events	47		32				

Heterogeneity: tau^2 = 000; chi^2 = 0.81, df = 1 (p = 0.37); I^2 = 0%
Test for overall effect: Z = 1.59 (p = 0.11)
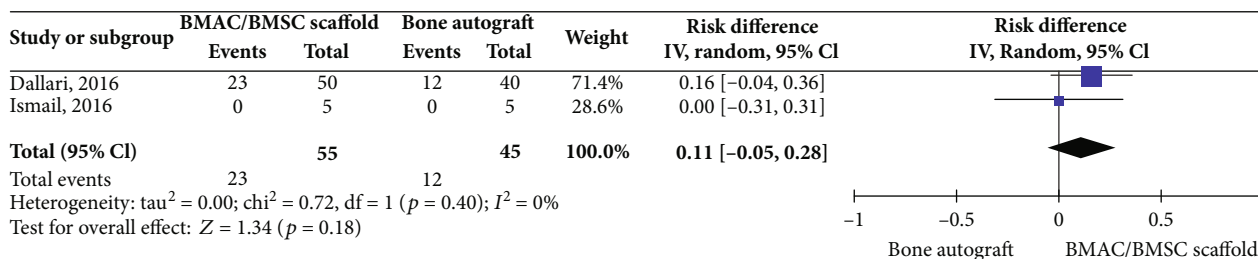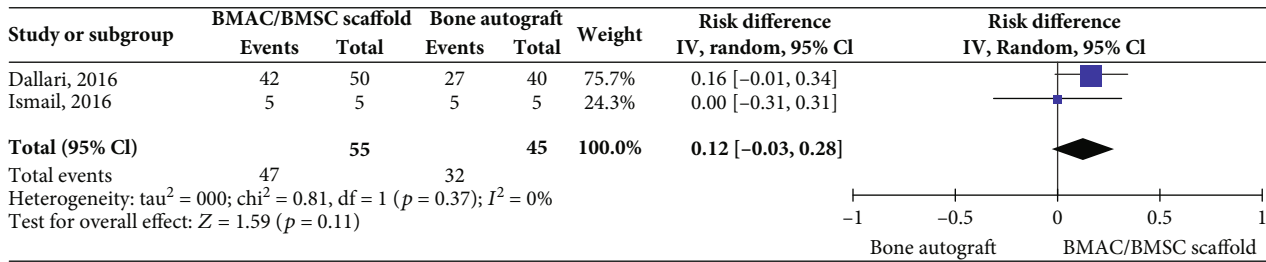
FIGURE 4: Bone healing rate at 12 months posttreatment for cell-based therapies vs. bone autograft.

3.4. Bone Healing Rate at 12 Months of Follow-Up. Two controlled studies investigating BMAC/Scaffold or BMSC/Scaffold interventions did not show any significant difference in bone healing rate versus the control intervention (bone autograft) (2 studies, 100 patients, RD 0.12 95% CI -0.03 to 0.28, I^2 = 0%; p = 0.11, Figure 4).

Looking at the cohort studies lacking the control group, 2 studies did not report the outcome data as planned (4.7%). Of the remainder, the mean pooled proportion of bone healing in the BMSC/Scaffold treatment group was 100% (95% CI 81%-100%, 9 cases, n = 3) followed by BMAC/Scaffold with 95% (95% CI 87%-100%, 117 cases, n = 8), BMSC alone with 87% (95% CI 58%-100%, 22 cases, 7 = 5), and BMAC alone with 81% (95% CI 65%-93%, 117 cases, n = 5). The combined overlapped 95% CIs suggested similar effects among the four interventions studied. Data are reported in Figure 5.

4. Discussion

The standard management of nonunions is based on surgeries that may or may not involve the replacement of the fixation implants and the use of autografts. Nonunions represent a major indication for the clinical use of cell-based therapies. In fact, as indicated by the growing literature, BMSC and bone marrow derivatives have raised interest for the treatment of this disorder. In this systematic review, we noticed a positive trend in bone healing in favour of stem cell-based therapies as compared to bone autograft. However, it must be underlined that this difference was not statistically significant and data were weakly supported by a paucity of studies. In fact, the most represented study designs were single cohort studies. Among these, we found that BMAC alone or combined with scaffolds yielded bone healing at 6 months of follow-up in 77% and 71% of patients, respectively. Conversely, interventions with BMSC and BMSC/Scaffold showed an inferior healing rate 6 months after treatment (59% and 4%, respectively). The bone healing rate significantly increased for the BMAC/Scaffold group at 12 months of follow-up (95%), while it was only slightly increased when BMAC alone was used (81%). At this time point, the healing rate associated with BMSC-based treatments was even better than that yielded by the corresponding BMAC-based treatments (BMSC: 87%; BMSC/Scaffold: 100%). However, no definitive conclusion can be derived about the use of BMSC combined with a scaffold due to the retrieval of only 3 studies for a total number of 9 patients. Even in the absence of strong

evidences coming from controlled studies, these preliminary results suggest that the use of bone scaffolds (demineralised bone, bioceramics, bone chips, etc.) in combination with cell-based therapies can be considered of great importance to locally deliver and engraft progenitor cells, while providing a structural support to the bone healing process.

In general, failures occurred mainly because of fracture instability, severe bone loss, or alcohol/drug addiction. We also speculated that one of the main causes of failure for cell-based treatment could be the presence of hypertrophic rather than atrophic nonunions which are usually not recommended for these kinds of orthobiologic approaches. Indeed, the efficacy of the cell-based therapies could be very limited in these cases where bone biological activity is retained compared to atrophic nonunions [42]. Moreover, hypertrophic nonunions are greatly affected by the fixation technique used to limit the micromovement of bone stumps, which may additionally complicate the situation. We considered these premises as particularly relevant to evaluate the efficacy of cell-based therapies in correlation with the type of nonunion. However, only half of the analysed articles reported the type of nonunion and the relative failure rate, which impeded us in investigating properly possible correlations between these two parameters. When treating long-bone nonunions, it is also important to keep in mind the type of injured bone. Indeed, leg and arm bones bear very different weights even in the same limb, which can significantly affect the clinical outcome. Albeit almost all the papers reported in which anatomical site the treatment was unsuccessful, the number of cases was still too low to clearly define a correlation between failure rate and fracture site. In the same way, it was not possible to investigate the correlation between the clinical outcome of each treatment and the type of fracture. Indeed, only about 50% of the studies declared whether the fracture was closed or open and/or provided a score in the case of open fractures. Additionally, in some studies where the fracture score was provided, the clinical outcome of each specific patient was not reported, thus impeding the correlation between these parameters.

Despite the mean age of treated patients being similar among the analysed studies, the age range was quite heterogeneous and widely distributed. Although the older age does not directly affect the healing outcomes of fracture nonunions [43], the quality of patients' mesenchymal stromal cells is known to be reduced in older patients [44–46]. According to this premise, the therapeutic efficacy of cell-based approaches should be weighted on the age of enrolled

Study	ES (95% CI)	% weight
A BMAC		
Connolly, 1991	0.90 (0.60, 0.98)	4.96
Garg, 1993	0.85 (0.64, 0.95)	7.58
Guimaraes, 2014	0.50 (0.28, 0.72)	6.68
Sugaya, 2014	0.76 (0.53, 0.90)	6.92
Flouzat–Lachaniette, 2016	0.91 (0.80, 0.96)	**11.57**
Subtotal ($I^2 = 65.62\%$, $p = 0.02$)	0.81 (0.65, 0.93)	37.71
B BMAC/Scaffold		
Kocialkowski, 1990	0.67 (0.21, 0.94)	2.06
Ateschrang, 2009	0.92 (0.65, 0.99)	5.60
Wojcik, 2012	1.00 (0.34, 1.00)	1.52
Fernandez–Bances, 2013	1.00 (0.65, 1.00)	**3.87**
Giannoudis, 2013	1.00 (0.78, 1.00)	6.17
Dallari, 2016	0.84 (0.71, 0.92)	11.28
Schröter, 2016	0.83 (0.61, 0.94)	**7.15**
Lovy, 2017	1.00 (0.74, 1.00)	5.29
Subtotal ($I^2 = 17.64\%$, $p = 0.29$)	0.95 (0.87, 1.00)	42.92
C BMSC		
Giannotti, 2013	1.00 (0.61, 1.00)	3.46
Qu, 2015	1.00 (0.44, 1.00)	2.06
Dell'Osso, 2016	1.00 (0.21, 1.00)	0.95
Labibzadeh, 2016	0.57 (0.25, 0.84)	3.87
Emadedin, 2017	0.60 (0.23, 0.88)	3.02
Subtotal ($I^2 = 29.32\%$, $p = 0.23$)	0.87 (0.58, 1.00)	13.35
D BMSC/Scaffold		
Bajada, 2007	1.00 (0.21, 1.00)	0.95
Wittig, 2016	1.00 (0.44, 1.00)	2.06
Ismail, 2016	1.00 (0.57, 1.00)	3.02
Subtotal ($I^2 = $ n.d., $p = $ n.d.)	1.00 (0.81, 1.00)	6.02
Heterogeneity between groups: $p = 0.328$		
Overall ($I^2 = 32.78\%$, $p = 0.07$);	0.92 (0.85, 0.97)	100.00

FIGURE 5: Bone healing rate at 12 months posttreatment.

patients, similarly to metabolic and social habits that have been indicated as possible determinants of treatment failure in some of the analysed studies.

In this meta-analysis, we found that detailed reporting on failure rate and causes is often inconsistent. This implies the impossibility to clearly identify the association between known or possible confounding bias and treatment failure.

Based on all these considerations, we would like to highlight a very poor reporting of useful data regarding the patients' cohort and the clinical outcomes and subsequently stress the need to conduct studies in accordance with the international standards of reporting, as indicated by the EQUATOR network initiative and implemented by the STROBE guidelines for observational studies (http://www .equator-network.org/). Poor reporting in many cases also reflects a poor quality of conduct of these studies, explaining the mismatch between the amount of research spent in the

last 20 years of *in vitro* and *in vivo* studies supporting the use of mesenchymal stromal cells in bone regeneration and the missing demonstration of their therapeutic efficacy for clinical practice. In fact, the present review retrieved only 2 controlled clinical trials comparing the efficacy of bone marrow-derived cell-based therapies to bone autograft, which represent the therapeutic gold standard [31, 41]. Anyway, these 2 studies were not randomized. Additionally, we noticed a huge variability in the procedures used in the analysed studies. For instance, both isolation and expansion protocols of BMSC and the protocols to obtain BMAC varied significantly among studies. Another variable, and often undefined, factor was the number of progenitor cells delivered either as BMAC or as expanded BMSCs. In fact, only few studies assessed the number of progenitor cells in BMAC [21–23, 28]. With regard to concerns on the use of expanded BMSC, we found studies delivering a variable number of

BMSCs but none of these studies analysed the correlation between cell number and treatment efficacy [34, 36–38]. In this scenario, we believe that the recently approved EU-H2020-ORTHOUNION project will provide interesting insights. This project is focused on testing the efficacy of different doses of *in vitro* expanded BMSC loaded onto biomaterials in a transnational multicentre, controlled (autograft), and randomized clinical trial. Due to these specific features, the EU-H2020-ORTHOUNION represents a promising attempt to prove the efficacy of cell-based therapies for the treatment of nonunions in a standardized setup (EudraCT number 2015-000431-32) [47]. This study will enrol more than 100 patients, implementing a sample size calculation based on an accurate power analysis. Considering that among the analysed studies, 7 were case reports describing data obtained from 1 to 3 patients and all the studies evaluating expanded BMSC included less than 10 patients, the EU-H2020-ORTHOUNION project will represent a significant step forward and a positive example of an efficient collaboration among European clinicians.

5. Conclusions

Overall, the data obtained in this meta-analysis should be interpreted with caution. Indeed, the heterogeneity of the studies along with limited reporting and nonsystematic study design makes difficult to draw clear and definitive recommendations regarding the best approach to heal bone nonunions. Clinical trials recapitulating a more accurate planning and data collection should be conducted in the future to obtain a reliable demonstration of the efficacy of cell-based therapies, the importance of using bone scaffolds to promote the engraftment of implanted progenitor cells, and the superiority of BMAC versus expanded BMSCs.

Conflicts of Interest

The authors declare that there is no conflict of interest regarding the publication of this paper.

Authors' Contributions

SL and SP have equally contributed to this study.

Acknowledgments

Supplementary Materials

Appendix S1: search strategy including the MeSH terms used for the literature search. Appendix S2: table including eligible studies that were excluded since they reported aggregated data for eligible and noneligible patients. *(Supplementary Materials)*

References

[1] G. Zimmermann and A. Moghaddam, "Trauma: Non-Union: New Trends," in *European Instructional Lectures. European Instructional Lectures, vol 10*, G. Bentley, Ed., Springer, Berlin, Heidelberg, 2010.

[2] M. A. Imam, J. Holton, L. Ernstbrunner et al., "A systematic review of the clinical applications and complications of bone marrow aspirate concentrate in management of bone defects and nonunions," *International Orthopaedics*, vol. 41, no. 11, pp. 2213–2220, 2017.

[3] E. Gómez-Barrena, P. Rosset, D. Lozano, J. Stanovici, C. Ermthaller, and F. Gerbhard, "Bone fracture healing: cell therapy in delayed unions and nonunions," *Bone*, vol. 70, pp. 93–101, 2015.

[4] D. Holmes, "Closing the gap," *Nature*, vol. 550, no. 7677, pp. S194–S195, 2017.

[5] D. Holmes, "Non-union bone fracture: a quicker fix," *Nature*, vol. 550, no. 7677, p. S193, 2017.

[6] D. J. Hak, D. Fitzpatrick, J. A. Bishop et al., "Delayed union and nonunions: epidemiology, clinical issues, and financial aspects," *Injury*, vol. 45, Suppl 2, pp. S3–S7, 2014.

[7] A. B. Lovati, C. L. Romanò, M. Bottagisio et al., "Modeling Staphylococcus epidermidis-induced non-unions: subclinical and clinical evidence in rats," *PLoS One*, vol. 11, no. 1, p. e0147447, 2016.

[8] A. Ho-Shui-Ling, J. Bolander, L. E. Rustom, A. W. Johnson, F. P. Luyten, and C. Picart, "Bone regeneration strategies: engineered scaffolds, bioactive molecules and stem cells current stage and future perspectives," *Biomaterials*, vol. 180, pp. 143–162, 2018.

[9] P. V. Giannoudis, S. Gudipati, P. Harwood, and N. K. Kanakaris, "Long bone non-unions treated with the diamond concept: a case series of 64 patients," *Injury*, vol. 46, Suppl 8, pp. S48–S54, 2015.

[10] S. S. Lin and M. G. Yeranosian, "The role of orthobiologics in fracture healing and arthrodesis," *Foot and Ankle Clinics*, vol. 21, no. 4, pp. 727–737, 2016.

[11] R. DerSimonian and N. Laird, "Meta-analysis in clinical trials," *Controlled Clinical Trials*, vol. 7, no. 3, pp. 177–188, 1986.

[12] J. P. T. Higgins and S. Green, "Cochrane handbook for systematic reviews of interventions," *Version 5.1.0 The Cochrane Collaboration*, 2011, March 2011, http://www.cochrane-handbook.org.

[13] V. N. Nyaga, M. Arbyn, and M. Aerts, "Metaprop: a Stata command to perform meta-analysis of binomial data," *Archives of Public Health*, vol. 72, no. 1, p. 39, 2014.

[14] R. J. Harris, J. J. Deeks, D. G. Altman, M. J. Bradburn, R. M. Harbord, and J. A. C. Sterne, "METAN: Fixed- and Random-Effects Meta-Analysis," *The Stata Journal: Promoting communications on statistics and Stata*, vol. 8, no. 1, pp. 3–28, 2008.

[15] J. F. Connolly, R. Guse, J. Tiedeman, and R. Dehne, "Autologous marrow injection as a substitute for operative grafting of tibial nonunions," *Clinical Orthopaedics and Related Research*, vol. 266, pp. 259–270, 1991.

[16] N. K. Garg, S. Gaur, and S. Sharma, "Percutaneous autogenous bone marrow grafting in 20 cases of ununited fracture," *Acta Orthopaedica Scandinavica*, vol. 64, no. 6, pp. 671-672, 1993.

[17] B. Sebecić, V. Gabelica, L. Patrlj, and T. Sosa, "Percutaneous autologous bone marrow grafting on the site of tibial delayed

union," *Croatian Medical Journal*, vol. 40, no. 3, pp. 429–432, 1999.

[18] A. Goel, S. S. Sangwan, R. C. Siwach, and A. M. Ali, "Percutaneous bone marrow grafting for the treatment of tibial non-union," *Injury*, vol. 36, no. 1, pp. 203–206, 2005.

[19] M. S. Kassem, "Percutaneous autogenous bone marrow injection for delayed union or non-union of fractures after internal fixation," *Acta Orthopaedica Belgica*, vol. 79, no. 6, pp. 711–717, 2013.

[20] A. K. Singh and A. Sinha, "Percutaneous autologous bone marrow injections for delayed or non-union of bones," *Journal of Orthopaedic Surgery*, vol. 21, no. 2, p. 267, 2013.

[21] J. A. M. Guimarães, M. E. L. Duarte, M. B. C. Fernandes et al., "The effect of autologous concentrated bone-marrow grafting on the healing of femoral shaft non-unions after locked intramedullary nailing," *Injury*, vol. 45, Suppl 5, pp. S7–S13, 2014.

[22] H. Sugaya, H. Mishima, K. Aoto et al., "Percutaneous autologous concentrated bone marrow grafting in the treatment for nonunion," *European Journal of Orthopaedic Surgery and Traumatology*, vol. 24, no. 5, pp. 671–678, 2014.

[23] C. H. Flouzat-Lachaniette, C. Heyberger, C. Bouthors et al., "Osteogenic progenitors in bone marrow aspirates have clinical potential for tibial non-unions healing in diabetic patients," *International Orthopaedics*, vol. 40, no. 7, pp. 1375–1379, 2016.

[24] A. Kocialkowski, W. A. Wallace, and H. G. Prince, "Clinical experience with a new artificial bone graft: preliminary results of a prospective study," *Injury*, vol. 21, no. 3, pp. 142–144, 1990.

[25] J. J. Tiedeman, K. L. Garvin, T. A. Kile, and J. F. Connolly, "The role of a composite, demineralized bone matrix and bone marrow in the treatment of osseous defects," *Orthopedics*, vol. 18, no. 12, pp. 1153–1158, 1995.

[26] A. Ateschrang, B. G. Ochs, M. Lüdemann, K. Weise, and D. Albrecht, "Fibula and tibia fusion with cancellous allograft vitalised with autologous bone marrow: first results for infected tibial non-union," *Archives of Orthopaedic and Trauma Surgery*, vol. 129, no. 1, pp. 97–104, 2009.

[27] K. Wójcik, R. Nowak, D. Polak, and T. Bielecki, "Locked intramedullary nailing in the treatment of non-union following humeral shaft fractures," *Ortopedia Traumatologia Rehabilitacja*, vol. 14, no. 3, pp. 279–288, 2012.

[28] I. Fernandez-Bances, M. Perez-Basterrechea, S. Perez-Lopez et al., "Repair of long-bone pseudoarthrosis with autologous bone marrow mononuclear cells combined with allogenic bone graft," *Cytotherapy*, vol. 15, no. 5, pp. 571–577, 2013.

[29] P. V. Giannoudis, M. A. Ahmad, G. V. Mineo, T. I. Tosounidis, G. M. Calori, and N. K. Kanakaris, "Subtrochanteric fracture non-unions with implant failure managed with the "diamond" concept," *Injury*, vol. 44, Suppl 1, pp. S76–S81, 2013.

[30] M. Scaglione, L. Fabbri, D. Dell'Omo, F. Gambini, and G. Guido, "Long bone nonunions treated with autologous concentrated bone marrow-derived cells combined with dried bone allograft," *Musculoskeletal Surgery*, vol. 98, no. 2, pp. 101–106, 2014.

[31] D. Dallari, N. Rani, G. Sabbioni, A. Mazzotta, A. Cenacchi, and L. Savarino, "Radiological assessment of the PRF/BMSC efficacy in the treatment of aseptic nonunions: a retrospective study on 90 subjects," *Injury*, vol. 47, no. 11, pp. 2544–2550, 2016.

[32] S. Schröter, A. Ateschrang, I. Flesch, U. Stöckle, and T. Freude, "First mid-term results after cancellous allograft vitalized with autologous bone marrow for infected femoral non-union," *Wiener Klinische Wochenschrift*, vol. 128, no. 21-22, pp. 827–836, 2016.

[33] A. J. Lovy, J. S. Kim, J. di Capua et al., "Intramedullary nail fixation of atypical femur fractures with bone marrow aspirate concentrate leads to faster union: a case-control study," *Journal of Orthopaedic Trauma*, vol. 31, no. 7, pp. 358–362, 2017.

[34] S. Giannotti, V. Bottai, M. Ghilardi et al., "Treatment of pseudoarthrosis of the upper limb using expanded mesenchymal stem cells: a pilot study," *European Review for Medical and Pharmacological Sciences*, vol. 17, no. 2, pp. 224–227, 2013.

[35] Z. Qu, S. Guo, G. Fang, Z. Cui, and Y. Liu, "AKT pathway affects bone regeneration in nonunion treated with umbilical cord-derived mesenchymal stem cells," *Cell Biochemistry and Biophysics*, vol. 71, no. 3, pp. 1543–1551, 2015.

[36] G. Dell'Osso, G. Bugelli, F. Celli et al., "Grafting of expanded mesenchymal stem cells without associated procedure in a healed case of ulna pseudarthrosis: a case report," *Surgical Technology International*, vol. 28, pp. 289–292, 2016.

[37] N. Labibzadeh, M. Emadedin, R. Fazeli et al., "Mesenchymal stromal cells implantation in combination with platelet lysate product is safe for reconstruction of human long bone nonunion," *Cell Journal*, vol. 18, no. 3, pp. 302–309, 2016.

[38] M. Emadedin, N. Labibzadeh, R. Fazeli et al., "Percutaneous autologous bone marrow-derived mesenchymal stromal cell implantation is safe for reconstruction of human lower limb long bone atrophic nonunion," *Cell Journal*, vol. 19, no. 1, pp. 159–165, 2017.

[39] S. Bajada, P. E. Harrison, B. A. Ashton, V. N. Cassar-Pullicino, N. Ashammakhi, and J. B. Richardson, "Successful treatment of refractory tibial nonunion using calcium sulphate and bone marrow stromal cell implantation," *Journal of Bone and Joint Surgery. British Volume (London)*, vol. 89-B, no. 10, pp. 1382–1386, 2007.

[40] O. Wittig, E. Romano, C. González et al., "A method of treatment for nonunion after fractures using mesenchymal stromal cells loaded on collagen microspheres and incorporated into platelet-rich plasma clots," *International Orthopaedics*, vol. 40, no. 5, pp. 1033–1038, 2016.

[41] H. D. Ismail, P. Phedy, E. Kholinne et al., "Mesenchymal stem cell implantation in atrophic nonunion of the long bones: a translational study," *Bone & Joint Research*, vol. 5, no. 7, pp. 287–293, 2016.

[42] S. Toosi, N. Behravan, and J. Behravan, "Nonunion fractures, mesenchymal stem cells and bone tissue engineering," *Journal of Biomedical Materials Research. Part A*, vol. 106, no. 9, pp. 2552–2562, 2018.

[43] D. P. Taormina, B. S. Shulman, R. Karia, A. B. Spitzer, S. R. Konda, and K. A. Egol, "Older age does not affect healing time and functional outcomes after fracture nonunion surgery," *Geriatric Orthopaedic Surgery & Rehabilitation*, vol. 5, no. 3, pp. 116–121, 2014.

[44] A. Stolzing, E. Jones, D. McGonagle, and A. Scutt, "Age-related changes in human bone marrow-derived mesenchymal stem cells: consequences for cell therapies," *Mechanisms of Ageing and Development*, vol. 129, no. 3, pp. 163–173, 2008.

[45] O. S. Beane, V. C. Fonseca, L. L. Cooper, G. Koren, and E. M. Darling, "Impact of aging on the regenerative properties of bone marrow-, muscle-, and adipose-derived mesenchymal stem/stromal cells," *PLoS One*, vol. 9, no. 12, p. e115963, 2014.

[46] L. de Girolamo, S. Lopa, E. Arrigoni, M. F. Sartori, F. W. Baruffaldi Preis, and A. T. Brini, "Human adipose-derived stem cells isolated from young and elderly women: their differentiation potential and scaffold interaction during in vitro osteoblastic differentiation," *Cytotherapy*, vol. 11, no. 6, pp. 793–803, 2009.

[47] E. Gómez-Barrena, N. G. Padilla-Eguiluz, C. Avendaño-Solá et al., "A multicentric, open-label, randomized, comparative clinical trial of two different doses of expanded hBM-MSCs plus biomaterial versus iliac crest autograft, for bone healing in nonunions after long bone fractures: study protocol," *Stem Cells International*, vol. 2018, Article ID 6025918, 13 pages, 2018.

Research Article

In Vivo Magic Angle Magnetic Resonance Imaging for Cell Tracking in Equine Low-Field MRI

Carolin Horstmeier [ID],[1] **Annette B. Ahrberg,**[2] **Dagmar Berner,**[3] **Janina Burk** [ID],[4] **Claudia Gittel,**[5] **Aline Hillmann** [ID],[6] **Julia Offhaus,**[1] **and Walter Brehm** [ID][1,6]

[1]*Department for Horses, Faculty of Veterinary Medicine, University of Leipzig, An den Tierkliniken 21, 04103 Leipzig, Germany*
[2]*Department of Orthopedics, Traumatology, and Plastic Surgery, University of Leipzig, Liebigstr. 20, 04103 Leipzig, Germany*
[3]*Royal Veterinary College, University of London, Hawkshead Lane, Hatfield, Hertfordshire AL9 7TA, UK*
[4]*Equine Clinic-Surgery, Justus Liebig University Giessen, Frankfurter Str. 108, 35392 Giessen, Germany*
[5]*Department of Veterinary Medicine, Queen's Veterinary School, Madingley Road, Cambridge CB3 0ES, UK*
[6]*Saxon Incubator for Clinical Translation, University of Leipzig, Philipp-Rosenthal-Str. 55, 04103 Leipzig, Germany*

Correspondence should be addressed to Carolin Horstmeier; carolin.horstmeier@uni-leipzig.de

The magic angle effect increases the MRI signal of healthy tendon tissue and could be used for more detailed evaluation of tendon structure. Furthermore, it could support the discrimination of hypointense artefacts induced by contrast agents such as superparamagnetic iron oxide used for cell tracking. However, magic angle MRI of the equine superficial digital flexor tendon has not been accomplished in vivo in standing low-field MRI so far. The aim of this in vivo study was to evaluate the practicability of this magic angle technique and its benefit for tracking superparamagnetic iron oxide-labelled multipotent mesenchymal stromal cells. Six horses with induced tendinopathy in their forelimb superficial digital flexor tendons were injected locally either with superparamagnetic iron oxide-labelled multipotent mesenchymal stromal cells or serum. MRI included standard and magic angle image series in T1- and T2∗-weighted sequences performed at regular intervals. Image analysis comprised blinded evaluation and quantitative assessment of signal-to-noise ratio. The magic angle technique enhanced the tendon signal-to-noise ratio ($P < 0.001$). Hypointense artefacts were observable in the cell-injected superficial digital flexor tendons over 24 weeks and artefact signal-to-noise ratio differed significantly from tendon signal-to-noise ratio in the magic angle images ($P < 0.001$). Magic angle imaging of the equine superficial digital flexor tendon is feasible in standing low-field MRI. The current data demonstrate that the technique improves discrimination of superparamagnetic iron oxide-induced artefacts from the surrounding tendon tissue.

1. Introduction

In equine practice, tendinopathies most commonly affect the superficial digital flexor tendon (SDFT) [1, 2] and treatment is challenging. Consequently, the SDFT is the focus of research activities aimed at understanding tendon healing and regenerative therapy options.

Standing low-field magnetic resonance imaging (MRI) offers good opportunities to closely monitor tendon healing, especially by using T2 and STIR sequences. It also allows longitudinal cell tracking after injecting superparamagnetic iron oxide- (SPIO-) labelled cells by the induction of hypointense artefacts based on inhomogeneities of the local magnetic field in T1- and T2∗-weighted sequences. Tendon signal is dependent on a particular angle θ between the tendon fibres and the main magnetic field B_0 [3]. The angle $\theta = 90°$ in standard MRI images leads to a rapid dephasing of the MR signal, resulting in a hypointense signal of healthy tendon tissue. The so-called magic angle effect with an angle of approximately $\theta = 55°$ could be useful to improve the value of the diagnostic procedure. The T2 relaxation time is extended, and the tendon signal intensity (SI) increases [3, 4]. The

magic angle effect is an artefact and can occur naturally in tendons and ligaments during MRI which could lead to misdiagnosis. But considering special clinical and scientific problems, it can provide additional information on the structure of tendons [5, 6] and could be advantageous for the discrimination of artefacts induced by contrast agents such as SPIO from the surrounding tissue [7, 8]. Intralesional injection of multipotent mesenchymal stromal cells (MSC) has been established with promising results [9–11]. However, little is known about the behaviour of the cells after injection. Therefore, MRI tracking would be favourable to monitor the fate of MSC and the healing process of the tendon lesions. However, while SPIO-labelled cells can be localised and distinguished in most tissues, a clear distinction between labelled cells and healthy tendon tissue is hampered as both display hypointense signals in standard images. Therefore, it appears favourable to use the magic angle technique to increase the tendon signal and support the discrimination of the labelled MSC after injection into the tendon. This beneficial effect of the magic angle has already been confirmed ex vivo [12, 13] and in vivo in rabbits [14], but it has not been performed in large animal in vivo studies so far [7, 8, 15]. Burk et al. in 2013 have shown that the magic angle effect is feasible in the SDFT of the midmetacarpal region.

We hypothesised that magic angle images can be obtained from the equine SDFT in standing low-field MRI. Furthermore, we aimed to evaluate the benefit of the thereby established technique for cell tracking in tendon lesions, hypothesising that the magic angle effect ($\theta = 55°$) improves visualisation of labelled cells inside the tendon tissue compared to standard ($\theta = 90°$) MRI.

2. Materials and Methods

2.1. Tendinopathy Induction. This study was approved by the local ethics committee (Landesdirektion Leipzig, TVV 34/13), and all ethical guidelines were observed. Six healthy standardbreds (3 female and 3 male, 3–10 years, 400–550 kg) were included.

Tendon lesions were induced by the same surgeon in the midmetacarpal region of the SDFT in both forelimbs under general anaesthesia. The horses were placed in lateral recumbency, and the surgical fields were prepared aseptically. Via a 2 cm vertical skin incision, an 11-gauge bone marrow aspiration needle (Walter Veterinär-Instrumente e.K., Baruth/-Mark, Germany) was advanced 2 cm in the proximal direction into the SDFT. During retraction of the needle, 0.4 ml collagenase I (4.8 mg/ml; Life Technologies GmbH, Darmstadt, Germany) was injected into the tendon tissue. Subsequently, peritendineum and skin were sutured and the limbs were bandaged. Postoperative management included standardised pain management with nonsteroidal antiinflammatory drugs (flunixin meglumine; pre- and 10 h postsurgery: 1.1 mg/kg bwt i.v.; day 1 to day 4 postsurgery: 0.55 mg/kg bwt p.o. twice daily; and day 5 to day 6 post surgery: 0.55 mg/kg bwt p.o. once daily). The horses were assessed for pain by a pain scoring system [16] 3 times daily over a period of 10 days after surgery and, if necessary, additional analgesics were administered.

2.2. MSC Isolation and Labelling. In the same surgery, subcutaneous adipose tissue was collected from the supragluteal region for the isolation of autologous MSC as described previously [17, 18]. The plastic-adherent cell fraction was expanded until passage 2 and was labelled with SPIO (Molday ION Rhodamine B™; iron concentration: 25 μg Fe/ml culture medium, incubation: 20 h; BioPAL, Inc., Worcester, MA, USA). The MSC were harvested and 10×10^6 cells per treated tendon were resuspended in 1 ml autologous serum for the intralesional injection. Labelled MSC from each animal were also used to confirm labelling by Prussian Blue staining and flow cytometry, trilineage differentiation potential, and MSC surface marker expression [19].

2.3. MSC Injection. Three weeks after induction of tendinopathy, treatment of the tendon lesions was performed. 10×10^6 resuspended MSC were injected intralesionally into 1 randomly chosen forelimb of each animal. 1 ml autologous serum was injected as a control into the contralateral forelimb. For this purpose, horses were sedated and perineural anaesthesia of the ulnar nerve and local anaesthesia were performed. The skin was prepared aseptically. A 20-gauge needle was placed in the tendon lesion under ultrasonographic monitoring (10 MHz linear transducer, LOGIQ 5 Expert; GE Healthcare, Munich, Germany), and the cell suspension or serum was injected by the same blinded veterinarian. From week 2 to week 24 after cell injection, the horses were subjected to an increasing exercise program [20].

2.4. MRI. For MSC tracking over 24 weeks, the SDFT of both forelimbs were examined in standing, sedated animals using an equine-dedicated low-field MRI system (0.27 Tesla MRI unit; Hallmarq Veterinary Imaging, Guildford, Surrey, UK) as described before [8]. Examinations were performed immediately before and after cell injection as well as 1, 2, 3, 4, 6, 8, 12, and 24 weeks postinjection. Each examination included transversal T1-weighted and T2∗-weighted gradient echo MRI sequences (Table 1), both as a standard series as well as a magic angle series. In the standard series, the whole injured area was scanned. In the magic angle series of the MSC-treated forelimb, imaging was limited to the area with SPIO-induced hypointense artefacts, and in the magic angle series of the contralateral forelimb, 8 slices were acquired from the region of the injection.

For the standard series, the poles of the MRI framed the metacarpus on its medial and lateral side resulting in an angle of $\theta = 90°$ between the SDFT and the static magnetic field B_0. For the magic angle series, the SDFT was positioned at an angle of approximately $\theta = 55°$ to the magnetic field B_0. To accomplish this, the animal was moved sideways into the magnet, leaving the poles of the MRI dorsal and palmar to the metacarpal region, while the carpus was bent and fixed manually by one person (Figure 1).

2.5. Image Analysis. Image analysis was performed using Synedra View Personal Version 3.4.0.2 (Synedra Information Technologies GmbH, Innsbruck, Austria) and Mathematica 10.1 (Wolfram Research, Inc., Champaign, IL, USA). All T1- and T2∗-weighted standard and magic angle image

TABLE 1: Settings of MRI sequences.

Sequence	TR (ms)	TE (ms)	FA (°)	ST (mm)	Gap (mm)	FOV (mm^2)	Matrix
T1w GRE	52	8	50	5	1	171×171	256×256
T2∗w GRE	68	13	25	5	1	171×171	256×256

GRE: gradient echo; TR: time to repeat; TE: time to echo; FA: flip angle; ST: slice thickness; FOV: field of view.

(a)

(b)

(c)

(d)

FIGURE 1: Position of the equine limb in the MRI scanner. (a) and (b) show the equine limb positioned between the poles of an equine-dedicated low-field MRI system. In (a), the SDFT of a left forelimb (posterior limb) was positioned in approximately the magic angle ($\theta = 55°$) to the main magnetic field B_0. In (b), the SDFT of a right forelimb was positioned in a $\theta = 90°$ angle (standard series) to the main magnetic field B_0. (c) and (d) show T1-weighted magic angle (c) and standard (d) images of healthy SDFT (arrows) in the midmetacarpal region. The signal intensity of the SDFT in the magic angle image increases compared to the SDFT in the standard image.

series were randomized, and the presence of a potential hypointense artefact in each image was determined qualitatively in consensus by two blinded observers. First of all, images displaying potential artefacts were assigned to one of two categories (category 1: "hypointense area most likely related to SPIO"; category 2: "questionable hypointense area") on the base of position, shape, and intensity (for example see Figure 2). Category 1 artefacts generally were characterised by lower SI and a larger area and were often localised in and around the SDFT. After this, only images with a potential hypointense artefact (categories 1 and 2) were used for further analysis. The SI of these artefacts were measured using a region of interest (circular ROI: 1 mm^2). Additionally, the artefact area and its SI were measured based on the whole
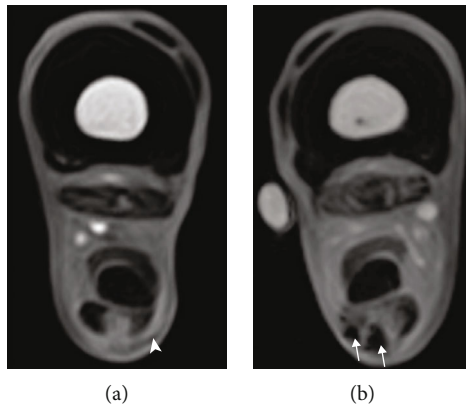
(a)   (b)

FIGURE 2: Categorisation of hypointense artefacts. Sample images of T1-weighted gradient echo MRI sequences with potential hypointense artefacts. (a) The arrowhead indicates a region of a category 2 artefact ("questionable hypointense area"). (b) The arrows indicate a region of a category 1 artefact ("hypointense area most likely related to SPIO").

visible artefact area. In all images assigned to category 1, the surrounding SDFT SI were measured additionally. In standard images assigned to category 1, tendon lesion SI were determined using a region of interest (circular ROI: $1\,mm^2$). This was not possible in magic angle images because of the difficult delineation between the tendon lesion and the surrounding tendon tissue. All measurements were repeated three times by a single observer, and mean values were used for further analysis. Furthermore, the standard deviation (SD) of the background noise, based on the whole background areas, was obtained.

For further analysis of all category 1 images, the signal-to-noise ratios of the different structures (SNR = SI/SD background) and the contrast-to-noise ratios (CNR) (CNR = (SI SDFT − SI artefact)/SD background) were used. In contrast, in category 2 images, only the artefact SNR were calculated for comparison. After all, the data were unblinded and the selected categorisation was evaluated. The artefact volumes displayed by all category 1 images within the whole limb series ($V = \Sigma$ artefact areas × 6 mm; 6 mm representing a slice thickness of 5 mm and a gap of 1 mm) were calculated.

2.6. Histology.
Within the framework of a different part of this study [19], histological sections of the tendons were obtained from the same horses at week 24 after euthanasia. Sections from the treated tendon were used to confirm that SPIO-labelled MSC were still present based on the rhodamine B component of the labelling agent. Briefly, the sections were subjected to counterstaining of nuclei with DAPI (Carl Roth GmbH & Co. KG, Karlsruhe, Germany). Other samples were stained with Prussian Blue with nuclear fast red counterstaining (Carl Roth GmbH & Co. KG, Karlsruhe, Germany) to evaluate the presence of fibroblast-like structures. All images were recorded using a Pannoramic Scan II (3DHIS-TECH Ltd., Budapest, Hungary). DAPI-stained sections were evaluated qualitatively by two observers in consensus, and Prussian Blue-stained sections were evaluated quantitatively by two blinded, independent observers.

2.7. Statistical Analysis.
Statistical analysis was performed using SPSS® Statistics 22 (IBM, Ehningen, Germany). For comparisons of SI within the same image, the Wilcoxon test was used; for comparisons between different images, Mann-Whitney's U tests were performed. P values < 0.05 were considered significant.

3. Results

3.1. Magic Angle Effect.
The magic angle effect was observed in all examined SDFT in low-field MRI. We obtained hyperintense signals in the healthy tendon tissue and significantly higher SDFT SNR in magic angle images compared to standard images in both T1- and T2∗-weighted sequences and at all time points ($P < 0.001$) (Figures 3 and 4(a)).

3.2. Artefact Discrimination.
Evaluation of the blind review showed that category 1 artefacts (images: $n = 1115$) were all part of the image series obtained from limbs injected with SPIO-labelled MSC, which demonstrates a correct identification of SPIO artefacts (Figure 2). However, among category 2 artefacts (images: $n = 140$), there were also images obtained from the control limbs ($n = 25$) or before MSC injection ($n = 10$), thus demonstrating that these images did not reliably display artefacts caused by SPIO-labelled MSC (Figure 2).

In contrast, artefacts appeared hypointense and with low SNR in both magic angle and standard category 1 images, with no significant differences observed at most time points (Figures 3 and 4(b)). Interestingly, SPIO SNR in the false-positive category 2 images was not as low as in images of category 1 ($P < 0.001$), the difference being most evident in T1-weighted magic angle images (Figure 5). However, a threshold SNR value delimiting SPIO-induced artefacts could not be defined.

All category 2 images were excluded from the following analyses. In standard images, when the SPIO artefact was surrounded by a hyperintense tendon lesion, its borders were clearly definable, but when it was localised within healthy tendon tissue, a clear distinction was only possible in magic angle images. This observation was reflected by the SNR values obtained from the artefact, the lesion, and the SDFT (Figure 4(b)). Lesion SNR measured in standard images was significantly higher than artefact SNR in both T1- and T2∗-weighted sequences and at all time points ($P < 0.001$). On the contrary, SDFT SNR in standard images was in a similar range as artefact SNR, especially considering the values obtained from the whole artefact area. However, in the magic angle images, SDFT SNR was significantly higher than artefact SNR in both T1- and T2∗-weighted sequences and at all time points ($P < 0.001$). This finding corresponds to the comparison of the CNR based on SI SDFT and SI artefact between magic angle and standard images (Figure 4(c)). It was significantly higher in magic angle images in both T1- and T2∗-weighted sequences and at all time points ($P < 0.001$). Nevertheless, despite these differences, artefact volume did not differ significantly between magic angle and 90° images (data not shown).
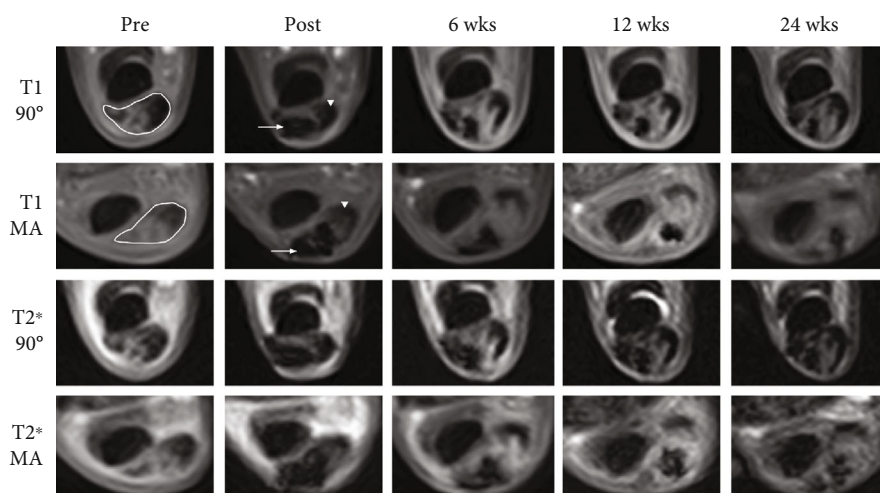
FIGURE 3: Exemplary MRI images. Exemplary images of T1- and T2*-weighted gradient echo MRI sequences before and immediately after as well as 6, 12, and 24 weeks after cell application at the same level of the limb. The first and third rows show standard images (90°), and the second and fourth rows show the corresponding magic angle (MA) images. The SDFT with its hyperintense lesion is identified by the white edging. After injection of labelled cells, they appear as pronounced hypointense artefacts (white arrows). Note that the healthy tendon tissue (white arrowheads) is difficult to discriminate from the artefact in $\theta = 90°$ images but not in the magic angle (MA) images.

3.3. Follow-Up. Category 1 artefacts could be distinguished at the MSC injection site over the whole follow-up period until week 24. Artefact SNR constantly remained low, and CNR correspondingly remained high and was not influenced by a decreasing signal during tendon healing over time in T1-weighted images. In contrast, T2*-weighted images showed a decreasing trend in SDFT SNR, which was also evident in magic angle images and reflected by CNR in these images. Nevertheless, the differences in CNR between standard and magic angle images still remained significant until week 24 ($P < 0.001$) (Figure 4).

Evaluation of the histological sections revealed that SPIO-labelled cells were still present at the lesion site at week 24, suggesting that the artefacts observed in MRI corresponded to labelled MSC (Figure 6).

4. Discussion

The first important finding of this study is that magic angle images can be obtained from the equine SDFT in standing low-field MRI resulting in images with higher SI in the SDFT. Therefore, it can be used for preclinical and clinical research in horses. As demonstrated here, this offers considerable advantages for cell tracking studies. Moreover, magic angle images could be used for more detailed diagnostics in tendon disease [5, 6]. However, while the current data demonstrate the feasibility of this technique, it should be acknowledged that the achievable angle between the SDFT and the main magnetic field is limited by the rigid poles of the used low-field MRI scanner and the animal size. Therefore, the standardisation of image acquisition is challenging and the use of a wedge was not possible. Furthermore, positioning of the animal should be performed with caution and there could be a high risk for injuries for both horse and person. Success and safety may depend on training and temper of the respective horse.

The second important finding of this study is that the magic angle technique improves the accuracy and reliability of SPIO-artefact discrimination in the SDFT. So far, the use of the magic angle effect for cell tracking in vivo had only been reported in one in vivo study in rabbits [14], in which comparison with standard images has not been performed.

Although in this study, the artefact volume determined in the standard image series was similar to those analysed in the magic angle image series, it should not be assumed that the cells are located solely within the tendon lesion at all times. They are likely to be distributed within the healthy tendon around the lesion and the tendon sheath after being injected into the lesion [8, 15, 21]. As demonstrated in our study, SPIO artefacts and healthy tendon tissue display an equally hypointense signal in standard images. Only the tendon lesion displays a higher SNR compared to the artefacts, thus they can be distinguished clearly. However, a reliable identification of the artefact area within the whole tendon is nearly impossible. These issues can be overcome using additional magic angle images to determine the artefact localisation more accurately. In magic angle images, only the SPIO artefacts display a hypointense signal. Therefore, it is possible to distinguish them from the surrounding tendon tissue, which is of particular importance for a detailed tracking of SPIO-labelled MSC.

Interestingly, a subjective blinded review was demonstrated to be surprisingly accurate, as no hypointense areas in control limbs or before MSC injection had been categorised as "most likely related to SPIO." In contrast, all hypointense areas found in control limbs or before cell injection had been considered as "questionable hypointense areas," demonstrating a correct identification of potential false-positive artefacts. Unspecific artefacts may arise as a result of high magnetisation at the transition of different tissues. However, due to few outlier SNR values in questionable and SPIO artefacts, it was not possible to define a fixed

(a)

(b)

(c)
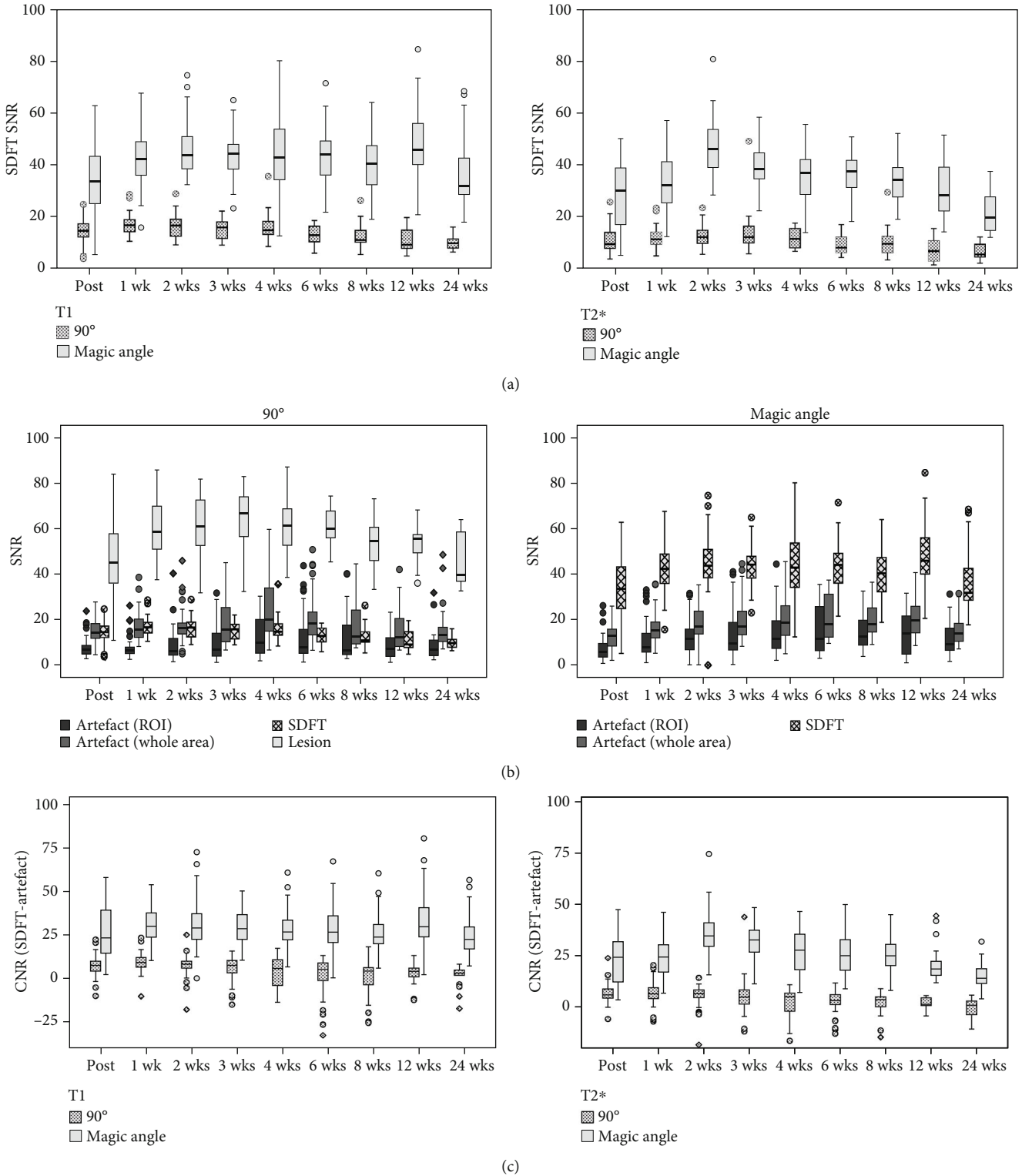
Figure 4: Signal-to-noise ratio (SNR) and contrast-to-noise ratio (CNR) in standard and magic angle images. (a) Boxplots illustrating significantly higher SDFT SNR in magic angle images ($\theta = 55°$) compared to standard images ($\theta = 90°$) in T1- and T2∗-weighted sequences and at all time points ($P < 0.001$). (b) Boxplots displaying the SNR of the artefact ROI, artefact of the whole area, SDFT, and lesion (only in standard images) in T1-weighted sequences over time. The SNR of hypointense artefacts and SDFT in standard images are similar, making it challenging to distinguish hypointense artefacts from healthy tendon tissue. In contrast, in the magic angle images, SDFT SNR was significantly higher than artefact SNR ($P < 0.001$). Lesion SNR in standard images was significantly higher than artefact SNR as well ($P < 0.001$). (c) Boxplots illustrating the significantly higher CNR between SDFT and artefact in magic angle images compared to standard images in both T1- and T2∗-weighted sequences and at all time points ($P < 0.001$). Circles and rhombs display outlier values; wk: week.

(a)

(b)
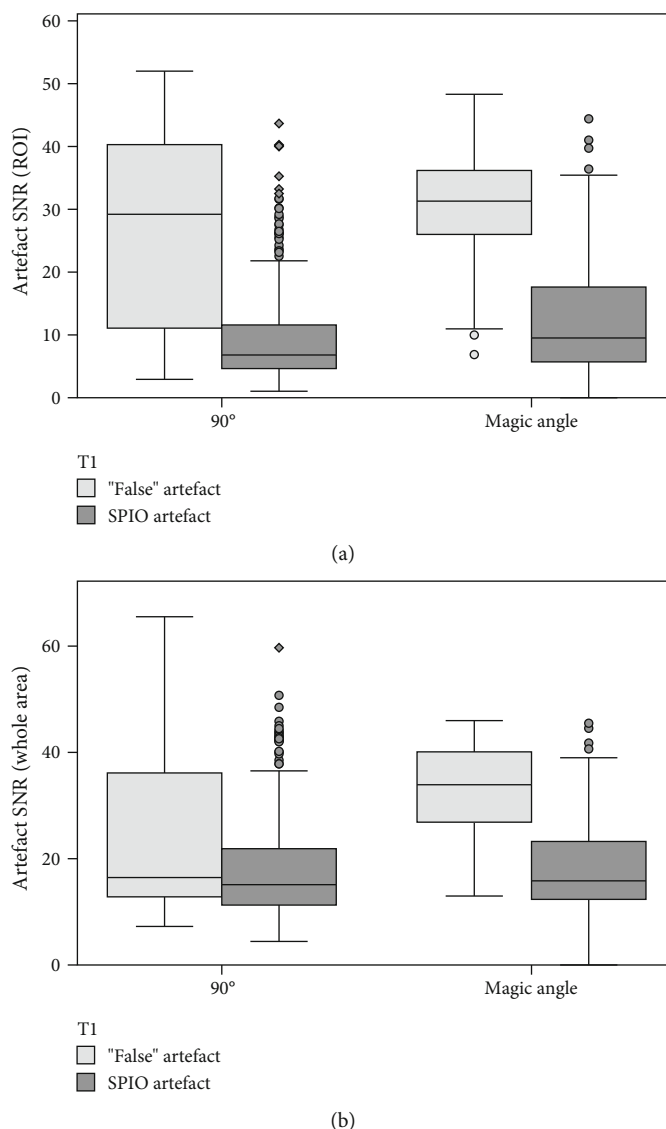
FIGURE 5: Differences in signal-to-noise ratio (SNR) between SPIO or "false" artefacts. Boxplots exhibiting the comparison of artefact SNR in images categorized as 1 ("hypointense area most likely related to SPIO"=SPIO artefact) and 2 ("questionable hypointense area"="false" artefact) in T1-weighted sequences obtained at $\theta = 90°$ or magic angle ($\theta = 55°$). It shows that the artefact SNR of the ROI (a) and area (b) in the potentially false-positive category 2 images was not as low as in the category 1 images ($P < 0.001$). However, a threshold SNR value for the discrimination of true SPIO artefacts and other hypointense artefacts was not definable. Circles and rhombs display outlier values; different assessment time points are summarized.

threshold SNR value delimiting true SPIO artefacts in standard and magic angle MRI images. Possibly, these outlier values in SPIO artefacts were caused by the partial-volume effect in MRI images which leads to the interference of signals and which can therefore increase the SI of especially small artefact areas. Regarding the lack of significant differences between artefact volume, it is a surprising finding and underlines that subjective discrimination of artefacts works well in most cases (as also shown by the subjective artefact categorization). However, the magic angle effect is still very useful in challenging cases.

To confirm that artefacts seen in MRI correspond to SPIO-labelled cells, histology can be considered as a gold standard technique [7, 14, 15]. In the current study, histology

showed that SPIO particles were present and localised in vital, spindle-shaped cells up to week 24 (Figure 6), as described in more detail previously [19]. However, while histology remains the most reliable method to validate MRI results, it is obviously not suitable for longitudinal in vivo tracking. Therefore, using MRI to obtain standard as well as magic angle image series, cell tracking was feasible over a long period of 24 weeks. Yet, it should be acknowledged that low-field MRI, despite using the magic angle technique, is not suitable to detect small numbers of labelled cells. Using low-field MRI, 100,000 SPIO-labelled MSC were visible in agar gel but lower concentrations can certainly not be distinguished [8]. The cell concentrations in the tendon decrease over time which is represented by the decreasing artefact
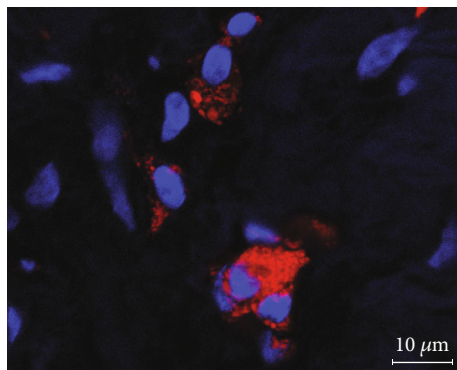
FIGURE 6: Fluorescence microscopy. Representative image of a tendon lesion 24 weeks after injection of SPIO-labelled MSC with red rhodamine B fluorescence of iron oxide particles and blue DAPI staining of nuclei.

volume in MRI and the examination of the histological sections [7, 19]. Besides this, there were different in vivo studies about longitudinal cell tracking of SPIO-labelled MSC in tendons with a detection period of 8 and 9 weeks but without further follow-up [7, 8] and in joints with a detection period of 12 weeks without further follow-up [22].

One limitation of this study was the use of a low-field MRI system, leading to reduced image resolution, relatively wide slice thickness, and risk of motion artefacts. However, due to the 1% risk of mortality, general anaesthesia required for examinations of horses in high-field systems is a major disadvantage [23]. Moreover, the recovery phase may lead to high strains within the SDFT, leading to a possible negative effect on tendon healing. Therefore, particularly for studies involving repeated examinations as well as examining equine patients, the use of standing low-field MRI with a lower risk for the animals is favourable.

5. Conclusion

In conclusion, in vivo magic angle imaging has not been described in large animals. The current data show for the first time that the approach is feasible in the horse, which is of high interest for future in vivo studies. At the same time, the results demonstrate the advantages of using the technique in practical implementation for long-term cell tracking.

Data Availability

The data used to support the findings of this study are available from the corresponding author upon request.

Conflicts of Interest

Each author certifies that he or she has no commercial associations that might pose a conflict of interest in connection with the submitted article.

Acknowledgments

References

[1] Y. Kasashima, T. Takahashi, R. K. W. Smith et al., "Prevalence of superficial digital flexor tendonitis and suspensory desmitis in Japanese thoroughbred flat racehorses in 1999," *Equine Veterinary Journal*, vol. 36, no. 4, pp. 346–350, 2004.

[2] C. T. Thorpe, P. D. Clegg, and H. L. Birch, "A review of tendon injury: why is the equine superficial digital flexor tendon most at risk?," *Equine Veterinary Journal*, vol. 42, no. 2, pp. 174–180, 2010.

[3] M. Bydder, A. Rahal, G. D. Fullerton, and G. M. Bydder, "The magic angle effect: a source of artifact, determinant of image contrast, and technique for imaging," *Journal of Magnetic Resonance Imaging*, vol. 25, no. 2, pp. 290–300, 2007.

[4] A. Oatridge, A. H. Herlihy, R. W. Thomas et al., "Magnetic resonance: magic angle imaging of the Achilles tendon," *The Lancet*, vol. 358, no. 9293, pp. 1610-1611, 2001.

[5] A. Oatridge, A. Herlihy, R. W. Thomas et al., "Magic angle imaging of the Achilles tendon in patients with chronic tendonopathy," *Clinical Radiology*, vol. 58, no. 5, pp. 384–388, 2003.

[6] M. Spriet, B. Murphy, S. A. Vallance, M. A. Vidal, M. B. Whitcomb, and E. R. Wisner, "Magic angle magnetic resonance imaging of diode laser induced and naturally occurring lesions in equine tendons," *Veterinary Radiology & Ultrasound*, vol. 53, no. 4, pp. 394–401, 2012.

[7] F. Geburek, K. Mundle, S. Conrad et al., "Tracking of autologous adipose tissue-derived mesenchymal stromal cells with in vivo magnetic resonance imaging and histology after intralesional treatment of artificial equine tendon lesions—a pilot study," *Stem Cell Research & Therapy*, vol. 7, no. 1, p. 21, 2016.

[8] D. Berner, W. Brehm, K. Gerlach et al., "Longitudinal cell tracking and simultaneous monitoring of tissue regeneration after cell treatment of natural tendon disease by low-field magnetic resonance imaging," *Stem Cells International*, vol. 2016, Article ID 1207190, 13 pages, 2016.

[9] R. K. W. Smith, M. Korda, G. W. Blunn, and A. E. Goodship, "Isolation and implantation of autologous equine mesenchymal stem cells from bone marrow into the superficial digital flexor tendon as a potential novel treatment," *Equine Veterinary Journal*, vol. 35, no. 1, pp. 99–102, 2003.

[10] R. K. W. Smith, N. J. Werling, S. G. Dakin, R. Alam, A. E. Goodship, and J. Dudhia, "Correction: Beneficial effects of autologous bone marrow-derived mesenchymal stem cells in naturally occurring tendinopathy," *PLoS One*, vol. 8, no. 10, 2013.

[11] A. Crovace, L. Lacitignola, G. Rossi, and E. Francioso, "Histological and immunohistochemical evaluation of autologous cultured bone marrow mesenchymal stem cells and bone marrow mononucleated cells in collagenase-induced tendinitis of equine superficial digital flexor tendon," *Veterinary Medicine International*, vol. 2010, Article ID 250978, 10 pages, 2010.

[12] J. Burk, D. Berner, I. Erbe, J. Offhaus, K. Winter, and W. Brehm, "MRI of superparamagnetic iron oxide-labeled mesenchymal stromal cells in tendon tissue using the magic-angle effect," *Regenerative Medicine*, vol. 8, no. 6, p. 69, 2013.

[13] C. E. Sherlock and T. S. Mair, "Magic angle effect on low field magnetic resonance images in the superficial digital flexor tendon in the equine proximal pastern region," *Veterinary Journal*, vol. 217, pp. 126–131, 2016.

[14] Y. Yang, J. Zhang, Y. Qian et al., "Superparamagnetic iron oxide is suitable to label tendon stem cells and track them in vivo with MR imaging," *Annals of Biomedical Engineering*, vol. 41, no. 10, pp. 2109–2119, 2013.

[15] A. Scharf, S. Holmes, M. Thoresen, J. Mumaw, A. Stumpf, and J. Peroni, "Superparamagnetic iron oxide nanoparticles as a means to track mesenchymal stem cells in a large animal model of tendon injury," *Contrast Media & Molecular Imaging*, vol. 10, no. 5, pp. 388–397, 2015.

[16] C. Gittel, J. Burk, C. Horstmeier, and W. Brehm, "Assessment of pain scoring systems in horses following induced orthopaedic pain," *Veterinary Anaesthesia and Analgesia*, vol. 42, no. 1, p. A39, 2014.

[17] A. Hillmann, A. B. Ahrberg, W. Brehm et al., "Comparative characterization of human and equine mesenchymal stromal cells: a basis for translational studies in the equine model," *Cell Transplantation*, vol. 25, no. 1, pp. 109–124, 2016.

[18] W. Brehm, J. Burk, and U. Delling, "Application of stem cells for the treatment of joint disease in horses," in *Animal Models for Stem Cell Therapy. Methods in Molecular Biology (Methods and Protocols), vol 1213*, B. Christ, J. Oerlecke, and P. Stock, Eds., pp. 215–228, Humana Press, New York, NY, USA, 2014.

[19] J. Burk, D. Berner, W. Brehm et al., "Long-term cell tracking following local injection of mesenchymal stromal cells in the equine model of induced tendon disease," *Cell Transplantation*, vol. 25, no. 12, pp. 2199–2211, 2016.

[20] R. K. W. Smith and C. W. Mcilwraith, "Consensus on equine tendon disease: building on the 2007 Havemeyer symposium," *Equine Veterinary Journal*, vol. 44, no. 1, pp. 2–6, 2012.

[21] D. J. Guest, M. R. W. Smith, and W. R. Allen, "Monitoring the fate of autologous and allogeneic mesenchymal progenitor cells injected into the superficial digital flexor tendon of horses: preliminary study," *Equine Veterinary Journal*, vol. 40, no. 2, pp. 178–181, 2008.

[22] U. Delling, W. Brehm, M. Metzger, E. Ludewig, K. Winter, and H. Jülke, "In vivo tracking and fate of intra-articularly injected superparamagnetic iron oxide particle-labeled multipotent stromal cells in an ovine model of osteoarthritis," *Cell Transplantation*, vol. 24, no. 11, pp. 2379–2390, 2015.

[23] G. M. Johnston, J. K. Eastment, J. L. N. Wood, and P. M. Taylor, "The confidential enquiry into perioperative equine fatalities (CEPEF): mortality results of phases 1 and 2," *Veterinary Anaesthesia and Analgesia*, vol. 29, no. 4, pp. 159–170, 2002.

Research Article

Autologous Microfragmented Adipose Tissue Reduces the Catabolic and Fibrosis Response in an In Vitro Model of Tendon Cell Inflammation

Marco Viganò [iD],[1] **Gaia Lugano,**[1] **Carlotta Perucca Orfei** [iD],[1] **Alessandra Menon** [iD],[2,3]
Enrico Ragni,[1] **Alessandra Colombini,**[1] **Paola De Luca,**[1] **Pietro Randelli** [iD],[2,3]
and Laura de Girolamo [iD][1]

[1]*Orthopedics Biotechnology Lab, IRCCS Istituto Ortopedico Galeazzi, Milan, Italy*
[2]*Laboratory of Applied Biomechanics, Department of Biomedical Sciences for Health, Università degli Studi di Milano, Via Mangiagalli 31, 20133 Milan, Italy*
[3]*1st Clinica Ortopedica, ASST Centro Specialistico Ortopedico Traumatologico Gaetano Pini-CTO, Piazza Cardinal Ferrari 1, 20122 Milan, Italy*

Correspondence should be addressed to Carlotta Perucca Orfei; carlotta.perucca@grupposandonato.it

Background. Mesenchymal stem cells (MSCs) emerged as a promising therapy for tendon pathologies. Microfragmented adipose tissue (μFAT) represents a convenient autologous product for the application of MSC-based therapies in the clinical setting. In the present study, the ability of μFAT to counteract inflammatory processes induced by IL-1β on human tendon cells (TCs) was evaluated. *Methods.* Cell viability and proliferation were evaluated after 48 hours of transwell coculture of TCs and autologous μFAT in the presence or absence of IL-1β. Gene expression of scleraxis, collagen type I and type III, metalloproteinases-1 and -3, and cyclooxygenase-2 was evaluated by real-time RT-PCR. The content of VEGF, IL-1Ra, TNFα, and IL-6 was evaluated by ELISA. *Results.* IL-1β-treated TCs showed augmented collagen type III, metalloproteases, and cyclooxygenase-2 expression. μFAT was able to reduce the expression of collagen type III and metalloproteases-1 in a significant manner, and at the same time, it enhanced the production of VEGF, IL-1Ra, and IL-6. *Conclusions.* In this in vitro model of tendon cell inflammation, the paracrine action of μFAT, exerted by anti-inflammatory molecules and growth factors, was able to inhibit the expression of fibrosis and catabolic markers. Then, these results suggest that the application of μFAT may represent an effective conservative or adjuvant therapy for the treatment of tendon disorders.

1. Introduction

Tendon disorders represent a common condition in the field of musculoskeletal injuries. Current treatment options often lead to unsatisfactory results, with persistence of pain and reduced physical activity level [1, 2]. Among the conservative approaches, the use of mesenchymal stem cells (MSCs) from the bone marrow and adipose tissue emerged as a promising treatment, capable to counteract the pathological processes characterizing degenerative disease in the orthopedic field [3], gathering interest also in the treatment of tendon disor-

ders. Indeed, successful applications of cultured MSCs were described for the treatment of tendon injuries in preclinical models [4]. The use of adipose-derived stem cells (ASCs), or autologous adipose-derived products, already showed efficacy in the context of tendon disorders in clinical and preclinical trials [5–8]. In vitro investigations demonstrated that the coculture of ASCs or μFAT improved proliferation, viability, and collagen and VEGF production in tendon cells (TCs) [9, 10]. In addition, in an in vitro model of TC inflammation, cultured adipose-derived MSCs were able to reduce the production of proinflammatory mediators [11]. Never-

theless, translation of MSC-based therapies implies extensive manipulation for the production of cells in good manufacturing practice (GMP) conditions and it is limited by the high costs of production and the regulatory issues related to the advanced therapy medicinal products [12, 13]. As a consequence, different solutions for adipose- and bone marrow-derived MSC isolation at the point of care have been proposed in recent years, with encouraging results [5, 14]. In particular, microfragmented adipose tissue (μFAT) represents a convenient compromise for the exploitation of MSCs in the clinical practice, avoiding extensive cell manipulation, and culture expansion [15]. μFAT is easily obtained by commercially available devices from autologous lipoaspirate, and it has been demonstrated to exert a therapeutic activity in clinical and preclinical settings, providing positive functional outcomes in particular for the treatment of knee osteoarthritis [16–20]. The procedure of μFAT production and injection is compatible with a single-stage surgery and may be combined with different surgical procedures. The aim of the present study was to investigate the paracrine effect of μFAT on the proinflammatory and catabolic response of TCs to tnterleukin-1β- (IL-1β-) mediated inflammation. This molecule has been described as the primary mediator of the inflammatory status preventing tissue healing in rotator cuff injury [21], and previous reports showed that IL-1β-treated TCs upregulated the expression of catabolic enzymes and the production of inflammatory cytokines [22–24]. Thus, the working hypothesis of the present study is that autologous μFAT would counteract the catabolic and proinflammatory response elicited by IL-1β on TCs, providing insights on the mechanism of action of this therapeutic approach and strengthening the rationale of its use in tendon disorders.

2. Materials and Methods

2.1. TCs and μFAT Isolation and Harvesting.

Long head of biceps tendon biopsies and μFAT were collected from 8 patients (5 females and 3 males, mean age: 60 ± 10 y/o) undergoing arthroscopic rotator cuff repair augmented with μFAT. An informed consent was obtained from all patients as per the protocol approved by the Institutional Review Board (no. 148/INT/2015, January 13, 2016). Lipoaspirate adipose tissue was collected before surgery and processed by Lipogems® device, following the manufacturer's instruction [25]. An aliquot of μFAT was harvested for in vitro experiments. Briefly, each μFAT sample was centrifuged at $376 \times g$ for 5 minutes at room temperature to separate the aqueous phase and the fragmented tissue. The former was stored at -20°C, while the latter was frozen at -80°C after the addition of 1 volume of freezing solution (90% FBS, 10% dimethyl sulfoxide; Sigma-Aldrich, St. Louis, MO, USA). Separation of the two phases was adopted to maintain the composition of injected μFAT even after thawing and removal of the aqueous freezing solution. This allowed for the use in the experiment of an identical product as injected during the surgical procedure.

Human tendon cells (TCs) were isolated from long head of the biceps tendon biopsies obtained during arthroscopic rotator cuff repair. Tendon tissue was digested with a 0.3%

w/v collagenase type I solution (Worthington, Lakewood, NJ, USA) for 16 hours at 37°C, as previously reported [26]. TCs were cultured in a complete medium composed by high-glucose Dulbecco's modified Eagle's medium (DMEM; Sigma-Aldrich) with 10% v/v fetal bovine serum (FBS; Euroclone, Pero, Italy), 100 U/ml penicillin, 100 μg/ml streptomycin, 0.29 mg/ml L-glutamine (Gibco, Waltham, MA, USA), and 5 ng/ml bFGF (Peprotech, London, UK). The medium was replaced every 3 days, and all the experiments have been performed at passage 3. After culture, TCs represent a mixed population of terminally differentiated and tendon progenitor cells at different stages of differentiation, as previously reported [26, 27].

2.2. Treatment of TCs with IL-1β and Coculture with μFAT.

TCs were seeded in 12-well plates at the density of 50000 cells/well. TCs were either maintained in normal culture medium or a medium added of 1 ng/ml IL-1β. In addition, cells treated with IL-1β and untreated cells were cocultured with 250 μl of μFAT, made of 125 μl of microfragmented tissue and 125 μl of the corresponding aqueous phase. The two phases were separated in order to maintain the aqueous part of μFAT, even after thawing and removal of the freezing solution. μFAT was added to the top portion of a transwell insert (pore size: 0.4 μm), while TCs were seeded on the bottom. Equal volume of phosphate-buffered saline (PBS) was added in the transwell top portion of the samples without μFAT. After 48 hours of treatment, the culture media were collected and stored at -20°C, while cells were trypsinized and the pellets stored at -80°C.

2.3. RNA Isolation and Gene Expression.

RNA was obtained from cell pellets using TRI reagent (Sigma-Aldrich). Briefly, cells were lysed by the addition of 300 μl TRI reagent, and then 100 μl of 1-bromo-3-chloropropane (Sigma-Aldrich) were added to the samples. After centrifugation at $12000 \times g$ for 10 minutes, the interphase was collected for DNA extraction while the RNA in the aqueous phase was precipitated with isopropanol, washed in 75% ethanol and then resuspended in 20 μl RNAse-free water for storage at -80°C.

Total RNA from each sample was transcribed to cDNA using iScript™ cDNA Synthesis Kit (Bio-Rad Laboratories, Hercules, CA, USA) as per manufacturer's instructions. Real-time PCR was performed starting from 10 ng of cDNA, using a PCR mix containing TaqMan® Universal PCR Master Mix and Assays-on-Demand Gene expression probes (Life Technologies, Waltham, MA, USA) for *SCX* (scleraxis; Hs03054634_g1), *COL1A1* (collagen type I alpha 1 chain; Hs01076777_m1), *COL3A1* (collagen type III alpha 1 chain; Hs00943809_m1), *MMP1* (metalloproteinase-1; Hs00899658_m1), *MMP3* (metalloproteinase-3; Hs00968305_m1), and *PTGS2* (cyclooxygenase-2; Hs00153133_m1). Applied Biosystems StepOnePlus® (Life Technologies) was used to perform all experiments (program: 1 cycle of 2 minutes at 50°C, 1 cycle of 10 minutes at 95°C, 40 cycles of 15 seconds at 95°C, and 1 minute at 60°C). The results were normalized against the mean expression of two housekeeping genes: *YWHAZ* (tyrosine 3-monooxygenase/tryptophan 5-monooxygenase activation

(a)

(b)
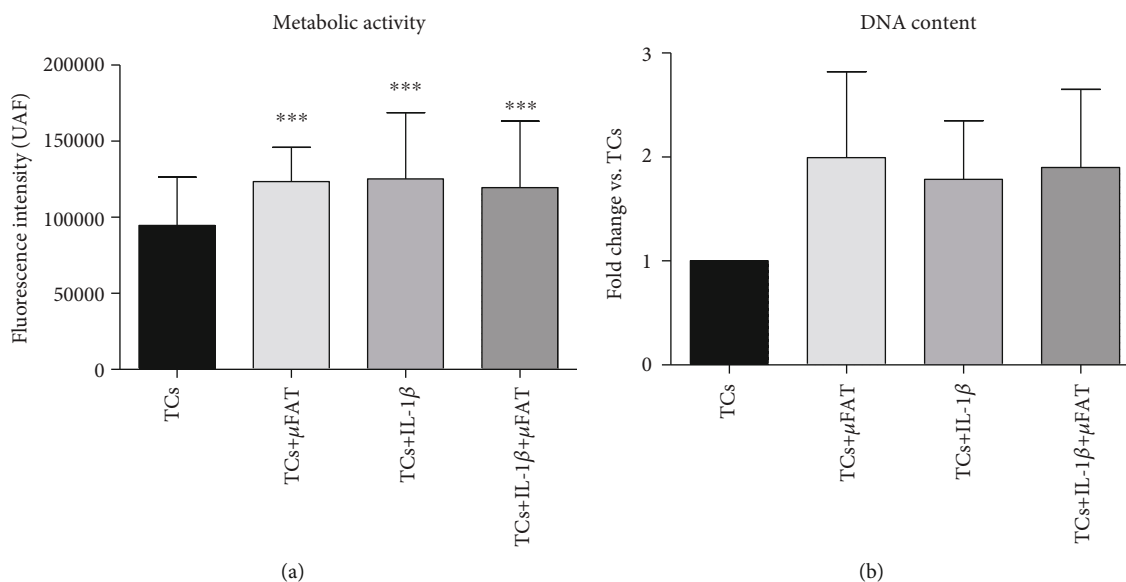
Figure 1: Metabolic activity (a) and DNA content (b) of untreated and differently treated TC samples ($n = 8$). $^*p < 0.05$, $^{***}p < 0.001$ vs. TCs.

protein zeta, Hs03044281_g1) and *ACTB* (β-actin, Hs99999903_m1) identified in a previous study [28]. Two replicates were analyzed for each sample, and data were presented according to the $\Delta\Delta$**Ct** method [29].

2.4. DNA Isolation and Quantification. DNA was separated from the interphase (obtained as described above) by the addition of 100% ethanol and centrifugation at $2000 \times g$ for 5 minutes. The DNA pellet was washed in 0.1 M trisodium citrate, 10% ethanol solution for 30 minutes, and then centrifuged at $2000 \times g$ for 5 minutes. DNA was then washed in 75% ethanol, and solubilized in $50\,\mu$l 8 mM NaOH for storage at -20°C. DNA content in each sample was measured by NanoDrop spectrophotometer at 260 nm absorbance using software version 3.7.1 (NanoDrop ND-1000, Thermo-Fisher Scientific) [30].

2.5. TC Metabolic Activity. Viability was assessed by alamarBlue assay after 48 hours of treatment (ThermoFisher Scientific, Waltham, MA, USA). Briefly, culture medium was removed and cells were incubated with a 10% *v/v* solution of alamarBlue in DMEM at 37°C. After 2 hours of incubation, fluorescence was measured by a spectrophotometer (Victor X3, Perkin Elmer, Waltham, MA, USA) with excitation of 540 nm and emission of 590 nm.

2.6. ELISA. The release of interleukine-6 (IL-6), interleukine-1 receptor antigen (IL-1Ra), tumor necrosis factor α (TNFα) (Peprotech), and vascular endothelial growth factor (VEGF) (R&D Systems, Minneapolis, MN, USA) in the culture media of TCs treated for 48 hours was analyzed by ELISA assays, following the manufacturer's instruction. The detection ranges were as follows: 24–1500 pg/mL for IL-6, 23–1500 pg/mL for IL-1Ra, 31–2000 pg/ml for TNFα, and 31.3-2000 pg/ml for VEGF.

2.7. μFAT Cell Count and Viability Assays. After thawing, an aliquot of μFAT was digested by 0.075% *w/v* collagenase type

I (Worthington) for 45 minutes at 37°C. The number of cells and viability was assessed by NucleoCounter NC-3000 using cell viability staining (Chemometech, Allerod, Denmark) [31]. The μFAT samples used in the study had a mean cell count of $2.3 \pm 1.3 \times 10^6$ cells/ml, while cell viability was $53.2 \pm 13.1\%$.

2.8. Statistical Analysis. All the analyses were performed using Prism 5.0 (Graphpad Software, La Jolla, CA, USA). Gaussian distribution of data was assessed by Shapiro-Wilk test. One-way repeated measures ANOVA test with Bonferroni's post test was applied to measure the differences among treatments when data presented a Gaussian distribution (Figures 1(a), 2(b), and 2(c)); otherwise, the Friedman's test with Dunn's post-test was used (Figures 1(b), 2(a), and 3). A level of $p < 0.05$ was considered statistically significant.

3. Results

3.1. IL-1β and μFAT Enhance TC Metabolic Activity. The metabolic activity of IL-1β-treated TCs was significantly increased with respect to untreated TCs ($p < 0.01$), and no further improvement was induced by the coculture with μFAT. In noninflammatory conditions, samples cocultured in transwell with μFAT demonstrated a higher metabolic activity with respect to untreated TCs ($p < 0.05$) (Figure 1(a)). DNA content resulted in increased in all conditions, even if in a nonsignificant manner (Figure 1(b)).

3.2. μFAT Reduces the Gene Expression of Catabolic and Fibrosis Markers. The presence of IL-1β significantly enhanced the TC expression of *SCX* ($p < 0.05$), *MMP1* ($p < 0.01$), *MMP3* ($p < 0.01$), *COL3A1* ($p < 0.001$), and *PTGS2* ($p < 0.01$) with respect to untreated TCs, while it did not exert any effect on *COL1A1* expression (Figure 3). In this inflammatory condition, the coculture with μFAT decreased the expression of *COL3A1* (-57%, $p < 0.001$) and

(a)

(b)

(c)
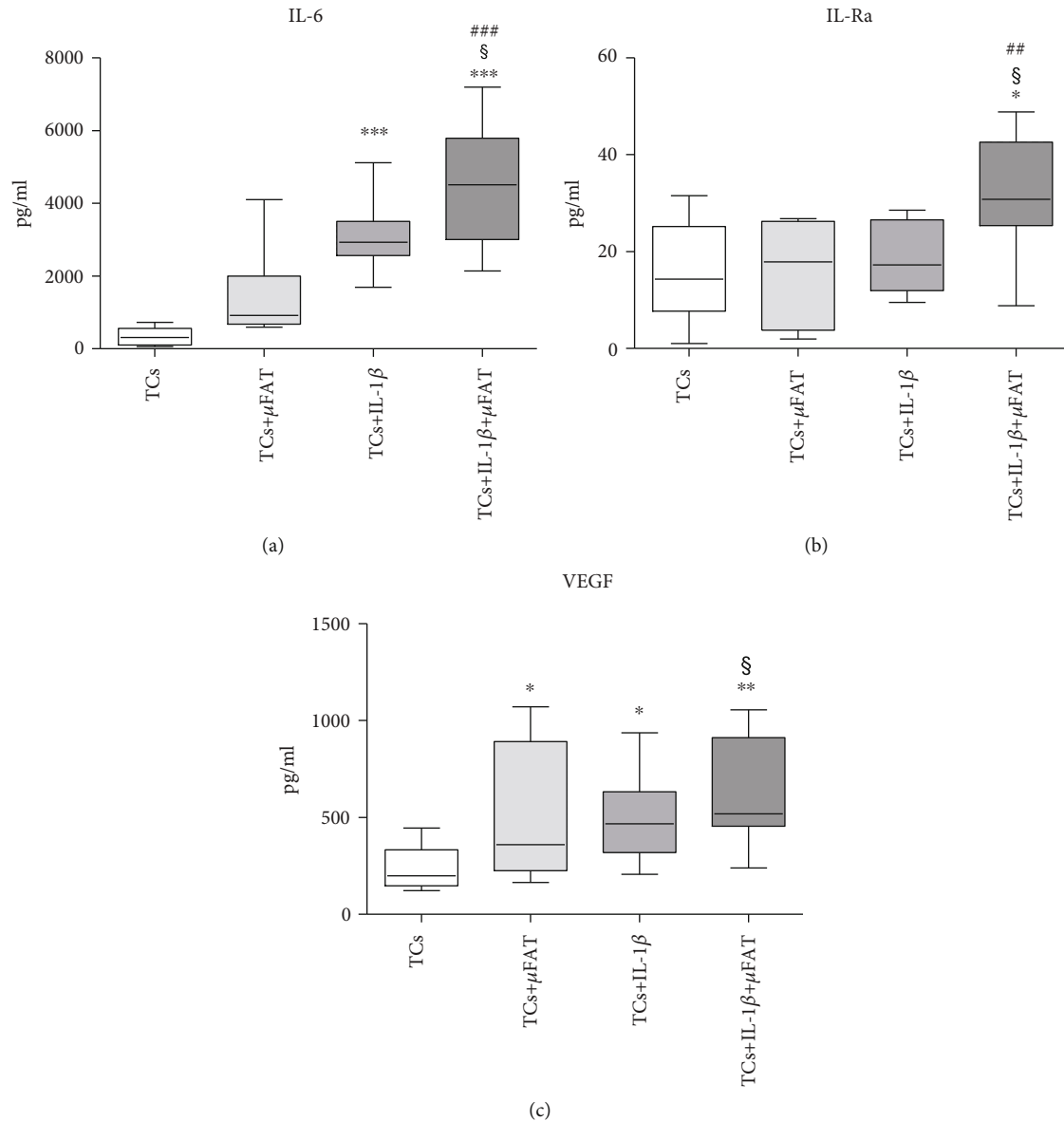
FIGURE 2: IL-1Ra, IL-6, and VEGF quantification in culture media of TCs treated with IL-1β and/or μFAT and untreated TCs ($n = 8$). $^*p < 0.05$, $^{**}p < 0.01$, $^{***}p < 0.001$ vs. TCs; $^{\#\#}p < 0.01$, $^{\#\#\#}p < 0.001$ vs. +μFAT; $^{\S}p < 0.05$ vs. +IL-1β.

MMP1 (-41%, $p = 0.08$) (Figures 3(c) and 3(d)), with little effect on the other parameters. No effect of μFAT on *MMP3* expression was observed, while it was strongly induced by IL-1β treatment (Figure 3(e)). Moreover, TCs cocultured with μFAT, with or without IL-1β, showed a reduced expression of *COL1A1* with respect to untreated TCs ($p = 0.06$ and $p < 0.001$ in the presence or absence of IL-1β, respectively) (Figure 3(b)). A slight increase in *SCX* expression was observed in TCs cocultured with μFAT and treated with IL-1β, with respect to IL-1β only treated cells (+12%, n.s.) (Figure 3(a)).

A fivefold increase in overall *COL3A1/COL1A1* expression ratio was observed in IL-1β-treated TCs with respect to untreated TCs ($p < 0.05$, data not shown). In inflammatory conditions (+IL-1β), the coculture with μFAT was able to reduce the ratio, even if in a nonstatistically significant

manner (-27%, n.s.), while in TCs+μFAT, the ratio was increased in a nonsignificant manner in comparison to untreated TCs samples, in both inflammatory and noninflammatory conditions.

3.3. Il-1β and μFAT Enhance the Production of Cytokines and VEGF. In the presence of IL-1β, an enhanced production of IL-6 ($p < 0.001$) was observed with respect to untreated TCs, and it was further increased by the coculture with μFAT (+45%, $p < 0.05$ with respect to TCs+IL-1β) (Figure 2(a)). On the contrary, IL-1Ra production was not induced by IL-1β or μFAT alone, while the contemporary presence of these factors significantly increased the production of this molecule (+217% and +290%, with respect to both untreated TCs and IL-1β-treated TCs; $p < 0.05$) (Figure 2(b)). The production of VEGF was induced by IL-1β (+109% with respect to

(a)

(b)

(c)

(d)

(e)

(f)
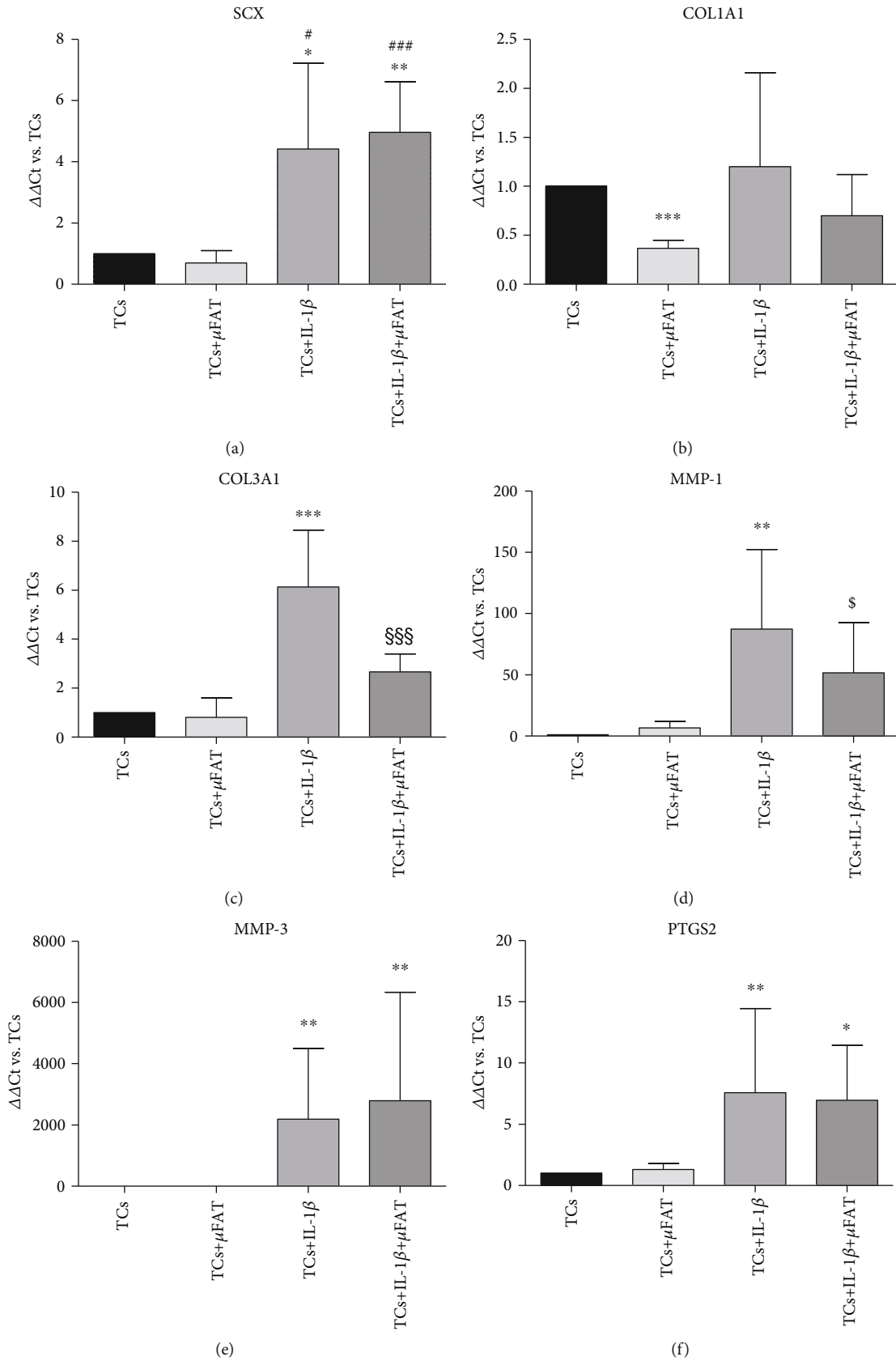
FIGURE 3: Gene expression of *SCX*, *COL1A1*, *COL3A1*, *MMP1*, *MMP3*, and *PTGS2* in TCs cultured in the presence of IL-1β and/or μFAT ($n = 8$). Data are expressed as mean $\Delta\Delta$Ct with respect to untreated controls (TCs = 1). $^*p < 0.05$, $^{**}p < 0.01$, $^{***}p < 0.001$ vs. TCs; $^\#p < 0.05$, $^{\#\#\#}p < 0.001$ vs. +μFAT; $^{\S\S\S}p < 0.001$ vs. +IL-1β; $^\$p < 0.1$ vs. +IL-1β (tendency).

untreated cells, $p < 0.05$) or μFAT coculture (+116% with respect to untreated cells, $p < 0.05$); the combination of both factors further increased VEGF production (+29% in comparison with TCs treated with IL-1β, $p < 0.05$) (Figure 2(c)). The content of TNFα was undetectable in all samples (data not shown).

4. Discussion

The present study aimed to test the ability of autologous μFAT in favouring tissue healing in the context of tendon cell inflammation. Our results demonstrated that the paracrine action of μFAT effectively reduces the expression of catabolic and fibrosis markers in pair-matched TCs cultured in inflammatory conditions. The strength of this work is the use of patient-matched TCs and μFAT, allowing for taking into account the inter-donor variability in both elements.

More in details, in cells exposed to IL-1β, the paracrine action of μFAT was able to significantly reduce the *COL3A1/-COL1A1* ratio which positively correlates with the deposition of rupture-prone fibrotic tendon matrix [32, 33], confirming previous findings obtained in cocultures of TCs and adipose-derived MSCs [34, 35]. IL-1β has been described as the key effector of tendon inflammation leading to the inhibition of the proper healing process [21, 23, 24], also enhancing the production of catabolic enzymes such as MMP1 and MMP3 involved in tendon matrix degradation [36, 37], and increasing collagen type III expression over collagen type I. Moreover, IL-1β directly induces the production of the enzyme cyclooxygenase-2 (COX-2), typical marker of inflammation [38]. Interestingly, cells cultured in inflammatory condition in presence of μFAT showed an overall reduction of the absolute expression of both collagen type I and III. The increase in collagen type III after injury is associated with the formation of scar tissue, which allows for prompt healing at the expense of tissue quality and functionality [39, 40]. In this view, a slower matrix deposition, where the proportion between the different types of collagen is similar to the physiological level, represents a therapeutic goal aimed to improve the quality of regenerated tissue.

In addition, μFAT was able to inhibit *MMP1* expression, suggesting a protective role towards tendon ECM integrity. Metalloproteases are crucial for the physiological maintenance of tendon extracellular matrix (ECM) homeostasis [41], to the extent that the inhibition of MMPs results in pathological changes and pain [42]. On the other hand, an excess of MMP expression is associated with aberrant matrix degradation, typical of degenerative tendon disorders [43]. In particular, MMP1 is clearly involved in tendon pathology in association with the action of IL-1β [44, 45]. The effect of μFAT on MMP expression is consistent with previous observations reported in a model of inflamed synoviocytes, supporting the inhibition of MMP-related matrix degradation as a mechanism of action of this product [46]. Moreover, when inflammatory processes are not involved, μFAT has little effect on the expression of MMPs, indicating that it would not inhibit the physiological remodeling of tendon ECM.

In this study, the influence of IL-1β on the expression of the tendon-specific transcription factor *SCX* was also assessed. While previous reports showed an inhibition of its transcription in inflammatory conditions [23, 47, 48], in our model, the presence of IL-1β significantly increased *SCX* expression. The discrepancy between the results described in literature and those reported in the present study is probably due to the different sources of TCs and to the inflammatory protocol. Since adipose-derived MSCs are known to produce trophic mediator-specific for TCs [49], a slight reduction of *SCX* expression was observed when TCs were cocultured with μFAT in basal conditions, and a downregulation of this marker have been already reported by other authors after TCs-MSCs coculture [34]. These observations suggest that μFAT (or MSCs) trophic action on TCs may be independent of *SCX* upregulation.

Our findings showed no effect of μFAT on *PTGS2* expression, neither in inflammatory nor in noninflammatory conditions. As expected, *PTGS2* transcription was enhanced by IL-1β treatment with respect to basal conditions, being IL-1β the main inducer of this gene encoding for COX2 [38]. Despite its role in inflammation, COX2 has been reported exerting an important role in the maintenance of tendon homeostasis and ECM maturation [50, 51]. Therefore, the expression of this enzyme may represent not only as a symptom of inflammation but also as a response of TCs towards tissue healing.

IL-1β and μFAT both demonstrated an enhancing effect on TC metabolic activity and DNA content, even if no statistical significance was found for the latter. Interestingly, this effect was not further enhanced by the use of IL-1β on TCs cocultured with μFAT, showing a lack of additive/synergistic action of the two elements on these parameters.

In our model, due to the use of a transwell system, the modifications induced by μFAT on TC gene expression and metabolic activity are ascribed to its paracrine activity. In particular, μFAT increased the content of soluble IL-1Ra, IL-6, and VEGF in the culture medium. IL-1Ra is a direct inhibitor of IL-1β, and it acts by competing with the cytokines for the binding to IL-1 receptor 1 [52], to the extent that IL-1Ra-based treatments have been developed for rheumatoid arthritis and other autoinflammatory diseases [53]. IL-1Ra production was elicited in μFAT samples only in the presence of inflammatory conditions, suggesting it is a reaction of the μFAT-embedded adipose-derived MSCs to this condition. Indeed, these cells are known to respond to IL-1β stimulation by releasing IL-1Ra [54], as well as MSCs from other sources [55].

As expected, in our model, the content of IL-6 was enhanced in the presence of IL-1β [56] and μFAT further increased its production. This effect is possibly related to the IL-1β-mediated induction of IL-6 in the cells contained in μFAT [54], and even if there are little evidences of direct pathological changes mediated by IL-6 on TCs and tendon matrix production [57], this aspect should be taken into account as a possible side effect when applying cell-based regenerative medicine products. The role of IL-6 in tendon pathologies has been confirmed by several studies, and it is considered one of the evidences of inflammation involvement in tendinopathy [58]. Indeed, IL-6 increased after tears and ruptures, as well as after intense exercise and injuries, in

both humans and animals [59]. Nevertheless, despite its role in inflammation, IL-6 exhibits an immunoregulatory activity and it demonstrated to support tenocyte proliferation and survival, thus resulting among the effectors of the early phases of tendon healing [60–62]. In addition, IL-6 induces the production of VEGF [63], a growth factor mainly known for its role in angiogenesis, that is also involved in tissue regeneration, exerting a homeostatic function [64]. Different to what is observed in IL-6, VEGF is induced by both IL-1β and μFAT treatments at similar intensities, and it was further enhanced by the combination of these factors. Then, since IL-6 was just slightly enhanced by μFAT treatment in comparison to untreated TCs, the μFAT-induced VEGF production appears to be at least partially independent from the IL-6 pathway. Despite the promotion of angiogenesis which may result detrimental for tendon ECM integrity [65], VEGF was able to improve tendon healing strength in several studies [66–68].

The ability of MSCs and μFAT paracrine mediators to counteract inflammation is well described, and it has been reported in several models involving different cells and tissues, comprising chondrocytes, synoviocytes, and the central nervous system [46, 69, 70]. Indeed, the increased production of VEGF and the augmented expression of *SCX* and, to some extent, *COL3A1*, demonstrate that IL-1β also elicits an initial reparative response in TCs [71]. This observation is consistent with the presence of a subpopulation of progenitor cells, demonstrating features of mesenchymal stem/stromal cells, within TCs [26, 72]. In pathological conditions and aging, the presence of progenitor cells may be reduced, leading to a loss of homeostatic function and thus tissue degeneration [73]. Then, the idea to supply the injured tissue with a convenient source of autologous MSCs with homeostatic and immunomodulatory activity perfectly represents the rationale of the application of cell concentrates in degenerative disorders.

Limitations of the present study are represented by the use of a nonphysiological inflammatory stimulus that may result in considerably stronger than the one occurring in vivo, and thus partially masking the ability of μFAT to counteract the catabolic response. In addition, the quantity of μFAT was chosen based on previous reports [9], but the proportion between cells and tissue hardly corresponds to the physiological ratio. Another limitation is given by the possible influence of patients' characteristics on the activity of μFAT, which was not taken into account in the present work while it may indeed identify a fraction of individuals who are nonresponders to the μFAT treatment due to pathology or adipose tissue-specific features [74] and thus representing a source of bias.

The results obtained in this work sustain the rationale of μFAT application to tendon disorders and they may provide evidences for the interpretation of future clinical data, identifying the possible mechanisms involved in μFAT-mediated effects on tendon healing. A clinical trial is now ongoing for the evaluation of the possible clinical benefit of μFAT injection as adjuvant therapy in the arthroscopic rotator cuff repair, especially in terms of possible reduction of retears.

5. Conclusions

In an inflammatory context, TCs demonstrated a catabolic and profibrosis pattern of gene expression, while at the same time, producing molecules with a role in tissue healing. The coculture with μFAT not only reduced the expression of fibrosis and catabolic markers but it also enhanced the production of cytokines and growth factors able to counteract the inflammatory process and to contribute to tissue regeneration. These observations provide a rationale for the clinical application of μFAT in the treatment of tendon disorders.

Data Availability

All data used to support the findings of this study are available from the corresponding author upon request.

Conflicts of Interest

The authors declare that there is no conflict of interest regarding the publication of this paper.

Acknowledgments

References

[1] J. G. Snedeker and J. Foolen, "Tendon injury and repair – a perspective on the basic mechanisms of tendon disease and future clinical therapy," *Acta Biomaterialia*, vol. 63, pp. 18–36, 2017.

[2] F. Wu, M. Nerlich, and D. Docheva, "Tendon injuries," *EFORT Open Reviews*, vol. 2, no. 7, pp. 332–342, 2017.

[3] M. B. Murphy, K. Moncivais, and A. I. Caplan, "Mesenchymal stem cells: environmentally responsive therapeutics for regenerative medicine," *Experimental & Molecular Medicine*, vol. 45, no. 11, p. e54, 2013.

[4] S. Chaudhury, "Mesenchymal stem cell applications to tendon healing," *Muscles Ligaments Tendons Journal*, vol. 2, no. 3, pp. 222–229, 2012.

[5] F. G. Usuelli, M. Grassi, C. Maccario et al., "Intratendinous adipose-derived stromal vascular fraction (SVF) injection provides a safe, efficacious treatment for Achilles tendinopathy: results of a randomized controlled clinical trial at a 6-month follow-up," *Knee Surgery, Sports Traumatology, Arthroscopy*, vol. 26, no. 7, pp. 2000–2010, 2018.

[6] S. Y. Lee, B. Kwon, K. Lee, Y. H. Son, and S. G. Chung, "Therapeutic mechanisms of human adipose-derived mesenchymal stem cells in a rat tendon injury model," *The American Journal of Sports Medicine*, vol. 45, no. 6, pp. 1429–1439, 2017.

[7] S. O. Canapp, D. A. Canapp, V. Ibrahim, B. J. Carr, C. Cox, and J. G. Barrett, "The use of adipose-derived progenitor cells and platelet-rich plasma combination for the treatment of supraspinatus tendinopathy in 55 dogs: a retrospective study," *Frontiers in Veterinary Science*, vol. 3, p. 61, 2016.

[8] M. V. Mora, S. A. Antuña, M. G. Arranz, M. T. Carrascal, and R. Barco, "Application of adipose tissue-derived stem cells in a rat rotator cuff repair model," *Injury*, vol. 45, Supplement 4, pp. S22–S27, 2014.

[9] P. Randelli, A. Menon, V. Ragone et al., "Lipogems product treatment increases the proliferation rate of human tendon stem cells without affecting their stemness and differentiation capability," *Stem Cells International*, vol. 2016, Article ID 4373410, 11 pages, 2016.

[10] C. Long, Z. Wang, A. Legrand, A. Chattopadhyay, J. Chang, and P. M. Fox, "Tendon tissue engineering: mechanism and effects of human tenocyte coculture with adipose-derived stem cells," *The Journal of Hand Surgery*, vol. 43, no. 2, pp. 183.e1–183.e9, 2018.

[11] C. N. Manning, C. Martel, S. E. Sakiyama-Elbert et al., "Adipose-derived mesenchymal stromal cells modulate tendon fibroblast responses to macrophage-induced inflammation in vitro," *Stem Cell Research & Therapy*, vol. 6, no. 1, p. 59, 2015.

[12] P. Salmikangas, M. Schuessler-Lenz, S. Ruiz et al., "Marketing regulatory oversight of advanced therapy medicinal products (ATMPs) in Europe: the EMA/CAT perspective," *Advances in Experimental Medicine and Biology*, vol. 871, pp. 103–130, 2015.

[13] A. J. Guess, B. Daneault, R. Wang et al., "Safety profile of good manufacturing practice manufactured interferon γ-primed mesenchymal stem/stromal cells for clinical trials," *Stem Cells Translational Medicine*, vol. 6, no. 10, pp. 1868–1879, 2017.

[14] S. J. Kim, E. K. Kim, S. J. Kim, and D. H. Song, "Effects of bone marrow aspirate concentrate and platelet-rich plasma on patients with partial tear of the rotator cuff tendon," *Journal of Orthopaedic Surgery*, vol. 13, no. 1, p. 1, 2018.

[15] C. Tremolada, V. Colombo, and C. Ventura, "Adipose tissue and mesenchymal stem cells: state of the art and Lipogems® technology development," *Current Stem Cell Reports*, vol. 2, pp. 304–312, 2016.

[16] O. Zeira, S. Scaccia, L. Pettinari et al., "Intra-articular administration of autologous micro-fragmented adipose tissue in dogs with spontaneous osteoarthritis: safety, feasibility, and clinical outcomes," *Stem Cells Translational Medicine*, vol. 7, no. 11, pp. 819–828, 2018.

[17] A. Bouglé, P. Rocheteau, M. Hivelin et al., "Micro-fragmented fat injection reduces sepsis-induced acute inflammatory response in a mouse model," *British Journal of Anaesthesia*, vol. 121, no. 6, pp. 1249–1259, 2018.

[18] G. Cattaneo, A. De Caro, F. Napoli, D. Chiapale, P. Trada, and A. Camera, "Micro-fragmented adipose tissue injection associated with arthroscopic procedures in patients with symptomatic knee osteoarthritis," *BMC Musculoskeletal Disorders*, vol. 19, no. 1, p. 176, 2018.

[19] A. Russo, V. Condello, V. Madonna, M. Guerriero, and C. Zorzi, "Autologous and micro-fragmented adipose tissue for the treatment of diffuse degenerative knee osteoarthritis," *Journal of Experimental Orthopaedics*, vol. 4, no. 1, p. 33, 2017.

[20] A. Schiavone Panni, M. Vasso, A. Braile et al., "Preliminary results of autologous adipose-derived stem cells in early knee osteoarthritis: identification of a subpopulation with greater response," *International Orthopaedics*, vol. 43, no. 1, pp. 7–13, 2019.

[21] F. G. Thankam, Z. K. Roesch, M. F. Dilisio et al., "Association of inflammatory responses and ECM disorganization with HMGB1 upregulation and NLRP3 inflammasome activation in the injured rotator cuff tendon," *Scientific Reports*, vol. 8, no. 1, p. 8918, 2018.

[22] M. Tsuzaki, G. Guyton, W. Garrett et al., "IL-1β induces COX2, MMP-1, -3 and -13, ADAMTS-4, IL-1β and IL-6 in human tendon cells," *Journal of Orthopaedic Research*, vol. 21, no. 2, pp. 256–264, 2003.

[23] K. Zhang, S. Asai, B. Yu, and M. Enomoto-Iwamoto, "IL-1β irreversibly inhibits tenogenic differentiation and alters metabolism in injured tendon-derived progenitor cells in vitro," *Biochemical and Biophysical Research Communications*, vol. 463, no. 4, pp. 667–672, 2015.

[24] C. H. Jo, S. Y. Lee, K. S. Yoon, and S. Shin, "Effects of platelet-rich plasma with concomitant use of a corticosteroid on tenocytes from degenerative rotator cuff tears in interleukin 1β-induced tendinopathic conditions," *The American Journal of Sports Medicine*, vol. 45, no. 5, pp. 1141–1150, 2017.

[25] F. Bianchi, M. Maioli, E. Leonardi et al., "A new nonenzymatic method and device to obtain a fat tissue derivative highly enriched in pericyte-like elements by mild mechanical forces from human lipoaspirates," *Cell Transplantation*, vol. 22, no. 11, pp. 2063–2077, 2013.

[26] D. Stanco, M. Viganò, C. Perucca Orfei et al., "Multidifferentiation potential of human mesenchymal stem cells from adipose tissue and hamstring tendons for musculoskeletal cell-based therapy," *Regenerative Medicine*, vol. 10, no. 6, pp. 729–743, 2015.

[27] M. Viganò, C. Perucca Orfei, A. Colombini et al., "Different culture conditions affect the growth of human tendon stem/progenitor cells (TSPCs) within a mixed tendon cells (TCs) population," *Journal of Experimental Orthopaedics*, vol. 4, no. 1, p. 8, 2017.

[28] M. Viganò, C. Perucca Orfei, L. de Girolamo et al., "Housekeeping gene stability in human mesenchymal stem and tendon cells exposed to tenogenic factors," *Tissue Engineering. Part C, Methods*, vol. 24, no. 6, pp. 360–367, 2018.

[29] M. W. Pfaffl, "A new mathematical model for relative quantification in real-time RT-PCR," *Nucleic Acids Research*, vol. 29, no. 9, pp. 45e–445, 2001.

[30] P. Desjardins and D. Conklin, "NanoDrop Microvolume Quantitation of Nucleic Acids," *Journal of Visualized Experiments*, vol. 45, no. 1, 2010.

[31] D. Shah, M. Naciri, P. Clee, and M. Al-Rubeai, "NucleoCounter-an efficient technique for the determination of cell number and viability in animal cell culture processes," *Cytotechnology*, vol. 51, no. 1, pp. 39–44, 2006.

[32] H. A. Eriksen, A. Pajala, J. Leppilahti, and J. Risteli, "Increased content of type III collagen at the rupture site of human Achilles tendon," *Journal of Orthopaedic Research*, vol. 20, no. 6, pp. 1352–1357, 2002.

[33] I. Shirachi, M. Gotoh, Y. Mitsui et al., "Collagen production at the edge of ruptured rotator cuff tendon is correlated with postoperative cuff integrity," *Arthroscopy: The Journal of Arthroscopic & Related Surgery*, vol. 27, no. 9, pp. 1173–1179, 2011.

[34] F. Veronesi, E. Della Bella, P. Torricelli, S. Pagani, and M. Fini, "Effect of adipose-derived mesenchymal stromal cells on tendon healing in aging and estrogen deficiency: an in vitro co-culture model," *Cytotherapy*, vol. 17, no. 11, pp. 1536–1544, 2015.

[35] R. Costa-Almeida, I. Calejo, R. L. Reis, and M. E. Gomes, "Crosstalk between adipose stem cells and tendon cells reveals a temporal regulation of tenogenesis by matrix deposition and remodeling," *Journal of Cellular Physiology*, vol. 233, no. 7, pp. 5383–5395, 2018.

[36] J. E. Baroneza, A. Godoy-Santos, B. F. Massa, F. B. de Araujo Munhoz, T. D. Fernandes, and M. C. L. G. dos Santos, "MMP-1 promoter genotype and haplotype association with posterior tibial tendinopathy," *Gene*, vol. 547, no. 2, pp. 334–337, 2014.

[37] A. Castagna, E. Cesari, A. Gigante, M. Conti, and R. Garofalo, "Metalloproteases and their inhibitors are altered in both torn and intact rotator cuff tendons," *Musculoskeletal Surgery*, vol. 97, no. S1, Supplement 1, pp. 39–47, 2013.

[38] N. K. Kordulewska, A. Cieślińska, E. Fiedorowicz, B. Jarmołowska, and E. Kostyra, "High Expression of IL-1RI and EP2 receptors in the IL-1β/COX-2 pathway, and a new alternative to non-steroidal drugs—osthole in inhibition COX-2," *International Journal of Molecular Sciences*, vol. 20, no. 1, p. 186, 2019.

[39] F. G. Thankam, D. K. Evan, D. K. Agrawal, and M. F. Dilisio, "Collagen type III content of the long head of the biceps tendon as an indicator of glenohumeral arthritis," *Molecular and Cellular Biochemistry*, vol. 454, no. 1-2, pp. 25–31, 2019.

[40] A. Pajala, J. Melkko, J. Leppilahti, P. Ohtonen, Y. Soini, and J. Risteli, "Tenascin-C and type I and III collagen expression in total Achilles tendon rupture. An immunohistochemical study," *Histology and histopathology*, vol. 24, no. 10, pp. 1207–1211, 2009.

[41] D. Sbardella, G. Tundo, G. Fasciglione et al., "Role of metalloproteinases in tendon pathophysiology," *Mini Reviews in Medicinal Chemistry*, vol. 14, no. 12, pp. 978–987, 2014.

[42] A. W. Millar, P. D. Brown, J. Moore et al., "Results of single and repeat dose studies of the oral matrix metalloproteinase inhibitor marimastat in healthy male volunteers," *British Journal of Clinical Pharmacology*, vol. 45, no. 1, pp. 21–26, 1998.

[43] A. Del Buono, F. Oliva, U. G. Longo et al., "Metalloproteases and rotator cuff disease," *Journal of Shoulder and Elbow Surgery*, vol. 21, no. 2, pp. 200–208, 2012.

[44] G. P. Riley, V. Curry, J. DeGroot et al., "Matrix metalloproteinase activities and their relationship with collagen remodelling in tendon pathology," *Matrix Biology*, vol. 21, no. 2, pp. 185–195, 2002.

[45] M. Gotoh, K. Hamada, H. Yamakawa, A. Tomonaga, A. Inoue, and H. Fukuda, "Significance of granulation tissue in torn supraspinatus insertions: an immunohistochemical study with antibodies against interleukin-1 beta, cathepsin D, and matrix metalloprotease-1," *Journal of Orthopaedic Research*, vol. 15, no. 1, pp. 33–39, 1997.

[46] F. Paolella, C. Manferdini, E. Gabusi et al., "Effect of microfragmented adipose tissue on osteoarthritic synovial macrophage factors," *Journal of Cellular Physiology*, vol. 234, no. 4, pp. 5044–5055, 2019.

[47] A. McClellan, R. Evans, C. Sze, S. Kan, Y. Paterson, and D. Guest, "A novel mechanism for the protection of embryonic stem cell derived tenocytes from inflammatory cytokine interleukin 1 beta," *Scientific Reports*, vol. 9, no. 1, p. 2755, 2019.

[48] F. Busch, A. Mobasheri, P. Shayan, C. Lueders, R. Stahlmann, and M. Shakibaei, "Resveratrol modulates interleukin-1β-induced phosphatidylinositol 3-kinase and nuclear factor κB signaling pathways in human tenocytes," *The Journal of Biological Chemistry*, vol. 287, no. 45, pp. 38050–38063, 2012.

[49] S. S. Polly, A. E. C. Nichols, E. Donnini et al., "Adipose-Derived Stromal Vascular Fraction and Cultured Stromal Cells as Trophic Mediators for Tendon Healing," *Journal of Orthopaedic Research*, vol. 37, no. 6, pp. 1429–1439, 2019.

[50] M. Hammerman, P. Blomgran, S. Ramstedt, and P. Aspenberg, "COX-2 inhibition impairs mechanical stimulation of early tendon healing in rats by reducing the response to microdamage," *Journal of Applied Physiology*, vol. 119, no. 5, pp. 534–540, 2015.

[51] C. H. Rundle, S.-T. Chen, M. J. Coen, J. E. Wergedal, V. Stiffel, and K.-H. W. Lau, "Direct lentiviral-cyclooxygenase 2 application to the tendon-bone interface promotes osteointegration and enhances return of the pull-out tensile strength of the tendon graft in a rat model of biceps tenodesis," *PLoS One*, vol. 9, no. 5, article e98004, 2014.

[52] M. P. Dabrowski, W. Stankiewicz, T. Płusa, A. Chciałowski, and S. Szmigielski, "Competition of IL-1 and IL-1ra determines lymphocyte response to delayed stimulation with PHA," *Mediators of Inflammation*, vol. 10, no. 3, 107 pages, 2001.

[53] J. Palomo, D. Dietrich, P. Martin, G. Palmer, and C. Gabay, "The interleukin (IL)-1 cytokine family – balance between agonists and antagonists in inflammatory diseases," *Cytokine*, vol. 76, no. 1, pp. 25–37, 2015.

[54] P. De Luca, D. Kouroupis, M. Viganò et al., "Human diseased articular cartilage contains a mesenchymal stem cell-like population of chondroprogenitors with strong immunomodulatory responses," *Journal of Clinical Medicine*, vol. 8, no. 4, p. 423, 2019.

[55] L. A. Ortiz, M. DuTreil, C. Fattman et al., "Interleukin 1 receptor antagonist mediates the antiinflammatory and antifibrotic effect of mesenchymal stem cells during lung injury," *Proceedings of the National Academy of Sciences of the United States of America*, vol. 104, no. 26, pp. 11002–11007, 2007.

[56] Z. Liu, R. J. Simpson, and C. Cheers, "Interaction of interleukin-6, tumour necrosis factor and interleukin-1 during Listeria infection," *Immunology*, vol. 85, no. 4, pp. 562–567, 1995.

[57] M. S. Katsma, S. H. Patel, E. Eldon et al., "The influence of chronic IL-6 exposure, in vivo, on rat Achilles tendon extracellular matrix," *Cytokine*, vol. 93, pp. 10–14, 2017.

[58] K. Legerlotz, E. R. Jones, H. R. C. Screen, and G. P. Riley, "Increased expression of IL-6 family members in tendon pathology," *Rheumatology*, vol. 51, no. 7, pp. 1161–1165, 2012.

[59] W. Morita, S. G. Dakin, S. J. B. Snelling, and A. J. Carr, "Cytokines in tendon disease," *Bone & Joint Research*, vol. 6, no. 12, pp. 656–664, 2017.

[60] S. Chen, G. Deng, K. Li et al., "Interleukin-6 promotes proliferation but inhibits tenogenic differentiation via the Janus kinase/signal transducers and activators of transcription 3 (JAK/STAT3) pathway in tendon-derived stem cells," *Medical Science Monitor*, vol. 24, pp. 1567–1573, 2018.

[61] T. W. Lin, L. Cardenas, D. L. Glaser, and L. J. Soslowsky, "Tendon healing in interleukin-4 and interleukin-6 knockout mice," *Journal of Biomechanics*, vol. 39, no. 1, pp. 61–69, 2006.

[62] T. John, D. Lodka, B. Kohl et al., "Effect of pro-inflammatory and immunoregulatory cytokines on human tenocytes," *Journal of Orthopaedic Research*, vol. 28, pp. n/a–1077, 2010.

[63] T. Cohen, D. Nahari, L. W. Cerem, G. Neufeld, and B. Z. Levi, "Interleukin 6 induces the expression of vascular endothelial growth factor," *The Journal of Biological Chemistry*, vol. 271, no. 2, pp. 736–741, 1996.

[64] J. Luo, Y. Xiong, X. Han, and Y. Lu, "VEGF non-angiogenic functions in adult organ homeostasis: therapeutic implications," *Journal of Molecular Medicine*, vol. 89, no. 7, pp. 635–645, 2011.

[65] T. Pufe, W. J. Petersen, R. Mentlein, and B. N. Tillmann, "The role of vasculature and angiogenesis for the pathogenesis of degenerative tendons disease," *Scandinavian Journal of Medicine & Science in Sports*, vol. 15, no. 4, pp. 211–222, 2005.

[66] W. F. Mao, Y. F. Wu, Q. Q. Yang et al., "Modulation of digital flexor tendon healing by vascular endothelial growth factor gene transfection in a chicken model," *Gene Therapy*, vol. 24, no. 4, pp. 234–240, 2017.

[67] J.-F. Kaux, L. Janssen, P. Drion et al., "Vascular endothelial growth factor-111 (VEGF-111) and tendon healing: preliminary results in a rat model of tendon injury," *Muscles Ligaments Tendons Journal*, vol. 4, no. 1, pp. 24–28, 2014.

[68] J. B. Tang, Y. F. Wu, Y. Cao et al., "Basic FGF or VEGF gene therapy corrects insufficiency in the intrinsic healing capacity of tendons," *Scientific Reports*, vol. 6, no. 1, p. 20643, 2016.

[69] G. Marfia, S. E. Navone, L. A. Hadi et al., "The adipose mesenchymal stem cell secretome inhibits inflammatory responses of microglia: evidence for an involvement of sphingosine-1-phosphate signalling," *Stem Cells and Development*, vol. 25, no. 14, pp. 1095–1107, 2016.

[70] R. Jin, M. Shen, L. Yu, X. Wang, and X. Lin, "Adipose-derived stem cells suppress inflammation induced by IL-1β through down-regulation of P2X7R mediated by miR-373 in chondrocytes of osteoarthritis," *Molecules and Cells*, vol. 40, no. 3, pp. 222–229, 2017.

[71] N. L. Millar, G. A. C. Murrell, and I. B. McInnes, "Inflammatory mechanisms in tendinopathy - towards translation," *Nature Reviews Rheumatology*, vol. 13, no. 2, pp. 110–122, 2017.

[72] Y. Bi, D. Ehirchiou, T. M. Kilts et al., "Identification of tendon stem/progenitor cells and the role of the extracellular matrix in their niche," *Nature Medicine*, vol. 13, no. 10, pp. 1219–1227, 2007.

[73] J. Kohler, C. Popov, B. Klotz et al., "Uncovering the cellular and molecular changes in tendon stem/progenitor cells attributed to tendon aging and degeneration," *Aging Cell*, vol. 12, no. 6, pp. 988–999, 2013.

[74] A. I. Caplan, "Cell-based therapies: the nonresponder," *Stem Cells Translational Medicine*, vol. 7, no. 11, pp. 762–766, 2018.

Research Article

Colony Formation, Migratory, and Differentiation Characteristics of Multipotential Stromal Cells (MSCs) from "Clinically Accessible" Human Periosteum Compared to Donor-Matched Bone Marrow MSCs

Heather E. Owston [ID],[1,2,3] **Payal Ganguly** [ID],[3] **Giuseppe Tronci**,[2] **Stephen J. Russell** [ID],[2] **Peter V. Giannoudis**,[3] **and Elena A. Jones** [ID][3]

[1]*Institute of Medical and Biological Engineering, University of Leeds, Leeds, UK*
[2]*Clothworkers' Centre for Textile Materials Innovation for Healthcare, University of Leeds, UK*
[3]*Leeds Institute of Rheumatic and Musculoskeletal Medicine, University of Leeds, Leeds, UK*

Correspondence should be addressed to Elena A. Jones; e.jones@leeds.ac.uk

Periosteum is vital for fracture healing, as a highly vascular and multipotential stromal cell- (MSC-) rich tissue. During surgical bone reconstruction, small fragments of periosteum can be "clinically accessible," yet periosteum is currently not ultilised, unlike autologous bone marrow (BM) aspirate. This study is aimed at comparing human periosteum and donor-matched iliac crest BM MSC content and characterising MSCs in terms of colony formation, growth kinetics, phenotype, cell migration patterns, and trilineage differentiation capacity. "Clinically accessible" periosteum had an intact outer fibrous layer, containing CD271+ candidate MSCs located perivasculary; the inner cambium was rarely present. Following enzymatic release of cells, periosteum formed significantly smaller fibroblastic colonies compared to BM (6.1 mm^2 vs. 15.5 mm^2, $n = 4$, $P = 0.0006$). Periosteal colonies were more homogenous in size (range 2-30 mm^2 vs. 2-54 mm^2) and on average 2500-fold more frequent (2.0% vs. 0.0008%, $n = 10$, $P = 0.004$) relative to total viable cells. When expanded *in vitro*, similar growth rates up to passage 0 (P0) were seen (1.8 population doublings (PDs) per day (periosteum), 1.6 PDs per day (BM)); however, subsequently BM MSCs proliferated significantly slower by P4 (4.3 PDs per day (periosteum) vs. 9.3 PDs per day (BM), $n = 9$, $P = 0.02$). In early culture, periosteum cells were less migratory at slower speeds than BM cells. Both MSC types exhibited MSC phenotype and trilineage differentiation capacity; however, periosteum MSCs showed significantly lower (2.7-fold) adipogenic potential based on Nile red : DAPI ratios with reduced expression of adipogenesis-related transcripts *PPAR-γ*. Altogether, these data revealed that "clinically accessible" periosteal samples represent a consistently rich source of highly proliferative MSCs compared to donor-matched BM, which importantly show similar osteochondral capacity and lower adipogenic potential. Live cell tracking allowed determination of unique morphological and migration characteristics of periosteal MSCs that can be used for the development of novel bone graft substitutes to be preferentially repopulated by these cells.

1. Introduction

Fracture nonunion represents a significant clinical challenge. The rate of fracture nonunion is reported to be between 2 and 10% of all fractures, dependent on fracture type, location, and patient demographics [1, 2]. Its treatment is not only costly to healthcare providers [3], but importantly to the patients

through loss of earnings and high rates of depression, all of which will have a detrimental effect on quality of life [4]. Therefore, improvements to standard-of-care treatments of bone fracture are needed and have been recently developed based on the diamond concept framework [5], which draws attention to the importance of ensuring the presence of all: osteogenic cells, osteoconductive scaffolds, osteoinductive

growth factors and a stable mechanical environment at the site of healing [5]. Most commonly, osteogenic cells are delivered to the fracture site in the form of bone marrow aspirate (BMA), BMA concentrate (BMAC), or combining BMAC with grafting material to fill larger defects to aid with fracture repair [6–10].

The critically important role of periosteum during bone fracture healing is well established. Following fracture periosteum reacts by thickening and entering into a proliferative state [11–13]. Periosteal-derived progenitor cells migrate into the fracture haematoma early on, where they differentiate into osteoblasts or chondrocytes, directly contributing to bone regeneration [12]. Periosteal stripping or damage during fracture results in decreased callus formation or delayed union [13–16]. However, despite the known critical impact of periosteum during fracture repair, the use of periosteal-derived cells for surgical repair of fractures, nonunions, or critical size bone defects remains unexploited.

Periosteum lines the outer aspect of most bones, contributing to appositional growth during childhood and adolescence as well as providing the vascular supply to bone [14]. This tissue, although thin, forms two distinct layers, the bone lining inner cambium layer being highly cellular and containing osteogenic progenitors, while the outer fibrous layer, predominantly consisting of collagen, is highly vascular but not particularly cellular in comparison [12, 17]. The cambium layer is tightly attached to the underlying bone by Sharpey's Fibres; thus, removal of periosteum with the cambium layer attached is difficult [18] and is furthermore considered inappropriate by the surgeons as potentially compromising the repair process. However, "clinically accessible" samples of periosteum, likely to be fibrous in nature, can be obtained as by-products of surgical debridement of the fracture site, but their osteogenic progenitor cell content has not yet been explored before.

The purpose of this study was to investigate "clinically accessible" samples of human periosteum for the presence of osteogenic progenitor multipotential stromal cells (MSCs) and to compare their functional capacities with iliac crest BMA samples from the same donors.

2. Materials and Methods

2.1. Tissue Collection and Processing.

Donor-matched samples of periosteum and BMA were obtained from 12 patients treated for fracture nonunion (median age 49 years, range 17-80) at the Trauma Orthopaedic Unit at Leeds General Infirmary, Leeds, UK. Periosteum (approximately 50 mm^2, 0.3 g) was harvested from near to the site of fracture using a scalpel, and BMA (volume range 16-60 mL) was aspirated from the anterior iliac crest. Iliac crest trabecular bone (approximately 1 cm^3) was collected from three patients, undergoing autograft procurement. Ethical approval was granted by the National Research Ethics Committee–Leeds East, with ethical approval number 06/Q1206/127 and informed written consent given by all patients.

For extraction of periosteum- and BMA-resident nucleated cells, BMA underwent processing with ammonium chloride (Stem Cell Technologies) to lyse red blood cells.

Briefly, 4 mL of ammonium chloride solution was added per 1 mL of BMA and incubated for 10 mins on ice. Cells were concentrated via centrifugation (650 g, 5 mins). Periosteum samples were digested in collagenase (600 U/mL, Stem Cell Technologies) at a ratio of 0.1 g of tissue to 0.5 mL of collagenase, for 4 h, incubated at 37°C, 5% CO$_2$. After digestion, the cell suspension was passed through a 70 μm cell strainer to remove large debris; the cell suspension was concentrated via centrifugation (650 g, 5 mins). Cells were used directly for in vitro assays, as described in the subsequent sections.

2.2. Histology of Periosteum.

Human periosteum and iliac crest bone samples were fixed in 3.75% formaldehyde for a week, and iliac crest bone was next decalcified using 0.1 M EDTA. Subsequently, samples were embedded in paraffin wax, and 5 μm thick slides were produced (SuperFrost Plus slides). Slides were dewaxed and hydrated using standard methods, followed by staining for haematoxylin and eosin and picro sirius red. Samples were also stained for CD271 (1 : 20, NGFRS, Abcam), the well-recognised marker of bone-resident MSCs [19]. Antigen retrieval was carried out using 10 mM/L citrate buffer, and immunohistochemistry was carried out using the Dako EnVision kit (Dako), as per the manufacturer's guidelines. Post staining, slides were dehydrated and cleared with xylene and covered with a coverslip, using DPX (Sigma). Slides were imaged using light microscopy (AxioCam MRc5, Zeiss) and under a polarised light.

2.3. Colony-Forming Fibroblast (CFU-F) Assay.

CFU-F assays were used to quantify colony-forming cells in BMA and periosteum digest samples and performed as previously described [20, 21]. After 14 days of culture in StemMACS MSC expansion media (Miltenyi Biotec, supplemented with 1% penicillin streptomycin), duplicate dishes were fixed, stained [20], and scanned. Colonies were counted and colony surface area was quantified using ImageJ [22]. The frequency distribution of colony surface area was plotted using Prism. The spread of colony surface area distribution data was quantified using "full width at half maximum" (FWHM) values [23].

2.4. MSC Expansion and Surface Marker Characterisation.

Following initial processing, nucleated cells from BMA and periosteum were plated at a density of 4×10^5 per cm^2 and 1×10^4 per cm^2, respectively, and incubated at 37°C, 5% CO$_2$ in StemMACS media. After 48 hours, media were replaced and cells were cultured until 60-80% confluence with biweekly half medium changes; flasks were trypsinised and reseeded at cell densities of 1.25×10^5 for periosteum [24] and 2.5×10^5 for BM [25], this was repeated until passage 6. Population doubling (PD) up to passage 0 (<P0) and after passage 0 (>P0) was calculated as follows: PD $(<P0) = \log_2$ (cell count at passage 0/seeded number of CFU − F) and PD $(>P0) = \log_2$ (cell count at passage/seeded cell count) as per Churchman et al. [26].

To confirm the MSC nature of expanded cells, flow cytometry of donor-matched BM and periosteum cultures was carried out using antibodies chosen in line with the International Society for Cellular Therapies (ISCT) approved

panel (Supplementary Table 1) [27], as previously described by [28]. In brief, trypsinised cells were resuspended in blocking buffer (10% mouse serum, 1% human IgG in FACS buffer (0.1% BSA, 0.01% sodium azide, 0.5 M EDTA in PBS)) for 15 mins at RT and stained with antibodies (Supplementary Table 1) for 30 mins on ice. Following one wash in FACS buffer, cells were resuspended in 500 μL 4′,6-diamidino-2-phenylindole (DAPI) buffer ready to be analysed by an LSRII flow cytometer (BD Pharmingen). Data was analysed using FACS DIVA software.

2.5. In Vitro Trilineage Differentiation Assays.

Cultured cells (passage 1-3) from donor-matched periosteum and BM underwent trilineage differentiation assessment; OsteoDIFF, AdipoDIFF, and ChondroDIFF media (Miltenyi Biotec) were used to induce differentiation. For osteogenesis ($n = 7$ donors), 2600 cells/cm^2 were plated onto 7 replicate flat bottom wells and incubated at 37°C, 5% CO$_2$ in OsteoDIFF for 2 or 3 weeks, with biweekly, half medium changes. At two weeks, alkaline phosphatase (ALP) activity was detected using fast blue. At three weeks, calcium deposition was stained with alizarin red [29] and calcium content was measured, as previously described [28]. For three donors, an extra well was set up to measure DNA content, cells were lysed in 200 μL of 0.1% Triton-X 100, and DNA content was quantified using a PicoGreen Assay (Thermo Scientific) [30].

Adipogenesis assays were seeded at 4200 cells/cm^2 into 5 replicate flat bottomed well plates, incubated at 37°C, 5% CO$_2$, and half medium (AdipoDIFF) changes were carried out biweekly for 3 weeks. After 3 weeks, plates were fixed with 3.75% formaldehyde and stained with either oil red ($n = 6$ donors) or Nile red and DAPI ($n = 3$ donors) [31], the latter of which was quantified using a fluorescent plate reader (Berthold) and Nile red absorbance levels were normalised to DAPI absorbance levels to establish Nile red/DAPI ratios [31].

Chondrogenic assays ($n = 5$ donors) were carried out in 5 replicate 1.5 mL screw cap Eppendorf tubes; 2.5×10^5 cells were added to each tube and centrifuged (800 g, 5 mins) to create a pellet culture and was resuspended in ChondroDIFF media. Tubes were placed in an incubator at 37°C, 5% CO$_2$ for 3 weeks, where half medium changes were made three times a week. After 3 weeks, 2 pellets were snap frozen in OCT, cut using a cryostat (Leica Biosystems), and dried onto histology slides where toluidine blue was used to stain GAGs. The remaining three pellets were digested in papain digest buffer at 65°C overnight, and the GAG content was quantified using a sulphated GAG assay kit (Blyscan), as previously described [28].

Extra wells or pellets were set up for each trilineage differentiation assay for 3 donors to allow quantification of change expression of key lineage markers following differentiation induction. Cells were lysed and RNA isolated using a Single Cell RNA Purification Kit (Norgen) and on-column DNase (Applied Biosystems) treatment. cDNA was produced using a High-Capacity cDNA Reverse Transcription Kit (Applied Biosystems) for use with TaqMan assays: osteogenesis markers—runt-related transcription factor 2 (RUNX2) and bone gamma-carboxyglutamate (gla) protein (BGLAP);

chondrogenesis markers—collagen, type 2, alpha 1 (COL2A1) and SRY- (sex-determining region Y-) box 9 (Sox9); and adipogenesis markers—fatty acid-binding protein 4 (FABP4) and peroxisome proliferator-activated receptor-gamma (PPAR-γ). The real time-PCR (RT-PCR) reaction was run using a QuantStudio™ 7 Flex Real-Time PCR System and SDS software, recording the fluorescence in real time. Analysis was carried out using the $2^{-\Delta(Ct)}$ method, to calculate normalised gene expression (normalised to hypoxanthine phosphoribosyltransferase 1 (HPRT1) expression) [32].

2.6. Live Holographic Imaging.

P0 vials of donor-matched (male, 17) BM and periosteum MSCs were seeded in duplicate (250 cells per well) onto a Lumox® multiwell 24-well cell culture plate (Sarstedt). The cultures were grown for 3 days at 37°C, 5% CO$_2$ in StemMACS media. On day 3, following a half medium change, the plate lid was replaced with PHI HoloLids™ imaging covers (PHI, phase holographic imaging) (sterilised in 70% EtOH, 10 mins). The plate was placed onto the xy motorised stage of a HoloMonitor M4 Microscope, set up inside an incubator. Using the Hstudio software, three coordinates in each well were manually focused and set to automatically image every hour for 2 days.

Post acquisition, the Hstudio software applied a "mask" to the images, where a threshold was set to distinguish cells from the bottom of the well, allowing for automatic cell identification. Automatic cell number assignment allowed for individual cell tracking over time, which was checked manually. All outputs were exported into Excel files and plotted using Prism.

2.7. Statistical Analysis.

To compare donor-matched periosteum and BM samples, statistical analysis was carried out using appropriate paired tests (Wilcoxon signed-rank test or paired t test depending on data distributions), where $P < 0.05$ was considered significant. Phase holographic imaging data sets were compared using an unpaired Student's t-test. The exact tests are specified in the figure legends, and the data is presented mean ± standard deviation.

3. Results

3.1. Location of CD271+ Candidate MSCs in Human Periosteum and Iliac Crest Bone.

The architecture of human samples of periosteum ($n = 5$), taken from the femur and humerus ($n = 1$), approximately 5 cm from a nonunion fracture site (within the surgical opening) was assessed. The mean donor age was 51.8 ± 24.6 years (range, 23-80 years), and periosteum samples were harvested 50 ± 37 weeks following initial injury, with each patient having undergone 0-2 previous orthopaedic surgeries (Table 1). In all the samples, apart from one (male, 47) (Figures 1(a)–1(c)), no cambium layer could be seen, reflecting the preferential harvesting of periosteum fibrous layer, as expected. When an intact cambium layer was seen (Figures 1(a) and 1(b)), it was shown to be attached to the underlying bone. Here, the periosteum could be clearly split into the bone lining cambium layer and the muscle facing fibrous layer.

Table 1: Breakdown of patient demographics, with respect to location of periosteum retrieval and time since initial injury for histological analysis and cellular work.

Sex & age (years)		Harvested from	Time since injury (weeks)	Previous surgeries	Surgery carried out
Histology	M, 23*	Femur	57	2	IMN
	M, 35*	Humerus	108	None	Bone graft with BMAC
	M, 47	Femur	19	None	RIA graft
	F, 74*	Femur	49	2	IMN, bone graft
	F, 80	Femur	17	2	2nd stage Masquelet
Cellular work	M, 17	Femur	65	2	IMN
	M, 44	Tibia	11	1	IMN
	F, 49	Femur	155	1	IMN
	M, 49	Femur	12	1	Plate fixation
	M, 55	Femur	41	1	2nd stage Masquelet
	M, 58	Tibia	71	1	Bone graft
	M, 59	Femur	127	2	Locking plate

M: male, F: female, none: sample harvested during first orthopaedic surgery, IMN: intramedullary nailing, BMAC: bone marrow aspirate concentrate, RIA: reamer irrigator aspirator, *sample also used for cellular work.

(a)

(b)

(c)

(d)
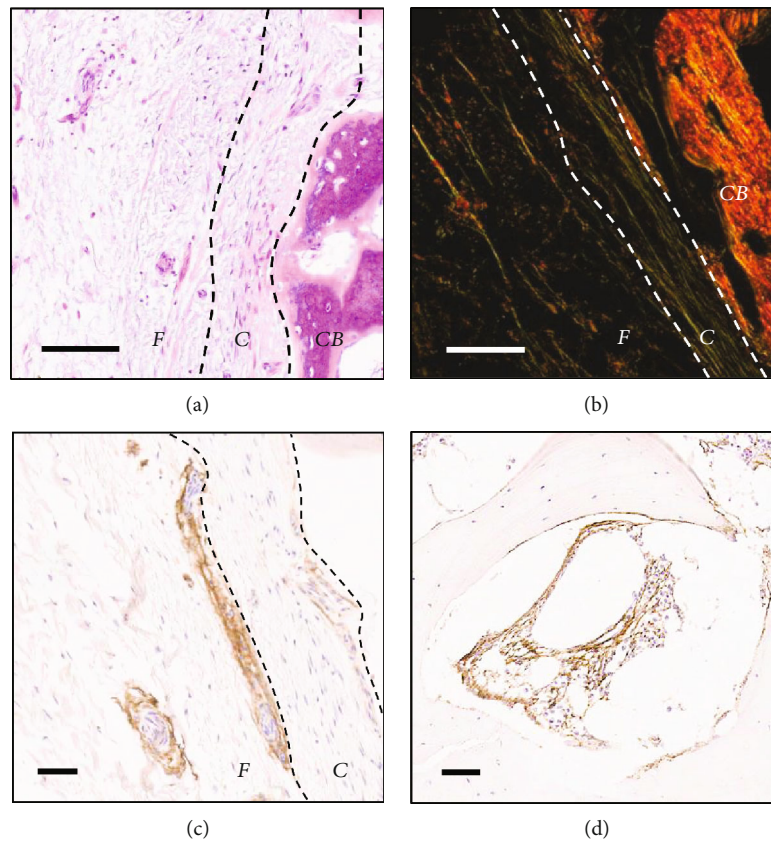
Figure 1: Histological staining of human periosteum samples, harvested close to a fracture site. (a) H&E staining of periosteum sample showing the cellular inner cambium layer (C), the lining cortical bone (CB), and the outer fibrous layer (F). (b) Picro sirius red, imaged using polarised light, showed collagen as the dominant feature of periosteum. CD271 candidate MSC marker immunohistochemistry staining was carried out on (c) periosteum, where staining was shown in the cambium layer and surrounding blood vessels throughout the fibrous layer and (d) iliac crest bone samples, where staining was within the bone marrow and lining the bone.
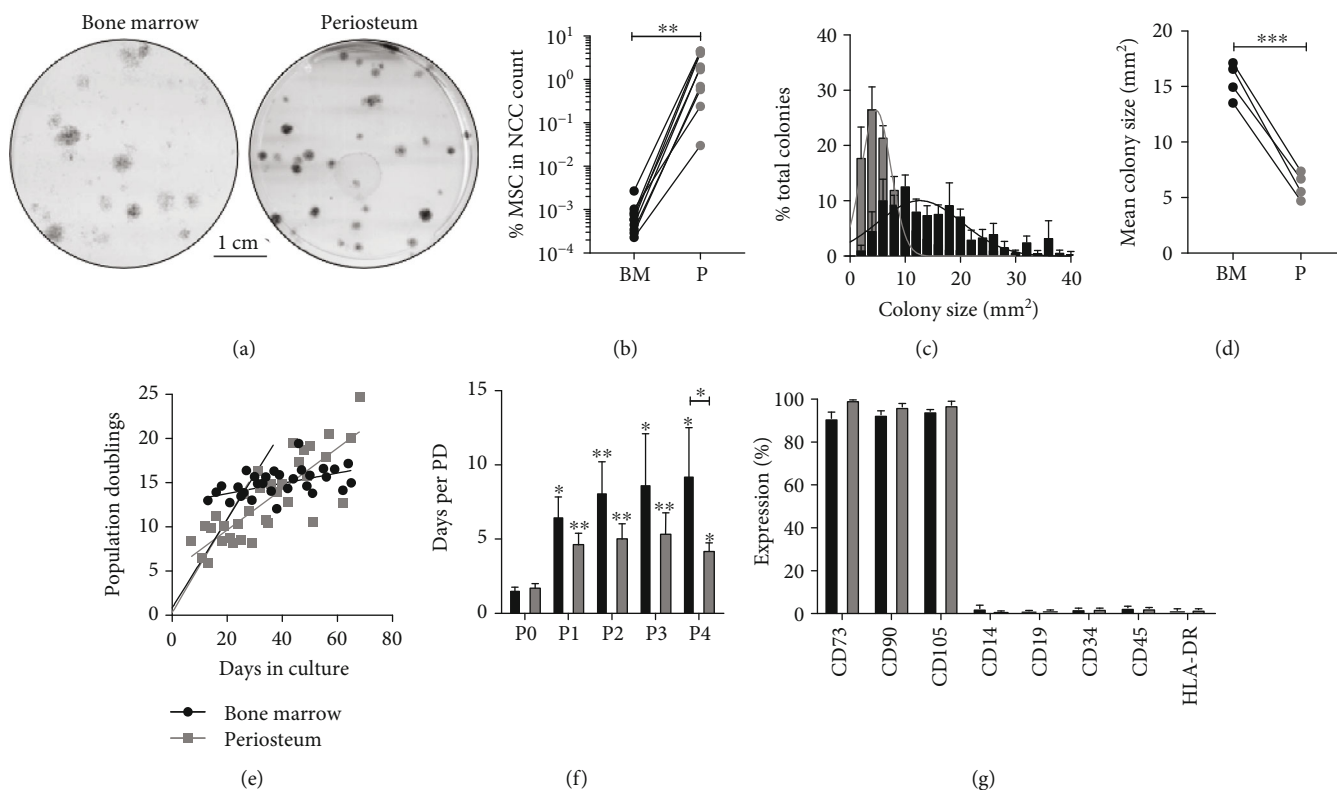
FIGURE 2: Quantification of MSC content, colony formation, and *in vitro* proliferation of periosteum and bone marrow-derived MSCs. (a) Colonies formed by MSCs during CFU-F assays. (b) Percentage MSCs in nucleated cell count. (c) Quantification of colony surface area ($n = 4$) distribution (Gaussian distribution). (d) Mean colony size ($n = 4$). (e) *In vitro* proliferation of MSCs, calculated by cumulative population doublings, showing two distinct growth curves prior to passage (<P0) and post passage (>P0). (f) Days per population doubling compared from P0 to P4. (g) Flow cytometry histograms for positive and negative MSC markers. Statistical analysis was carried out, Wilcoxon signed-rank test $^{**}P = 0.004$ (a), paired Student's t-test $^{***}P = 0.0006$ (d), Kruskal-Wallis test (comparison of P0 to P1-P4) $^*P < 0.02$, $^{**}P < 0.001$ (f), and Wilcoxon signed-rank test (comparison of bone marrow to periosteum) $^*P < 0.05$ (f). BM: bone marrow (black), P: periosteum (grey), NCC: nucleated cell, PD: population doubling.

To investigate the location of candidate MSCs throughout the periosteum, CD271 staining was carried out. CD271 positivity was found throughout both layers of the periosteum, localised to the outer edge of blood vessels (Figure 1(c)). CD271 positivity was also seen in the BM cavities of the control iliac crest bone as expected (Figure 1(d)) [33].

3.2. *Colony Formation and Growth Kinetics of Periosteum-Derived Cultures.* CFU-F assays were carried out to quantify colony formation as a measure of MSC frequency in donor-matched iliac crest BM and periosteum samples ($n = 10$) (Figures 2(a) and 2(b)). The mean donor age was 46.3 ± 17.3 years (range, 17-74 years), periosteum was harvested mainly from the femur ($n = 7$), but also the tibia ($n = 2$) and humerus ($n = 1$), all from nonunion cases, 70 ± 47 weeks following initial injury, and patients had undergone 0-2 previous orthopaedic surgeries.

In the BM, CFU-F frequency in relation to total nucleated cells was on average $0.0008 \pm 0.0002\%$ consistent with previous studies [21, 34]. In donor-matched periosteum digests, CFU-F frequency was significantly ($P = 0.004$, Wilcoxon signed-rank test) higher (2500-fold) ($2.0 \pm 0.6\%$) (Figure 2(b)).

In order to assess the visual differences in colony formation (Figure 2(a)), colony surface area was quantified, from donor-matched dishes containing more than 20 colonies ($n = 4$). Periosteum colonies were more homogenous, with a smaller size distribution compared to BM colonies (Figure 2(c)), which were more heterogeneous and larger. Periosteum colonies were significantly smaller at 6.1 ± 0.6 mm^2 (range, 2.0-29.6 mm^2) compared to BM colonies at 15.5 ± 0.8 mm^2 (range, 2.1-54.3 mm^2) (paired Student's t-test, $P = 0.0006$) (Figure 2(d)). Of particular interest was that BM had a subset of larger colonies > 30 mm^2, accounting for $6.4 \pm 2.2\%$ of all BM colonies, which were not seen in periosteum samples.

Growth kinetics of donor-matched BM and periosteum cultures was next investigated, and two clear growth patterns were noticeable (Figures 2(e) and 2(f)) and thus split before P0 (<P0) and after P0 (>P0) for the analysis. Growth rates measured as PDs per day for <P0 cultures were similar between BM (1.6 ± 0.1 days per PD) and periosteum (1.8 ± 0.2 days per PD), also shown through similar slope gradient (0.50 (BM) and 0.52 (P)) following linear regression analysis (r^2 values, 0.87 (BM) and 0.91 (periosteum)) (Figure 2(e)). However, differences could be seen following

quantification of number of PDs at P0; BM cultures were started with a lower number of MSCs compared to periosteum (Figure 2(b)) and therefore went through significantly higher number of PDs (BM: 13.3 ± 0.5 PDs at P0, periosteum: 8.5 ± 1.1 PDs at P0, Wilcoxon signed-rank test, $P = 0.02$).

Following the first passage, the PD rate significantly slowed (P1-P4) for both culture types (Figures 2(e) and 2(f)), by P4 proliferation rates were reduced to 9.3 ± 3.2 days per PD (BM) and 4.3 ± 0.5 days per PD (periosteum) (Figure 2(f)). The ISCT MSC phenotype was tested on donor-matched cultures [27] at passage 4, and both culture types were >91% positive for MSC markers CD73 (ecto-5′-NT), CD90 (Thy1), and CD105 (Endoglin) and <3% positive for hematopoietic lineage markers: CD14 (monocyte differentiation antigen), CD19 (B-lymphocyte antigen), CD34 (haematopoietic progenitor cell antigen), CD45 (haematopoietic cell marker), and HLA-DR (MHC class II cell surface receptor) (Figure 2(g)).

Overall, these data revealed high CFU-F content and a more homogenous nature of colony-forming cells in "clinically accessible" periosteal samples, compared to donor-matched BM samples. Additionally, in our chosen experimental conditions, periosteum MSC cultures had achieved lower cumulative PDs than their BM counterparts at the same passage.

3.3. Live Cell Tracking of Periosteum and Bone Marrow MSC Cultures. To explore if the observed differences seen in colony size between periosteum and BM MSCs could be due to different cell migration patterns, live cell imaging and tracking of cell movement over time was carried out using holographic imaging. Thawed P0 cell cultures (previously grown in culture for 13 days, 6.6 PD (periosteum) and 13 PD (BM)) were tracked from one donor (male, 17). Thawed freshly digested periosteum cultures were grown and shown to be not significant to their P0 counterparts (data not shown); therefore, P0 cultures were taken as surrogate to represent MSC migration for up to 2 weeks in culture (the end time point of a CFU-F assay).

Following thresholding of individual images and identification of cells, the morphology of the cells within each culture could be quantified and compared. There were two differing cell morphologies within both MSC populations. The first of which was "dividing" cells (Figure 3(a)), with high average cell thickness (>2.5 μm) but a small cell surface area (<1100 μm^2), reflecting a spherical shape just prior to cell division, which made up 2.05% (periosteum) and 2.12% (BM) of all cells (Figures 3(b) and 3(c)). The second, which formed the majority (97.95%: periosteum, 97.88%: BM), was "spindle-" shaped cells (Figure 3(a)), representing the classical MSC morphology, with an average cell thickness of 0.6-2.5 μm and cell surface area ranging from 79 to 2965 μm^2 (Table 2).

With respect to the "dividing" cells, the average thickness of periosteum cells (6.1 ± 2.5 μm) was significantly higher (unpaired Student's t-test, $P < 0.0001$) than BM cells (3.4 ± 0.6 μm); however, cell surface area was similar (Table 2). In addition, the periosteum "spindle-" shaped cells

had significantly higher cell surface area and cell thickness (unpaired Student's t-test, $P < 0.0001$) compared to BM cells. Overall, these data indicated that periosteal cells MSCs appear to have a larger cell volume than their BM counterparts.

The cell migration and movement patterns of periosteal and BM MSCs were assessed by live tracking of individual cells. Maps of cell movement (Figure 4(a)) revealed visual differences in MSC migration patterns of individual cells, whereby some cells were relatively nonmigratory, remaining in the same area, and other cells were seen to migrate across the field of view. "Cell migration" refers to the displacement of a tracked cell from the first measured coordinates, in comparison to "cell motility" which refers to the cumulative distance travelled at each time point. From three fields of view per culture, the whole cell population was quantified over 25 hours and mean cell migration was calculated as well as split into the migratory (>100 μm cell migration) or the nonmigratory (<100 μm cell migration) cells (Figure 4(a)).

To track changes in migration patterns over time, mean cell migration after 5 and 20 hours of cell tracking was compared. BM MSCs showed significantly higher mean cell migration (unpaired Student's t-test, $P < 0.0001$ (5 hours), $P = 0.001$ (20 hours)) at 5 hours (102.6 ± 54.6 μm (BM), 53.5 ± 32.6 μm (periosteum)) and 20 hours (209.1 ± 129.2 μm (BM) and 123.6 ± 67.6 μm (periosteum)) (Figure 4(b)). A similar trend was seen with cell motility, where BM MSCs were significantly more motile over time (unpaired Student's t-test, $P < 0.05$). At 5 hours, total cell motility (distance travelled) was 151.4 ± 53.6 μm (BM) compared to 95.6 ± 35.0 μm (periosteum), and by 20 hours, this difference had increased to 594 ± 136.0 μm (BM) and 384.2 ± 81.5 μm (periosteum) (Figure 4(c)).

The proportion of nonmigratory to migratory MSCs within the periosteum and BM cultures was 42% ($n = 45$) and 63% ($n = 94$), respectively, suggestive that there is a slightly lower proportion of cells classified as nonmigratory within periosteum cultures (Table 3). When comparing nonmigratory to migratory MSCs over time, significant increases in cell migration or displacement away from the initial tracked point were seen from 5 hours onwards between the migratory and nonmigratory cells for both culture types (unpaired Student's t-test, $P < 0.05$) (Figure 4(b)). Similar trends were seen, where cell migration steadily increased in a linear fashion and then started to plateau; however, while the plateau was seen at approximately 8 hours (>100 μm) and 5 hours (<100 μm) for BM cultures, this was extended to about 15 hours (<100 μm) or not well defined for >100 μm within periosteum cultures (Figure 4(b)).

Based on this data, it could be concluded that cell migration was not only "faster" in BM MSCs compared to their periosteum counterparts but also "further away" from the tracked start point (approximately 190 μm (BM) vs. 150 μm (periosteum)) (Figure 4(b)), indicating that the speed of cell movement was greater in BM cultures.

Significant increases in cell motility or distance (rather than displacement) migrated over time were seen with the migratory cells (>100 μm), compared to the nonmigratory cells (<100 μm) from 5 hours onwards (unpaired Student's t-test, $P < 0.005$), irrespective of culture type (Figure 4(c)).

(a)

• Dividing
• Spindle

(b)

• Dividing
• Spindle

(c)
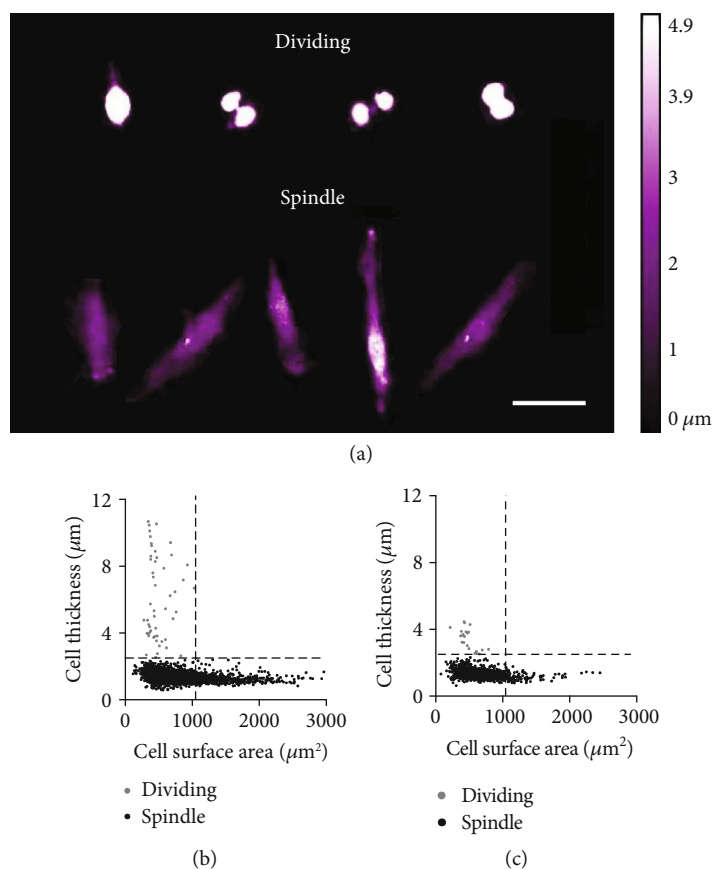
Figure 3: Distinct morphology types of MSCs described as "dividing" and "spindle" shaped. (a) Four individual cells in the process of cell division (top row) and five individual "spindle-" shaped cells, the classical MSC phenotype (bottom row). All quantified cells were plotted cell surface area vs. cell thickness to show the two different morphologies for (b) periosteum and (c) bone marrow cultures. Scale bar represents 50 μm. Dividing cells (grey) and spindle-shaped cells (black). Separation of cell types at $y = 2.5$ μm and $x = 1100$ μm^2.

Table 2: Summary of cell morphology of periosteum and bone marrow cultures. Periosteum (P) vs. bone marrow (BM), unpaired Student's t-test, ****$P < 0.0001$.

Cell morphology characteristic		Number of cells measured	Average cell thickness (μm)	Cell surface area (μm^2)
Dividing	P	51	6.1±2.5****	497 ± 172
	BM	23	3.4 ± 0.6	493 ± 126
Spindle	P	2438	1.4±0.3****	827±414****
	BM	1061	1.3 ± 0.3	668 ± 297

Cell motility was linear, irrespective of either class of migration, with r^2 values of >0.994 for both culture types. Therefore, cell speed (μm/h) was calculated from the gradient of the cell motility graphs (Figure 4(c)); as expected, the speed of the migratory cells was higher than the nonmigratory cells (Table 3). Furthermore, BM MSCs were shown to migrate at either 22.3 μm/h (<100 μm) or 32.0 μm/h (>100 μm), confirming that BM MSCs move with greater speed than periosteum MSCs (17.5 μm/h (<100 μm), 20.4 μm/h (>100 μm)) (Table 3).

Migration directness is a ratio of migration (displacement) to motility (distance), where 1 refers to movement in a straight line and 0 to a cell moving completely randomly. This parameter can be used to calculate whether cells migrate randomly or with apparent "purpose." In contrast to the previous parameters, no significant differences were seen between the MSC culture types over time (Figure 4(d)). Cell migration directness reduced over time, with the nonmigratory cells showing significantly reduced cell directness at 5 and 10 hours for both MSC types (unpaired Student's t-test, $P < 0.05$); however, after this, differences were not seen, suggestive that with time both MSC types migrated in a more random fashion.

Overall, these data provided new insights into BM and periosteum MSC behaviour in culture. Smaller volumes of BM MSCs could facilitate their faster migration capacities, which in turn could in part explain their ability to form larger colonies, compared to periosteal MSCs, in standard CFU-F assays.

3.4. MSC Differentiation Capacity.

Quantitative trilineage differentiation assays were carried out on donor-matched cultures in addition to qPCR for lineage-specific markers comparing day 0 (before differentiation) and day 21

(a)

(b)

(c)

(d)
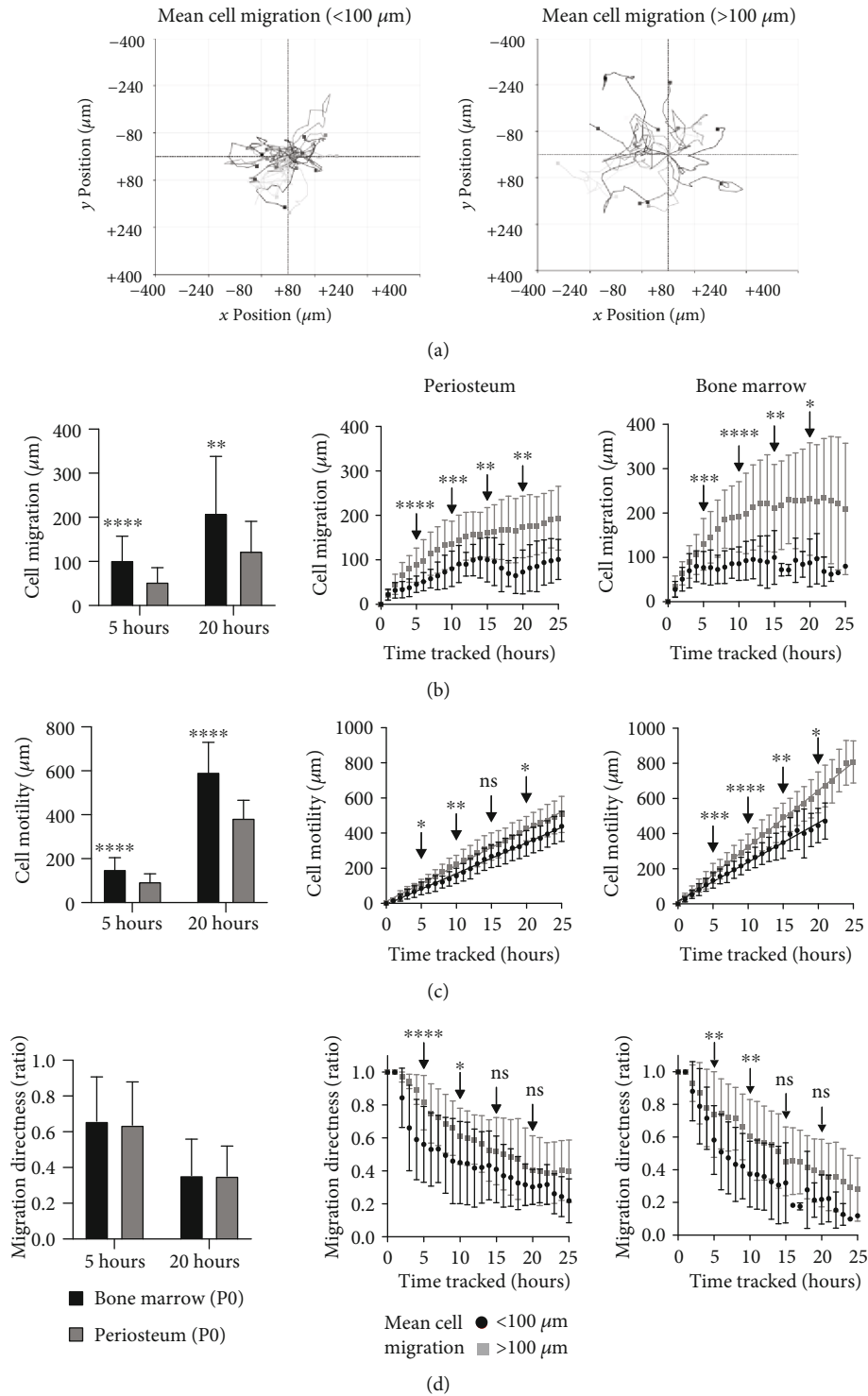
Figure 4: Live cell tracking of migration patterns of periosteum and bone marrow cultures. (a) Cell migration map of individually tracked cells with </>100 μm mean cell migration, multiple cells represented. (b) Quantification of cell migration, (c) cell motility, and (d) cell migration directness for periosteum and bone marrow cultures over time. (A) Quantified at 5 and 20 hours; (B, C) individually tracked cells were split into </>100 μm mean cell migration for periosteum (B) and bone marrow (C). Unpaired Student's t-test, $P < 0.05$, ****$P < 0.0001$, ***$P < 0.001$, **$P < 0.005$, and *$P < 0.05$, ns: not significant.

(following three weeks of differentiation induction). Osteogenic cultures were stained for ALP after two weeks and then for calcium deposition after three weeks, where visually similar staining could be seen for both culture types, with a

tendency for visually higher confluency in the periosteum cultures (Figure 5(b)). Calcium content was quantified ($n = 7$) at three weeks and was found to be slightly higher (but not significant, Wilcoxon signed-rank test, $P = 0.08$) in

TABLE 3: Summary of confluency, cell migration, and cell motility speed—split into nonmigratory and migratory cells, following cell tracking of periosteum and bone marrow MSC cultures.

Passage 0 MSC culture	Confluency (% cell coverage)		Number of cells split by cell migration (%)		Cell motility (μm/h)	
	0 hours	25 hours	<100 μm	>100 μm	<100 μm	>100 μm
Periosteum	5.0 ± 1.2	9.9 ± 3.3	42.2 ($n = 55$)	57.8 ($n = 26$)	17.5	20.4
Bone marrow	0.9 ± 0.3	2.7 ± 0.6	62.8 ($n = 59$)	37.2 ($n = 35$)	22.3	32.0

periosteum than BM cultures. Of note, there was high donor variation that was not shown to correlate with donor age (r^2 value, 0.17 (BM), 0.22 (periosteum)). qPCR showed reduction in the early osteogenic marker, *RUNX2* expression, but increases in the late osteogenic marker *BGLAP* expression at day 21 ($n = 3$) for both culture types, as expected.

In chondrogenic conditions, after three weeks, pellets of similar sizes were seen to form for periosteum and BM cultures and staining for GAG (toluidine blue) was confirmed for both (Figure 5(b)). Following quantification of GAG content, no significant differences were seen between periosteum and BM pellets (Wilcoxon signed-rank test, $n = 5$, $P = 0.99$) (Figure 5(b)). As with osteogenesis, there was high donor variability; however, donor age was seen to negatively affect GAG production for BM cultures ($r^2 = 0.77$), but not periosteum cultures ($r^2 = 0.22$). Chondrogenic differentiation markers, *COL2A1* and *SOX9*, were increased in both periosteum and BM pellets by day 21 (Figure 5(b)).

Noticeably, greater fat deposition was seen in BM cultures compared to periosteum, following three weeks of adipogenic induction and oil red staining ($n = 6$) (Figure 5(b)). Quantification of fat deposition (Nile red) and DNA (DAPI) levels revealed that BM cultures had higher fat per cell content (Wilcoxon signed-rank test, $P < 0.05$). *FABP4* was seen to increase in both culture types following adipogenic induction (Figure 5(b)); however, *PPAR-γ* increased in BM cultures but reduced in periosteum cultures.

4. Discussion

In this study, the potential for the utilisation of periosteum-derived MSCs as a source of MSCs during bone defect surgical repair was investigated. Currently, there is a lack of direct comparisons of MSCs derived from human periosteum and BMA, especially when donor matched [24, 35]. Here, for the first time, donor-matched comparisons of "clinically accessible" periosteum (from within the surgical opening of a fracture site) were compared to iliac crest BMA, a supply of MSCs currently used in surgery [36].

Both MSC sources were compared histologically to locate CD271+ candidate MSCs within each tissue [21, 37–39]. The cambium layer of periosteum has been historically described as a rich source of osteoprogenitors, whereas the fibrous layer is thought to be less cellular [16, 17, 40, 41]. However, this study has shown the presence of CD271+ cells in human samples located throughout the outer fibrous layer. These cells were localised surrounding blood vessels throughout the fibrous layer; therefore, even though the cambium layer was often not harvested, these data indicated that "clinically accessible" human periosteum could still contain a supply of MSCs.

CFU-F assays are the gold standard for MSC quantification in BM aspirates or solid connective tissues enzymatically processed to release viable cells [42]. Despite this, very few studies have so far quantified human periosteum MSC frequency [20, 42] and none of them compared it to donor-matched BMA. Our data on the 2500-fold higher frequency of MSCs present within "clinically accessible" periosteum samples, which most commonly do not include the cambium layer, present periosteum as a viable alternative to BM aspirates with high and consistent supply of MSCs. Of note, the MSC counts within BM samples (0.0008%) in this study were lower compared to the literature, which estimates 0.001-0.01% MSC [43]. This could be due to the fact that most of the BMA in our study were collected in large volumes (>50 mL) prior to concentration to generate BMAC, and it is known to result in BM dilution with peripheral blood [21, 32, 43]. Nevertheless, even at the highest MSC content for BMA (0.0027%) within this study, the donor-matched periosteum had >1500-fold more MSCs, thus confirming the superiority of periosteum samples with respect to their MSC content.

Until recently, CFU-F colony size measurements have not been routinely performed in MSC tissue comparison studies; however, these data can provide valuable information on MSC heterogeneity within the tissues under investigation. When this was carried out on BM aspirates, MSC subpopulations with different sizes and densities have been found indicating a high degree of MSC heterogeneity, which in one study was linked to donor age [22] but could be also related to different MSC topographies [44, 45]. Here, periosteum colonies were significantly smaller (half in size), and more homogenous than donor-matched BM counterparts, which aids in the predictability of periosteum MSC outcomes over BM MSCs.

In order to underpin the differences seen in colony formation between periosteum and BM MSC cultures, live cell imaging of early *in vitro* (2 weeks in culture) MSCs was carried out. Phase holographic imaging was utilised as a noninvasive, unlabeled high throughput method for quantifying cellular morphology and live cell tracking [46–48]. MSC morphology in both MSC sources was variable over time, changing hour by hour, with approximately 98% of the cells measured retaining the classical "spindle" shape, and the remaining 2% of the measured cells were retracted into
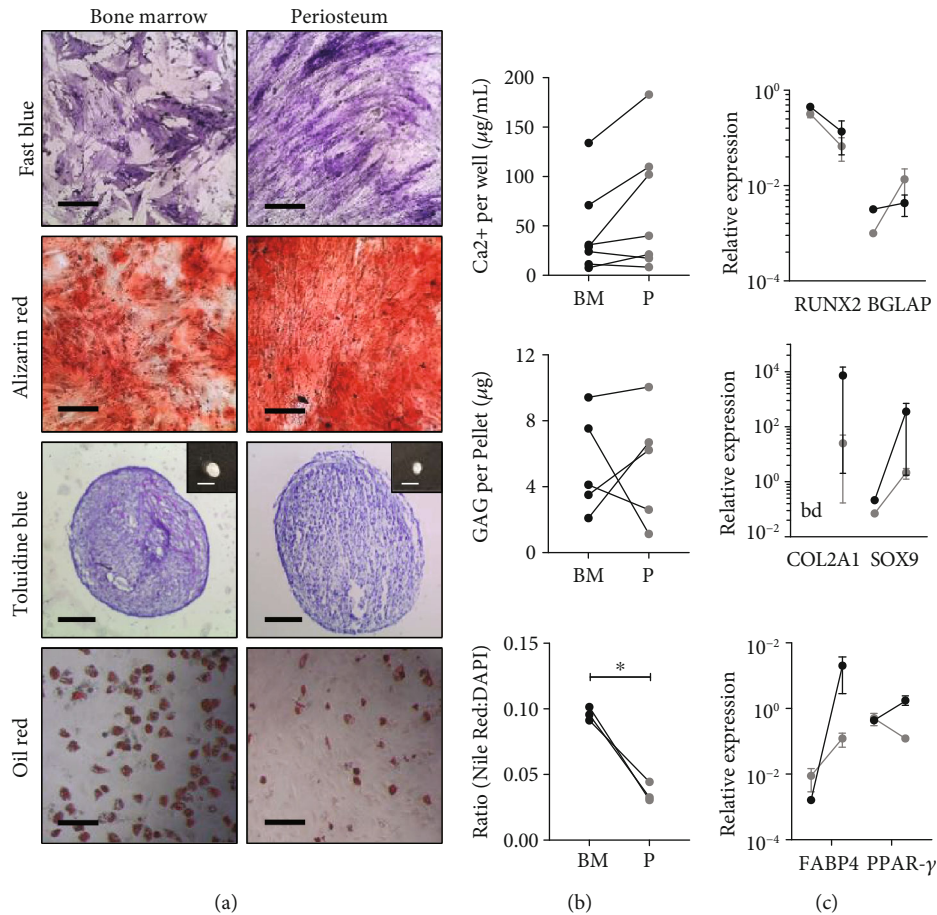
FIGURE 5: Trilineage differentiation assays, comparing donor-matched periosteum and bone marrow MSCs. Each assay was assessed using (a) histology staining, (b) quantitative assays, and (c) qPCR for specific markers of differentiation. Osteogenic assays stained for alkaline phosphatase (fast blue) and calcium deposition (alizarin red), with quantified Ca^{2+} content and assessment of runt-related transcription factor 2 (*RUNX2*) and bone gamma-carboxyglutamate (gla) protein (*BGLAP*) expression levels. Chondrogenic assay macro images (insert) stained for glycosaminoglycans (GAG) (toluidine blue), quantified GAG content and collagen, type 2, alpha 1 (*COL2A1*), and SRY- (sex-determining region Y-) box 9 (*Sox9*) expression levels. Adipogenic assays stained for fat deposition (oil red), quantified fat deposition (Nile red) and nuclei content (DAPI), and fatty acid-binding protein 4 (*FABP4*) and peroxisome proliferator-activated receptor-gamma (*PPAR-γ*) expression levels. Wilcoxon signed-rank test was carried out, $^{*}P < 0.05$. Scale bars represent $500\,\mu$m (fast blue, alizarin red, and oil red), $200\,\mu$m (macro insert), and $200\,\mu$m (toluidine blue). BM: bone marrow, P: periosteum, bd: below detection.

spheres, undergoing division. Similar proportions of dividing cells seen in these experiments are consistent with our data on similar growth rates between paired periosteum and BM cultures prior to passage zero. Based on these and our CFU-F data, we therefore hypothesised that smaller periosteum colony sizes could be due to their reduced cell area and/or poorer ability for migration rather than their reduced proliferation.

When individual cells were analysed over a 24-hour period, it was observed that as MSCs proliferate and occupy more surface, their migration plateaus and cell directness becomes more random, for both cell types. Indeed, periosteum MSCs were less migratory and moving at slower speeds than BM MSCs. This was also true when cells were divided into two subpopulations, nonmigratory and migratory, based on chosen arbitrary cut-off point of $100\,\mu$m. The speed at which MSCs migrate was also quantified; for the first time,

periosteum MSCs were shown to migrate at $17.5\,\mu$m/h (nonmigratory) and $20.4\,\mu$m/h (migratory), which was slower than their BM MSC counterparts at $22.3\,\mu$m/h (nonmigratory) and $30.0\,\mu$m/h (migratory). BM MSC migration speed within a collagen type I gel has been quantified previously in one study ($15\,\mu$m/h), which could reflect that migration speed is influenced by the substrate on which MSCs are in contact with [49]. This was also shown by Salam et al. [50], whereby fibrinogen matrix concentration was shown to inversely affect BM MSC migration, through reduction in pore size and changes in substrate stiffness. These characteristics may help to develop more rational approaches for bone scaffold design for repopulation by periosteal cells, for example, their optimal porosity. Related to this, a recent study utilised holographic imaging to assess growth and differentiation of BM MSCs onto a glass and a titanium oxide (TiO_2), showing favorable cell adhesion and

spreading on the TiO$_2$ coating [51], highlighting the potential of this technology in the tissue engineering field. Future work would aim at increasing donor numbers to assess donor variability and impact of donor age, as well as a more precise study of how cell confluence affects individual cells' behaviours.

With respect to cell size analysis, periosteum MSC cell area was 20% larger compared to donor-matched BM cells. This confirmed that despite higher cumulative PDs accrued by BM MSCs, they were not approaching senescence (senescent cells are larger) [52], which is consistent with our observations of similar proportions of dividing cells for both MSC types. Although this investigation was limited to a single pair of donor-matched cultures, the available evidence points towards slower motility of early-culture periosteal cells compared to BM cells in our experimental conditions, rather than their lower proliferation or smaller cell area. A larger cell surface area of periosteum MSCs could affect the traction forces required to overcome fractional and adhesive resistances required to allow for cell movement [53]. Confluence is another factor that can affect cell velocity or migration; however, this did not appear to influence the seen differences in this study, thus other factors must be at play.

We have shown that differing tissue sources of MSCs, from the same donor and grown *in vitro* for the same time period, are potentially interacting with the same substrate (in this case tissue culture plastic) in different ways, thus resulting in changes in cell surface area, migration distance, and velocity. It is known that migration of spindle-shaped cells, like MSCs, is dependent on the formation focal adhesions with actin filaments that mechanically link the extracellular matrix to the cytoskeleton and contractile stress fibres [53]. Levels of integrins and cytoskeleton within MSCs have previously been linked to influencing MSC differentiation, whereby increased focal adhesions and a stiff spread cytoskeleton appear to influence osteogenesis [54]. Goessler et al. [55] showed that adipose tissue MSCs and BM MSCs grown *in vitro* express different levels of various integrins, which influence focal adhesion formation. However, little is known about differences in integrin and focal adhesion levels between periosteum and BM MSCs; future developments to this work would involve ascertaining whether there are inherent differences in the cytoskeleton and focal adhesion formation.

For periosteum to be utilised as a source of MSCs for fracture healing, osteogenic and chondrogenic capacities are of particular importance [56, 57]. While osteogenic and chondrogenic differentiation capacities of periosteum MSC cultures were shown to be similar to donor-matched BM MSCs, adipogenic differentiation showed clear differences, whereby periosteal adipogenic potential was significantly lower than donor-matched BM MSCs. Differences could be partially explained through a reduction in *PPAR-γ* levels, a molecule critical to initiating adipocyte differentiation [58], in day 21 periosteum MSCs, whereas in BM MSCs, it was upregulated, consistent with previous studies [24, 31]. Mastoid periosteum MSC clones showed variation in trilineage differentiation capacity, whereby nearly all clones showed

osteochondral capacity, whereas only 53% were considered to be adipogenic [59]. Based on this and our data, it could be suggested that periosteum MSCs have a preferential commitment to osteochondral differentiation, needed for fracture repair.

As with harvesting of bone autograft for filling of critical size bone defects, a key point to consider with advocating for the use of periosteum is creating a minimal donor site morbidity. Currently, free vascularised corticoperiosteal bone grafts, where the periosteum and underlying cortical graft bone can be 4 cm^2, are harvested from the medial femoral condyle, to wrap around a defect site [60–63]. The femoral condyle is found to consolidate well following the harvesting process [60, 61]. Additionally, proof-of-concept studies in critical size bone defect sheep models have shown maximal defect bridging, where autologous periosteal strips were used, harvested with a periosteal elevator, thus removing the cambium layer [64, 65]. Together, this suggests that harvesting small graft(s) with a scalpel of the fibrous layer of periosteum as in this study, leaving the cambium mainly intact, would not create a donor site morbidity. This would allow for periosteum as a proliferative "MSC-rich" source to be transplanted into or around defect areas for the treatment of complex fracture or critical size bone defects, as a conjunct with other healing stimulating factors and cell sources that are currently in use.

5. Conclusions

"Clinically accessible" samples of long bone periosteum, a vital component of bone fracture repair has been shown to be a rich source of highly proliferative MSCs, compared to the current "gold-standard" BMA, with lower adipogenic but similar osteochondral potential. A novel live cell tracking technique permitted extensive quantification of morphological and migratory characteristics of periosteal MSCs that can be used to inform the development of novel bone graft substitutes to be repopulated by these cells. Further investigation into "minimally manipulated" periosteum samples, for example, periosteal micrografts, is needed for future clinical translation of this tissue source for use during single surgical procedure.

Data Availability

The data used to support the findings of this study are available from the corresponding author upon request.

Conflicts of Interest

The authors declare no conflict of interest with respect to the authorship, research, and/or publication of this article.

Acknowledgments

Supplementary Materials

Details of the antibodies used to phenotype MSCs with flow cytometry can be found in Supplementary Table 1. *(Supplementary Materials)*

References

[1] L. A. Mills, S. A. Aitken, and A. H. R. W. Simpson, "The risk of non-union per fracture: current myths and revised figures from a population of over 4 million adults," *Acta Orthopaedica*, vol. 88, no. 4, pp. 434–439, 2017.

[2] C. Tzioupis and P. V. Giannoudis, "Prevalence of long-bone non-unions," *Injury*, vol. 38, Supplement 2, pp. S3–S9, 2007.

[3] L. A. Mills and A. H. R. W. Simpson, "The relative incidence of fracture non-union in the Scottish population (5.17 million): a 5-year epidemiological study," *BMJ Open*, vol. 3, article e002276, 2013.

[4] E. Antonova, T. K. Le, R. Burge, and J. Mershon, "Tibia shaft fractures: costly burden of nonunions," *BMC Musculoskeletal Disorders*, vol. 14, no. 1, article 42, 2013.

[5] P. V. Giannoudis, T. A. Einhorn, and D. Marsh, "Fracture healing: the diamond concept," *Injury*, vol. 38, Supplement 4, pp. S3–S6, 2007.

[6] J. J. El-Jawhari, C. Sanjurjo-Rodríguez, E. Jones, and P. V. Giannoudis, "Collagen-containing scaffolds enhance attachment and proliferation of non-cultured bone marrow multipotential stromal cells," *Journal of Orthopaedic Research*, vol. 34, no. 4, pp. 596–606, 2016.

[7] T. A. Elsattar, A. I. Alseedy, and A. A. E. Khalil, "Bone marrow injection in treatment of long bone nonunion," *Menoufia Medical Journal*, vol. 27, no. 4, pp. 632–635, 2014.

[8] J. A. M. Guimarães, M. E. L. Duarte, M. B. C. Fernandes et al., "The effect of autologous concentrated bone-marrow grafting on the healing of femoral shaft non-unions after locked intramedullary nailing," *Injury*, vol. 45, no. S5, pp. S7–S13, 2014.

[9] D. Kouroupis, T. G. Baboolal, E. Jones, and P. V. Giannoudis, "Native multipotential stromal cell colonization and graft expander potential of a bovine natural bone scaffold," *Journal of Orthopaedic Research*, vol. 31, no. 12, pp. 1950–1958, 2013.

[10] R. L. Sahu, "Percutaneous autogenous bone marrow injection for delayed union or non-union of long bone fractures after internal fixation," *Revista Brasileira de Ortopedia*, vol. 53, no. 6, pp. 668–673, 2018.

[11] A. D. Mercurio, T. Motta, E. Green, G. Noble, R. T. Hart, and M. J. Allen, "Effects of extensive circumferential periosteal stripping on the microstructure and mechanical properties of the murine femoral cortex," *Journal of Orthopaedic Research*, vol. 30, no. 4, pp. 561–568, 2012.

[12] T. Wang, X. Zhang, and D. D. Bikle, "Osteogenic differentiation of periosteal cells during fracture healing," *Journal of Cellular Physiology*, vol. 232, no. 5, pp. 913–921, 2017.

[13] X. Zhang, C. Xie, A. S. P. Lin et al., "Periosteal progenitor cell fate in segmental cortical bone graft transplantations: implications for functional tissue engineering," *Journal of Bone and Mineral Research*, vol. 20, no. 12, pp. 2124–2137, 2005.

[14] D. Bisseret, R. Kaci, M. H. Lafage-Proust et al., "Periosteum: characteristic imaging findings with emphasis on radiologic-pathologic comparisons," *Skeletal Radiology*, vol. 44, no. 3, pp. 321–338, 2015.

[15] C. Colnot, X. Zhang, and M. L. K. Tate, "Current insights on the regenerative potential of the periosteum: molecular, cellular, and endogenous engineering approaches," *Journal of Orthopaedic Research*, vol. 30, no. 12, pp. 1869–1878, 2012.

[16] J. R. Dwek, "The periosteum: what is it, where is it, and what mimics it in its absence?," *Skeletal Radiology*, vol. 39, no. 4, pp. 319–323, 2010.

[17] C. Colnot, "Skeletal cell fate decisions within periosteum and bone marrow during bone regeneration," *Journal of Bone and Mineral Research*, vol. 24, no. 2, pp. 274–282, 2009.

[18] H. C. Brownlow, A. Reed, C. Joyner, and A. H. R. W. Simpson, "Anatomical effects of periosteal elevation," *Journal of Orthopaedic Research*, vol. 18, no. 3, pp. 500–502, 2000.

[19] E. Jones, A. English, S. M. Churchman et al., "Large-scale extraction and characterization of CD271+ multipotential stromal cells from trabecular bone in health and osteoarthritis implications for bone regeneration strategies based on uncultured or minimally cultured multipotential stromal cells," *Arthritis & Rheumatism*, vol. 62, no. 7, pp. 1944–1954, 2010.

[20] R. J. Cuthbert, S. M. Churchman, H. B. Tan, D. McGonagle, E. Jones, and P. V. Giannoudis, "Induced periosteum a complex cellular scaffold for the treatment of large bone defects," *Bone*, vol. 57, no. 2, pp. 484–492, 2013.

[21] R. Cuthbert, S. A. Boxall, H. B. Tan, P. V. Giannoudis, D. McGonagle, and E. Jones, "Single-platform quality control assay to quantify multipotential stromal cells in bone marrow aspirates prior to bulk manufacture or direct therapeutic use," *Cytotherapy*, vol. 14, no. 4, pp. 431–440, 2012.

[22] P. Ganguly, J. J. El-Jawhari, A. N. Burska, F. Ponchel, P. V. Giannoudis, and E. A. Jones, "The analysis of in vivo aging in human bone marrow mesenchymal stromal cells using colony-forming unit-fibroblast assay and the $CD45^{low}CD271^+$ phenotype," *Stem Cells International*, vol. 2019, Article ID 5197983, 14 pages, 2019.

[23] S. Pat, Ş. Korkmaz, S. Özen, and V. Şenay, "Heavily carbon doped GaAs nanocrystalline thin film deposited by thermionic vacuum arc method," *Journal of Alloys and Compounds*, vol. 657, no. 1, pp. 711–716, 2016.

[24] J. Eyckmans, G. L. Lin, and C. S. Chen, "Adhesive and mechanical regulation of mesenchymal stem cell differentiation in human bone marrow and periosteum-derived progenitor cells," *Biology Open*, vol. 1, no. 11, pp. 1058–1068, 2012.

[25] E. Fossett and W. S. Khan, "Optimising human mesenchymal stem cell numbers for clinical application: a literature review," *Stem Cells International*, vol. 2012, Article ID 465259, 5 pages, 2012.

[26] S. M. Churchman, S. A. Boxall, D. McGonagle, and E. A. Jones, "Predicting the remaining lifespan and cultivation-related loss of osteogenic capacity of bone marrow multipotential stromal

cells applicable across a broad donor age range," *Stem Cells International*, vol. 2017, Article ID 6129596, 10 pages, 2017.

[27] M. Dominici, K. le Blanc, I. Mueller et al., "Minimal criteria for defining multipotent mesenchymal stromal cells. The International Society for Cellular Therapy position statement," *Cytotherapy*, vol. 8, no. 4, pp. 315–317, 2006.

[28] E. M. Fragkakis, J. J. El-Jawhari, R. A. Dunsmuir et al., "Vertebral body versus iliac crest bone marrow as a source of multipotential stromal cells: comparison of processing techniques, tri-lineage differentiation and application on a scaffold for spine fusion," *PLoS One*, vol. 13, no. 5, pp. 1–20, 2018.

[29] C. A. Gregory, W. Grady Gunn, A. Peister, and D. J. Prockop, "An alizarin red-based assay of mineralization by adherent cells in culture: comparison with cetylpyridinium chloride extraction," *Analytical Biochemistry*, vol. 329, no. 1, pp. 77–84, 2004.

[30] J. El-Jawhari, K. Moisley, E. Jones, and P. V. Giannoudis, "A crosslinked collagen membrane versus a non-crosslinked bilayer collagen membrane for supporting osteogenic function of human bone marrow-multipotent stromal cells," *European Cells and Materials*, vol. 37, no. 1, pp. 292–309, 2019.

[31] A. Aldridge, D. Kouroupis, S. Churchman, A. English, E. Ingham, and E. Jones, "Assay validation for the assessment of adipogenesis of multipotential stromal cells––a direct comparison of four different methods," *Cytotherapy*, vol. 15, no. 1, pp. 89–101, 2013.

[32] S. M. Churchman, F. Ponchel, S. A. Boxall et al., "Transcriptional profile of native CD271+ multipotential stromal cells: evidence for multiple fates, with prominent osteogenic and Wnt pathway signaling activity," *Arthritis & Rheumatism*, vol. 64, no. 8, pp. 2632–2643, 2012.

[33] D. C. Ilas, S. M. Churchman, T. Baboolal et al., "The simultaneous analysis of mesenchymal stem cells and early osteocytes accumulation in osteoarthritic femoral head sclerotic bone," *Rheumatology*, vol. 58, no. 10, pp. 1777–1783, 2019.

[34] S. Churchman, D. Kouroupis, S. A. Boxall et al., "Yield optimisation and molecular characterisation of uncultured CD271+ mesenchymal stem cells in the reamer irrigator aspirator waste bag," *European Cells and Materials*, vol. 26, pp. 252–262, 2013.

[35] D. Chen, H. Shen, J. Shao et al., "Superior mineralization and neovascularization capacity of adult human metaphyseal periosteum-derived cells for skeletal tissue engineering applications," *International Journal of Molecular Medicine*, vol. 27, no. 14, pp. 707–713, 2011.

[36] R. Dimitriou, E. Jones, D. McGonagle, and P. V. Giannoudis, "Bone regeneration: current concepts and future directions," *BMC Medicine*, vol. 9, no. 1, article 66, 2011.

[37] D. Alexander, F. Schäfer, A. Munz et al., "LNGFR induction during osteogenesis of human jaw periosteum-derived cells," *Cellular Physiology and Biochemistry*, vol. 24, no. 3–4, pp. 283–290, 2009.

[38] D. Alexander, F. Schäfer, M. Olbrich et al., "MSCA-1/TNAP selection of human jaw periosteal cells improves their mineralization capacity," *Cellular Physiology and Biochemistry*, vol. 26, no. 6, pp. 1073–1080, 2010.

[39] S. A. Boxall and E. Jones, "Markers for characterization of bone marrow multipotential stromal cells," *Stem Cells International*, vol. 2012, Article ID 975871, 12 pages, 2012.

[40] H. Chang and M. K. Tate, "Concise review : the periosteum : tapping into a reservoir of clinically useful progenitor cells,"

[41] S. F. Evans, J. B. Parent, C. E. Lasko et al., "Periosteum, bone's "smart" bounding membrane, exhibits direction-dependent permeability," *Journal of Bone and Mineral Research*, vol. 28, no. 3, pp. 608–617, 2013.

[42] Y. Sakaguchi, I. Sekiya, K. Yagishita, and T. Muneta, "Comparison of human stem cells derived from various mesenchymal tissues: superiority of synovium as a cell source," *Arthritis & Rheumatism*, vol. 52, no. 8, pp. 2521–2529, 2005.

[43] M. E. Bernardo, F. Locatelli, and W. E. Fibbe, "Mesenchymal stromal cells," *Annals of the New York Academy of Sciences*, vol. 1176, no. 1, pp. 101–117, 2009.

[44] D. Gothard, J. I. Dawson, and R. O. C. Oreffo, "Assessing the potential of colony morphology for dissecting the CFU-F population from human bone marrow stromal cells," *Cell and Tissue Research*, vol. 352, no. 2, pp. 237–247, 2013.

[45] A. Tormin, O. Li, J. C. Brune et al., "CD146 expression on primary nonhematopoietic bone marrow stem cells is correlated with in situ localization," *Blood*, vol. 117, no. 19, pp. 5067–5077, 2011.

[46] T. Kawase, K. Okuda, M. Nagata, M. Tsuchimochi, H. Yoshie, and K. Nakata, "Non-invasive, quantitative assessment of the morphology of γ-irradiated human mesenchymal stem cells and periosteal cells using digital holographic microscopy," *International Journal of Radiation Biology*, vol. 92, no. 12, pp. 796–805, 2016.

[47] A. Mölder, M. Sebesta, M. Gustafsson, L. Gisselson, A. G. Wingren, and K. Alm, "Non-invasive, label-free cell counting and quantitative analysis of adherent cells using digital holography," *Journal of Microscopy*, vol. 232, no. 2, pp. 240–247, 2008.

[48] J. Persson, A. Mölder, S. Pettersson, and K. Alm, "Cell motility studies using digital holographic microscopy," in *Microscopy: Science, Technology, Applications and Education*, A. Meńdez-Vilas and J. Diáz Álvarez, Eds., pp. 1063–1072, Formatex Research Center, 2010.

[49] G. Kallifatidis, B. M. Beckermann, A. Groth et al., "Improved lentiviral transduction of human mesenchymal stem cells for therapeutic intervention in pancreatic cancer," *Cancer Gene Therapy*, vol. 15, no. 4, pp. 231–240, 2008.

[50] N. Salam, S. Toumpaniari, P. Gentile, A. M. Ferreira, K. Dalgarno, and S. Partridge, "Assessment of migration of human mscs through fibrin hydrogels as a tool for formulation optimisation," *Materials*, vol. 11, no. 9, article 1781, 2018.

[51] L. Petecchia, C. Usai, M. Vassalli, and P. Gavazzo, "Biophysical characterization of nanostructured TiO_2 as a good substrate for hBM-MSC adhesion, growth and differentiation," *Experimental Cell Research*, vol. 358, no. 2, pp. 111–119, 2017.

[52] W. Zhai, D. Yong, J. J. El-Jawhari et al., "Identification of senescent cells in multipotent mesenchymal stromal cell cultures: current methods and future directions," *Cytotherapy*, vol. 21, no. 8, pp. 803–819, 2019.

[53] F. Qu, F. Guilak, and R. L. Mauck, "Cell migration: implications for repair and regeneration in joint disease," *Nature Reviews Rheumatology*, vol. 15, no. 3, pp. 167–179, 2019.

[54] P. S. Mathieu and E. G. Loboa, "Cytoskeletal and focal adhesion influences on mesenchymal stem cell shape, mechanical properties, and differentiation down osteogenic, adipogenic, and chondrogenic pathways," *Tissue Engineering - Part B: Reviews*, vol. 18, no. 6, pp. 436–444, 2012.

Stem Cells: Translational Medicine, vol. 1, no. 6, pp. 480–491, 2012.

[55] U. R. Goessler, P. Bugert, K. Bieback et al., "Integrin expression in stem cells from bone marrow and adipose tissue during chondrogenic differentiation," *International Journal of Molecular Medicine*, vol. 21, no. 3, pp. 271–279, 2008.

[56] R. Marsell and T. Einhorn, "The biology of fracture healing," *Injury*, vol. 42, no. 6, pp. 551–555, 2011.

[57] A. Phillips, "Overview of the fracture healing cascade," *Injury*, vol. 36, no. 3, pp. S5–S7, 2005.

[58] C. J. Rosen, C. Ackert-Bicknell, J. P. Rodriguez, and A. M. Pino, "Marrow fat and the bone microenvironment: developmental, functional, and pathological implications," *Critical Reviews™ in Eukaryotic Gene Expression*, vol. 19, no. 2, pp. 109–124, 2012.

[59] S. Stich, A. Loch, S.-J. Park, T. Häupl, J. Ringe, and M. Sittinger, "Characterization of single cell derived cultures of periosteal progenitor cells to ensure the cell quality for clinical application," *PLoS One*, vol. 12, no. 5, article e0178560, 2017.

[60] K. Bakri, A. Shin, and S. Moran, "The vascularized medial femoral corticoperiosteal flap for reconstruction of bony defects within the upper and lower extremities," *Seminars in Plastic Surgery*, vol. 22, no. 3, pp. 228–233, 2008.

[61] U. H. Choudry, K. Bakri, S. L. Moran, Z. Karacor, and A. Y. Shin, "The vascularized medial femoral condyle periosteal bone flap for the treatment of recalcitrant bony nonunions," *Annals of Plastic Surgery*, vol. 60, no. 2, pp. 174–180, 2008.

[62] B. Fuchs, S. P. Steinmann, and A. T. Bishop, "Free vascularized corticoperiosteal bone graft for the treatment of persistent nonunion of the clavicle," *Journal of Shoulder and Elbow Surgery*, vol. 14, no. 3, pp. 264–268, 2005.

[63] M. F. Meek and W. F. A. Den Dunnen, "Porosity of the wall of a neurolac nerve conduit hampers nerve regeneration," *Microsurgery*, vol. 29, no. 6, pp. 473–478, 2009.

[64] M. L. Knothe Tate, H. Chang, S. R. Moore, and U. R. Knothe, "Surgical membranes as directional delivery devices to generate tissue: testing in an ovine critical sized defect model," *PLoS One*, vol. 6, no. 12, pp. 1–9, 2011.

[65] S. R. Moore, C. Heu, N. Y. C. Yu et al., "Translating periosteum's regenerative power: insights from quantitative analysis of tissue genesis with a periosteum substitute implant," *Stem Cells Translational Medicine*, vol. 5, no. 12, pp. 1739–1749, 2016.

Review Article

Adipose Stem Cell-Based Clinical Strategy for Neural Regeneration: A Review of Current Opinion

Yu-hao Wang ⓘ,[1,2,3] Yu-chen Guo ⓘ,[1,2] Dian-ri Wang ⓘ,[1,2,3] Ji-yuan Liu ⓘ,[1,2] and Jian Pan ⓘ[1,2,3]

[1]*State Key Laboratory of Oral Disease, West China Hospital of Stomatology, Sichuan University, Chengdu 610041, China*
[2]*National Clinical Research Center for Oral Diseases & Department of Oral and Maxillofacial Surgery, West China Hospital of Stomatology, Sichuan University, Chengdu 610041, China*
[3]*National Engineering Laboratory for Oral Regenerative Medicine, West China Hospital of Stomatology, Sichuan University, Chengdu, Sichuan Province 610041, China*

Correspondence should be addressed to Jian Pan; jianpancn@scu.edu.cn

Nerve injury is a critical problem in the clinic. Nerve injury causes serious clinic issues including pain and dysfunctions for patients. The disconnection between damaged neural fibers and muscles will result in muscle atrophy in a few weeks if no treatment is applied. Moreover, scientists have discovered that nerve injury can affect the osteogenic differentiation of skeletal stem cells (SSCs) and the fracture repairing. In plastic surgery, muscle atrophy and bone fracture after nerve injury have plagued clinicians for many years. How to promote neural regeneration is the core issue of research in the recent years. Without obvious effects of traditional neurosurgical treatments, research on stem cells in the past 10 years has provided a new therapeutic strategy for us to address this problem. Adipose stem cells (ASCs) are a kind of mesenchymal stem cells that have differentiation potential in adipose tissue. In the recent years, ASCs have become the focus of regenerative medicine. They play a pivotal role in tissue regeneration engineering. As a type of stem cell, ASCs are becoming popular for neuroregenerative medicine due to their advantages and characteristics. In the various diseases of the nervous system, ASCs are gradually applied to treat the related diseases. This review article focuses on the mechanism and clinical application of ASCs in nerve regeneration as well as the related research on ASCs over the past decades.

1. Introduction

Nerve injury is common in the clinic and leads to many other complications, such as muscle atrophy and abnormal bone reconstruction. The treatments of nerve injury cost USA medical insurance $150 billion every year, and these diseases affect 20 million Americans' lives [1]. Nerve injury occurs in 2% to 3% of citizens, and more than 50,000 peripheral nerve injury repair operations are performed per year in the United States [2]. Therefore, nerve injury and its complications cause huge financial burdens for social development and affect patients' life quality. Thus, it is critical for clinicians to solve these urgent problems.

Nerve injury results in muscle atrophy and abnormal bone reconstruction which leads motor dysfunction. In gen-

eral, satellite cells, as stem cells in skeletal muscle tissue, can repair atrophied and damaged skeletal muscles [3–7]. However, the recovery of damaged musculoskeletal tissue requires the involvement of nerve endings. It will form scar tissues without the involvement of nerve endings [8]. The loss of axonal continuity, nerve demyelination, and neuron cell death after nerve injury can lead to the denervation of skeletal muscle [2]. Some studies have demonstrated that muscle atrophy will happen after denervation within 2 weeks [9]. Furthermore, the accumulation ability of skeletal stem cells (SSCs) will decrease in the mandible with inferior alveolar nerve injury according to the Annual Clinical Congress of the American College of Surgeons in Boston, May 2018 [10]. Scientists attending the meeting have proved that nerve injury can affect the osteogenic differentiation of SSCs and

delay the procedure of bone fracture repair [10]. The mandible is the core component of the masticatory system, and any damage to the mandible can cause masticatory muscle disorder. The recovery of damaged nerve may have a positive impact on the bone fracture repair, and briefly, it may provide a new strategy for skeletal muscle dysfunction and bone diseases.

The orthodox treatment for nerve injury can be divided into two major categories: surgical methods and nonsurgical methods. However, both surgical and nonsurgical methods have their own limitations. For example, Robinson et al. found that only 4 of 53 patients who underwent neurological direct suture had some degree of recovery [11]. The possible reason is that the length of nerve defect is so long that the sutured nerve has a large tension between the sutural endings. The majority of clinicians reject to use medication alone for treatment due to the long periodicity of drug therapy. At present, there are no effective methods to treat nerve injury in the clinic. Fortunately, the research on stem cells and tissue engineering in the past decades may make it possible.

2. Stem Cells

Stem cells can self-renew and differentiate into multiple lineages. Currently, scientists have isolated several kinds of adult stem cells, such as bone marrow mesenchymal stem cells (BM-MSCs), skeletal stem cells (SSCs), dental pulp stem cells (DPSCs), adipose stem cells (ASCs), neural stem cells (NSCs), fetal-derived stem cells (FDSCs), human periapical cyst-mesenchymal stem cells (hPCy-MSCs), induced pluripotent stem cells (iPSCs), skin epidermal stem cells (SESCs), human amniotic-mesenchymal stem cells (hAMSCs), and hair follicle stem cells (HFSCs) [12–14].

Stem cells in different tissues can expand their quantities by symmetrical division during the growth and development of the human body. Meanwhile, stem cells can self-renew and have great ability of multidirectional differentiation to replace damaged cells by asymmetric division when some injuries occur in different tissues. It has been reported that intravenous injection of MSCs can treat acute lung and kidney injuries in preclinical trials with mouse disease models [15, 16]. ASCs derive from adipose tissues with some shared characteristics of all stem cells. More importantly, it is potential for ASCs to repair damaged tissues including nervous tissues.

3. The Fate and Biological Characteristics of ASCs

Easy obtainable methods with little damage for stem cell harvesting are the main ambition. The quantity of ASCs in adipose tissues is 100- to 500-fold compared with that of MSCs in bone marrow tissues. There are two types of human adipose tissue: white adipose tissue and brown adipose tissue. Subcutaneous adipose tissue in white adipose tissue is the main source of ASCs, and this kind of ASCs has a stronger antiapoptotic ability than ASCs located in brown adipose tissue [17]. However, ASCs from brown adipose tissue more easily undergo skeletal myogenic differentiation in the spe-

cific microenvironment [18, 19]. The characteristics of ASCs make them popular in the field of regeneration.

3.1. The Obtainable Method and Multipotential Differentiation of ASCs. It is widely accepted that ASCs can be harvested from adipose tissues and have great ability of multidirectional differentiation. With 0.075% collagenase type II digestion, ASCs can be harvested from the stromal vascular fraction (SVF) of adipose tissues. The ingredients of SVF include ASCs (15~30%), endothelial cells (10-20%), pericytes (3~5%), and immune cells (25~45%) [20, 21]. Due to the mesodermal origin of ASCs, they can differentiate into adipogenic, osteogenic, and chondrogenic lineages induced by selective medium *in vitro* [22, 23]. Among them, the neural differentiation of ASCs has attracted scientists' attention and created a new cell-based clinical strategy for neurodegenerative diseases.

3.2. Neural Differentiation. Safford et al. firstly induced ASCs to differentiate into neuronal phenotype cells which express nestin and neuronal nuclei protein (NeuN) in 2002 [24]. The inducing and differentiation medium they used for neural differentiation of ASCs contained valproic acid, butyl hydroxyanisole, insulin, and hydrocortisone. However, this chemical method is not suitable to induce differentiation *in vivo* due to its disability to construct the corresponding microenvironment in the body for neural regeneration [25]. Moreover, chemical reagents in the medium can cause some extra damage to tissues, which brings pain to patients.

Biological induction methods are more suitable for repairing damaged tissues *in vivo*. ASCs can be induced to differentiate into neural cells if the medium contains some soluble factors secreted from nerve tissues which include cerebellum, hippocampus, and cerebral cortex [26]. ASCs can also secrete some neurotrophic factors in the process of neural differentiation, such as nerve growth factor (NGF), brain-derived neurotrophic factor (BDNF), glial-derived neurotrophic factor (GDNF), ciliary neurotrophic factor (CNTF), and fibroblast growth factor (FGF) [27]. The current problem lies in how to control the direction of neural differentiation. Both neurons and glial cells can promote the remyelination of nerve which is of great importance for neural regeneration and express the similar markers [28–30]. However, some differences can be pointed out. A higher tendency of neuronal phenotype can be recognized when ASCs are induced by olfactory ensheathing cell conditioned medium (OEC-CM) [31, 32]. Instead, ASCs are more likely to differentiate into glial cells in Schwann cell conditioned medium (SC-CM) with high concentration of GFAP [31, 32].

ASCs can promote axonal regeneration, myelination, and functional recovery [33]. ASCs upregulate the expression of myelin protein zero, peripheral myelin protein-22, and myelin basic protein, which promotes self-regulation of ASC differentiation and reestablishes the connection between damaged nerve and target organs [34]. Some animal models have proved that ASCs have neuroprotection abilities and provide trophic supports for axon regeneration in optic nerve transection, glaucoma, and retinitis pigmentosa [35–37].

Furthermore, ASCs were applied to the preclinical trials for the CNS diseases, such as Alzheimer's disease (AD) and Parkinson's disease (PD) [38].

4. The Regulation and Mechanism in the Neural Differentiation of ASCs

There is a complex regulatory network in the neural differentiation of ASCs. In addition to neurotrophic factors secreted by ASCs, parts of signaling pathways are also involved in the differentiation courses. Most importantly, ASCs can promote their own neural differentiation by regulating the microenvironment. It is widely accepted that the microenvironment regulation interacts with the neural differentiation of ASCs [39]. The neural differentiation of ASCs takes place under complex regulatory mechanisms and promotes neural regeneration in order to repair damaged nervous tissues.

4.1. The Neurotrophic Effect. The paracrine function of stem cells is a kind of mechanism that accelerates the process of neural differentiation. Undifferentiated ASCs can secrete neuroprotective factors to enhance neural regeneration and reduce muscle atrophy [40, 41]. These neuroprotective factors include BDNF, GDNF, CNTF, and neurotrophin-4 [41]. Furthermore, some angiogenesis and antiapoptotic factors are also secreted by ASCs, including hepatocyte growth factor (HGF), transforming growth factor-β (TGF-β), and vascular endothelial growth factor (VEGF) [42–46]. Some scientists believe that the inhibition of apoptosis is a crucial step in tissue regeneration, which is decided by the concentration of antiapoptotic factors in the microenvironment [47]. Antiapoptotic factors and neurotrophic factors can promote neuron proliferation and survival [48, 49]. Another important point is that the activation and proliferation of microglia accelerate the process of some neurodegenerative diseases, for example, traumatic brain injury (TBI) [50–54]. Jha et al. have proved that trophic factors secreted by ASCs can normalize microglia and slow down the development of neurodegenerative diseases [55].

Neurotrophic factor is a sort of protein molecule necessary for the growth and survival of neurons [56]. Among the known neurotrophic factors, BDNF is one of the most important factors in the development of the nervous system [41]. BDNF is a neural-related protein encoded early during the embryonic period and its genome is made of eight promoters, each of which binds to a common BDNF full-length protein-encoding exon [57]. Transcription of BDNF is regulated by several mechanisms [58–60]. For example, the cAMP response element-binding protein (CREB) controls the transcription of exon IV and it is a key factor for the synaptic plasticity of neurons and cognition [61–64]. Furthermore, forskolin is a cAMP-elevating agent that can upregulate the expression of BDNF [65]. Recent studies have shown that the use of BDNF has a positive impact on synaptic plasticity, neuron-glia communication, and regulation of neurite outgrowth [66, 67]. The neuron-glia communication is the foundation of neural maintenance. Glial cells can upregulate the expression of BDNF by receiving the signals from neurons [67–69].

4.2. The Microenvironment Regulation of ASCs. ASCs can improve the microenvironment for neural regeneration by inhibiting inflammatory responses [70]. Inflammation is induced by proinflammatory immune cells and cytokines and ASCs can secrete angiogenic factors to inhibit that process [71–74]. The newborn blood vessels ameliorate the microenvironment for tissue recovery while the inhibition of angiogenesis aggravates the progression and pathology of inflammation [75]. Black et al. found that ASCs reduced inflammatory response and demonstrated positive therapeutic effects on chronic inflammatory bowel disease in dogs [76]. ASCs can inhibit neural cell apoptosis by releasing anti-inflammatory factors and cytokines, which provide a stable microenvironment for the neural differentiation of ASCs [77].

The main anti-inflammatory factors secreted by ASCs include tumour necrosis factor-inducible gene 6 protein (TSG-6) and STC-1 [78–81]. TSG-6 is a component of the negative feedback mechanism and it can downregulate the inflammatory response [82]. Increasing evidences indicate that some paracrine factors secreted by ASCs are enough to alleviate inflammatory diseases in animal neural disease models [78, 80, 83, 84]. The anti-inflammatory and immunomodulatory effects of these cytokines and chemokines are not only affected by the status of ASCs but are also affected by the concentration of TGF-β1, tumour necrosis factor-α (TNF-α), lipopolysaccharide (LPS), and hypoxia in microenvironments [85–88]. Taken together, the interaction between the neural differentiation of ASCs and the regulation of the microenvironment has a positive influence on inflammatory inhibition.

4.3. The Regulation of Signaling Pathways. Since the discovery of the signaling pathways was introduced, scientists have discovered that most of cell physiology can be explained by the regulation of signaling pathways. The neural differentiation of ASCs is also regulated by multiple signaling pathways. Here, we reviewed several known signaling pathways involved in the neural differentiation process.

Researchers have discovered that the Wnt signaling pathway is involved in the formation of the brain. The Wnt/LEF/TCF genes work synergistically to participate in the development of the hippocampal gyrus, and Wnt3a knockout can stop the development of hippocampus in mouse embryos [89–91]. In addition, the Wnt signaling pathway is also involved in the initiation of axon formation. Wnt7a can induce the reconstitution of axons and growth cones in mossy nerve fibers, as well as the collection of receptors I [91]. In contrast, Jang et al. have demonstrated that the classical Wnt signaling pathway does not regulate the neural differentiation of ASCs. Instead, they have proved that the noncanonical Wnt signaling pathway activates the neural differentiation of ASCs by regulating the activation/phosphorylation of Wnt5a/JNK signaling pathway [92].

Some other signaling pathways have been found to participate in the neural differentiation process, such as ROCK and BDNF/TrkB signaling pathway. Ren et al. have proved that the ROCK pathway inhibitor, namely, Y-27632, could accelerate the neural differentiation of ASCs in their

experiment. After adding Y-27632 into the culture medium, the shape of mouse ASCs switched to neuronal-like cells. Furthermore, the cells lost their neuron-like morphology once Y-27632 was removed from the medium [93]. It indicates that the ROCK signaling pathway inhibits the neural differentiation of ASCs. Some scholars have pointed out that ASCs may be also regulated by the BDNF/TrkB signaling pathway during the neural differentiation [84]. The BDNF/TrkB signaling pathway induces the secretion of BDNF which is a neurotrophic factor which can promote the neural differentiation of ASCs as previously mentioned [85]. However, scientists are not sure how these multiple signaling pathways interplay in the neural differentiation of ASCs. More research is needed in this field.

5. The Prospects for Clinical Application of ASCs in Neural Disease

Due to the limited therapeutic effect of clinical methods, treatment for nerve injury cannot keep pace with the life quality of people. Many elderly people suffer from nervous system diseases around the world. For example, the organic chemical pollution in water always causes serious nervous system diseases in developing countries and backward regions. Nerve injury not only leads to neurological disorders but also musculoskeletal system damage. Taking into account the limitations of current therapeutic methods, the application of stem cell-based therapy is extremely urgent.

The occurrence of neurodegenerative diseases involves a variety of pathophysiological mechanisms that determine the progress and severity of the diseases including neuroinflammation, mitochondrial dysfunction, and protein aggregation [94]. There are several common neurodegenerative diseases in the clinic, such as AD, PD, TBI, and spinal cord injury (SCI). In addition to their own ability to differentiate into nerve cells, ASCs can also secrete various neurotrophic factors and immune regulatory mediators. In the recent years, clinical application of ASCs has attracted much attention in the field of regenerative medicine.

5.1. AD. AD is a neurological degenerative disease with family heritability [95]. It is characterized by generalized dementia, such as memory impairment, loss of recognition, abnormal motion, and personality and behavioural change. AD may be a heterogeneous group of diseases, which is regulated by a variety of factors, including biological and psychosocial factors. Entanglement of amyloid-β plaques and neuronal fibers, neurodegeneration of the limbic system, and neural progressive decline are the main pathological features of AD [96].

Kim et al. have proved that the application of ASCs in the AD mouse experimental models was feasible [97]. In their study, the Morris water maze test (MWM) of mice was significantly improved. They found that Aβ plaque formations were reduced in the cerebral cortex. Amyloid precursor protein (APP) levels were reduced and Aβ-degrading enzyme levels were also upregulated. These phenomena clearly showed that the symptom of AD has been ameliorated. In another experiment, ASCs increased the secretion of anti-inflammatory factors, enhancing the expression of Aβ-degrading enzymes and raising the response levels in cognitive and memory tests [38]. Furthermore, ASCs increased the secretion of interleukin-10 and induced microglia to polarize the activation phenotype as well as express several vascular and neurotrophic factors [38, 97, 98]. In the recent years, Pérez-González et al. found that ASCs could secrete leptin during neural differentiation. Leptin is a kind of protein hormone which promotes the neural regeneration of stem cells *in vitro* and slows down the process of neurodegenerative diseases *in vivo* [99].

5.2. PD. PD is a common degenerative disease of the nervous system in the elderly. The main pathological features of PD are progressive dopaminergic neuron loss in the substantia nigra pars compacta. Tremor, muscle rigidity, and decreased motion are the main clinical features of PD. Zhang et al. have found that PD patients always had chest muscle tissue tension which lead to breath function disorder [100]. It shows that the nervous system damage of PD is not the most fatal factor for patients. Dyspnea and its complications caused by PD are the greatest harm to the human body.

In animal experimental models of PD, ASCs upregulated the secretion of soluble growth factors including anti-inflammatory factors and BDNF [101]. BDNF is an important neurotropic factor which can promote differentiation of stem cells and anti-inflammatory can improve the micro-environment as described earlier. The ASC-based regenerative therapy has a huge potential to treat PD and provides us a new strategy to improve neural and musculoskeletal tissue function for PD patients. However, Schwerk et al. found that the function of regenerative dopaminergic neurons induced by ASCs cannot completely replace that of lost dopaminergic neurons [102]. Furthermore, some scientists demonstrated that ASCs cannot improve the survival rate of PD patients after clinical treatment [103]. More research is required to clarify whether ASCs are useful in the treatment of PD.

5.3. SCI. SCI is one of the common symptoms in serious traumas caused by car accidents or falls. Serious injury to the limbs and muscle atrophy due to disconnection between muscles and damaged nerves disturb the ordinary life of patients. Thousands of SCI patients impose a huge burden on the development of social economy, and it costs billions of dollars every year [1]. The prevention, treatment, and rehabilitation of SCI have become a major issue in the medical field due to its urgency for patients and society.

Some studies have shown that ASCs can survive and migrate to damaged nerve tissue in animal experimental models [104]. Meanwhile, transplanted ASCs express GFAP and neuronal nuclear antigens in ischaemic encephalopathy [105]. In a previous study, the expression of GFAP, NF160, and Tuj-1 of ASCs was positive after transplanted ASCs were inserted into lentiviral vectors that were GFP-tagged in SCI models [8]. It is suggested that the implantation of ASCs can differentiate into astrocytes and oligodendrocytes as well as neurons. Neurons deriving from differentiation can

convey regenerative information from proximal-disrupting-ending neural fibers to the distal side [106].

The neural regeneration in SCI has a positive effect on innervation to muscle after peripheral nerve injury. When the peripheral nerve breaks down, the skeletal muscle which is innervated by the damaged nerve degenerates and muscle atrophy occurs. The neural transdifferentiation process may be the consequence of cytokine secretion, the interactions of ASCs and intercellular signaling pathways of ASCs [107]. Also, ASCs have been shown to secrete a variety of angiogenic and antiapoptotic cytokines, which support tissue regeneration and minimize tissue damage [108].

5.4. TBI. TBI is a type of disruption or alteration of brain function caused by external forces. Skull fracture and intracranial hypertension caused by TBI can lead to conscious disturbance, headache, and vomiting which are transient or long-lasting clinical symptoms of patients. External forces that cause TBI include acceleration or deceleration, direct compression, penetration of objects, and explosion damage. In the United States, the top three causes of TBI are fall (28%), motor vehicle accidents (20%), and pedestrian impact (19%) [109]. Masel and Dewitt thought that TBI is a cascade process involving primary and secondary brain injury instead of a simple external force injury process [110]. Primary damage refers to mechanical damage to the brain tissue caused by external forces. Secondary damage is a cellular metabolic event that occurs after an external force injury [111]. Within 24 hours after the brain tissue injury, the blood-brain barrier has been damaged and inflammatory cells enter the brain tissue leading to the occurrence of inflammation.

Tajiri et al. have proved that ASCs and ASC-associated secreted proteins can reduce cortical damage in mouse TBI models [112]. But the experimental mice were killed at an early stage, and the relevant mechanisms have not been proved. However, a possible mechanism is increasingly supported in scholars: inflammatory suppression theory [113]. Regarding these patients suffering TBI, inflammatory cells release kinds of immune-mediated factors. It is often considered as a secondary brain injury [114, 115]. TNF-α, as a kind of inflammatory factor, mainly predominates the inflammatory response [116, 117]. Controlling the inflammatory response after injury can be thought as a target for the TBI treatment. Kappy et al. have demonstrated that ASCs and its own secreting proteins downregulate the secretion of inflammatory factors and inhibit the inflammation in TBI [118–120].

Furthermore, β-APP is thought to be an important marker of nerve damage [121]. β-APP is a complete membrane protein with a high concentration in neuronal synapses. The role of β-APP in the brain has not been clarified, but the concentration of β-APP has been found increasing in the mouse TBI model [121]. β-APP can be used as a marker for diagnosing nerve damage and assessing the severity of TBI [122]. In Kappy's experiment, inserting ASCs into TBI mouse maintains the β-APP concentration instead of making the concentration of β-APP continuously increasing

[118]. It suggests that ASCs play a neuroprotective role in the TBI model.

6. Conclusion

Stem cells have great abilities of multidirectional differentiation and are widely found in nearly all organs and tissues except the heart. When human tissues or organs are damaged or diseased, stem cells can differentiate into corresponding progenitor cells and replenish the cell pools to recover normal function of organs. However, due to the particularity of the nervous system, nerves are less able to self-regenerate. The nerve injury is not only limited to the nerve tissues but also often affects the musculoskeletal tissues. Muscle atrophy and scar formation can be effectively prevented by neural regeneration. At present, the clinical therapy for neurodegenerative diseases mainly includes surgical and nonsurgical means, such as neurolysis, direct nerve suture, and drug treatment. Although these methods have been proved to have a degree of curative effect, it has not lived up to expectations. In recent years, stem cell-based therapies are expected to replace orthodox treatment.

ASCs that are isolated from adipose tissue can differentiate into other kinds of cells with a low mortality rate *in vivo* and *in vitro*. ASCs have advantages of easy material extraction, which means that they could be extracted from many types of tissues with slight damage to the body. Most importantly, ASCs are characterized by low immunogenicity and are not susceptible to immune rejection. Considering the advantages above, we are looking forward to a fact that ASCs will play a crucial role in the treatment of various tissue and organ diseases. In particular, in the nervous system, ASCs are important for promoting neural regeneration. The neurogenic and osteogenic differentiation of ASCs accelerates the recovery of damaged tissues. It will provide a new method for orthodox treatments. However, there are still many issues in the field of neural regeneration with ASCs. For example, the neural differentiation ability of ASCs extracted from different tissues should be clarified in order to identify the most efficacious ASC source for neural regeneration. More research is needed in the field for clinical application. We truly believe that ASCs would play a signature role for neural regeneration in the future.

Abbreviations

AD:	Alzheimer's disease
APP:	Amyloid precursor protein
ASCs:	Adipose stem cells
BDNF:	Brain-derived neurotrophic factor
BM-MSCs:	Bone marrow mesenchymal stem cells
CNS:	Central nervous system
CNTF:	Ciliary neurotrophic factor
CREB:	cAMP response element-binding protein
DPSCs:	Dental pulp stem cells
FDSCs:	Fetal-derived stem cells
FGF:	Fibroblast growth factor
GDNF:	Glial-derived neurotrophic factor
GFAP:	Glial fibrillary acidic protein

HGF: Hepatocyte growth factor
HFSCs: Hair follicle stem cells
hPCy-MSCs: Human apical cyst-mesenchymal stem cells
iPSCs: Induced pluripotent stem cells
LPS: Lipopolysaccharide
MSCs: Mesenchymal stem cells
MWM: Morris water maze test
NeuN: Neuronal nuclei protein
NGF: Nerve growth factor
NSCs: Neural stem cells
OEC-CM: Olfactory ensheathing cell conditioned medium
PD: Parkinson's disease
PNS: Peripheral nervous system
SC-CM: Schwann cell conditioned medium
SCI: Spinal cord injury
SESCs: Skin epidermal stem cells
SSCs: Skeletal stem cells
SVF: Stromal vascular fraction
TBI: Traumatic brain injury
TGF-β: Transforming growth factor-β
TNF-α: Tumour necrosis factor-α
TSG-6: Tumour necrosis factor-inducible gene 6 protein
VEGF: Vascular endothelial growth factor.

Conflicts of Interest

The authors declare no conflict of interests.

Acknowledgments

References

[1] D. Grinsell and C. P. Keating, "Peripheral nerve reconstruction after injury: a review of clinical and experimental therapies," *Biomed Research International*, vol. 2014, Article ID 698256, 13 pages, 2014.

[2] L. Yue, M. A. Talukder, A. Gurjar et al., "4-Aminopyridine attenuates muscle atrophy after sciatic nerve crush injury in mice," *Muscle & Nerve*, vol. 60, no. 2, pp. 192–201, 2019.

[3] J. Gros, M. Manceau, V. Thomé, and C. Marcelle, "A common somitic origin for embryonic muscle progenitors and satellite cells," *Nature*, vol. 435, no. 7044, pp. 954–958, 2005.

[4] P. Seale, L. A. Sabourin, A. Girgis-Gabardo, A. Mansouri, P. Gruss, and M. A. Rudnicki, "Pax7 is required for the specification of myogenic satellite cells," *Cell*, vol. 102, no. 6, pp. 777–786, 2000.

[5] M. Cerletti, S. Jurga, C. A. Witczak et al., "Highly efficient, functional engraftment of skeletal muscle stem cells in dystrophic muscles," *Cell*, vol. 134, no. 1, pp. 37–47, 2008.

[6] S. Fukada, S. Higuchi, M. Segawa et al., "Purification and cell-surface marker characterization of quiescent satellite cells from murine skeletal muscle by a novel monoclonal antibody," *Experimental Cell Research*, vol. 296, no. 2, pp. 245–255, 2004.

[7] S. Kuang, K. Kuroda, F. le Grand, and M. A. Rudnicki, "Asymmetric self-renewal and commitment of satellite stem cells in muscle," *Cell*, vol. 129, no. 5, pp. 999–1010, 2007.

[8] H. H. Ryu, J. H. Lim, Y. E. Byeon et al., "Functional recovery and neural differentiation after transplantation of allogenic adipose-derived stem cells in a canine model of acute spinal cord injury," *Journal of Veterinary Science*, vol. 10, no. 4, pp. 273–284, 2009.

[9] V. Moresi, A. H. Williams, E. Meadows et al., "Myogenin and class II HDACs control neurogenic muscle atrophy by inducing E3 ubiquitin ligases," *Cell*, vol. 143, no. 1, pp. 35–45, 2010.

[10] R. E. Jones, R. C. Ransom, A. Salhotra, D. S. Foster, D. C. Wan, and M. T. Longaker, "Nerve-dependent mandibular regeneration by skeletal stem cells in fracture repair," *Journal of the American College of Surgeons*, vol. 227, no. 4, p. S197, 2018.

[11] P. P. Robinson, A. R. Loescher, and K. G. Smith, "A prospective, quantitative study on the clinical outcome of lingual nerve repair," *British Journal of Oral & Maxillofacial Surgery*, vol. 38, no. 4, pp. 255–263, 2000.

[12] N. G. Fairbairn, A. M. Meppelink, J. Ng-Glazier, M. A. Randolph, and J. M. Winograd, "Augmenting peripheral nerve regeneration using stem cells: a review of current opinion," *World Journal of Stem Cells*, vol. 7, no. 1, pp. 11–26, 2015.

[13] Y. Guo, W. Wu, X. Ma, M. Shi, and X. Yang, "Comparative gene expression profiling reveals key pathways and genes different in skin epidermal stem cells and corneal epithelial cells," *Genes & Genomics*, vol. 41, no. 6, pp. 679–688, 2019.

[14] H. C. Pan, D. Y. Yang, Y. T. Chiu et al., "Enhanced regeneration in injured sciatic nerve by human amniotic mesenchymal stem cell," *Journal of Clinical Neuroscience*, vol. 13, no. 5, pp. 570–575, 2006.

[15] A. Monsel, Y. G. Zhu, S. Gennai, Q. Hao, J. Liu, and J. W. Lee, "Cell-based therapy for acute organ injury: preclinical evidence and on-going clinical trials using mesenchymal stem cells," *Anesthesiology*, vol. 121, no. 5, pp. 1099–1121, 2014.

[16] S. Bruno and B. Bussolati, "Therapeutic effects of mesenchymal stem cells on renal ischemia–reperfusion injury: a matter of genetic transfer?," *Stem Cell Research & Therapy*, vol. 4, no. 5, p. 55, 2013.

[17] J. W. Kuhbier, B. Weyand, C. Radtke, P. M. Vogt, C. Kasper, and K. Reimers, "Isolation, characterization, differentiation, and application of adipose-derived stem cells," in *Bioreactor Systems for Tissue Engineering II*, vol. 123, pp. 55–105, Springer, Berlin, Heidelberg, 2010.

[18] E. Raposio and N. Bertozzi, "Isolation of ready-to-use adipose-derived stem cell (ASC) pellet for clinical applications and a comparative overview of alternate methods for ASC isolation," *Current Protocols in Stem Cell Biology*, vol. 41, no. 1, pp. 1F.17.1–1F.17.12, 2017.

[19] E. Raposio and N. Bertozzi, "How to isolate a ready-to-use adipose-derived stem cells pellet for clinical application," *European Review for Medical and Pharmacological Sciences*, vol. 21, no. 18, pp. 4252–4260, 2017.

[20] O. DelaRosa, B. Sánchez-Correa, S. Morgado et al., "Human adipose-derived stem cells impair natural killer cell function and exhibit low susceptibility to natural killer-mediated lysis," *Stem Cells and Development*, vol. 21, no. 8, pp. 1333–1343, 2012.

[21] J. M. Gimble, A. J. Katz, and B. A. Bunnell, "Adipose-derived stem cells for regenerative medicine," *Circulation Research*, vol. 100, no. 9, pp. 1249–1260, 2007.

[22] C. Radtke, B. Schmitz, M. Spies, J. D. Kocsis, and P. M. Vogt, "Peripheral glial cell differentiation from neurospheres derived from adipose mesenchymal stem cells," *International Journal of Developmental Neuroscience*, vol. 27, no. 8, pp. 817–823, 2009.

[23] S. G. Almalki and D. K. Agrawal, "Key transcription factors in the differentiation of mesenchymal stem cells," *Differentiation*, vol. 92, no. 1-2, pp. 41–51, 2016.

[24] K. M. Safford, K. C. Hicok, S. D. Safford et al., "Neurogenic differentiation of murine and human adipose-derived stromal cells," *Biochemical and Biophysical Research Communications*, vol. 294, no. 2, pp. 371–379, 2002.

[25] A.-M. Rodriguez, C. Elabd, E. Z. Amri, G. Ailhaud, and C. Dani, "The human adipose tissue is a source of multipotent stem cells," *Biochimie*, vol. 87, no. 1, pp. 125–128, 2005.

[26] C. Han, L. Song, Y. Liu, W. Zou, C. Jiang, and J. Liu, "Rat cortex and hippocampus-derived soluble factors for the induction of adipose-derived mesenchymal stem cells into neuron-like cells," *Cell Biology International*, vol. 38, no. 6, pp. 768–776, 2014.

[27] J. D. Kocsis, K. L. Lankford, M. Sasaki, and C. Radtke, "Unique in vivo properties of olfactory ensheathing cells that may contribute to neural repair and protection following spinal cord injury," *Neuroscience Letters*, vol. 456, no. 3, pp. 137–142, 2009.

[28] M. Barton, J. John, M. Clarke, A. Wright, and J. Ekberg, "The glia response after peripheral nerve injury: a comparison between Schwann cells and olfactory ensheathing cells and their uses for neural regenerative therapies," *International Journal of Molecular Sciences*, vol. 18, no. 2, p. 287, 2017.

[29] M. Gu, Z. Gao, X. Li et al., "Conditioned medium of olfactory ensheathing cells promotes the functional recovery and axonal regeneration after contusive spinal cord injury," *Brain Research*, vol. 1654, no. Part A, pp. 43–54, 2017.

[30] R. Pellitteri, M. Spatuzza, S. Stanzani, and D. Zaccheo, "Biomarkers expression in rat olfactory ensheathing cells," *Frontiers in Bioscience*, vol. S2, no. 1, pp. 289–298, 2010.

[31] D. Lo Furno, G. Mannino, R. Giuffrida et al., "Neural differentiation of human adipose-derived mesenchymal stem cells induced by glial cell conditioned media," *Journal of Cellular Physiology*, vol. 233, no. 10, pp. 7091–7100, 2018.

[32] D. Lo Furno, G. Mannino, R. Pellitteri et al., "Conditioned media from glial cells promote a neural-like connexin expression in human adipose-derived mesenchymal stem cells," *Frontiers in Physiology*, vol. 9, p. 1742, 2018.

[33] K. Tomita, T. Madura, C. Mantovani, and G. Terenghi, "Differentiated adipose-derived stem cells promote myelination and enhance functional recovery in a rat model of chronic denervation," *Journal of Neuroscience Research*, vol. 90, no. 7, pp. 1392–1402, 2012.

[34] C. Mantovani, D. Mahay, M. Kingham, G. Terenghi, S. G. Shawcross, and M. Wiberg, "Bone marrow- and adipose-derived stem cells show expression of myelin mRNAs and proteins," *Regenerative Medicine*, vol. 5, no. 3, pp. 403–410, 2010.

[35] S. Sugitani, K. Tsuruma, Y. Ohno et al., "The potential neuroprotective effect of human adipose stem cells conditioned medium against light-induced retinal damage," *Experimental Eye Research*, vol. 116, pp. 254–264, 2013.

[36] B. Mead, L. J. Hill, R. J. Blanch et al., "Mesenchymal stromal cell-mediated neuroprotection and functional preservation of retinal ganglion cells in a rodent model of glaucoma," *Cytotherapy*, vol. 18, no. 4, pp. 487–496, 2016.

[37] T. V. Johnson, N. D. Bull, D. P. Hunt, N. Marina, S. I. Tomarev, and K. R. Martin, "Neuroprotective effects of intravitreal mesenchymal stem cell transplantation in experimental glaucoma," *Investigative Ophthalmology & Visual Science*, vol. 51, no. 4, pp. 2051–2059, 2010.

[38] T. Ma, K. Gong, Q. Ao et al., "Intracerebral transplantation of adipose-derived mesenchymal stem cells alternatively activates microglia and ameliorates neuropathological deficits in Alzheimer's disease mice," *Cell Transplantation*, vol. 22, 1_suppl, pp. 113–126, 2013.

[39] A. C. E. Graziano, R. Avola, V. Perciavalle et al., "Physiologically based microenvironment for *in vitro* neural differentiation of adipose-derived stem cells," *World Journal of Stem Cells*, vol. 10, no. 3, pp. 23–33, 2018.

[40] L. Y. Santiago, J. Clavijo-Alvarez, C. Brayfield, J. P. Rubin, and K. G. Marra, "Delivery of adipose-derived precursor cells for peripheral nerve repair," *Cell Transplantation*, vol. 18, no. 2, pp. 145–158, 2009.

[41] X. Wei, L. Zhao, J. Zhong et al., "Adipose stromal cells-secreted neuroprotective media against neuronal apoptosis," *Neuroscience Letters*, vol. 462, no. 1, pp. 76–79, 2009.

[42] A. Miranville, C. Heeschen, C. Sengenès, C. A. Curat, R. Busse, and A. Bouloumié, "Improvement of postnatal neovascularization by human adipose tissue-derived stem cells," *Circulation*, vol. 110, no. 3, pp. 349–355, 2004.

[43] H. Nakagami, K. Maeda, R. Morishita et al., "Novel autologous cell therapy in ischemic limb disease through growth factor secretion by cultured adipose tissue–derived stromal cells," *Arteriosclerosis, Thrombosis, and Vascular Biology*, vol. 25, no. 12, pp. 2542–2547, 2005.

[44] V. Planat-Benard, J. S. Silvestre, B. Cousin et al., "Plasticity of human adipose lineage cells toward endothelial cells: physiological and therapeutic perspectives," *Circulation*, vol. 109, no. 5, pp. 656–663, 2004.

[45] J. Rehman, D. Traktuev, J. Li et al., "Secretion of angiogenic and antiapoptotic factors by human adipose stromal cells," *Circulation*, vol. 109, no. 10, pp. 1292–1298, 2004.

[46] S. Sadat, S. Gehmert, Y. H. Song et al., "The cardioprotective effect of mesenchymal stem cells is mediated by IGF-I and VEGF," *Biochemical and Biophysical Research Communications*, vol. 363, no. 3, pp. 674–679, 2007.

[47] O. Ekshyyan and T. Aw, "Apoptosis: a key in neurodegenerative disorders," *Current Neurovascular Research*, vol. 1, no. 4, pp. 355–371, 2004.

[48] A. Blesch, "Neurotrophic factors in neurodegeneration," *Brain Pathology*, vol. 16, no. 4, pp. 295–303, 2006.

[49] M. Dragunow, G. A. MacGibbon, P. Lawlor et al., "Apoptosis, neurotrophic factors and neurodegeneration," *Reviews in the Neurosciences*, vol. 8, no. 3-4, pp. 223–265, 1997.

[50] J. R. Perez-Polo, H. C. Rea, K. M. Johnson et al., "Inflammatory consequences in a rodent model of mild traumatic brain injury," *Journal of Neurotrauma*, vol. 30, no. 9, pp. 727–740, 2013.

[51] T. Cao, T. C. Thomas, J. M. Ziebell, J. R. Pauly, and J. Lifshitz, "Morphological and genetic activation of microglia after

diffuse traumatic brain injury in the rat," *Neuroscience*, vol. 225, pp. 65–75, 2012.

[52] A. Kumar, D. M. Alvarez-Croda, B. A. Stoica, A. I. Faden, and D. J. Loane, "Microglial/macrophage polarization dynamics following traumatic brain injury," *Journal of Neurotrauma*, vol. 33, no. 19, pp. 1732–1750, 2016.

[53] M. Das, S. Mohapatra, and S. S. Mohapatra, "New perspectives on central and peripheral immune responses to acute traumatic brain injury," *Journal of Neuroinflammation*, vol. 9, no. 1, 2012.

[54] J. B. Redell and P. K. Dash, "Traumatic brain injury stimulates hippocampal catechol- O -methyl transferase expression in microglia," *Neuroscience Letters*, vol. 413, no. 1, pp. 36–41, 2007.

[55] K. Jha, M. Pentecost, R. Lenin et al., "Concentrated conditioned media from adipose tissue derived mesenchymal stem cells mitigates visual deficits and retinal inflammation following mild traumatic brain injury," *International Journal of Molecular Sciences*, vol. 19, no. 7, p. 2016, 2018.

[56] A. I. Caplan and J. E. Dennis, "Mesenchymal stem cells as trophic mediators," *Journal of Cellular Biochemistry*, vol. 98, no. 5, pp. 1076–1084, 2006.

[57] T. Aid, A. Kazantseva, M. Piirsoo, K. Palm, and T. Timmusk, "Mouse and rat BDNF gene structure and expression revisited," *Journal of Neuroscience Research*, vol. 85, no. 3, pp. 525–535, 2007.

[58] A. E. West, E. C. Griffith, and M. E. Greenberg, "Regulation of transcription factors by neuronal activity," *Nature Reviews Neuroscience*, vol. 3, no. 12, pp. 921–931, 2002.

[59] A. E. West, W. G. Chen, M. B. Dalva et al., "Calcium regulation of neuronal gene expression," *Proceedings of the National Academy of Sciences*, vol. 98, no. 20, pp. 11024–11031, 2001.

[60] P. L. Greer and M. E. Greenberg, "From synapse to nucleus: calcium-dependent gene transcription in the control of synapse development and function," *Neuron*, vol. 59, no. 6, pp. 846–860, 2008.

[61] X. Tao, S. Finkbeiner, D. B. Arnold, A. J. Shaywitz, and M. E. Greenberg, "Ca^{2+} Influx Regulates *BDNF* Transcription by a CREB Family Transcription Factor-Dependent Mechanism," *Neuron*, vol. 20, no. 4, pp. 709–726, 1998.

[62] P. B. Shieh, S. C. Hu, K. Bobb, T. Timmusk, and A. Ghosh, "Identification of a signaling pathway involved in calcium regulation of BDNF expression," *Neuron*, vol. 20, no. 4, pp. 727–740, 1998.

[63] Z. Zhou, E. J. Hong, S. Cohen et al., "Brain-Specific Phosphorylation of MeCP2 Regulates Activity-Dependent *Bdnf* Transcription, Dendritic Growth, and Spine Maturation," *Neuron*, vol. 52, no. 2, pp. 255–269, 2006.

[64] F. D. Lubin, T. L. Roth, and J. D. Sweatt, "Epigenetic regulation of bdnf gene transcription in the consolidation of fear memory," *Journal of Neuroscience*, vol. 28, no. 42, pp. 10576–10586, 2008.

[65] K. H. Tse, L. N. Novikov, M. Wiberg, and P. J. Kingham, "Intrinsic mechanisms underlying the neurotrophic activity of adipose derived stem cells," *Experimental Cell Research*, vol. 331, no. 1, pp. 142–151, 2015.

[66] R. D. Fields and G. Burnstock, "Purinergic signalling in neuron-glia interactions," *Nature Reviews Neuroscience*, vol. 7, no. 6, pp. 423–436, 2006.

[67] I. Takasaki, S. Takarada, S. Tatsumi et al., "Extracellular adenosine $5'$-triphosphate elicits the expression of brain-derived neurotrophic factor exon IV mRNA in rat astrocytes," *Glia*, vol. 56, no. 13, pp. 1369–1379, 2008.

[68] C. Verderio, F. Bianco, M. P. Blanchard et al., "Cross talk between vestibular neurons and Schwann cells mediates BDNF release and neuronal regeneration," *Brain Cell Biology*, vol. 35, no. 2-3, pp. 187–201, 2006.

[69] M. E. Gomez-Casati, J. C. Murtie, C. Rio, K. Stankovic, M. C. Liberman, and G. Corfas, "Nonneuronal cells regulate synapse formation in the vestibular sensory epithelium via erbB-dependent BDNF expression," *Proceedings of the National Academy of Sciences*, vol. 107, no. 39, pp. 17005–17010, 2010.

[70] Z. Zhu, Z. Q. Yuan, C. Huang et al., "Pre-culture of adipose-derived stem cells and heterologous acellular dermal matrix: paracrine functions promote post-implantation neovascularization and attenuate inflammatory response," *Biomedical Materials*, vol. 14, no. 3, 2019.

[71] M. Duijvestein, M. E. Wildenberg, M. M. Welling et al., "Pretreatment with interferon-γ enhances the therapeutic activity of mesenchymal stromal cells in animal models of colitis," *Stem Cells*, vol. 29, no. 10, pp. 1549–1558, 2011.

[72] K. Nagaishi, Y. Arimura, and M. Fujimiya, "Stem cell therapy for inflammatory bowel disease," *Journal of Gastroenterology*, vol. 50, no. 3, pp. 280–286, 2015.

[73] C. Grégoire, C. Lechanteur, A. Briquet et al., "Review article: mesenchymal stromal cell therapy for inflammatory bowel diseases," *Alimentary Pharmacology & Therapeutics*, vol. 45, no. 2, pp. 205–221, 2017.

[74] M. Dave, P. Jaiswal, and F. Cominelli, "Mesenchymal stem/stromal cell therapy for inflammatory bowel disease: an updated review with maintenance of remission," *Current Opinion in Gastroenterology*, vol. 33, no. 1, pp. 59–68, 2017.

[75] J. H. Chidlow Jr., D. Shukla, M. B. Grisham, and C. G. Kevil, "Pathogenic angiogenesis in IBD and experimental colitis: new ideas and therapeutic avenues," *American Journal of Physiology-Gastrointestinal and Liver Physiology*, vol. 293, no. 1, pp. G5–G18, 2007.

[76] L. L. Black, J. Gaynor, D. Gahring et al., "Effect of adipose-derived mesenchymal stem and regenerative cells on lameness in dogs with chronic osteoarthritis of the coxofemoral joints: a randomized, double-blinded, multicenter, controlled trial," *Veterinary Therapeutics*, vol. 8, no. 4, pp. 272–284, 2007.

[77] K. Marycz, I. Michalak, I. Kocherova, M. Maredziak, and C. Weiss, "The Cladophora glomerata enriched by biosorption process in Cr(III) improves viability, and reduces oxidative stress and apoptosis in equine metabolic syndrome derived adipose mesenchymal stromal stem cells (ASCs) and their extracellular vesicles (MV's)," *Marine Drugs*, vol. 15, no. 12, p. 385, 2017.

[78] H. Choi, R. H. Lee, N. Bazhanov, J. Y. Oh, and D. J. Prockop, "Anti-inflammatory protein TSG-6 secreted by activated MSCs attenuates zymosan-induced mouse peritonitis by decreasing TLR2/NF-κB signaling in resident macrophages," *Blood*, vol. 118, no. 2, pp. 330–338, 2011.

[79] E. Sala, M. Genua, L. Petti et al., "Mesenchymal stem cells reduce colitis in mice via release of TSG6, independently of their localization to the intestine," *Gastroenterology*, vol. 149, no. 1, pp. 163–176.e20, 2015.

[80] J. Xie, H. E. Broxmeyer, D. Feng et al., "Human adipose-derived stem cells ameliorate cigarette smoke-induced

murine myelosuppression via secretion of TSG-6," *Stem Cells*, vol. 33, no. 2, pp. 468–478, 2015.

[81] G. J. Block, S. Ohkouchi, F. Fung et al., "Multipotent stromal cells are activated to reduce apoptosis in part by upregulation and secretion of stanniocalcin-1," *Stem Cells*, vol. 27, no. 3, pp. 670–681, 2009.

[82] C. M. Milner and A. J. Day, "TSG-6: a multifunctional protein associated with inflammation," *Journal of Cell Science*, vol. 116, Part 10, pp. 1863–1873, 2003.

[83] Y. Liu, R. Zhang, K. Yan et al., "Mesenchymal stem cells inhibit lipopolysaccharide-induced inflammatory responses of BV2 microglial cells through TSG-6," *Journal of Neuroinflammation*, vol. 11, no. 1, p. 135, 2014.

[84] R. Zhang, Y. Liu, K. Yan et al., "Anti-inflammatory and immunomodulatory mechanisms of mesenchymal stem cell transplantation in experimental traumatic brain injury," *Journal of Neuroinflammation*, vol. 10, no. 1, 2013.

[85] M. J. Lee, J. Kim, M. Y. Kim et al., "Proteomic analysis of tumor necrosis factor-alpha-induced secretome of human adipose tissue-derived mesenchymal stem cells," *Journal of Proteome Research*, vol. 9, no. 4, pp. 1754–1762, 2010.

[86] E. R. Andreeva, M. V. Lobanova, O. O. Udartseva, and L. B. Buravkova, "Response of adipose tissue-derived stromal cells in tissue-related O2 microenvironment to short-term hypoxic stress," *Cells, Tissues, Organs*, vol. 200, no. 5, pp. 307–315, 2015.

[87] T. M. Rodríguez, A. Saldías, M. Irigo, J. V. Zamora, M. J. Perone, and R. A. Dewey, "Effect of TGF-β1 stimulation on the secretome of human adipose-derived mesenchymal stromal cells," *Stem Cells Translational Medicine*, vol. 4, no. 8, pp. 894–898, 2015.

[88] A. A. Ostanin, Y. L. Petrovskii, E. Y. Shevela, and E. R. Chernykh, "Multiplex analysis of cytokines, chemokines, growth factors, MMP-9 and TIMP-1 produced by human bone marrow, adipose tissue, and placental mesenchymal stromal cells," *Bulletin of Experimental Biology and Medicine*, vol. 151, no. 1, pp. 133–141, 2011.

[89] S. Jessberger, R. E. Clark, N. J. Broadbent et al., "Dentate gyrus-specific knockdown of adult neurogenesis impairs spatial and object recognition memory in adult rats," *Learning & Memory*, vol. 16, no. 2, pp. 147–154, 2009.

[90] N. Toni, D. A. Laplagne, C. Zhao et al., "Neurons born in the adult dentate gyrus form functional synapses with target cells," *Nature Neuroscience*, vol. 11, no. 8, pp. 901–907, 2008.

[91] A. Shruster, H. Eldar-Finkelman, E. Melamed, and D. Offen, "Wnt signaling pathway overcomes the disruption of neuronal differentiation of neural progenitor cells induced by oligomeric amyloid β-peptide," *Journal of Neurochemistry*, vol. 116, no. 4, pp. 522–529, 2011.

[92] S. Jang, J. S. Park, and H. S. Jeong, "Neural differentiation of human adipose tissue-derived stem cells involves activation of the Wnt5a/JNK signalling," *Stem Cells International*, vol. 2015, 7 pages, 2015.

[93] H. Y. Ren, H. Xu, W. Y. Yu et al., "Potentiation of neuroal—like differentiation from rat adipose mesenchymal stem cells by Rho-associated coiled kinase inhibitor Y-27632," *Chinese Journal of Anatomy*, vol. 36, no. 4, pp. 772–809, 2013.

[94] R. A. Sabol, A. C. Bowles, A. Côté, R. Wise, N. Pashos, and B. A. Bunnell, "Therapeutic potential of adipose stem cells," in *Advances in Experimental Medicine and Biology*, Springer, New York, NY, 2018.

[95] B. F. Darst, R. L. Koscik, B. P. Hermann et al., "Heritability of cognitive traits among siblings with a parental history of Alzheimer's disease," *Journal of Alzheimer's Disease*, vol. 45, no. 4, pp. 1149–1155, 2015.

[96] R. E. Tanzi, "A brief history of Alzheimer's disease gene discovery," *Journal of Alzheimer's Disease*, vol. 33, Suppl 1, pp. S5–13, 2013.

[97] S. Kim, K. A. Chang, J. . Kim et al., "The preventive and therapeutic effects of intravenous human adipose-derived stem cells in Alzheimer's disease mice," *Plos One*, vol. 7, no. 9, p. e45757, 2012.

[98] X. Hu, R. K. Leak, Y. Shi et al., "Microglial and macrophage polarization–new prospects for brain repair," *Nature Reviews Neurology*, vol. 11, no. 1, pp. 56–64, 2015.

[99] R. Pérez-González, D. Antequera, T. Vargas, C. Spuch, M. Bolós, and E. Carro, "Leptin induces proliferation of neuronal progenitors and neuroprotection in a mouse model of Alzheimer's disease," *Journal of Alzheimer's Disease*, vol. 24, no. s2, pp. 17–25, 2011.

[100] W. Zhang, L. Zhang, N. Zhou et al., "Dysregulation of respiratory center drive (P0.1) and muscle strength in patients with early stage idiopathic Parkinson's disease," *Frontiers in Neurology*, vol. 10, p. 724, 2019.

[101] M. K. McCoy, T. N. Martinez, K. A. Ruhn et al., "Autologous transplants of Adipose-Derived Adult Stromal (ADAS) cells afford dopaminergic neuroprotection in a model of Parkinson's disease," *Experimental Neurology*, vol. 210, no. 1, pp. 14–29, 2008.

[102] A. Schwerk, J. Altschüler, M. Roch et al., "Human adipose-derived mesenchymal stromal cells increase endogenous neurogenesis in the rat subventricular zone acutely after 6-hydroxydopamine lesioning," *Cytotherapy*, vol. 17, no. 2, pp. 199–214, 2015.

[103] H. S. Choi, H. J. Kim, J. H. Oh et al., "Therapeutic potentials of human adipose-derived stem cells on the mouse model of Parkinson's disease," *Neurobiology of Aging*, vol. 36, no. 10, pp. 2885–2892, 2015.

[104] S. K. Kang, D. H. Lee, Y. C. Bae, H. K. Kim, S. Y. Baik, and J. S. Jung, "Improvement of neurological deficits by intracerebral transplantation of human adipose tissue-derived stromal cells after cerebral ischemia in rats," *Experimental Neurology*, vol. 183, no. 2, pp. 355–366, 2003.

[105] L. R. Zhao, W. M. Duan, M. Reyes, C. D. Keene, C. M. Verfaillie, and W. C. Low, "Human bone marrow stem cells exhibit neural phenotypes and ameliorate neurological deficits after grafting into the ischemic brain of rats," *Experimental Neurology*, vol. 174, no. 1, pp. 11–20, 2002.

[106] B. S. Bregman, E. Kunkel-Bagden, P. J. Reier, H. N. Dai, M. McAtee, and D. Gao, "Recovery of function after spinal cord injury: mechanisms underlying transplant-mediated recovery of function differ after spinal cord injury in newborn and adult rats," *Experimental Neurology*, vol. 123, no. 1, pp. 3–16, 1993.

[107] L. Cova, A. Ratti, M. Volta et al., "Stem cell therapy for neurodegenerative diseases: the issue of transdifferentiation," *Stem Cells and Development*, vol. 13, no. 1, pp. 121–131, 2004.

[108] A. Efimenko, E. Starostina, N. Kalinina, and A. Stolzing, "Angiogenic properties of aged adipose derived mesenchymal stem cells after hypoxic conditioning," *Journal of Translational Medicine*, vol. 9, no. 1, p. 10, 2011.

[109] I. K. Moppett, "Traumatic brain injury: assessment, resuscitation and early management," *British Journal of Anaesthesia*, vol. 99, no. 1, pp. 18–31, 2007.

[110] B. E. Masel and D. S. DeWitt, "Traumatic brain injury: a disease process, not an event," *Journal of Neurotrauma*, vol. 27, no. 8, pp. 1529–1540, 2010.

[111] A. Dekmak, S. Mantash, A. Shaito et al., "Stem cells and combination therapy for the treatment of traumatic brain injury," *Behavioural Brain Research*, vol. 340, pp. 49–62, 2018.

[112] N. Tajiri, S. A. Acosta, M. Shahaduzzaman et al., "Intravenous transplants of human adipose-derived stem cell protect the brain from traumatic brain injury-induced neurodegeneration and motor and cognitive impairments: cell graft biodistribution and soluble factors in young and aged rats," *Journal of Neuroscience*, vol. 34, no. 1, pp. 313–326, 2014.

[113] T. Mert, A. H. Kurt, M. Arslan, A. Çelik, B. Tugtag, and A. Akkurt, "Anti-inflammatory and anti-nociceptive actions of systemically or locally treated adipose-derived mesenchymal stem cells in experimental inflammatory model," *Inflammation*, vol. 38, no. 3, pp. 1302–1310, 2015.

[114] J. M. Ziebell and M. C. Morganti-Kossmann, "Involvement of pro- and anti-inflammatory cytokines and chemokines in the pathophysiology of traumatic brain injury," *Neurotherapeutics*, vol. 7, no. 1, pp. 22–30, 2010.

[115] N. V. Selianina, I. V. Karakulova, and O. A. Eroshina, "The role of neuromediators and cytokines in the pathogenesis of acute traumatic brain injury," *Zhurnal Voprosy Neirokhirurgii Imeni NN Burdenko*, vol. 77, no. 6, pp. 22–26, 2013.

[116] S. M. Knoblach, L. Fan, and A. I. Faden, "Early neuronal expression of tumor necrosis factor-α after experimental brain injury contributes to neurological impairment," *Journal of Neuroimmunology*, vol. 95, no. 1-2, pp. 115–125, 1999.

[117] V. Trembovler, E. Beit-Yannai, F. Younis, R. Gallily, M. Horowitz, and E. Shohami, "Antioxidants attenuate acute toxicity of tumor necrosis factor-alpha induced by brain injury in rat," *Journal of Interferon & Cytokine Research*, vol. 19, no. 7, pp. 791–795, 1999.

[118] N. S. Kappy, S. Chang, W. M. Harris et al., "Human adipose-derived stem cell treatment modulates cellular protection in both in vitro and in vivo traumatic brain injury models," *Journal of Trauma and Acute Care Surgery*, vol. 84, no. 5, pp. 745–751, 2018.

[119] Y. Zhang, M. Chopp, Y. Meng et al., "Effect of exosomes derived from multipluripotent mesenchymal stromal cells on functional recovery and neurovascular plasticity in rats after traumatic brain injury," *Journal of Neurosurgery*, vol. 122, no. 4, pp. 856–867, 2015.

[120] S. K. Kapur and A. J. Katz, "Review of the adipose derived stem cell secretome," *Biochimie*, vol. 95, no. 12, pp. 2222–2228, 2013.

[121] S. M. Bird, H. R. Sohrabi, T. A. Sutton et al., "Cerebral amyloid-β accumulation and deposition following traumatic brain injury–a narrative review and meta-analysis of animal studies," *Neuroscience & Biobehavioral Reviews*, vol. 64, pp. 215–228, 2016.

[122] Y. Kishimoto, H. Shishido, M. Sawanishi et al., "Data on amyloid precursor protein accumulation, spontaneous physical activity, and motor learning after traumatic brain injury in the triple-transgenic mouse model of Alzheimer's disease," *Data in Brief*, vol. 9, no. C, pp. 62–67, 2016.

Research Article

Prx1-Expressing Progenitor Primary Cilia Mediate Bone Formation in response to Mechanical Loading in Mice

Emily R. Moore [iD], Julia C. Chen, and Christopher R. Jacobs

Department of Biomedical Engineering, Columbia University, 500 W 120th Street New York, NY 10027, USA

Correspondence should be addressed to Emily R. Moore; erm17@case.edu

Increases in mechanical loading can enhance the addition of new bone, altering geometry and density such that bones better withstand higher forces. Bone-forming osteoblasts have long been thought to originate from progenitors, but the exact source is yet to be identified. Previous studies indicate osteogenic precursors arise from Prx1-expressing progenitors during embryonic development and adult fracture repair. However, it is unknown whether this cell population is also a source for mechanically induced active osteoblasts. We first identified that Prx1 is expressed in skeletally mature mouse periosteum, a thin tissue covering the surface of the bone that is rich in osteoprogenitors. We then traced Prx1 progenitor lineage using a transgenic mouse model carrying both a Prx1-driven tamoxifen-inducible Cre and a ROSA-driven lacZ reporter gene. Cells that expressed Prx1 when compressive axial loading was applied were detected within the cortical bone days after stimulation, indicating osteocytes are of Prx1-expressing cell origin. In addition, we evaluated how these cells sense and respond to physical stimulation *in vivo* by disrupting their primary cilia, which are antenna-like sensory organelles known to enhance mechanical and chemical signaling kinetics. Although Prx1-driven primary cilium disruption did not affect osteoblast recruitment to the bone surface, the relative mineral apposition and bone formation rates were decreased by 53% and 34%, respectively. Thus, this cell population contributes to load-induced bone formation, and primary cilia are needed for a complete response. Interestingly, Prx1-expressing progenitors are easily extracted from periosteum and are perhaps an attractive alternative to marrow stem cells for bone tissue regeneration strategies.

1. Introduction

One way the skeleton structurally adapts to its mechanical environment is by stimulating the addition of new bone and subsequently altering its geometry and density to better withstand higher forces. Bone formation in response to mechanical loading involves multiple cell types and requires a sequence of events to occur. Specifically, mechanosensitive osteocytes sense physical loading and secrete paracrine factors that recruit cells to the bone surface [1]. These cells eventually transform into matrix-producing osteoblasts and, potentially, embedded osteocytes. With innovative regenerative bone therapies rapidly emerging, it is more important than ever to finally determine the origin of cells recruited to the bone surface. Bone-forming cells have long been thought to originate from progenitors, so approaches were developed to extract osteoblast precursors from bone marrow. How-

ever, these procedures are very invasive, and the acquired progenitors require further treatment in order to encourage proper differentiation. An appealing alternative is to harvest periosteum, which surrounds bones and is rich in progenitor cells known to preferentially differentiate towards the osteogenic lineage [2–4].

Previous *in vitro* studies demonstrate that immortalized murine and primary human mesenchymal stem cells directly sense physical stimulation, which enhances differentiation towards the osteogenic lineage [5, 6]. In addition, mechanical forces on the periosteum are known to enhance osteogenic lineage commitment *in vivo* and *in vitro*. Henderson et al. observed the localization of cells with osteogenic gene expression to areas of tension on the outer edges of embryonic mouse rudiment tissues [7], and Kanno et al. found osteogenic markers were upregulated when mechanical strain was applied to human periosteal cells [8]. These studies

suggest that physical stimulation activates and encourages osteogenic differentiation of progenitors within the periosteum. Although progenitors are clearly receptive to mechanical cues, how they sense and react to physical stimulation *in vivo* remain unknown.

The inner cambium layer of the periosteum contains a wealth of osteogenic precursors, a subset of which express paired-related homeobox 1 (Prx1). During embryonic development, Prx1 expression is rampant in the limb bud and gives rise to many skeletal tissues [4]. Prx1 tracking studies in adult mice have identified recombination in perivascular stromal cells [9, 10], mature osteoblasts [9, 10], osteocytes [9], and adipocytes [11]. These results suggest the Prx1Cre transgene is associated with multipotent mesenchymal progenitors in the appendicular skeleton [9]. We recently determined that Prx1 is highly restricted to the periosteum and perichondrium after birth [12] and are further confined to the periosteum in adulthood [13]. Prx1-expressing cells populate the callus during fracture healing [4, 14], but their presence under normal physiological conditions has yet to be confirmed. Thus, we investigate the role of Prx1-expressing progenitors during mechanical loading in this study.

One potential mechanism by which progenitor cells may become mechanically activated is through the primary cilium. Primary cilia are antenna-like organelles that extend from the cell surface and serve as signaling microdomains. Impairment of primary cilium formation and signaling is known to influence bone development and formation [15–17]. For example, when an intraflagellar retrograde transport protein important for primary cilium function (Kif3a) was deleted in osteoblasts and osteocytes, load-induced bone formation was diminished [18]. Primary cilia are also critical for mechano- and chemosensation in mesenchymal progenitor cells *in vitro* [5, 19]. Interestingly, Prx1-driven deletion of primary cilia in murine embryos alters lineage commitment, resulting in severe defects in endochondral bone formation and, ultimately, death [16]. We recently determined that the osteogenic response to fluid shear is lost when periosteal progenitor primary cilia are disrupted *in vitro* [13]. Despite the implications, whether Prx1-expressing progenitor cell primary cilia mediate the *in vivo* bone formation response to mechanical stimulation has yet to be investigated.

The objectives of this study are twofold. First, we traced Prx1-expressing cells in skeletally mature adults to examine their fate in load-induced bone formation. Second, we measured changes in load-induced bone formation with and without Prx1-expressing progenitor primary cilia to evaluate their role in adult adaptation. Overall, we determined that Prx1-expressing cells become embedded osteocytes in response to physical loading and this mechanism requires the primary cilium.

2. Methods

2.1. Generation of Prx1CreER-GFP; Kif3a$^{fl/fl}$ and Prx1CreER-GFP; R26R-lacZ Mice.
All mice were maintained in the animal facility at Columbia University with protocols approved by the Institutional Animal Care and Use Committee at Columbia University. C57BL/6 mice carrying floxed alleles

of Kif3a were recovered from the UC Davis Mutant Mice Regional Resource Center cryoarchive. C57BL/6 mice carrying the Prx1CreER^{T2} transgene were transferred from Case Western University. Mice carrying ROSA26-lacZ (R26R) were obtained from Jackson Laboratories (Bar Harbor, ME) and bred with Prx1CreER-GFP animals to generate the Prx1CreER-GFP; R26R$^{tg/+}$ model for the lineage-tracing experiment. For ulnar loading studies, Kif3a$^{fl/fl}$ and Prx1CreER-GFP animals were crossed to generate experimental Prx1CreER-GFP; Kif3a$^{fl/fl}$ mice (Figure 1(a)). The control group includes multiple genotypes that retain both copies of Kif3a upon tamoxifen administration: (1) Kif3a$^{fl/fl}$, (2) Prx1CreER; Kif3a$^{+/+}$, (3) Prx1CreER; Kif3a$^{+/+}$; R26R$^{tg/+}$, and (4) Kif3a$^{fl/+}$. Genotypes were verified by extracting DNA from tail biopsies and performing PCR analysis [4, 20]. Both female and male mice were used for all experiments. All applicable institutional and/or national guidelines for the care and use of animals were followed.

2.2. In Vitro Cilium Disruption and Immunocytochemistry.
16-week-old Prx1CreER-GFP; Kif3a$^{fl/fl}$ mice were sacrificed, and the limbs were dissected. The skin, muscle, and connective tissues were removed to expose the periosteum. The periosteum was gently scored with a scalpel, peeled from the bone, cut into 1 mm × 1 mm sections, and placed into culture media (MEMα+10% FBS+1% PenStrep, Thermo Fisher Scientific, Waltham, MA) in a fibronectin-coated (Sigma Chemical Co., St. Louis, MO) 35 mm tissue culture dish (Falcon, Corning, NY). Tissue sections were cultured at 37°C for 7–10 days, and the resulting isolated cells were seeded on fibronectin-coated glass bottom dishes (MatTek Corporation, Ashland, MA). Cells were cultured in reduced-serum media (MEMα+5% FBS+1% PenStrep) for 48 hours prior to fixation and received either 5 μg/mL 4-hydroxytamoxifen (Sigma) dissolved in 90% ethanol or vehicle control for 24 hours prior to fixation. Cells were fixed in 10% formalin solution (Sigma), blocked in 10% goat serum (Thermo Fisher), incubated in a primary antibody against acetylated α-tubulin obtained from a C3B9 hybridoma (Sigma), and incubated in 1 : 500 Alexa Fluor 488 secondary antibody (Thermo Fisher). All blocking and antibody steps were for 1 hr at ambient temperature. Cell nuclei were stained with NucBlue solution (Thermo Fisher) for 5 minutes at ambient temperature. To quantify primary cilium length and incidence, a laser scanning confocal microscope (Leica TCS SP5, Leica Microsystems Inc., Buffalo Grove, IL) was used to collect at least 10 slices and create Z-stacks of cell nuclei and their associated cilia. These stacks were imported into ImageJ, and cilium length and incidence were measured manually by two separate investigators for accuracy and repeatability. Length was measured using a pixel to μm conversion, and incidence was calculated using fields that were 80% confluent and contained 20-25 nuclei since primary cilium growth is influenced by cell density.

2.3. Mechanical Loading.
One week prior to loading, peritoneal injections of 75 mg/kg body weight tamoxifen (1.5-2 mg dissolved in corn oil, Sigma) were administered once a day for 5 days to induce Cre recombination. Tamoxifen
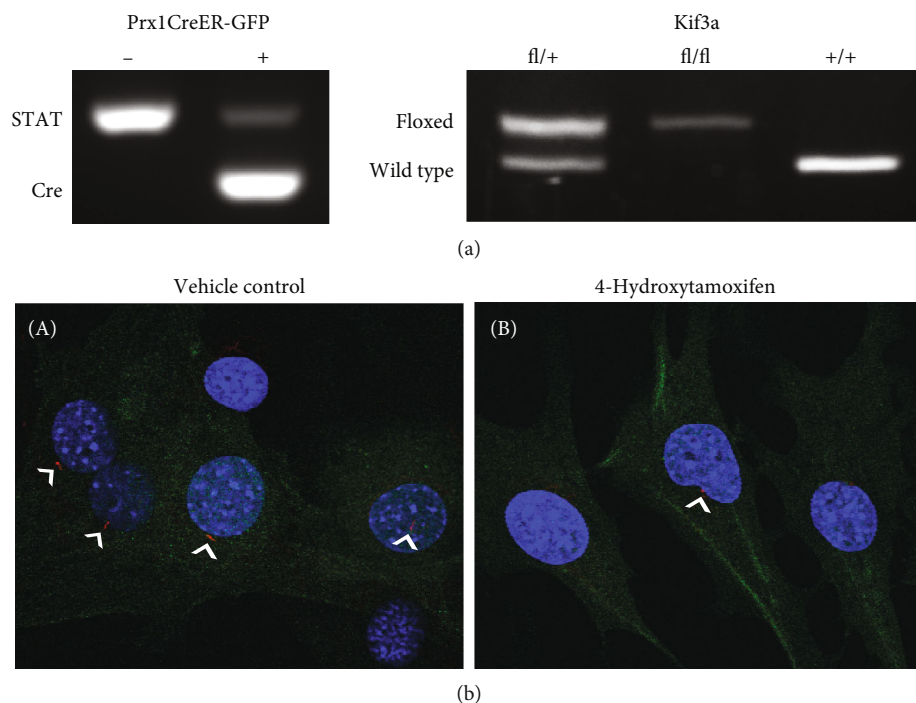
(a)

(b)

Figure 1: Generation of experimental Prx1CreER-GFP; Kif3a$^{fl/fl}$ and control mice. Genotype was confirmed using PCR to detect the Prx1CreER-GFP transgene and Kif3a wild-type and floxed alleles (a). The signal transducer and activator of transcription (STAT) gene served as a positive control for the PCR reaction. IHC for acetylated α-tubulin was performed to visualize primary cilia (b). Cilium (red, white arrows) incidence and length decreased in Prx1CreER-GFP; Kif3a$^{fl/fl}$ primary periosteal cells (green) treated with 4-hydroxytamoxifen (B) compared to controls (A). Nuclei (blue) were stained using DAPI, and micrographs were collected at 100x magnification.

injections were also administered each day of loading for 3 days total and on days 4 and 8 after initiation of loading. At 16 ± 1 weeks of age, the right ulna of skeletally mature mice was exposed to compressive axial loading (3 N at 2 Hz for 120 cycles per day) for 3 consecutive days using an electromagnetic loading system (EnduraTEC, Bose, Eden Prairie, MN) [15, 21]. The left ulna was not loaded and served as an internal control. Mice revived from anesthesia within 5 minutes of completion of loading and normal gait were observed.

2.4. Dynamic Histomorphometry. Subcutaneous injections of calcein (30 mg/kg body weight, Sigma) and Alizarin Red S (70 mg/kg body weight, Sigma) were administered 4 and 8 days, respectively, after the first day of loading. Mice were sacrificed 14 days after initiation of loading, and ulnae were dissected, stored in 70% ethanol up to a week, dehydrated, and embedded in methyl methacrylate and dibutyl phthalate, using benzoyl peroxide as a catalyst. A diamond saw (IsoMet Low Speed Saw, Buehler, Lake Bluff, IL) was used to create transverse sections at the midshaft. Sections were imaged using a laser scanning confocal microscope (Leica TCS SP5, Leica Microsystems Inc., Buffalo Grove, IL). With ImageJ software, the following were measured for the periosteal surface: bone perimeter (B.Pm), single label perimeter (sL.Pm), double label perimeter (dL.Pm), and double label area (dL.Ar). These measures were used to calculate bone formation parameters: mineralizing surface (MS/BS = $[1/2$ sL. Pm + dL.Pm]/B.Pm $\times 100$; %), mineral apposition rate

(MAR = dL.Ar/dL.Pm/4 days; μm per day), and bone formation rate (BFR/BS = MAR $\times$ MS/BS $\times 3.65$; $\mu m^3/\mu m^2$ per day). Relative (r) measurements reflect bone formation that is attributed to mechanical loading and were calculated by subtracting nonloaded from the loaded forelimb values for individual animals.

2.5. Immunohistochemistry. Animals were injected and euthanized following loading as explained above. Both ulnae were dissected, fixed in 10% formalin (Sigma), decalcified in RDO, dehydrated, and embedded in paraffin. Transverse sections 5 μm thick were cut at the midshaft. Sections were deparaffinized, rehydrated, blocked in 10% goat serum for 1 hr (Sigma), and then incubated with primary antibodies against GFP (1 : 500, Life Technologies, A11122) or beta-galactosidase overnight (1 : 3000, ab9361, abcam, Cambridge, UK). Sections were then incubated with biotinylated secondary antibodies for 30 min before adding ABC reagent (Vector Laboratories, Burlingame, CA) for 30 min. Development of color occurred through incubation in diaminobenzidine (DAKO, Carpinteria, CA) substrate solution. Finally, sections were counterstained with hematoxylin for 10 min. All incubations took place at ambient temperature.

2.6. Statistical Analysis. Data are presented as mean $\pm$ SEM and p values were calculated in GraphPad Prism (GraphPad Software, Inc., La Jolla, CA). One-way ANOVA revealed there were no statistical differences based on gender, so males and females were grouped together. Furthermore, one-way

ANOVA demonstrated there was no difference in reported values due to the specific genotype for control animals with intact Kif3a. For dynamic histomorphometry comparisons, we could not assume normality ($n < 30$), so the nonparametric Mann-Whitney U test was used to identify any differences. Tests were performed with $\alpha = 0.05$, and sample size was determined to achieve at least 80% power.

3. Results

3.1. Tamoxifen-Induced Cilium Disruption in Primary Periosteal Cells. The Prx1CreER-GFP; Kif3a$^{fl/fl}$ and Prx1CreER-GFP genotypes were confirmed via standard PCR and gel electrophoresis (Figure 1(a)). We then isolated primary cells to evaluate our model's ability to disrupt primary cilia. Isolated Prx1CreER − GFP ; Kif3a$^{fl/fl}$ periosteal cells were identified via GFP expression *in vitro*. Indeed, Prx1-expressing cells treated with the active compound of tamoxifen had visually shorter cilia compared to vehicle controls (Figure 1(b)). More importantly, cilium incidence was $79 \pm 1.4\%$ ($n = 4$) in controls and $32 \pm 1.4\%$ ($n = 5$) in treated samples. Thus, we conclude that tamoxifen treatment effectively disrupts primary cilia in our transgenic mouse model.

3.2. Expression of Prx1 in Adults. Since there are conflicting reports on Prx1 expression in adults [4, 10–12, 22], we sought to determine whether cells containing the Prx1CreER-GFP transgene were present in the periosteum of skeletally mature mice. Immunohistochemistry was used to visualize GFP and therefore identify Prx1 expression (Figure 2(a)). We detected cells carrying the Prx1CreER-GFP transgene in the periosteum of loaded and nonloaded ulnae, indicating Prx1 is expressed under normal static conditions, as well as when mechanical loads are introduced. Not all cells in the periosteum expressed Prx1, which was absent in osteoblasts, osteocytes, bone marrow, and muscle surrounding the ulna.

3.3. Prx1-Expressing Cells Contribute to Load-Induced Bone Formation. We then tracked the fate of Prx1-expressing cells in the nonloaded and loaded ulna by staining for beta-galactosidase in our Prx1CreER-GFP; R26R reporter. We observed beta-galactosidase-positive cells within the periosteum of both loaded and nonloaded limbs (Figure 2(b)). Recombined cells were also uniquely present near the periosteal edge of the cortical bone in loaded limbs. Since osteocytes do not express the Prx1CreER-GFP transgene, this suggests that mechanical loading promotes osteogenic differentiation of Prx1-expressing progenitors.

3.4. Prx1-Driven Kif3a Deletion Diminishes Load-Induced Bone Formation. We then explored whether Prx1-expressing cells require primary cilia to contribute to adult bone formation. Mice with and without intact Prx1-expressing progenitor primary cilia were exposed to ulnar loading, and bone formation parameters were quantified using dynamic histomorphometry. Indeed, animals lacking cilia exhibited diminished bone formation (Figure 3(a)). Specifically, the relative bone formation rate (Figure 3(d)), which is a combination of mineralizing surface percentage and mineral apposition rate, was attenuated in experimental animals

(381.7 ± 28.4 $\mu m^3/\mu m^2/year$) compared to controls (578.5 ± 28.4 $\mu m^3/\mu m^2/year$). The attenuated bone formation rate in mutants is due to a decrease in relative mineral apposition rate (1.0 ± 0.1 $\mu m/day$ compared to 1.8 ± 0.1 $\mu m/day$ for controls), which indicates how quickly new bone is formed at active surfaces (Figure 3(c)). Interestingly, we found no significant change ($p = 0.11$) in relative mineralizing surface (Figure 3(b)), or the percent of the surface that is active in bone formation, between animals with disrupted cilia (37.7 ± 3.0) compared to controls ($44.2 \pm 2.4\%$). Overall, our results indicate that Prx1-expressing progenitors require primary cilia to contribute to load-induced bone adaptation in adult mice.

4. Discussion

In this study, we identified Prx1-expressing cells as a source for osteoblasts active in load-induced bone formation. Osteoblast repopulation via progenitor cells has long been thought to drive adult bone formation, but no previous study has specifically traced the source of progenitors. Turner et al. used BrdU labeling to identify proliferating cells derived from progenitors after loading. On the endocortical surface, only 30-40% of osteoblasts were progenitor derived; however, on the periosteal surface, 90% of osteoblasts were newly created [23]. In a study of growing animals, bone formation was impaired when differentiated osteoblasts were ablated, while osteoprogenitors remained intact [24]. Once ablation ceased, bone formation returned to typical rates within 4 weeks, indicating that the osteoblast store had been repopulated from progenitor cells. These studies demonstrate that progenitors contribute to bone formation, but our work is the first to suggest active osteoblasts originate from Prx1-expressing progenitors. Specifically, our tracking studies reveal that some osteocytes near the periosteal surface arise from Prx1-expressing progenitors. A fraction of osteoblasts at the mineralizing surface eventually differentiate into osteocytes; therefore, the lacZ+ osteocytes we identified were once active osteoblasts.

Our results suggest that Prx1-expressing progenitors are recruited from the periosteum during load-induced bone formation. We identify four pieces of evidence that support this theory. First, our histological analysis and preexisting literature suggest Prx1 expression is confined to the periosteum in adult mice. Various tracking studies in constitutive Prx1Cre models report labeled cells in a variety of tissues [9–11], but these studies do not examine Prx1 expression specifically in adulthood. Kawanami et al. first reported that Prx1 expression becomes highly restricted after birth [4]. Duchamp De Lageneste et al. demonstrated that rare periosteal Prx1-expressing cells persist in the periosteum after healing is complete [14]. In our prior research, we detected Prx1 expression using a fluorescent reporter and concluded it was highly restricted to the periosteum with age [12, 13]. Here, we stained for GFP in skeletally mature adults and determined the Prx1CreER-GFP transgene was present in the periosteum in loaded and nonloaded bone, but not found in osteoblasts, osteocytes, muscle, or bone marrow. It is important to note that we only evaluated tissues spatially relevant to the ulna,

Nonloaded (A) Ulna Prx1CreER-GFP(+) Periosteum

Loaded (B) Prx1CreER-GFP(+) Ulna Periosteu

Nonloaded (A) Ulna
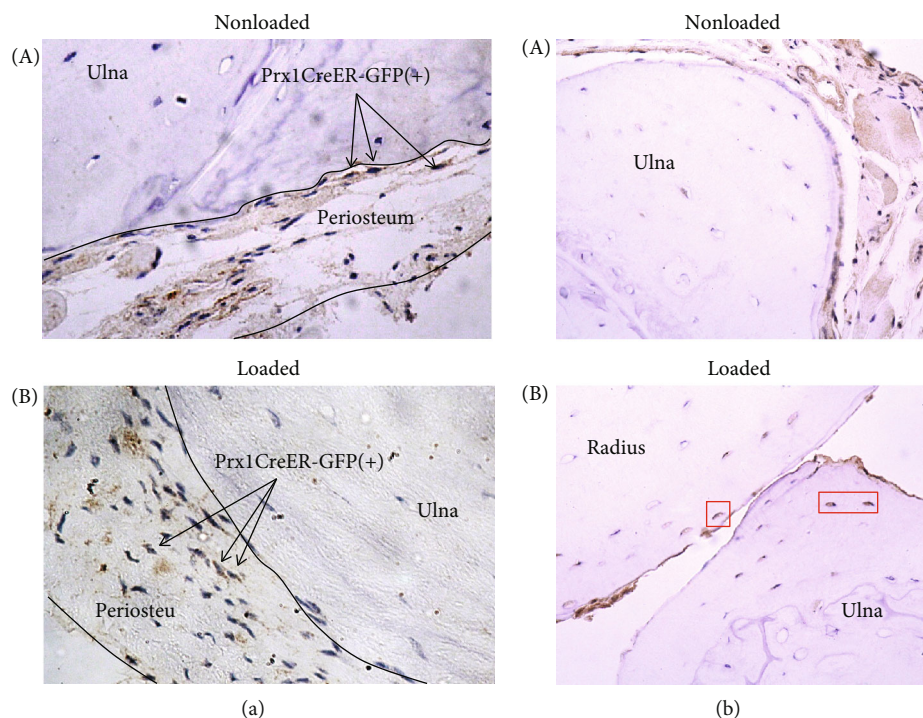
Loaded (B) Radius Ulna

(a) (b)

FIGURE 2: Prx1-expressing cells become embedded osteocytes in response to mechanical loading. (a) Prx1CreER-GFP(+) cells (brown) were detected in the periosteum surrounding the nonloaded (A) and loaded bone (B). Arrows denote examples of these cells for clarity. Osteocytes, muscle cells, bone marrow cells, and other cells in the periosteum were negative for GFP staining. (b) Beta-galactosidase staining was used to detect cells in which recombination had occurred (brown). Osteocytes near the periosteal surface demonstrated recombination in the loaded bone ((B), red boxes), but these cells were absent from nonloaded limbs (A). Brown coloration observed in the periosteum, muscle, and lacunae without corresponding nuclei (blue) was also seen in negative controls and thus deemed nonspecific staining. Nuclei were stained with hematoxylin, and micrographs were collected at 20x magnification.

so Prx1 may be expressed elsewhere. For example, Prx1 expression is also present in the calvaria after birth [25], but we do not anticipate that the expression in the areas of the body outside the area we evaluated would influence our findings.

Second, Kawanami et al. found that primary Prx1-expressing cells isolated from long bones of Prx1CreER-GFP mice were periosteal in nature [4]. Specifically, Prx1-expressing cells were sorted using the GFP tag, and quantitative PCR was performed to measure typical cell markers associated with various skeletal cells. The expression patterns of the primary cells were by far most consistent with periosteal cells, especially when compared to the expression patterns of osteoblast, preadipocyte, and macrophage cell lines.

Third, since bone formation primarily occurs at the periosteal surface in mice, it is widely believed that active osteoblasts are recruited from the periosteum, which is intimately connected to the periosteal bone surface [23, 26]. In fact, the recombined osteocytes we found in our tracking studies were all located near the periosteal surface. This spatial positioning strongly suggests active osteoblasts are derived from Prx1-expressing progenitors in the periosteum. Furthermore, in the tracking studies of their Prx1CreER-GFP model, Kawanami et al. noted that recombined cells were predominantly in the inner cambium layer [4], which is connected to the bone surface and readily provides osteoprogenitors [27].

Fourth, our dynamic histomorphometry data suggest Prx1-expressing progenitors are not derived from bone marrow, which is another expected source. We previously demonstrated that marrow-derived MSCs require primary cilia to populate the cortical bone at the periosteal surface in response to mechanical loading [28]. This suggests that Prx1-expressing progenitors containing disrupted cilia in the marrow would not mobilize to the periosteal surface. However, we found that the mineralizing surface is unchanged in mutants, meaning active osteoblasts still arrive at the periosteal surface. These phenomena are therefore inconsistent, and our data further implicate the periosteum as the source of Prx1-expressing progenitors. Additionally, we did not detect Prx1 expression in bone marrow when we visualized GFP. Collectively, our results provide compelling evidence to suggest Prx1-expressing progenitors that participate in load-induced bone formation are recruited from the periosteum.

The bone-forming activity of osteoblasts derived from Prx1-expressing progenitors is dependent on primary cilia, but recruitment and differentiation occur independently. The relative percent mineralizing surfaces (rMS/BS) were equivalent between experimental and control animals. This is surprising since the majority of active osteoblasts are derived from recruited progenitors at the time points we evaluated [23] and therefore suggests that primary cilia do not influence progenitor recruitment in this instance. We

	Loaded	Nonloaded
Control		
Cilium KO		

(a)

(b) Mineralizing surface
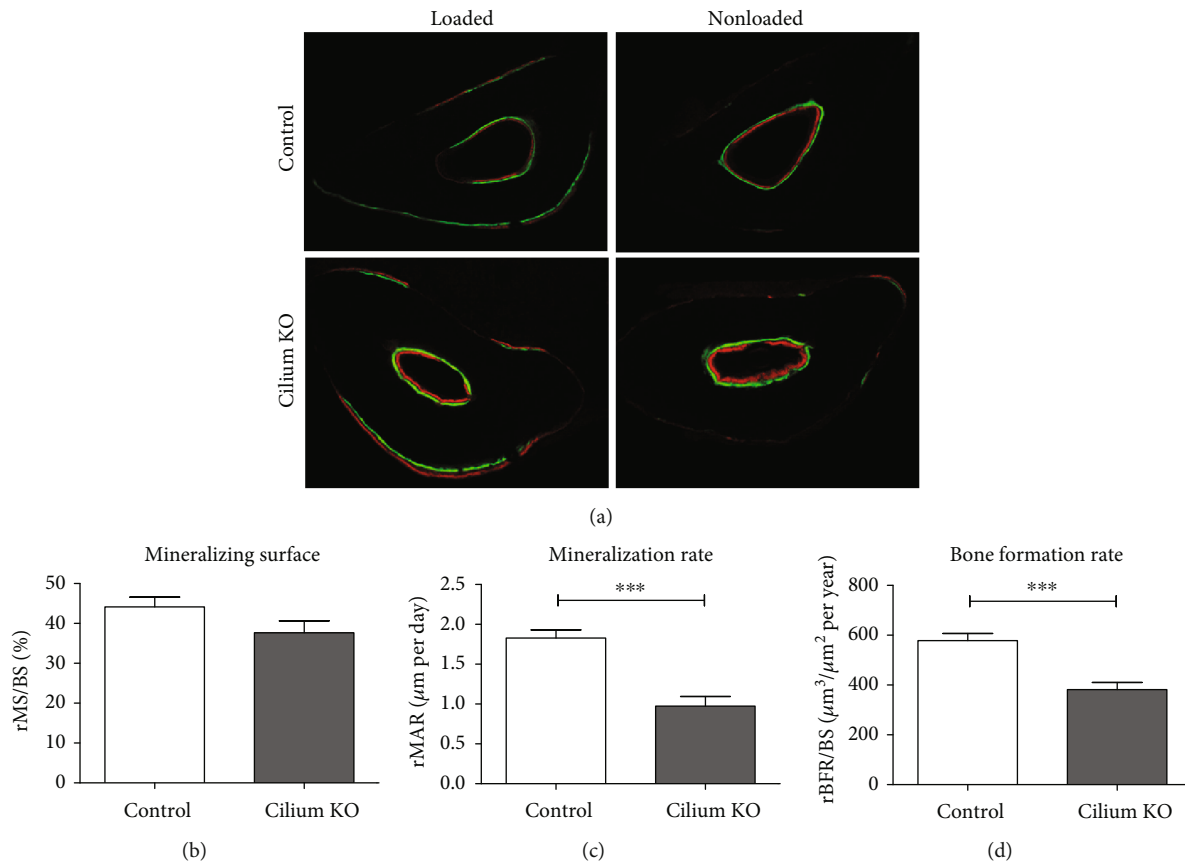

(c) Mineralization rate

(d) Bone formation rate

FIGURE 3: Load-induced bone formation is attenuated in mice with a Prx1-driven cilium knockout. Fluorochrome labels depicting load-induced bone formation at the periosteal surface (a). Dynamic histomorphometry to quantify bone formation parameters (c-d). Micrographs were collected at 10x magnification. $n = 22$ control and $n = 28$ experimental animals, $^{***}p < 0.001$.

also found that the relative rate of mineral apposition (rMAR) of mutant animals was approximately half the rate of controls, indicating primary cilia play a potent role in osteoblast activity. In a previous study by Temiyasathit et al., deletion of Kif3a in osteoblasts and osteocytes also resulted in a decrease in rMAR (~30%), with no change in rMS/BS [18]. The greater decrease in rMAR in our current study may be due to the deletion occurring prior to osteoblast differentiation. Mutants maintain some mineral apposition, suggesting that other cell types also contribute to adaptation. For example, the earliest active osteoblasts in response to loading are likely derived from bone lining cells [23]. Despite these alternative contributions, the severity of attenuated bone formation in mutants suggests Prx1-expressing cells have a significant impact.

Although our data indicate Prx1-expressing cells contribute to mechanically induced bone formation in a primary cilium-mediated process, the exact mechanism is unknown. The primary cilium is both a mechano- and chemosensor, so disrupting this organelle potentially abrogates a progenitor cell's ability to detect both physical and biochemical stimuli. One intriguing possibility is that mechanical stimulation alone directs progenitors to embark on a preprogrammed path of becoming active osteoblasts. Without functional primary cilia, Prx1-expressing progenitors are

not properly encoded to form bone once they arrive at the bone surface (Figure 4). This situation may not be entirely novel, since bone loss due to disuse is a consequence of decreased bone formation by osteoblasts in the basic multicellular unit [29]. Another possibility is that osteocytes sense loading and signal to Prx1-expressing cells, triggering differentiation. In this scenario, Prx1-expressing cells without primary cilia would exhibit dysfunctional chemosensation and fail to properly transduce signals from mechanically stimulated osteocytes. These two phenomena are not mutually exclusive so a third speculation is that Prx1-expressing progenitors both directly sense mechanical stimulation and receive signals from osteocytes.

One limitation of this study is that Kif3a has been linked to nonciliary functions. Loss of Kif3a results in constitutive phosphorylation of Dishevelled, leading to overactivation of the canonical Wnt pathway [30], which is believed to mediate progenitor differentiation [31, 32]. However, deletion of Ift88, another gene that affects ciliogenesis, did not cause constitutive phosphorylation of Dishevelled. Deletion of Ift88 may therefore be a more specific model for disrupting primary cilia, but Prx1-driven *in vivo* deletion of Kif3a and Ift88 in embryonic studies produced identical results [16]. Regardless, the results presented here are novel in showing that disruption of a key
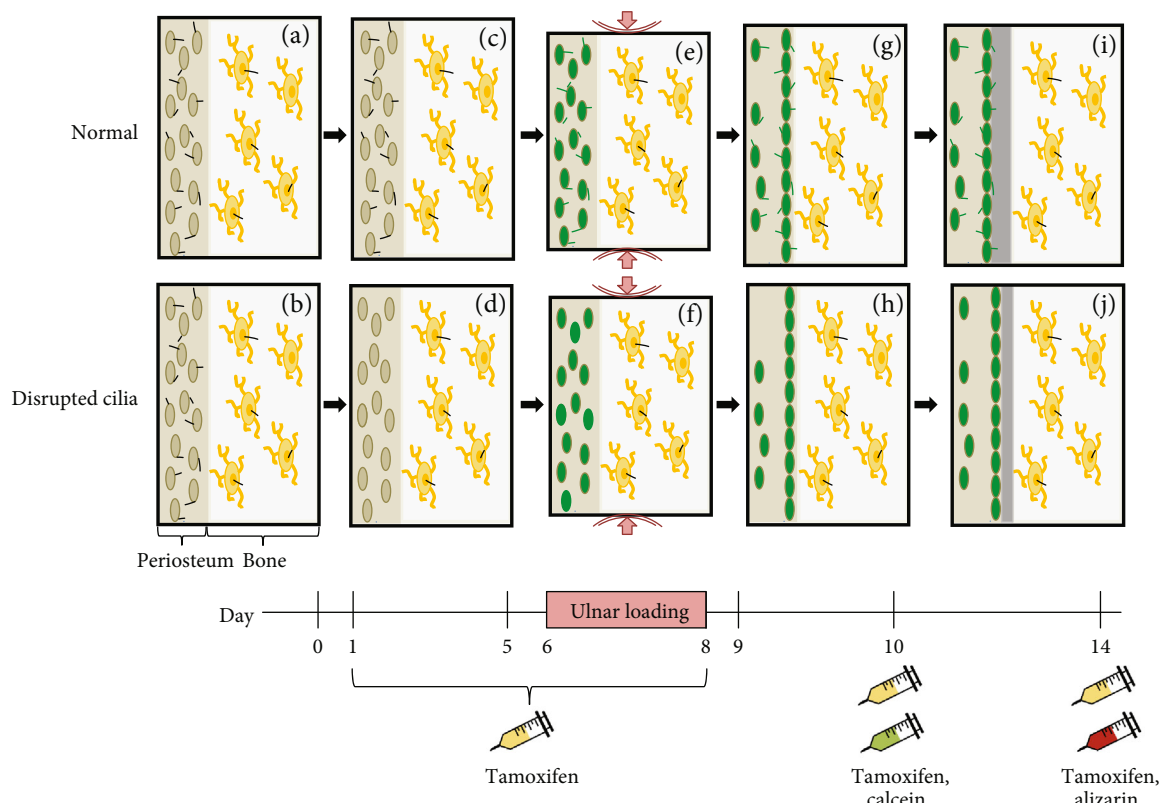
Figure 4: Proposed effect of Prx1-driven primary cilium disruption on load-induced bone formation. Prx1-expressing periosteal progenitor cells (tan) and osteocytes (yellow) contain functional primary cilia (black) prior to experimentation (a, b). Tamoxifen is injected prior to loading, and periosteal progenitor primary cilia are uniquely disrupted in mutant mice (c, d). Ulnar loading is applied and both periosteal progenitors and osteocytes sense the mechanical stimulus. Periosteal progenitors are activated (green) by loading, regardless of whether their primary cilia are functional (e) or disrupted (f). The majority of activated progenitors migrate to the cortical surface (g, h). A continuous layer of matrix is deposited on the periosteal surface, but periosteal progenitors with disrupted cilia (j) produce less newly formed bone than those with functional cilia (i).

ciliary protein in a progenitor source causes a deficiency in load-induced bone formation.

5. Conclusions

In this study, we demonstrate for the first time that Prx1-expressing cells contribute to mechanically induced bone formation. We also found evidence that, while functional primary cilia are not necessary for these progenitors to arrive at the bone surface, they are important for bone apposition activity once these cells differentiate into osteoblasts. The primary cilium may serve as a microdomain that facilitates signaling by enhancing reaction kinetics or bringing specific reaction partners together. Although this organelle's role in bone apposition remains unknown, understanding activation of periosteal progenitors through primary cilium-mediated mechanisms would greatly focus the search for bone regeneration strategies.

Data Availability

Primer sequences and data used to support the findings of this study are available from the corresponding author upon request.

Conflicts of Interest

The authors have no conflicts to disclose.

References

[1] R. T. Brady, F. J. O'Brien, and D. A. Hoey, "Mechanically stimulated bone cells secrete paracrine factors that regulate osteoprogenitor recruitment, proliferation, and differentiation," *Biochemical and Biophysical Research Communications*, vol. 459, no. 1, pp. 118–123, 2015.

[2] E. J. Arnsdorf, L. M. Jones, D. R. Carter, and C. R. Jacobs, "The periosteum as a cellular source for functional tissue engineering," *Tissue Engineering Part A*, vol. 15, no. 9, pp. 2637–2642, 2009.

[3] I. I. Castro-Silva, W. F. Zambuzzi, L. de Oliveira Castro, and J. M. Granjeiro, "Periosteal-derived cells for bone bioengineering: a promising candidate," *Clinical Oral Implants Research*, vol. 23, no. 10, pp. 1238–1242, 2012.

[4] A. Kawanami, T. Matsushita, Y. Y. Chan, and S. Murakami, "Mice expressing GFP and CreER in osteochondro progenitor cells in the periosteum," *Biochemical and Biophysical Research Communications*, vol. 386, no. 3, pp. 477–482, 2009.

[5] D. A. Hoey, S. Tormey, S. Ramcharan, F. J. O'Brien, and C. R. Jacobs, "Primary Cilia-Mediated Mechanotransduction in Human Mesenchymal Stem Cells," *Stem Cells*, vol. 30, no. 11, pp. 2561–2570, 2012.

[6] E. J. Arnsdorf, P. Tummala, R. Y. Kwon, and C. R. Jacobs, "Mechanically induced osteogenic differentiation - the role of RhoA, ROCKII and cytoskeletal dynamics," *Journal of Cell Science*, vol. 122, no. 4, pp. 546–553, 2009.

[7] J. H. Henderson, L. Fuentede la, D. Romero et al., "Rapid growth of cartilage rudiments may generate perichondrial structures by mechanical induction," *Biomechanics and Modeling in Mechanobiology*, vol. 6, no. 1–2, pp. 127–137, 2007.

[8] T. Kanno, T. Takahashi, W. Ariyoshi, T. Tsujisawa, M. Haga, and T. Nishihara, "Tensile mechanical strain up-regulates Runx2 and osteogenic factor expression in human periosteal cells: implications for distraction osteogenesis," *Journal of Oral and Maxillofacial Surgery*, vol. 63, no. 4, pp. 499–504, 2005.

[9] A. Greenbaum, Y.-M. S. Hsu, R. B. Day et al., "CXCL12 in early mesenchymal progenitors is required for haematopoietic stem- cell maintenance," *Nature*, vol. 495, no. 7440, pp. 227–230, 2013.

[10] L. Ding and S. J. Morrison, "Haematopoietic stem cells and early lymphoid progenitors occupy distinct bone marrow niches," *Nature*, vol. 495, no. 7440, pp. 231–235, 2013.

[11] J. Sanchez-Gurmaches, W.-Y. Hsiao, and D. A. Guertin, "Highly selective in vivo labeling of subcutaneous white adipocyte precursors with Prx1-Cre," *Stem Cell Reports*, vol. 4, no. 4, pp. 541–550, 2015.

[12] E. R. Moore, Y. Yang, and C. R. Jacobs, "Primary cilia are necessary for Prx1-expressing cells to contribute to postnatal skeletogenesis," *Journal of Cell Science*, vol. 131, no. 16, p. jcs217828, 2018.

[13] E. R. Moore, Y. X. Zhu, H. S. Ryu, and C. R. Jacobs, "Periosteal progenitors contribute to load-induced bone formation in adult mice and require primary cilia to sense mechanical stimulation," *Stem Cell Research & Therapy*, vol. 9, no. 1, p. 190, 2018.

[14] O. D. de Lageneste, A. Julien, R. Abou-Khalil et al., "Periosteum contains skeletal stem cells with high bone regenerative potential controlled by periostin," *Nature Communications*, vol. 9, no. 1, p. 773, 2018.

[15] K. L. Lee, D. A. Hoey, M. Spasic, T. Tang, H. K. Hammond, and C. R. Jacobs, "Adenylyl cyclase 6 mediates loading-induced bone adaptation in vivo," *FASEB Journal : Official Publication of the Federation of American Societies for Experimental Biology*, vol. 28, no. 3, pp. 1157–1165, 2014.

[16] C. J. Haycraft, Q. Zhang, B. Song et al., "Intraflagellar transport is essential for endochondral bone formation," *Development*, vol. 134, no. 2, pp. 307–316, 2007.

[17] R. Serra, "Role of intraflagellar transport and primary cilia in skeletal development," *The Anatomical Record: Advances in Integrative Anatomy and Evolutionary Biology*, vol. 291, no. 9, pp. 1049–1061, 2008.

[18] S. Temiyasathit, W. J. Tang, P. Leucht et al., "Mechanosensing by the primary cilium: deletion of Kif3A reduces bone formation due to loading," *PLoS One*, vol. 7, no. 3, article e33368, 2012.

[19] D. A. Hoey, D. J. Kelly, and C. R. Jacobs, "A role for the primary cilium in paracrine signaling between mechanically stimulated osteocytes and mesenchymal stem cells," *Biochemical and Biophysical Research Communications*, vol. 412, no. 1, pp. 182–187, 2011.

[20] J. R. Marszalek, P. Ruiz-Lozano, E. Roberts, K. R. Chien, and L. S. B. Goldstein, "Situs inversus and embryonic ciliary morphogenesis defects in mouse mutants lacking the KIF3A subunit of kinesin-II," *Proceedings of the National Academy of Sciences of the United States of America*, vol. 96, no. 9, pp. 5043–5048, 1999.

[21] A. G. Robling and C. H. Turner, "Mechanotransduction in bone: genetic effects on mechanosensitivity in mice," *Bone*, vol. 31, no. 5, pp. 562–569, 2002.

[22] Z. Ouyang, Z. Chen, M. Ishikawa et al., "*Prx1* and 3.2 kb *Col1a1* promoters target distinct bone cell populations in transgenic mice," *Bone*, vol. 58, pp. 136–145, 2014.

[23] C. H. Turner, I. Owan, T. Alvey, J. Hulman, and J. M. Hock, "Recruitment and proliferative responses of osteoblasts after mechanical loading in vivo determined using sustained-release bromodeoxyuridine," *Bone*, vol. 22, no. 5, pp. 463–469, 1998.

[24] D. A. Corral, M. Amling, M. Priemel et al., "Dissociation between bone resorption and bone formation in osteopenic transgenic mice," *Proceedings of the National Academy of Sciences of the United States of America*, vol. 95, no. 23, pp. 13835–13840, 1998.

[25] K. Wilk, S.-C. A. Yeh, L. J. Mortensen et al., "Postnatal calvarial skeletal stem cells expressing PRX1 reside exclusively in the calvarial sutures and are required for bone regeneration," *Stem Cell Reports*, vol. 8, no. 4, pp. 933–946, 2017.

[26] C. Colnot, "Skeletal cell fate decisions within periosteum and bone marrow during bone regeneration," *Journal of Bone and Mineral Research*, vol. 24, no. 2, pp. 274–282, 2009.

[27] J. R. Dwek, "The periosteum: what is it, where is it, and what mimics it in its absence?," *Skeletal Radiology*, vol. 39, no. 4, pp. 319–323, 2010.

[28] J. C. Chen, D. A. Hoey, M. Chua, R. Bellon, and C. R. Jacobs, "Mechanical signals promote osteogenic fate through a primary cilia-mediated mechanism," *FASEB Journal : Official Publication of the Federation of American Societies for Experimental Biology*, vol. 30, no. 4, pp. 1504–1511, 2016.

[29] H. M. Frost, "Perspectives: the role of changes in mechanical usage set points in the pathogenesis of osteoporosis," *Journal of Bone and Mineral Research*, vol. 7, no. 3, pp. 253–261, 1992.

[30] K. C. Corbit, A. E. Shyer, W. E. Dowdle, J. Gaulden, V. Singla, and J. F. Reiter, "Kif3a constrains β-catenin-dependent Wnt signalling through dual ciliary and non-ciliary mechanisms," *Nature Cell Biology*, vol. 10, no. 1, pp. 70–76, 2008.

[31] X. Peng, L. Yang, H. Chang et al., "Wnt/β-catenin signaling regulates the proliferation and differentiation of mesenchymal progenitor cells through the p53 pathway," *PLoS One*, vol. 9, no. 5, article e97283, 2014.

[32] E. D. Cohen, Y. Tian, and E. E. Morrisey, "Wnt signaling: an essential regulator of cardiovascular differentiation, morphogenesis and progenitor self-renewal," *Development (Cambridge, England)*, vol. 135, no. 5, pp. 789–798, 2008.

Research Article

The Manufacture of GMP-Grade Bone Marrow Stromal Cells with Validated In Vivo Bone-Forming Potential in an Orthopedic Clinical Center in Brazil

Rhayra B. Dias,[1,2] **João A. M. Guimarães** [iD],[2,3] **Marco B. Cury** [iD],[4] **Leonardo R. Rocha** [iD],[2,3] **Elaine S. da Costa** [iD],[5] **Liebert P. Nogueira** [iD],[6] **Camila Hochman-Mendez** [iD],[7,8] **Anneliese Fortuna-Costa,**[2] **Anna Karoline F. Silva** [iD],[9] **Karin S. Cunha** [iD],[9] **Sergio A. L. de Souza** [iD],[10] **Maria Eugênia L. Duarte** [iD],[2] **Rafaela C. Sartore,**[2] **and Danielle C. Bonfim** [iD][2]

[1]*Master Program in Musculoskeletal Sciences, National Institute of Traumatology and Orthopedics, Rio de Janeiro 20940-070, Brazil*
[2]*Research Division, National Institute of Traumatology and Orthopedics, Rio de Janeiro 20940-070, Brazil*
[3]*Trauma Center, National Institute of Traumatology and Orthopedics, Rio de Janeiro 20940-070, Brazil*
[4]*Hip Surgery Center, National Institute of Traumatology and Orthopedics, Rio de Janeiro 20940-070, Brazil*
[5]*Institute of Paediatrics and Puericulture Martagão Gesteira, Federal University of Rio de Janeiro, Rio de Janeiro 21941-912, Brazil*
[6]*Institute of Clinical Dentistry, University of Oslo, Oslo 0317, Norway*
[7]*Institute of Biophysics Carlos Chagas Filho, Federal University of Rio de Janeiro, Rio de Janeiro 21941-902, Brazil*
[8]*Texas Heart Institute, Regenerative Medicine Research, Texas 77030, USA*
[9]*Graduate Program in Pathology, Fluminense Federal University, Rio de Janeiro 24030-215, Brazil*
[10]*Department of Radiology, Clementino Fraga Filho University Hospital, Federal University of Rio de Janeiro, Rio de Janeiro 21941-913, Brazil*

Correspondence should be addressed to Danielle C. Bonfim; danibom@gmail.com

In vitro-expanded bone marrow stromal cells (BMSCs) have long been proposed for the treatment of complex bone-related injuries because of their inherent potential to differentiate into multiple skeletal cell types, modulate inflammatory responses, and support angiogenesis. Although a wide variety of methods have been used to expand BMSCs on a large scale by using good manufacturing practice (GMP), little attention has been paid to whether the expansion procedures indeed allow the maintenance of critical cell characteristics and potency, which are crucial for therapeutic effectiveness. Here, we described standard procedures adopted in our facility for the manufacture of clinical-grade BMSC products with a preserved capacity to generate bone in vivo in compliance with the Brazilian regulatory guidelines for cells intended for use in humans. Bone marrow samples were obtained from trabecular bone. After cell isolation in standard monolayer flasks, BMSC expansion was subsequently performed in two cycles, in 2- and 10-layer cell factories, respectively. The average cell yield per cell factory at passage 1 was of $21.93 \pm 12.81 \times 10^6$ cells, while at passage 2, it was of $83.05 \pm 114.72 \times 10^6$ cells. All final cellular products were free from contamination with aerobic/anaerobic pathogens, mycoplasma, and bacterial endotoxins. The expanded BMSCs expressed CD73, CD90, CD105, and CD146 and were able to differentiate into osteogenic, chondrogenic, and adipogenic lineages in vitro. Most importantly, nine out of 10 of the cell products formed bone when transplanted in vivo. These validated procedures will serve as the basis for in-house BMSC manufacturing for use in clinical applications in our center.

1. Introduction

Bone marrow stromal cells (BMSCs) have extensively been tested at the preclinical and clinical levels for the treatment of complex bone-related injuries, such as nonunion [1–4], avascular osteonecrosis [5, 6], critical-sized defects [1, 7–12], and osteochondral lesions [13–19] because of their inherent potential to differentiate into multiple skeletal cell types [20–22], modulate inflammatory responses [23–28], and support angiogenesis [29–32].

The treatment of these conditions requires the correct combination of biological (cells and scaffolds) and mechanical factors [33–35]. To replace bone autografts—the current gold standard—in the biological component, BMSCs must be expanded in vitro on a large scale by using good manufacturing practice (GMP) [36–45]. Although a wide variety of methods have been reported to manufacture GMP-grade BMSCs, a still major challenge for the generation of BMSC products is to scale up the processes while maintaining critical cell phenotypic and functional characteristics [25, 26]. Until now, there is no consensus as to which reagents, cell culture medium, and culture systems should be used and which tests should be performed to ensure the safety and efficacy of the final product [27–29].

Therefore, for the successful translation of BMSC potential to the clinic, it is imperative to develop standard procedures for cell production, which, in addition to being evidence-based, well-documented, cost-effective, clinically practical, and incorporating GMP, also guarantee the preservation of BMSC potency [46, 47]. As one of the main orthopedic centers in Brazil, we have established an in-house facility for the isolation and large-scale expansion of functionally certified clinical-grade BMSCs. Here, we report our general procedures, which comply both with GMP standards and the Brazilian regulatory rules for cell manufacturing for therapeutic purposes. These procedures will serve as the basis for BMSC production for future applications in our center, aiming at bone repair.

2. Materials and Methods

2.1. Reagents and Materials. All reagents and materials used for BMSC isolation, expansion, and cryopreservation were certified to be of clinical grade. None of these reagents were aliquoted. To assure traceability, the lot and/or serial numbers of all reagents and materials used in each assay were registered. Reagents used in in vitro differentiation assays and immunophenotyping, when not of clinical grade, were certified to have been produced under good laboratory practices and had defined chemical purity standards. A complete list of all reagents used with all related information is available in Supplementary Materials (Supplementary Table 1). The technical procedures described herein were adapted to comply with the rules of the Brazilian Health Regulatory Agency (ANVISA, Collegiate Board Resolution—RDC Nos. 09/2011 and 214/2018) for the development of cell products intended for use in humans.

2.2. Sample Donor Eligibility Criteria. The study design, the procedures used for its execution, and sample collection were approved by the institutional ethics committee (No. 41660415.3.0000.5273). Subjects of both sexes who were older than 18 years old with indications for total hip replacement were invited to donate the discarded acetabular bone/marrow. After providing written informed consent to donate the samples, a brief questionnaire was used to assess the risk of blood-borne infections. The donors were also questioned about previously diagnosed comorbidities, such as rheumatoid arthritis, diabetes mellitus, bone marrow dysplasia, and malignant tumors, the use of immunosuppressant drugs, and any history of drug and/or alcohol abuse. If any of these were disclosed, the donor was excluded from the study. To those selected, further inclusion criteria were applied: a platelet count > 150×10^9/L, a hemoglobin concentration > 11.5 g/dL for women and 12.5 g/dL for men (the reference values for blood donation—ANVISA, RDC No. 153/2004), and a negative pregnancy test. Donor blood samples were also tested for HIV-1/2, hepatitis B virus surface antigen, hepatitis B virus core antigen, hepatitis C virus, HTLV-1, HTLV-2, cytomegalovirus, *Mycobacterium tuberculosis*, *Treponema pallidum*, and *Trypanosoma cruzi* infection. In the case of any positive test, the donor was excluded from the study. The data for the final selected donors is summarized in Table 1.

2.3. Preparation of Total Bone Marrow Cell Suspensions. Acetabular bone fragments were processed immediately after harvesting or after a maximum of 12 h of storage at 2-8°C in α-minimum essential medium (α-MEM, LGC Biotechnology, São Paulo, SP, BRA) supplemented with 20% fetal bovine serum (FBS, Gibco-Thermo Fisher, Waltham, MA, USA) [37, 48–50]. The samples were added to 50 mL tubes, and phosphate-buffered saline (PBS, Amresco, Solon, OH, USA) was added at a 1 : 4 (*w/v*) ratio. After vigorous mechanical homogenization with a 10 mL pipette (the speed of the hand pipettor must be set to high), bone spicules were allowed to settle, and the cell suspension was collected and transferred to a new 50 mL tube. Fresh PBS was added to the tube containing the spicules, at the same ratio, and a second round of homogenization was performed. After brief spicule sedimentation, the supernatant was collected and transferred to a new tube. This step was repeated at least three times or until the bones were visually clean of marrow. The collected marrow suspensions were centrifuged at 300 × *g* for 5 minutes. After centrifugation, a 5 mL sample of the supernatant was collected for bacterial contamination testing. The pelleted cells were resuspended in α-MEM supplemented with 20% FBS. To determine the number of total nucleated cells obtained, an aliquot of the marrow suspension was diluted in an appropriate amount of 2% glacial acetic acid for red blood cell lysis and subsequently loaded in a modified Neubauer chamber for cell counting.

2.4. Colony-Forming Efficiency (CFE) Assay. To estimate the number of colony-forming units (CFU-Fs) in the obtained marrow suspensions, nucleated cells were plated in triplicate at a density of $8,0 \times 10^3$/cm² (Corning Incorporated, New York, NY, USA) in 2 mL of α-MEM supplemented with 20% FBS. After 3 days of incubation at 37°C in 5% CO_2, the

TABLE 1: Characteristics of donor patients and colony-forming efficiency (CFE) results.

	Gender	Age	TNC (10^5)	CFU-F/10^5	Colony diameter (mm)
BMSC 01	M	54	620	7.66	9.1
BMSC 02	F	61	520	8.33	8.4
BMSC 03	F	54	600	19.33	5.0
BMSC 04	M	48	590	17.33	4.8
BMSC 05	F	55	350	13.5	4.0
BMSC 06	M	65	150	45.33	3.9
BMSC 07	F	75	150	23.66	4.3
BMSC 08	F	75	150	20.33	2.5
BMSC 09	F	64	280	45	4.8
BMSC 10	M	71	250	48	1.8
BMSC 11	M	57	370	31	3.8
BMSC 12	F	54	210	20.33	3.3
BMSC 13	F	74	540	23	4.0
BMSC 14	F	70	250	31.33	3.3
Mean ± SD	—	62.0 ± 9.30	359.28 ± 173.55	25.29 ± 13.20	4.5 ± 1.86

TNC: total nucleated cells; CFU-F: colony-forming unit-fibroblast.

nonadherent hematopoietic cells were removed, and the medium was changed. At day 14, the colonies were fixed with 4% paraformaldehyde (Sigma-Aldrich, St. Louis, MO, USA) and stained with 1% crystal violet (Sigma-Aldrich). Colonies with more than 50 cells were counted [48]. The efficiency of colony formation was expressed as the mean colony number relative to the 100000 bone marrow nucleated cells plated.

2.5. BMSC Isolation. To determine the optimal cell seeding density for BMSC isolation, nucleated cells from samples 01 to 04 were resuspended at $0.08 \times 10^5/cm^2$, $0.4 \times 10^5/cm^2$, and $2.0 \times 10^5/cm^2$ in 10 mL of α-MEM supplemented with 20% FBS and plated in triplicate in T-75 cm^2 flasks (Corning Incorporated). After plating, the cells were allowed to adhere for 3 days in a humidified atmosphere of 5% CO$_2$ at 37°C. Then, the nonadherent cells were removed, the adherent cells were washed three times with PBS, and the medium was changed. Thereafter, the adherent cells were allowed to proliferate for 11 additional days. Complete medium exchange was performed every 3 days. At day 14, a 5 mL aliquot of the culture medium was collected for bacterial contamination testing. The cells were washed twice with PBS and harvested with recombinant trypsin (TrypLE® Express, Invitrogen, Carlsbad, CA, USA). The cell number was determined by manual counting with a Neubauer chamber. The cell viability was assessed by the Trypan Blue exclusion method. If the cell viability was <70%, the cells were discarded and expansion was stopped. For samples 05 to 14, nucleated cells were plated only at $0.4 \times 10^5/cm^2$, and the isolation was performed as described.

2.6. Large-Scale BMSC Expansion. Large-scale BMSC expansion was performed in multilayer cell factories, in a two-step process [37, 45]. In the first expansion cycle (passage 1—P1), BMSCs were seeded in 2-layer cell factories (1264 cm^2, Corning Incorporated) at a density of 2.0×10^3 cells/cm^2 in

500 mL of α-MEM supplemented with 20% FBS. The cells were incubated at 37°C in 5% CO$_2$ and allowed to proliferate until the monolayers reached 70% confluence. The medium was changed every 3 days. To estimate the degree of confluence of the cells in the cell factories, sentinel T-75 cm^2 flasks were simultaneously seeded with BMSCs and kept under the same culture conditions [37]. During harvesting, the cells were washed two times with PBS and incubated for 10 minutes with 150 mL of TrypLE® Express to induce detachment. After centrifugation at $300 \times g$ for 5 minutes, the cells were resuspended in fresh expansion medium and counted in a Neubauer chamber as described above. Expansion was discontinued if the cell viability was <70%.

For the second expansion cycle, BMSCs were seeded in 10-layer cell factories (6320 cm^2, Corning Incorporated) at a density of 2.0×10^3 cells/cm^2 in 1.5 L of α-MEM supplemented with 20% FBS. When the cells reached 70% confluence, a 5 mL aliquot of the culture medium was collected for bacterial contamination testing, and the cells were washed twice with PBS. After 10 minutes of incubation with TrypLE® Express, the cell suspension was collected, diluted 1 : 2 (v/v) in Ringer's lactate solution (Fresenius Kabi, Bad Homburg vor der Höhe, GER) supplemented with 5% human albumin (Alburex® 20, CSL Behring AGB, Berna, SWE), and centrifuged at $300 \times g$ for 5 minutes. The cell pellets were then washed five times with Ringer's lactate solution supplemented with 0.5% human albumin to remove the FBS proteins [37]. Finally, the cells were resuspended in Ringer's lactate solution with 5% human albumin and counted in a Neubauer chamber. The cell viability was assessed with Trypan Blue staining. If the cell viability was >70%, the cells were either used in subsequent experiments or processed for cryopreservation.

2.7. Population Doubling Analysis. In each expansion cycle, the number of population doublings (PD) was calculated

using the formula PD = (Log N_f-Log N_i)/Log 2, in which N_f is the final harvested cell number and N_i is the initial seeded cell number. The cumulative PD (cPD) was calculated by adding PD_1 and PD_2. The doubling time (dT) was determined by dividing the time in days required for total cell expansion by the cumulative PD (dT = Δt/cPD) [51].

2.8. Cryopreservation and Storage.

A total of 5.0×10^6 BMSCs were resuspended in 1.0 mL of cryopreservation solution consisting of 5% dimethylsulfoxide (DMSO, Sigma-Aldrich), 5% human serum albumin, and 6% hydroxyethyl starch solution (Voluven®, Fresenius Kabi) in Ringer's lactate solution. The cryotubes were placed in a room temperature Mr. Frosty freezing container (Nalgene®, Sigma-Aldrich), which was immediately transferred to a -80°C freezer. After overnight incubation, the vials were transferred to boxes that were stored in the vapor phase of a liquid nitrogen tank.

2.9. Viability of the Cryopreserved Cells.

After four and 40 weeks of cryopreservation in the aforementioned conditions, one vial from five BMSC products (07–11) was thawed in a water bath at 37°C. The cell suspension was immediately diluted 1:10 (v/v) in α-MEM supplemented with 20% FBS and centrifuged at $300 \times g$ for 5 minutes. The supernatants were discarded, and the cells were resuspended in 4 mL α-MEM supplemented with 20% FBS. The number of dead and live cells was determined by manual counting with a Neubauer chamber, using the Trypan Blue exclusion method.

2.10. Bacterial, Endotoxin, and Mycoplasma Contamination Testing.

To evaluate the sterility of the final BMSC products, the presence of aerobic and anaerobic bacteria and mycoplasma and the levels of endotoxin were evaluated. For aerobic and anaerobic bacterial contamination testing, 1 mL of the cell culture media collected at the end of bone marrow cell suspension preparations and at the end of P0 (isolation) and P2 was inoculated into BD BACTEC™ Plus Aerobic/F and BD BACTEC™ Plus Anaerobic/F (Becton Dickenson, New Jersey, USA) culture vials and incubated for 10 days.

Mycoplasma contamination and endotoxin levels were evaluated in P2 culture media with the detection kits MycoAlert™ and LAL Pyrogent™-5000 (both from Lonza, Basel, SWI), respectively. Measurements were performed in accordance with the manufacturer's protocol. Values ≤ 1.2 for mycoplasma and 5 UE/mL for endotoxin (reference values) were considered negative.

2.11. Quantification of Bovine Transferrin.

Levels of FBS proteins in the final cell products were estimated by the quantification of bovine transferrin concentration by ELISA. After the cells' washing step with Ringer's lactate, a 2 mL sample of the cell suspension was collected and measurements were performed according to the manufacturer's instructions (Abnova, Taipei, TWN). Values ≤ 10 ng/mL (assay reference value) were considered negative.

2.12. Immunophenotyping.

For immunophenotypic characterization of cells, 1.0×10^6 BMSCs per tube were washed with FACS buffer consisting of PBS supplemented with 1% bovine serum albumin (BSA, Sigma). Then, the cells were incubated for 30 minutes in the dark at room temperature with the following fluorochrome-conjugated primary antibodies: anti-CD90-Percp-Cy5.5, anti-CD73-APC, anti-CD105-FITC, anti-CD146-PE (all from BioLegend, San Diego, CA, USA), anti-CD14-FITC (Immunostep, Salamanca, SPA), anti-CD34-FITC, anti-CD45-Percp-Cy5.5 (both from Agilent DAKO, Santa Clara, CA, USA), and anti-CD11b-PE (Santa Cruz Biotechnology, Dallas, TX, USA). The isotype controls were IgG2A-FITC, IgG1A-APC, IgG1A-Percp-Cy5.5, IgG1-PE, IgG1-FITC, and IgG2A-PE (all from Santa Cruz Biotechnology). Next, the cells were washed with FACS buffer and resuspended in 300 μL buffer for acquisition with a BD FACSCanto™ cytometer (BD Biosciences). The data were analyzed with FlowJo software (Tree Star, Ashland, OR, USA).

2.13. In Vitro Osteogenic Differentiation and Von Kossa Staining.

BMSCs were plated at a density of 1.3×10^4 cells/cm^2 in triplicate in α-MEM supplemented with 20% FBS and allowed to grow until 100% confluence was reached. Osteogenic differentiation was induced by incubation with α-MEM containing 10 mM β-glycerophosphate, 5 μg/mL ascorbic acid 2-phosphate, and 10^{-6} M dexamethasone (all from Sigma) supplemented with 20% FBS for 21 days, and the medium was changed every 3 days [51]. To assess the mineralization, monolayers were stained with Von Kossa. The cells were fixed in 4% paraformaldehyde for 10 minutes at room temperature and incubated with 2% silver nitrate (Sigma) aqueous solution for 40 minutes while protected from light. The cells were washed three times with distilled water and exposed to UV light for 10 minutes. The wells were photographed using an Eclipse TS100 inverted microscope (Nikon, Tokyo, JPN).

2.14. In Vitro Adipogenic Differentiation and Oil Red O Staining.

BMSCs were plated as described above. After reaching 100% confluence, the cells were incubated with α-MEM containing 0.5 mM isobutylmethylxanthine, 200 mM indomethacin, 10^{-6} M dexamethasone (all from Sigma), and 10 mM insulin (Humulin®, Lilly, São Paulo, SP, BRA) supplemented with 20% FBS for 21 days, and the medium was changed every 3 days [51]. To confirm the lipidic composition of the cell vacuoles, BMSCs were fixed in 4% paraformaldehyde for 10 minutes at room temperature, washed with propylene glycol PA (Vetec Quimica, Rio de Janeiro, RJ, BRA), and incubated with 0.5% Oil Red O solution (Sigma) in propylene glycol for 20 minutes. After two washes with 85% propylene glycol, the cells were photographed using a Nikon Eclipse TS100 inverted microscope.

2.15. In Vitro Chondrogenic Differentiation.

BMSCs were resuspended in α-MEM supplemented with 20% FBS at a density of 1.0×10^7 cells/mL. One 10 μL drop of this cell suspension was placed in each well in a U-shaped 96-well plate, which was incubated at 37°C in 5% CO$_2$ for 30 minutes. Then, 100 μL of StemPro® chondrogenic medium (Thermo Fischer) was added to each well. The medium was changed every 2 days for 21 days [50, 52–55]. The formed

micromasses were fixed in 4% paraformaldehyde for 3 h at room temperature, embedded in paraffin, cut into 5 μm sections, and stained with H&E or Masson's Trichrome stain (EasyPath, São Paulo, SP, BRA) according to the manufacturer's instructions. The slides were photographed using a Nikon E600 microscope.

2.16. Type II Collagen Immunofluorescence. To confirm type II collagen deposition in the chondrogenically induced micromasses, 5 μm paraffin sections were obtained as described above and incubated in citrate buffer (pH 6.0) at 96°C for 40 minutes. After blocking with 10% BSA for 1 h, the sections were incubated overnight at 4°C with an anti-collagen type II primary antibody (sc-288887, Santa Cruz Biotechnology) diluted 1 : 50 in Tris-buffered saline (TBS) with 1% BSA. Subsequently, the slides were washed three times with TBS and incubated for 2 h with an Alexa Fluor 546-conjugated secondary antibody (Life Technologies, Thermo Fisher) in the dark at room temperature. The nuclei were stained with 1 μg/mL DAPI solution (sc-3598, Santa Cruz Biotechnology). Fluorescence images were obtained using a Leica TCS SP5 laser scanning confocal microscope (Leica Microsystems, Wetzlar, GER).

2.17. Subcutaneous Xenotransplantation Assay. To evaluate the in vivo bone-forming potential of the expanded BMSCs, 1.0×10^6 cells were mixed with 30 mg of hydroxyapatite/tricalcium phosphate powder (HA/TCP, Osteoset® T, Wright Medical, Arlington, TN, USA) in 1 mL of α-MEM supplemented with 20% FBS in a 1.5 mL tube. The cell/HA/TCP mixture was incubated overnight at 37°C to allow sedimentation and cell attachment to the HA/TCP particles. Then, the supernatant was carefully aspirated, and 15 μL of 3.2 mg/mL human fibrinogen and 100 U/mL human thrombin (both from Sigma) were added to form a fibrin glue [55–58]. After 3 h of incubation, the cell/HA/TCP implant was collected and subcutaneously transplanted into the flank of an immunocompromised mouse (beige BALB/c nu/nu, IPEN, São Paulo, SP, BR) aged between 6 and 8 weeks [50, 55]. For each BMSC sample, three implants were transplanted per mouse: one cell-free (negative control) and two containing the cells; and two mice were used. Surgeries were performed under general anesthesia with intraperitoneal injections of 80-100 mg/g ketamine hydrochloride and 10 mg/kg xylazine. After 12 weeks, the mice were euthanized by deep anesthesia, and the implants were harvested. All animal procedures were performed in accordance with the guidelines of the Institutional Animal Care and Use Committee (002/2014).

2.18. Implant Histology and Immunohistochemistry. Following harvesting, the implants were fixed for 24 h in 4% paraformaldehyde in PBS. For routine histology, the implants were decalcified by incubation in 10% nitric acid (Vetec) for 3 days, processed for paraffin embedding, cut into 6 μm sections, and stained with H&E.

For immunohistochemistry, the implants were decalcified in 10% EDTA (Sigma) for 8-12 weeks and processed for paraffin embedding and sectioning as previously described. The sections were incubated overnight at 4°C with

rabbit anti-lamin A/C antibody (M00438, Boster, Pleasanton, CA, USA) diluted 1 : 100 or with mouse anti-collagen type I antibody (Abcam, Cambridge, UK) diluted 1 : 300. After 2 washes with EnVision™ FLEX Wash Buffer (DAKO Agilent, Santa Clara, CA, USA), the sections were incubated for 2 h with EnVision Flex (DAKO Agilent). The signal was developed in EnVision Flex Substrate Buffer containing 20 μL/mL DAB—EnVision Flex DAB+ Chromogen (DAKO Agilent)—for 3 min. All images of the glass slides were obtained by digital scanning with an Aperio CS2 scanner and ImageScope software (both from Leica Biosystems).

2.19. Assessment of Bone Density by Micro-CT. Micro-CT scans were performed using the desktop SkyScan1172 scanner (Bruker, Brussels, BEL). One implant from each sample was placed in customized tubes and wrapped in gauze dampened with 4% formalin to avoid shrinkage. The scanning parameters were as follows: 4.0 μm isotropic pixel size and an X-ray source with 70 kV accelerating voltage and 141 μA current with a 500 μm Al filter. The samples were rotated 180° around their vertical axis with a rotational step of 0.4°, an exposure time of 1770 ms, and frame averaging of 3. The total scan time per sample was approximately 1.2 h. The images were reconstructed with NRecon v.1.7.1.0 software (Bruker) using a filtered back-projection algorithm. The 3D images were rendered using CTVox software (Bruker). To discriminate bone from HA/TCP, the grayscale images were binarized. For binarization, the threshold value was chosen based on a visual comparison of the original grayscale image and the binary image for each tissue slice. The binary samples were quantified in CTAn software (Bruker).

2.20. Statistical Analysis. The values were expressed either individually and/or as the mean/median, as appropriate. The Gaussian distribution was evaluated by the Shapiro-Wilk and Kolmogorov-Smirnov tests. Comparisons between groups were evaluated either by one-way ANOVA with Tukey's multiple comparisons test or by Kruskal Wallis with Dunn's multiple comparisons test. P values ≤ 0.05 were considered significant. Analyses were performed with GraphPad Prism software (GraphPad software version 8.0, La Jolla, CA, USA).

3. Results

3.1. Patient and Sample Characteristics. Trabecular bone containing marrow was collected from nine females and five males with ages ranging between 48 and 75 years old (Table 1). The frequency of clonogenic cells in the samples was estimated by the colony-forming efficiency (CFE) assay. The average number of colonies harvested from each sample was heterogeneous and ranged from 7.66 to 48.0 CFU-Fs per 100000 nucleated cells (mean of 25.29 ± 13.20 colonies). The size of the colonies also varied, with average diameters ranging from 1.8 mm to 9.1 mm (mean of 4.5 ± 1.86 mm) (Table 1).

3.2. Optimization of Cell Seeding Density for BMSC Isolation. To determine the optimal conditions for improved BMSC isolation from the bone marrow total nucleated cell fractions,
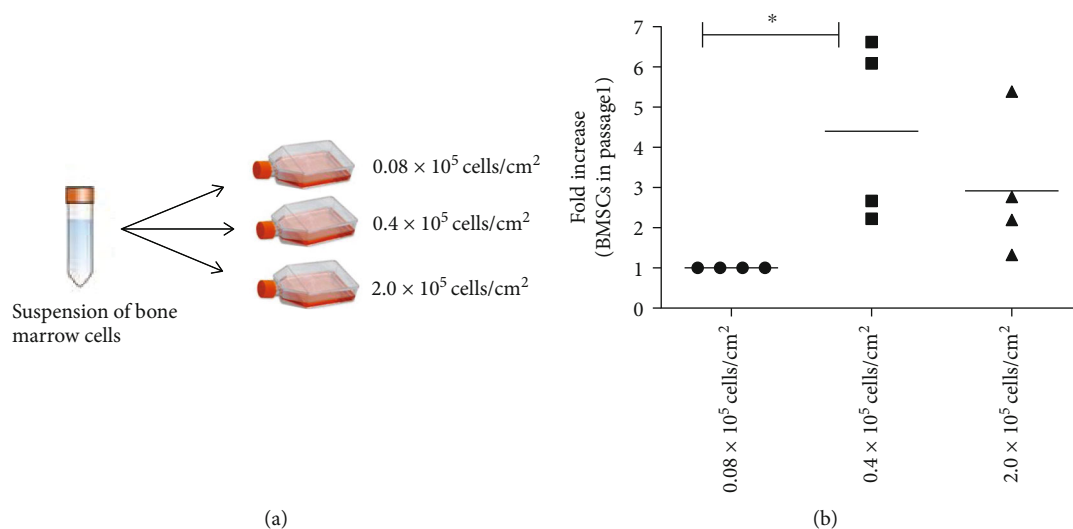
(a)

(b)

Figure 1: Standardization of cell isolation. (a) Schematic representation of the protocol used for determining the optimal initial seeding densities. (b) Fold increase in cell number (BMSCs in passage 1). $n = 4$; $p = 0.015$.
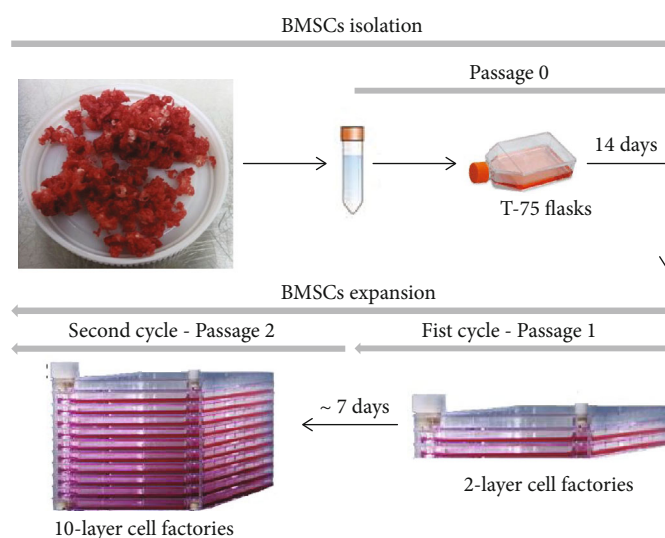
Figure 2: Schematic representation of the in vitro bone marrow stromal cells manufacturing in a GMP-compliant semiclosed system. After bone marrow dissociation from bone spicules, nucleated cells were seeded in T-75 flasks for BMSC isolation (P0), followed by expansion in 2-layer cell factories (P1) and subsequent expansion in 10-layer cell factories (P2).

BMSC samples 01–04 were seeded at three cell densities: $0.08 \times 10^5/cm^2$, which was the density used in the CFE assays, $0.4 \times 10^5/cm^2$, and $2.0 \times 10^5/cm^2$ (Figure 1(a)). The density of 0.4×10^5 cells/cm² yielded a significantly higher number of BMSCs in comparison with the clonal density of $0.08 \times 10^5/cm^2$ (Figure 1(b)) and, therefore, was used as the standard for BMSC isolation in subsequent samples.

3.3. BMSC Manufacturing.
BMSC manufacturing was performed in three steps: isolation in T-75 flasks (P0), followed by two rounds of expansion in 2- and 10-layer cell factories (Figure 2). The average BMSC harvest per T-75 flask at the end of P0 was $0.49 \pm 0.20 \times 10^6$ cells (Table 2). The minimal BMSC number required to initiate expansion in a 2-layer cell factory was obtained for all 10 bone marrow samples. Average viability was of $95.67\% \pm 4.33\%$.

In P1, the cells reached 70% confluence in 5.8 ± 1.75 days. The average BMSC yield per 2-layer cell factory was $21.93 \pm 12.81 \times 10^6$ cells, and the average viability was $95.29\% \pm 3.51\%$ (Table 2). Once again, all samples reached the minimum cell number required for subculture. In P2, the cells reached confluence after 6.6 ± 0.69 days, and an average of $83.05 \pm 114.72 \times 10^5$ cells were harvested per 10-layer cell factory. Viability was of $93.53\% \pm 5.14\%$. Considering both cycles of expansion, the total time needed to obtain the final cell product was 26.4 ± 2.33 days (Table 2).

3.4. Analysis of Population Doubling.
With the adopted procedures for BMSC manufacturing, cells doubled an average

TABLE 2: Yield (number) and viability of BMSCs at each culture step.

	BMSC isolation (P0)			Passage 1 (P1)				Passage 2 (P2)				Total production time (days)
	Cells seeded (10^6)/T-75	Yield (10^6)/T-75	%viability	Cells seeded (10^6)	Yield (10^6)	%viability	Time (days)	Cells seeded (10^6)	Yield (10^6)	%viability	Time (days)	
BMSC 05	3.0	0.35	100	2.5	42.0	95	6	12	118.0	95	7	27
BMSC 06	3.0	0.92	90.5	2.5	30.0	98.1	3	12	56.0	95.2	6	23
BMSC 07	3.0	0.72	100	2.5	43.7	100	3	12	34.0	100	6	23
BMSC 08	3.0	0.52	92.3	2.5	12.0	96	4	12	40.0	98.7	5	23
BMSC 09	3.0	0.62	87.9	2.5	27.0	92.8	7	12	400.0	85.6	7	28
BMSC 10	3.0	0.37	100	2.5	12.0	90	7	12	26.0	92	7	28
BMSC 11	3.0	0.32	96.7	2.5	12.1	90.2	7	12	60.0	89.5	7	28
BMSC 12	3.0	0.41	97.3	2.5	15.0	98	7	12	20.0	97.5	7	28
BMSC 13	3.0	0.37	93.7	2.5	12.5	98.7	7	12	40.0	96.1	7	28
BMSC 14	3.0	0.31	98.3	2.5	13.0	94.1	7	12	36.5	85.7	7	28
Mean ± SD	—	0.49 ± 0.20	95.67 ± 4.33	—	21.93 ± 12.81	95.29 ± 3.51	5.8 ± 1.75	—	83.05 ± 114.72	93.53 ± 5.14	6.6 ± 0.69	26.4 ± 2.33

TABLE 3: Number of population doublings and the doubling time for each BMSC passage.

	Population doubling				Time for population doubling (days)		
	P0	P1	P2	Cpd		P0	P1	P2
BMSC 05	9.75	4.07	3.30	17.12		1.43	1.47	2.12
BMSC 06	3.23	3.58	2.22	9.04		4.33	0.84	2.70
BMSC 07	12.31	4.13	1.50	17.94		1.13	0.73	3.99
BMSC 08	12.05	2.26	2.00	16.31		1.16	1.77	2.50
BMSC 09	11.85	3.43	5.06	20.34		1.18	2.04	1.38
BMSC 10	11.02	2.26	1.50	15.51		1.26	3.09	4.66
BMSC 11	11.74	2.28	2.58	16.60		1.19	3.08	2.71
BMSC 12	11.99	2.58	0.74	15.31		1.16	2.71	9.50
BMSC 13	12.08	2.32	2.00	16.04		1.15	3.01	3.50
BMSC 14	11.37	2.38	1.99	15.74		1.23	2.94	3.52
Mean ± SD	**10.74 ± 2.60**	**2.93 ± 0.75**	**2.29 ± 1.18**	**15.99 ± 2.85**	*Median*	**1.18**	**2.37**	**3.10***

Cpd: cumulative population doubling. *$P = 0,004$ vs. P0; Kruskal Wallis with Dunn's multiple comparisons test.

TABLE 4: Purity and safety analysis of the BMSCs.

	Anaerobic and aerobic bacteria*	Mycoplasma<1.2**	Endotoxin < 5 EU/mL**	Bovine transferrin < 10 ng/mL***
BMSC 05	ND	0.57	<0.005	7.43
BMSC 06	ND	0.43	<0.005	0.04
BMSC 07	ND	0.33	<0.005	0.04
BMSC 08	ND	0.42	<0.005	0.03
BMSC 09	ND	1.08	<0.005	0.04
BMSC 10	ND	0.82	<0.005	0.05
BMSC 11	ND	0.37	<0.005	ND
BMSC 12	ND	0.47	<0.005	ND
BMSC 13	ND	0.63	<0.022	ND
BMSC 14	ND	0.70	<0.005	ND

ND: not detected. *Assessed in the cell supernatant during sample collection, BMSC isolation, and expansion (passages 0 and 2). **Assessed in the supernatant from passage 2 BMSCs. ***Assessed in the supernatant from passage 2 BMSCs washed for 5 cycles with Ringer's lactate solution containing 0.5% human albumin to reduce the residual level of bovine contaminants.

of 10.74 ± 2.60 times during P0, 2.93 ± 0.75 times during P1, and 2.29 ± 1.18 during P2 (Table 3). The time for population doubling was of 1.18 days during P0 and 2.37 days during P1, reaching 3.10 days during P2, which was significantly increased in comparison to P0 (Table 3).

3.5. Sterility Analysis of BMSC Products. To attest the sterility of bone samples and BMSCs and ultimately the quality of the technical procedures and the whole facility environment, tests for aerobic and anaerobic pathogens were performed at P0 and P2 in cell supernatants. No bacterial growth was ever detected (Table 4). The tests for mycoplasma and pyrogenic substances were also all negative (Table 4).

3.6. Assessment of Animal Protein Content in Final BMSC Products. At the end of expansion, BMSCs were washed five times with Ringer's lactate solution containing 0.5% human albumin. Then, the levels of residual animal-derived proteins in the final cell products were evaluated by the quantification of bovine transferrin. None of the samples showed a level above the limiting value of 10 ng/mL

(Table 4), indicating that the BMSC products were compliant with GMP conditions.

3.7. Immunophenotypic Characterization and In Vitro Differentiation of Expanded BMSCs. To characterize the cell products, we first assessed the expression of BMSC-related cell surface markers by FACS. The expanded BMSCs homogenously expressed CD73, CD90, CD105, and CD146 and were negative for the hematopoietic lineage markers CD34, CD45, CD14, and CD11b (Table 5 and Supplementary Figure 1). Next, we evaluated their differentiation potential in vitro. The induced BMSCs were able to differentiate into osteoblasts, adipocytes, and chondrocytes (Figure 3 and Supplementary Figure 2), as shown by the deposition of mineralized nodules with positive Von Kossa staining (Figure 3(b)), intracellular lipid accumulation with positive Oil Red O staining (Figure 3(c)), and collagen type II-rich cartilaginous matrix as revealed by Masson's Trichrome stain (Figures 3(e) and 3(f)) and immunofluorescence analysis (Figures 3(g)–3(i)).

TABLE 5: Immunophenotypic characterization of the lots of BMSCs that were produced.

	%CD73	%CD90	%CD105	%CD146	%CD73/CD90/CD105/CD146	%CD11b	%CD14	%CD34	%CD45
BMSC 05	99.8	99.8	62.3	99.7	70.2	0.59	2.20	1.34	3.21
BMSC 06	100	100	82.3	99.9	82.3	0.86	1.85	0.56	2.85
BMSC 07	100	100	83.3	99.1	73.4	2.38	0.69	0.16	3.32
BMSC 08	97.6	97.6	100	100	95	0.25	0.11	0.45	0.98
BMSC 09	100	98.1	66.4	98.3	50.1	0.69	1.24	0.55	2.39
BMSC 10	92.7	99.6	99.4	99.3	98.8	0.62	0.18	0.22	2.85
BMSC 11	99.7	97.1	95.8	88.4	62.9	1.35	1.14	2.17	2.67
BMSC 12	99.9	99.4	75.2	100	86.1	1.03	0.11	0.11	1.26
BMSC 13	100	100	89.2	100	72.2	3.56	0.19	0.80	4.18
BMSC 14	99.7	98.9	98.3	99.1	82.9	0.12	0.08	1.09	0.26
Mean ± SD	98.94 ± 2.19	99.06 ± 1.02	85.24 ± 13.09	98.38 ± 3.36	77.39 ± 13.95	1.14 ± 1.00	0.77 ± 0.74	0.74 ± 0.60	2.39 ± 1.14

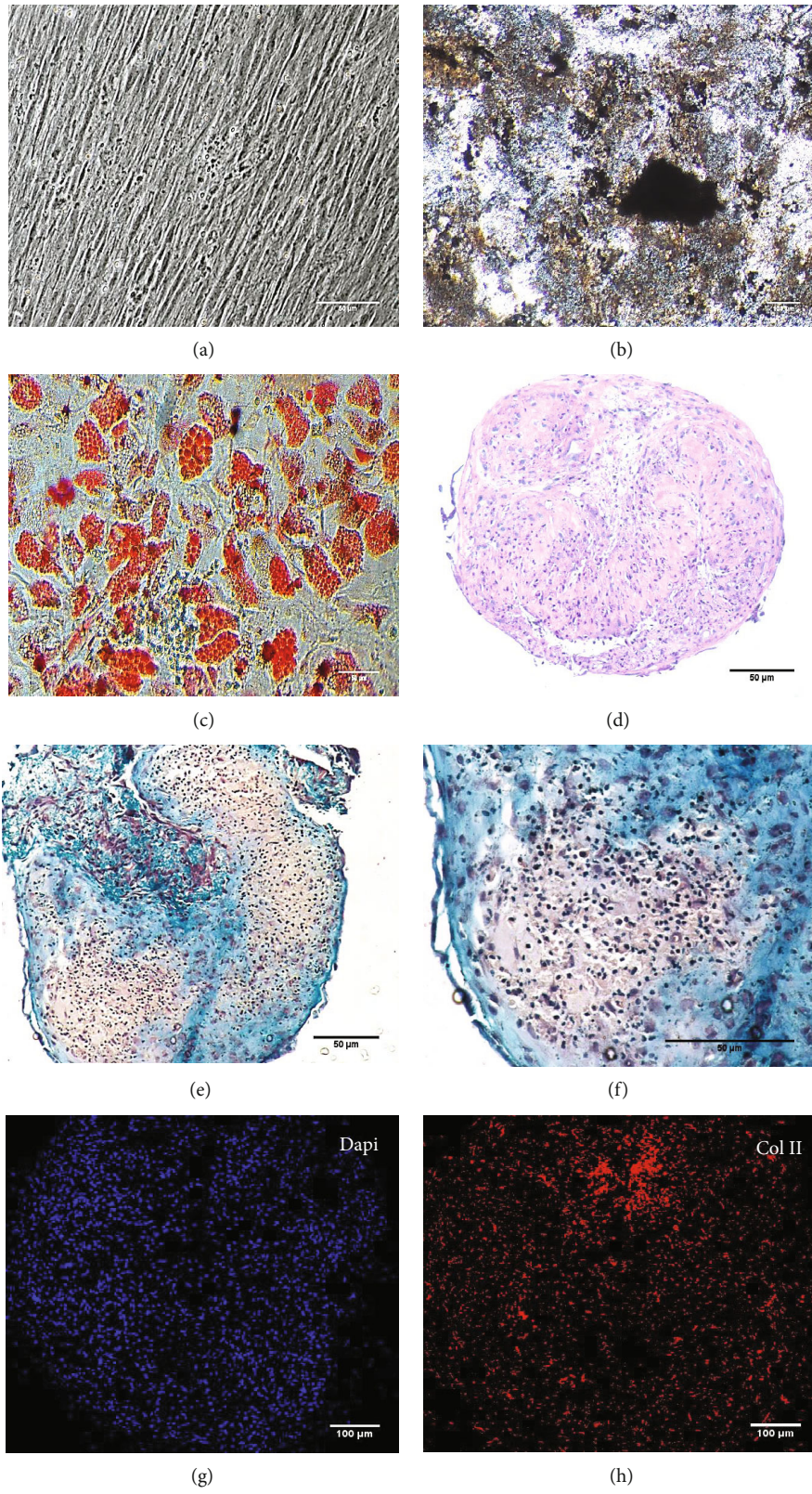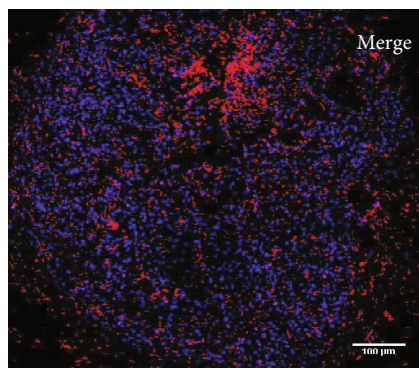(a)

(b)

(c)

(d)

(e)

(f)

(g)

(h)

Figure 3: Continued.

(i)

FIGURE 3: In vitro osteogenic, adipogenic, and chondrogenic potential of BMSC products. Representative images of (a) a noninduced BMSC layer, (b) mineralized nodules visualized by Von Kossa staining, and (c) intracellular lipid accumulation stained with Oil Red O. (d–i) Chondrogenic differentiation: (d) H&E staining, (e, f) Masson Trichrome staining, and (g-i) immunofluorescence staining of collagen II in representative BMSC micromass pellet cultures with differentiation towards the chondrogenic lineage. Cartilage matrix deposition (blue) in the extracellular matrix was assessed by Masson Trichrome staining and confirmed by immunofluorescence staining for collagen II. Representative images of $n = 10$ experiments. For the immunofluorescence analysis, $n = 3$.

3.8. Assessment of the In Vivo Bone-Forming Potential. To verify whether the BMSCs in the final cell products indeed retained the ability to differentiate and form bone in vivo, the cells were subcutaneously transplanted into immunodeficient mice. The histological examination of the implants revealed the formation of ossicles for nine out of 10 BMSC products (Table 6).

The bone matrix was deposited over the surfaces of the HA/TCP particles and resembled trabecular bone architecture (Figures 4(b), 4(d), and 4(f)). Osteocytes were embedded in the newly synthesized matrix (Figure 4(b), arrowheads), and the reconstituted marrow stroma was filled with hematopoietic cells (Figure 4(b), asterisk). The human origin of the cells inside the ossicles was corroborated through human lamin A/C and type I collagen detection within the woven bone (Figures 4(d) and 4(f) and Supplementary Figure 3). Micro-CT-based 3D reconstruction of the BMSC implants (Supplementary Figure 4) showed that the neoformed bone density ranged from 994 to 1946 HU (Hounsfield unit), which was in accordance with the reference density values described for human cancellous and cortical bone (Table 6).

3.9. Analysis of Cryopreservation Conditions. Finally, to evaluate the quality of the cryopreservation procedures, vials of five BMSC lots were thawed after four and 40 weeks of storage. Cell viability was similar at both time points and did not significantly differ from the percent viability at the time of cryopreservation (Table 7).

4. Discussion

Because of their osteogenic, immunomodulatory, and angiogenesis-promoting potential, BMSCs have been the focus of extensive research of their clinical application in orthopedics [59]. However, the translation to the bedside still faces important bottlenecks, one being the lack of regulatory and technical consensus determining the overall conditions that should be adopted for BMSC manufacturing and what

TABLE 6: Osteogenic potential of the lots of BMSCs produced.

	Tissues formed	Bone density (HU)*
BMSC 05	Bone/bone marrow	1572
BMSC 06	Bone	1233
BMSC 07	Bone/bone marrow	994
BMSC 08	Bone	1209
BMSC 09	Bone	1605
BMSC 10	Bone/bone marrow	1363
BMSC 11	Bone	1946
BMSC 12	Bone	1074
BMSC 13	Bone/bone marrow	1356
BMSC 14	Fibrous tissue	—

*Reference values: 700 HU (cancellous bone); 3000 HU (cortical bone).

assays should be performed in order to validate the cell potency [25, 26]. In this sense, centers in different countries have adopted its own procedures, resulting in the manufacturing of BMSC products with distinct gene expression signatures and functional potentials. In Brazil, the sanitary regulatory health agency (ANVISA) provided general regulatory rules for the establishment of facilities for cell manufacturing and/or processing for therapeutic purposes but left to the facilities the decision about what technical procedures should be adopted for primary tissue harvesting, processing, cell isolation, expansion, and characterization, according to the particularities of the cells to be manufactured. In this report, we described our procedures to generate functionally validated BMSC products that conform to both GMP standards and national regulatory policies.

In order to have a parameter for comparison, our protocols were based on the previous experience of the NIH BMSC bank [37]. But differently from their protocol, in which cells were expanded in three cycles (one in 2-layer and two in 10-layer cell factories), in our manufacturing process, cells were expanded in only two subsequent rounds in 2- and 10-layer
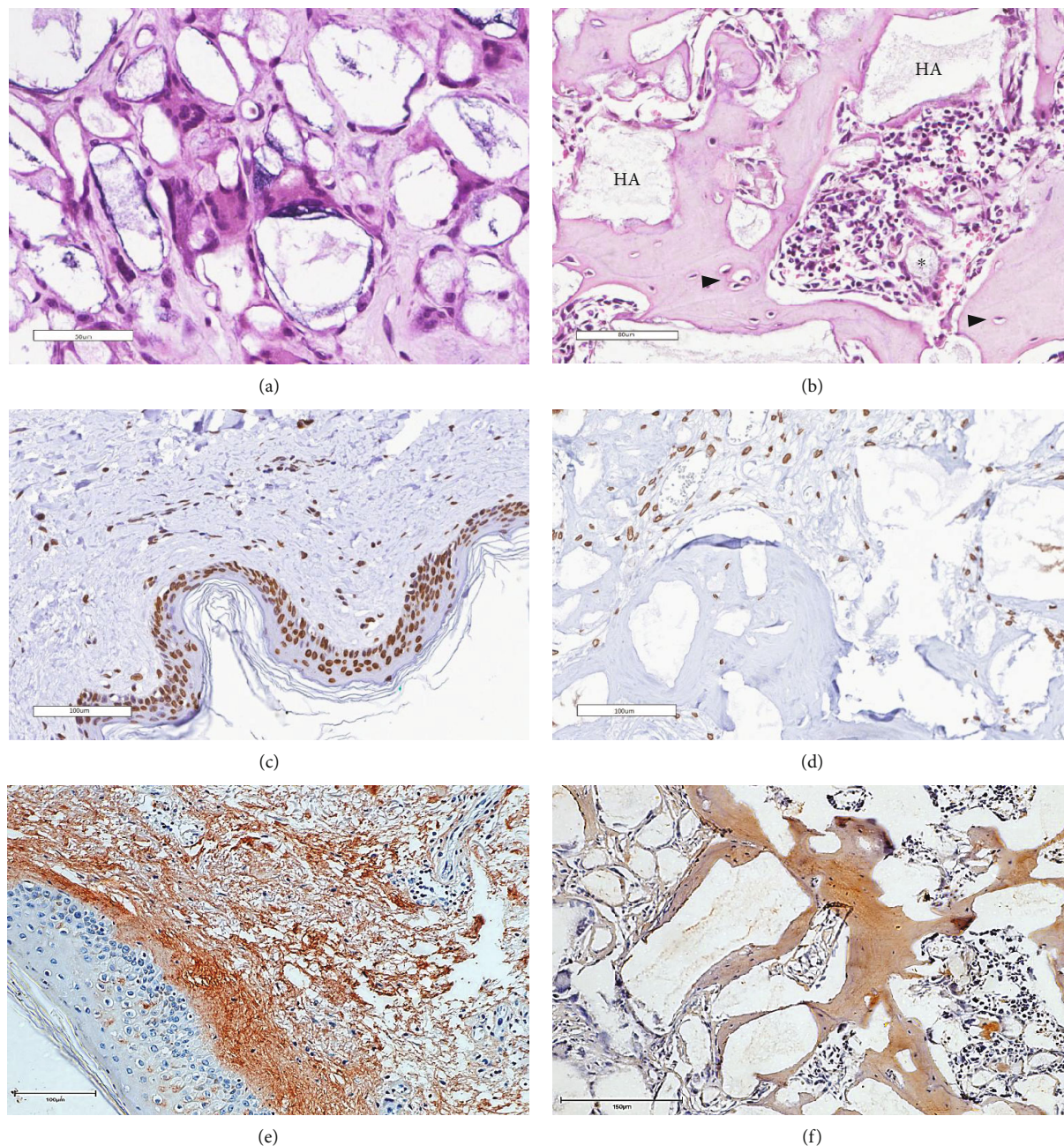
(a)

(b)

(c)

(d)

(e)

(f)

FIGURE 4: Osteogenic potential of BMSCs in vivo. In vivo transplantation assays were performed by combining BMSCs with HA/TCP followed by subcutaneous transplantation into immunocompromised mice. (a, b) H&E staining. (a) Negative control (HA/TCP transplantation without BMSC). (b) BMSCs formed ectopic ossicles that were sometimes populated by host hematopoietic marrow (asterisk). The arrowheads indicate osteocytes. HA = hydroxyapatite/tricalcium phosphate particles. (c–f) The human origin of the woven bone by immunohistochemical analysis. (c, e) Positive control of lamin A/C and collagen I stains, respectively, in human skin. (d, f) Expression of human lamin A/C and collagen I within the woven bone (for the immunohistochemistry analysis, $n = 3$).

cell factories, respectively. Another difference was the source of bone marrow. Instead of using bone marrow aspirates from volunteered donors, we used trabecular bone discards. The main reason for this choice was the fact that at this initial point our goal was simply to set and evaluate the procedures for BMSC manufacturing in our in-house facility. Because we are housed in an orthopedic hospital, bone discards from primary total hip arthroplasties (THA) are always available and can be obtained without subjecting donors to any additional

procedures. And from previous studies of our group using BMSCs isolated from THA as a model, the capacity of these cells to proliferate and differentiate in vitro and in vivo was already known [50], thus proving its usefulness to validate our procedures.

Indeed, the number of clonogenic cells in the bone marrow of the THA samples, as assessed by the CFE assay, was within the previously reported range of CFE measured in bone specimens from eight healthy adults [48] and was, on

TABLE 7: Viability evaluation of the cryopreserved lots of BMSCs.

	At the time of cryopreservation (%)	After 4 weeks of cryopreservation (%)	After 40 weeks of cryopreservation (%)
BMSC 07	100	78	85
BMSC 08	98.7	92	84
BMSC 09	85.6	93	95
BMSC 10	92	91	75
BMSC 11	89.5	88	78
Mean ± SD	**93.16 ± 6.11**	**88.4 ± 6.10**	**83.4 ± 7.70**

$P = 0.11$ (one-way ANOVA with Tukey's multiple comparisons test).

average, three times higher than the CFE of bone marrow aspirates reported in the NIH BMSC bank manuscript [37]. This was not surprising because marrow aspirates are usually more contaminated with peripheral blood, which dilutes the marrow, decreasing CFE counts. Also, BMSCs were successfully isolated from all 14 samples.

Although the time for population doubling progressively increased during expansion—which can be a reflex of the donors' age—the total average cell yield obtained using just one cell factory per cycle (our minimal infrastructure capacity) showed that a significant number of cells can be produced with our protocol, considering a lot unit of 100×10^6 BMSCs as proposed by the NIH facility [37]. Maintaining proliferation limited to 15–20 population doublings (including both the isolation and the two expansion cycles), cell output can be increased just by scaling up the number of T-75 flasks and cell factories accordingly to sample availability, the cell yield at each passage, and the maximum infrastructure capacity of the facility. Noteworthily, we did not use the whole amount of THA bone discards for cell isolation, as we did not aim to produce the highest number of cells as possible, but rather to determine the average yield of cells at each step.

Because ANVISA and international regulatory organizations, such as the US Food and Drug Administration (FDA), have recommended that reagents from animal sources should be avoided when manufacturing cells for human use because of the risk of zoonoses and xenogeneic immunological reactions, efforts have been made in the field to identify substitutes for fetal bovine serum, such as chemically defined media [60–63], human serum [64], and activated platelet lysates [65–68]. Although platelet lysates were shown to induce BMSC proliferation as efficiently as FBS [43, 66], strong evidence that these BMSC products have similar functional potency as FBS-expanded BMSCs has not been provided so far. Indeed, Ren and colleagues [65] showed that the substitution of FBS with platelet lysates during BMSC isolation and expansion resulted in BMSCs with different genes and microRNA expression profiles. While FBS-cultured BMSCs expressed genes involved in the MAPK, TGF-β, adhesion, and extracellular matrix pathways, BMSCs cultured with platelet lysates expressed genes related to metabolic, proliferation, cell cycle, and immune response pathways. Functional assays with either of these BMSC products were

not performed [65]. Therefore, in line with the standard protocol used by the NIH cell bank [37], we included FBS in the BMSC isolation and expansion media but added washing steps for the final cell products to reduce the animal protein content. The BMSC lots were shown to have animal protein concentrations below the threshold limit stipulated by the FDA, indicating that the cell products had no increased risks of infection that would hamper their use in patients.

Finally, because at present no known phenotypic or genetic characteristic allows the prospective determination of the differentiation ability of a given population of BMSCs once transplanted in vivo [69, 70] and in vitro assays are believed to have a high probability of being artifactual [49, 71–73], we established the in vivo differentiation assay as the critical test to ascertain BMSC potency. Although the in vivo assay takes months to complete and to obtain a result, it is long recognized by scientists of the field as the best available method to evaluate the intrinsic differentiation potential of a given cell population, as it allows the inherent expression of cell potency without any exogenous chemical inducer [21, 49, 58, 74, 75]. By using this functional quality control method, we showed that nine out of 10 of our BMSC products formed bone in vivo with the expected histology and matrix microarchitecture. Additionally, of the nine samples that formed bone, four developed a supportive hematopoietic stroma, which is an indicator of the presence of multipotential skeletal stem cells in a BMSC population [20, 49, 70, 76]. Therefore, we concluded that the protocol we established for large-scale BMSC manufacturing preserved the potential of cells to form bone in vivo, and we confirmed its suitability for the future generation of cells for bone repair strategies. This protocol can be equally used for BMSC isolation from any source sample. The only adaptation needed if the source sample is a bone marrow aspirate is the adjustment of the initial total nucleated cell seeding density for BMSC isolation, which needs to be higher because of the decreased CFE counts of the aspirates. For this adaptation, we refer the reader to the report of the NIH BMSC bank [37].

Although we have shown that BMSCs isolated from THA bone discards can form bone in vivo, which suggests that these samples could be useful for BMSC banking for allogeneic use, we emphasize that the choice for autologous or allogeneic cell applications, as well as the decision of the best bone marrow source material, needs to be carefully evaluated on a case by case basis. Because cell application itself was beyond our present objective, we did not conduct immunogenicity and/or HLA compatibility tests, but in any allogenic strategy scenario, these tests should be conducted, in addition to the tests presented herein.

5. Conclusion

Due to the implementation of regulatory rules for the establishment of facilities for cell manufacturing by the Brazilian sanitary agency, a significant step towards the clinical use of BMSCs in orthopedics was taken. However, definition of the procedures for the large-scale production of clinical-grade BMSCs with validated bone-forming potential in vivo is still needed. In this study, we described a protocol for the

generation of BMSC products with certified phenotype and capacity to form bone after in vivo transplantation, which will serve as the basis for in-house BMSC manufacturing for future clinical applications in our center.

Data Availability

All data used to support the findings of this study are included within the article and the supplementary information file.

Conflicts of Interest

The authors indicated no potential conflicts of interest.

Acknowledgments

Supplementary Materials

Supplementary Figure 1: immunophenotypic characterization of BMSC products. Figure a shows representative flow cytometry histograms used to obtain the percentage of cells expressing the surface marker in question. In b, it is shown the gating strategy for the simultaneous analysis of CD73, CD90, CD105, and CD146 surface markers. Supplementary Figure 2: quantifications of the mineralized nodules positive for Von Kossa stain, the number of vacuoles with intracellular lipid accumulation positive for Oil Red O, and cartilaginous matrix positive for Masson's Trichrome stain. Supplementary Figure 3: negative controls of the immunohistochemistry analysis showing no recognition of mouse collagen type I and lamin A/C by the primary antibodies designed to recognize the given human proteins. Supplementary Figure 4: reconstruction of bone implants by micro-CT. The images show the contrast generated in the micro-CT images in function of the density, the thickness, and the energy of the X-rays, which were used to discriminate the new bone and the HA/TCP scaffold. Supplementary Table 1: list of all reagents and materials used. (Supplementary Materials)

References

[1] A. S. Shekkeris, P. K. Jaiswal, and W. S. Khan, "Clinical applications of mesenchymal stem cells in the treatment of fracture non-union and bone defects," *Current Stem Cell Research & Therapy*, vol. 7, no. 2, pp. 127–133, 2012.

[2] S. Prat, S. Gallardo-Villares, M. Vives et al., "Clinical translation of a mesenchymal stromal cell-based therapy developed in a large animal model and two case studies of the treatment of atrophic pseudoarthrosis," *Journal of Tissue Engineering and Regenerative Medicine*, vol. 12, no. 1, pp. e532–e540, 2018.

[3] S. Giannotti, V. Bottai, M. Ghilardi et al., "Treatment of pseudoarthrosis of the upper limb using expanded mesenchymal stem cells: a pilot study," *European Review for Medical and Pharmacological Sciences*, vol. 17, no. 2, pp. 224–227, 2013.

[4] M. L. Ferreira, P. C. Silva, L. H. Alvarez Silva et al., "Heterologous mesenchymal stem cells successfully treat femoral pseudarthrosis in rats," *Journal of Translational Medicine*, vol. 10, no. 1, 2012.

[5] A. Lebouvier, A. Poignard, M. Cavet et al., "Development of a simple procedure for the treatment of femoral head osteonecrosis with intra-osseous injection of bone marrow mesenchymal stromal cells: study of their biodistribution in the early time points after injection," *Stem Cell Research & Therapy*, vol. 6, no. 1, 2015.

[6] G. Wang, Y. Li, T. Sun et al., "BMSC affinity peptide-functionalized β-tricalcium phosphate scaffolds promoting repair of osteonecrosis of the femoral head," *Journal of Orthopaedic Surgery and Research*, vol. 14, no. 1, 2019.

[7] I. H. Dilogo, A. F. Kamal, B. Gunawan, and R. V. Rawung, "Autologous mesenchymal stem cell (MSCs) transplantation for critical-sized bone defect following a wide excision of osteofibrous dysplasia," *International Journal of Surgery Case Reports*, vol. 17, pp. 106–111, 2015.

[8] N. Harada, Y. Watanabe, K. Sato et al., "Bone regeneration in a massive rat femur defect through endochondral ossification achieved with chondrogenically differentiated MSCs in a degradable scaffold," *Biomaterials*, vol. 35, no. 27, pp. 7800–7810, 2014.

[9] S. Agacayak, B. Gulsun, M. C. Ucan, E. Karaoz, and Y. Nergiz, "Effects of mesenchymal stem cells in critical size bone defect," *European Review for Medical and Pharmacological Sciences*, vol. 16, no. 5, pp. 679–686, 2012.

[10] M. Stiehler, F. P. Seib, J. Rauh et al., "Cancellous bone allograft seeded with human mesenchymal stromal cells: a potential good manufacturing practice-grade tool for the regeneration of bone defects," *Cytotherapy*, vol. 12, no. 5, pp. 658–668, 2010.

[11] P. Niemeyer, T. S. Schönberger, J. Hahn et al., "Xenogenic transplantation of human mesenchymal stem cells in a critical size defect of the sheep tibia for bone regeneration," *Tissue Engineering Part A*, vol. 16, no. 1, pp. 33–43, 2010.

[12] B. G. Kurkalli, O. Gurevitch, A. Sosnik, D. Cohn, and S. Slavin, "Repair of bone defect using bone marrow cells and demineralized bone matrix supplemented with polymeric materials," *Current Stem Cell Research & Therapy*, vol. 5, no. 1, pp. 49–56, 2010.

[13] A. Q. A. Teo, K. L. Wong, L. Shen et al., "Equivalent 10-year outcomes after implantation of autologous bone marrow-derived mesenchymal stem cells versus autologous chondrocyte implantation for chondral defects of the knee," *The American Journal of Sports Medicine*, vol. 47, no. 12, pp. 2881–2887, 2019.

[14] Y. Hashimoto, Y. Nishida, S. Takahashi et al., "Transplantation of autologous bone marrow-derived mesenchymal stem cells under arthroscopic surgery with microfracture versus microfracture alone for articular cartilage lesions in the knee: a multicenter prospective randomized control clinical trial," *Regenerative Therapy*, vol. 11, pp. 106–113, 2019.

[15] T. D. Bornes, A. B. Adesida, and N. M. Jomha, "Articular cartilage repair with Mesenchymal stem cells after Chondrogenic priming: a pilot study," *Tissue Engineering Part A*, vol. 24, no. 9-10, pp. 761–774, 2018.

[16] S. Yamasaki, Y. Hashimoto, J. Takigami et al., "Effect of the direct injection of bone marrow mesenchymal stem cells in hyaluronic acid and bone marrow stimulation to treat chondral defects in the canine model," *Regenerative Therapy*, vol. 2, pp. 42–48, 2015.

[17] S. Jia, T. Zhang, Z. Xiong, W. Pan, J. Liu, and W. Sun, "In vivo evaluation of a novel oriented scaffold-BMSC construct for

enhancing full-thickness articular cartilage repair in a rabbit model," *PLoS One*, vol. 10, no. 12, 2015.

[18] S. Yamasaki, H. Mera, M. Itokazu, Y. Hashimoto, and S. Wakitani, "Cartilage repair with autologous bone marrow mesenchymal stem cell transplantation: review of preclinical and clinical studies," *Cartilage*, vol. 5, no. 4, pp. 196–202, 2014.

[19] S. Wakitani, T. Okabe, S. Horibe et al., "Safety of autologous bone marrow-derived mesenchymal stem cell transplantation for cartilage repair in 41 patients with 45 joints followed for up to 11 years and 5 months," *Journal of Tissue Engineering and Regenerative Medicine*, vol. 5, no. 2, pp. 146–150, 2011.

[20] A. J. Friedenstein, R. K. Chailakhyan, N. V. Latsinik, A. F. Panasyuk, and I. V. Keiliss-Borok, "Stromal cells responsible for transferring the microenvironment of the hemopoietic tissues," *Transplantation*, vol. 17, no. 4, pp. 331–340, 1974.

[21] P. Bianco, M. Riminucci, S. Gronthos, and P. G. Robey, "Bone marrow stromal stem cells: nature, biology, and potential applications," *Stem Cells*, vol. 19, no. 3, pp. 180–192, 2001.

[22] P. Bianco, P. G. Robey, I. Saggio, and M. Riminucci, ""Mesenchymal" stem cells in human bone marrow (skeletal stem cells): a critical discussion of their nature, identity, and significance in incurable skeletal disease," *Human Gene Therapy*, vol. 21, no. 9, pp. 1057–1066, 2010.

[23] O. Ringdén, M. Uzunel, I. Rasmusson et al., "Mesenchymal stem cells for treatment of therapy-resistant graft-versus-host disease," *Transplantation*, vol. 81, no. 10, pp. 1390–1397, 2006.

[24] I. Muller, S. Kordowich, C. Holzwarth et al., "Application of multipotent mesenchymal stromal cells in pediatric patients following allogeneic stem cell transplantation," *Blood Cells, Molecules, and Diseases*, vol. 40, no. 1, pp. 25–32, 2008.

[25] M. Duijvestein, A. C. W. Vos, H. Roelofs et al., "Autologous bone marrow-derived mesenchymal stromal cell treatment for refractory luminal Crohn's disease: results of a phase I study," *Gut*, vol. 59, no. 12, pp. 1662–1669, 2010.

[26] N. Perico, F. Casiraghi, E. Gotti et al., "Mesenchymal stromal cells and kidney transplantation: pretransplant infusion protects from graft dysfunction while fostering immunoregulation," *Transplant International*, vol. 26, no. 9, pp. 867–878, 2013.

[27] A. Skrahin, R. K. Ahmed, G. Ferrara et al., "Autologous mesenchymal stromal cell infusion as adjunct treatment in patients with multidrug and extensively drug-resistant tuberculosis: an open-label phase 1 safety trial," *The Lancet Respiratory Medicine*, vol. 2, no. 2, pp. 108–122, 2014.

[28] B. A. Tompkins, D. L. DiFede, A. Khan et al., "Allogeneic mesenchymal stem cells ameliorate aging frailty: a phase II randomized, double-blind, placebo-controlled clinical trial," *The Journals of Gerontology: Series A*, vol. 72, no. 11, pp. 1513–1522, 2017.

[29] P. K. Gupta, A. Chullikana, R. Parakh et al., "A double blind randomized placebo controlled phase I/II study assessing the safety and efficacy of allogeneic bone marrow derived mesenchymal stem cell in critical limb ischemia," *Journal of Translational Medicine*, vol. 11, no. 1, 2013.

[30] S. K. Wang, L. A. Green, N. A. Drucker, R. L. Motaganahalli, A. Fajardo, and M. P. Murphy, "Rationale and design of the Clinical and Histologic Analysis of Mesenchymal Stromal Cells in AmPutations (CHAMP) trial investigating the therapeutic mechanism of mesenchymal stromal cells in the treatment of critical limb ischemia," *Journal of Vascular Surgery*, vol. 68, no. 1, pp. 176–181.e1, 2018.

[31] J. G. J. Wijnand, M. Teraa, H. Gremmels et al., "Rationale and design of the SAIL trial for intramuscular injection of allogeneic mesenchymal stromal cells in no-option critical limb ischemia," *Journal of Vascular Surgery*, vol. 67, no. 2, pp. 656–661, 2018.

[32] L. Deng, Q. Peng, H. Wang et al., "Intrathecal injection of allogenic bone marrow-derived mesenchymal stromal cells in treatment of patients with severe ischemic stroke: study protocol for a randomized controlled observer-blinded trial," *Translational Stroke Research*, vol. 10, no. 2, pp. 170–177, 2019.

[33] P. V. Giannoudis, T. A. Einhorn, and D. Marsh, "Fracture healing: the diamond concept," *Injury*, vol. 38, pp. S3–S6, 2007.

[34] Y. Watanabe, N. Harada, K. Sato, S. Abe, K. Yamanaka, and T. Matushita, "Stem cell therapy: is there a future for reconstruction of large bone defects?," *Injury*, vol. 47, pp. S47–S51, 2016.

[35] R. Shi, Y. Huang, C. Ma, C. Wu, and W. Tian, "Current advances for bone regeneration based on tissue engineering strategies," *Frontiers of Medicine*, vol. 13, no. 2, pp. 160–188, 2019.

[36] N. Fekete, M. T. Rojewski, D. Fürst et al., "GMP-compliant isolation and large-scale expansion of bone marrow-derived MSC," *PLoS One*, vol. 7, no. 8, 2012.

[37] M. Sabatino, J. Q. Ren, V. David-Ocampo et al., "The establishment of a bank of stored clinical bone marrow stromal cell products," *Journal of Translational Medicine*, vol. 10, no. 1, p. 23, 2012.

[38] B. Cunha, T. Aguiar, S. B. Carvalho et al., "Bioprocess integration for human mesenchymal stem cells: from up to downstream processing scale-up to cell proteome characterization," *Journal of Biotechnology*, vol. 248, pp. 87–98, 2017.

[39] P. Nold, C. Brendel, A. Neubauer, G. Bein, and H. Hackstein, "Good manufacturing practice-compliant animal-free expansion of human bone marrow derived mesenchymal stroma cells in a closed hollow-fiber-based bioreactor," *Biochemical and Biophysical Research Communications*, vol. 430, no. 1, pp. 325–330, 2013.

[40] M. T. Rojewski, N. Fekete, S. Baila et al., "GMP-compliant isolation and expansion of bone marrow-derived MSCs in the closed, automated device quantum cell expansion system," *Cell Transplantation*, vol. 22, no. 11, pp. 1981–2000, 2013.

[41] M. Codinach, M. Blanco, I. Ortega et al., "Design and validation of a consistent and reproducible manufacture process for the production of clinical-grade bone marrow-derived multipotent mesenchymal stromal cells," *Cytotherapy*, vol. 18, no. 9, pp. 1197–1208, 2016.

[42] C. Lechanteur, A. Briquet, O. Giet, O. Delloye, E. Baudoux, and Y. Beguin, "Clinical-scale expansion of mesenchymal stromal cells: a large banking experience," *Journal of Translational Medicine*, vol. 14, no. 1, 2016.

[43] V. Becherucci, L. Piccini, S. Casamassima et al., "Human platelet lysate in mesenchymal stromal cell expansion according to a GMP grade protocol: a cell factory experience," *Stem Cell Research & Therapy*, vol. 9, no. 1, 2018.

[44] A. L. Russell, R. C. Lefavor, and A. C. Zubair, "Characterization and cost–benefit analysis of automated bioreactor-expanded mesenchymal stem cells for clinical applications," *Transfusion*, vol. 58, no. 10, pp. 2374–2382, 2018.

[45] P. G. Robey, S. A. Kuznetsov, J. Ren, H. G. Klein, M. Sabatino, and D. F. Stroncek, "Generation of clinical grade human bone

marrow stromal cells for use in bone regeneration," *Bone*, vol. 70, pp. 87–92, 2015.

[46] Y. Zhou, T. L. Tsai, and W. J. Li, "Strategies to retain properties of bone marrow–derived mesenchymal stem cells *ex vivo*," *Annals of the New York Academy of Sciences*, vol. 1409, no. 1, pp. 3–17, 2017.

[47] J. Carmen, S. R. Burger, M. McCaman, and J. A. Rowley, "Developing assays to address identity, potency, purity and safety: cell characterization in cell therapy process development," *Regenerative Medicine*, vol. 7, no. 1, pp. 85–100, 2012.

[48] S. A. Kuznetsov, M. H. Mankani, P. Bianco, and P. G. Robey, "Enumeration of the colony-forming units-fibroblast from mouse and human bone marrow in normal and pathological conditions," *Stem Cell Research*, vol. 2, no. 1, pp. 83–94, 2009.

[49] P. G. Robey, S. A. Kuznetsov, M. Riminucci, and P. Bianco, "Bone marrow stromal cell assays: in vitro and in vivo," in *Skeletal Development and Repair*, M. Hilton, Ed., vol. 1130 of Methods in molecular biology, pp. 279–293, Humana Press, Totowa, NJ, USA, 2014.

[50] V. F. Vianna, D. C. Bonfim, A. S. Cavalcanti et al., "Late Adherent Human Bone Marrow Stromal Cells Form Bone and Restore the Hematopoietic Microenvironment *In Vivo*," *BioMed Research International*, vol. 2013, Article ID 790842, 11 pages, 2013.

[51] D. C. Bonfim, R. B. Dias, A. Fortuna-Costa et al., "PS1/ _γ_ -Secretase-Mediated Cadherin Cleavage Induces _β_ -Catenin Nuclear Translocation and Osteogenic Differentiation of Human Bone Marrow Stromal Cells," *Stem Cells International*, vol. 2016, Article ID 3865315, 14 pages, 2016.

[52] M. Jamal, S. L. Lewandowski, M. L. Lawton, G. T. J. Huang, and L. Ikonomou, "Derivation and characterization of putative craniofacial mesenchymal progenitor cells from human induced pluripotent stem cells," *Stem Cell Research*, vol. 33, pp. 100–109, 2018.

[53] L. A. Solchaga, K. J. Penick, and J. F. Welter, "Chondrogenic differentiation of bone marrow-derived mesenchymal stem cells: tips and tricks," *Methods in Molecular Biology*, vol. 698, pp. 253–278, 2011.

[54] D. Nasrabadi, S. Rezaeiani, M. B. Eslaminejad, and A. Shabani, "Improved protocol for chondrogenic differentiation of bone marrow derived mesenchymal stem cells -effect of PTHrP and FGF-2 on TGFβ1/BMP2-induced chondrocytes hypertrophy," *Stem Cell Reviews*, vol. 14, no. 5, pp. 755–766, 2018.

[55] F. C. Vallim, J. A. M. Guimarães, R. B. Dias et al., "Atrophic nonunion stromal cells form bone and recreate the bone marrow environment in vivo," *Orthopaedic Trauma International*, vol. 1, no. 3, 2018.

[56] P. Janicki, P. Kasten, K. Kleinschmidt, R. Luginbuehl, and W. Richter, "Chondrogenic pre-induction of human mesenchymal stem cells on β-TCP: enhanced bone quality by endochondral heterotopic bone formation," *Acta Biomaterialia*, vol. 6, no. 8, pp. 3292–3301, 2010.

[57] J. Brocher, P. Janicki, P. Voltz et al., "Inferior ectopic bone formation of mesenchymal stromal cells from adipose tissue compared to bone marrow: rescue by chondrogenic pre-induction," *Stem Cell Research*, vol. 11, no. 3, pp. 1393–1406, 2013.

[58] M. H. Mankani, S. A. Kuznetsov, G. W. Marshall, and P. G. Robey, "Creation of new bone by the percutaneous injection of human bone marrow stromal cell and HA/TCP suspensions," *Tissue Engineering Part A*, vol. 14, no. 12, pp. 1949–1958, 2008.

[59] R. M. Samsonraj, M. Raghunath, V. Nurcombe, J. H. Hui, A. J. van Wijnen, and S. M. Cool, "Concise review: multifaceted characterization of human mesenchymal stem cells for use in regenerative medicine," *Stem Cells Translational Medicine*, vol. 6, no. 12, pp. 2173–2185, 2017.

[60] L. G. Chase, U. Lakshmipathy, L. A. Solchaga, M. S. Rao, and M. C. Vemuri, "A novel serum-free medium for the expansion of human mesenchymal stem cells," *Stem Cell Research & Therapy*, vol. 1, no. 1, p. 8, 2010.

[61] L. Solmesky, S. Lefler, J. Jacob-Hirsch, S. Bulvik, G. Rechavi, and M. Weil, "Serum free cultured bone marrow mesenchymal stem cells as a platform to characterize the effects of specific molecules," *PLoS One*, vol. 5, no. 9, 2010.

[62] J. van der Valk, D. Brunner, K. De Smet et al., "Optimization of chemically defined cell culture media - Replacing fetal bovine serum in mammalian _in vitro_ methods," *Toxicology in Vitro*, vol. 24, no. 4, pp. 1053–1063, 2010.

[63] S. Mimura, N. Kimura, M. Hirata et al., "Growth factor-defined culture medium for human mesenchymal stem cells," *The International Journal of Developmental Biology*, vol. 55, no. 2, pp. 181–187, 2011.

[64] M. Cimino, R. M. Gonçalves, E. Bauman et al., "Optimization of the use of a pharmaceutical grade xeno-free medium for in vitro expansion of human mesenchymal stem/stromal cells," *Journal of Tissue Engineering and Regenerative Medicine*, vol. 12, no. 3, pp. e1785–e1795, 2018.

[65] J. Ren, D. Ward, S. Chen et al., "Comparison of human bone marrow stromal cells cultured in human platelet growth factors and fetal bovine serum," *Journal of Translational Medicine*, vol. 16, no. 1, 2018.

[66] G. Astori, E. Amati, F. Bambi et al., "Platelet lysate as a substitute for animal serum for the ex-vivo expansion of mesenchymal stem/stromal cells: present and future," *Stem Cell Research & Therapy*, vol. 7, no. 1, 2016.

[67] M. T. Rojewski, R. Lotfi, C. Gjerde et al., "Translation of a standardized manufacturing protocol for mesenchymal stromal cells: a systematic comparison of validation and manufacturing data," *Cytotherapy*, vol. 21, no. 4, pp. 468–482, 2019.

[68] K. Bieback, "Platelet lysate as replacement for fetal bovine serum in mesenchymal stromal cell cultures," *Transfusion Medicine and Hemotherapy*, vol. 40, no. 5, pp. 326–335, 2013.

[69] B. J. Sworder, S. Yoshizawa, P. J. Mishra et al., "Molecular profile of clonal strains of human skeletal stem/progenitor cells with different potencies," *Stem Cell Research*, vol. 14, no. 3, pp. 297–306, 2015.

[70] P. Bianco and P. G. Robey, "Skeletal stem cells," *Development*, vol. 142, no. 6, pp. 1023–1027, 2015.

[71] P. G. Robey, ""Mesenchymal stem cells": fact or fiction, and implications in their therapeutic use," *F1000Research*, vol. 6, 2017.

[72] D. D. Diascro Jr., R. L. Vogel, T. E. Johnson et al., "High Fatty Acid Content in Rabbit Serum Is Responsible for the Differentiation of Osteoblasts Into Adipocyte-like Cells," *Journal of Bone and Mineral research*, vol. 13, no. 1, pp. 96–106, 1998.

[73] L. F. Bonewald, S. E. Harris, J. Rosser et al., "von Kossa staining alone is not sufficient to confirm that mineralization *in vitro* represents bone formation," *Calcified tissue international*, vol. 72, no. 5, pp. 537–547, 2003.

[74] S. A. Kuznetsov, P. H. Krebsbach, K. Satomura et al., "Single-colony derived strains of human marrow stromal fibroblasts

form bone after transplantation in vivo," *Journal of Bone and Mineral Research*, vol. 12, no. 9, pp. 1335–1347, 1997.

[75] P. H. Krebsbach, S. A. Kuznetsov, P. Bianco, and P. G. Robey, "Bone marrow stromal cells: characterization and clinical application," *Critical Reviews in Oral Biology and Medicine*, vol. 10, no. 2, pp. 165–181, 1999.

[76] B. Sacchetti, A. Funari, S. Michienzi et al., "Self-renewing osteoprogenitors in bone marrow sinusoids can organize a hematopoietic microenvironment," *Cell*, vol. 131, no. 2, pp. 324–336, 2007.

Research Article

Achilles Tendon Repair by Decellularized and Engineered Xenografts in a Rabbit Model

Marta Bottagisio,[1] **Daniele D'Arrigo,**[2] **Giuseppe Talò,**[2] **Matilde Bongio,**[2] **Marco Ferroni,**[3] **Federica Boschetti,**[3] **Matteo Moretti** (ID)**,**[2,4,5] **and Arianna B. Lovati** (ID)[2]

[1]*Laboratory of Clinical Chemistry and Microbiology, IRCCS Istituto Ortopedico Galeazzi, Milan 20161, Italy*
[2]*Cell and Tissue Engineering Laboratory, IRCCS Istituto Ortopedico Galeazzi, Milan 20161, Italy*
[3]*Department of Chemistry, Materials and Chemical Engineering Giulio Natta, Politecnico di Milano, Milan 20133, Italy*
[4]*Regenerative Medicine Technologies Lab, Ente Ospedaliero Cantonale, Lugano 6900, Switzerland*
[5]*Cardiocentro Ticino, Lugano 6900, Switzerland*

Correspondence should be addressed to Arianna B. Lovati; arianna.lovati@grupposandonato.it

Tendon tissue ruptures often require the replacement of damaged tissues. The use of auto- or allografts is notoriously limited due to the scarce supply and the high risks of immune adverse reactions. To overcome these limitations, tissue engineering (TE) has been considered a promising approach. Among several biomaterials, decellularized xenografts are available in large quantity and could represent a possible solution for tendon reconstruction. The present study is aimed at evaluating TE xenografts in Achilles tendon defects. Specifically, the ability to enhance the biomechanical functionality, while improving the graft interaction with the host, was tested. The combination of decellularized equine-derived tendon xenografts with or without the matrix repopulation with autologous bone marrow mesenchymal stem cells (BMSCs) under stretch-perfusion dynamic conditions might improve the side-to-side tendon reconstruction. Thirty-six New Zealand rabbits were used to create 2 cm long segmental defects of the Achilles tendon. Then, animals were implanted with autograft (AG) as the gold standard control, decellularized graft (DG), or in vitro tissue-engineered graft (TEG) and evaluated postoperatively at 12 weeks. After sacrifice, histological, immunohistochemical, biochemical, and biomechanical analyses were performed along with the matrix metalloproteinases. The results demonstrated the beneficial role of undifferentiated BMSCs loaded within decellularized xenografts undergoing a stretch-perfusion culture as an immunomodulatory weapon reducing the inflammatory process. Interestingly, AG and TEG groups exhibited similar results, behaved similarly, and showed a significant superior tissue healing compared to DG in terms of newly formed collagen fibres and biomechanical parameters. Whereas, DG demonstrated a massive inflammatory and giant cell response associated with graft destruction and necrosis, absence of type I and III collagen, and a higher amount of proteoglycans and MMP-2, thus unfavourably affecting the biomechanical response. In conclusion, this in vivo study suggests a potential use of the proposed tissue-engineered constructs for tendon reconstruction.

1. Introduction

The increasing number of traumatic events resulting in tendon loss and/or degenerative tendinopathy causing complicated ruptures often requires the replacement of the damaged tissue, especially in elderly patients and athletes. As a matter of fact, the tendon self-repairing ability is poor due to both the scarce presence and the metabolic activity of resident cells that cannot properly guide the healing process required to restore the native tissue function [1, 2]. The surgical procedures commonly performed to treat tendon ruptures with auto- or allografts might not guarantee the successful restoration of the tendon function and, besides that, relapses are frequent [3]. Furthermore, the use of either auto- or allografts is notoriously limited due to the scarce supply and the high risks connected to immune adverse

reactions or disease transmission following the tendon substitution, respectively. In this context, the reconstruction of the tissue with synthetic grafts has been extensively investigated [4], together with several tissue engineering strategies to enhance the regenerative potential of implanted grafts [5]. However, the use of synthetic biomaterials has been proposed with questionable results in terms of biocompatibility and biomechanical properties [6].

Undeniably, there is no better way to substitute a damaged tissue with a homologous healthy structure. Hence, the ideal graft for tendon substitution is a nonimmunogenic, easily available extracellular matrix (ECM) with mechanical properties resembling those of the native tissue offering a valid scaffold to host cell ingrowth [6]. In this regard, the decellularization of xenografts appeared to be a promising strategy for the treatment of tendon tears and ruptures. In particular, equine tendon biomechanical properties, large quantity supply, and less uncontrolled cross-species diseases compared to other animals (swine, bovine, etc.) offer several advantages over both human-derived and synthetic scaffolds [7]. Previous studies demonstrated that the decellularization of equine tendons appeared to be a promising strategy for the generation of an acellular matrix lacking in antigens by preserving matrix and offering cells a natural environment [7, 8]. However, an implanted decellularized matrix will take a long time to eventually be repopulated with host resident cells and to become a vital biological scaffold. Hence, a stem cell-based approach might be exploited to encourage the decellularized matrix colonization while guiding the tendon regeneration [9]. Several researches demonstrated the ability of both human and animal bone marrow-derived mesenchymal stem cells (BMSCs) to differentiate into tenocyte-like cells in response to chemical and physical stimuli in vitro as well as in vivo [10–12]. To support the cell alignment, differentiation, and ECM deposition within the acellular matrix, an oscillating stretch-perfusion bioreactor (OSPB) was recently designed and validated in vitro for the functionalization of cell-seeded decellularized equine tendons [13]. In this study, it has been described how the use of OSPB confers to undifferentiated cells the mechanical stimuli required to highly orient both seeded cells and the newly deposed collagen while preserving the biomechanical properties of the scaffolds, thus guaranteeing a high cell engraftment within the engineered constructs [13]. Despite the promising results obtained in vitro, the use of an animal model to test the feasibility of the proposed regenerative therapy for injured tendons is mandatory. In order to identify the most appropriate animal model to verify the proposed scientific hypothesis, a review of the literature evaluating animal models and treatments for the reconstruction of Achilles and flexor tendons has been recently carried out [14]. From this analysis, rabbit resulted the most frequently used animal species due to the intrinsic advantages, such as the easy handling and appropriate tendon size and biomechanical properties resembling those of human flexor tendons [14, 15]. Considering the excellent above-mentioned results obtained in vitro, the present study is aimed at testing novel biofabricated tendon xenografts in a rabbit model of the Achilles tendon full transection. Specifically, the ability to increase the biomechanical

functionality, while improving the tendon graft interaction with the host, will be tested and compared to standard autografts as the control. The combination of a complete decellularized equine xenograft together with autologous cell repopulation of the matrix under dynamic conditions might be a promising approach to repair tendon ruptures in clinics.

2. Materials and Methods

2.1. Ethics Statement. The whole study was approved by the Institutional Animal Care and Use Committees (IACUC) of the University of Modena and Reggio Emilia (Permit N. 915/2016-PR). The animals were housed in the Institute's Animal Care Facilities that meet international standards. The University of Modena and Reggio Emilia adheres to the principles set out in the following laws, regulations, and policies governing the care and use of laboratory animals: Italian Governing Law (D. legs 26/2014) and EU directives and guidelines (EEC Council Directive 2010/63/UE). The animals were regularly checked by a certified veterinarian responsible for health monitoring, animal welfare supervision, experimental protocols, and procedure revision. All surgeries were performed under general anaesthesia, and all efforts were made to minimize animal suffering.

2.2. Study Design. Thirty-six male New Zealand white rabbits (Oryctolagus cuniculus; body weight 3.68 ± 0.55 kg, 15 weeks old) were used in this study (Envigo RMS Srl, S. Pietro al Natisone, Udine, Italy). All animals were singly caged and maintained under controlled conditions: room temperature 20-22°C, 45% humidity, 15 air changes per hour, and a light/dark cycle of 12 h. Rabbits had free access to water and standard food pellets ab libitum (diet 2RB15, Mucedola s.r.l., Settimo Milanese, Italy). Animals were acclimatized for two weeks before surgery; thereafter, the subjects were randomly divided into three groups: (1) autograft ($n = 12$) (AG, reversed autograft), (2) decellularized graft ($n = 12$) (DG), and (3) in vitro tissue-engineered graft ($n = 12$) (TEG). Each animal underwent surgical treatment of one hind limb, and the contralateral limb served as the native tendon (NT).

2.3. Anaesthesia and Postoperative Treatments. All the procedures on rabbits were performed under general anaesthesia. Rabbits were anaesthetized with an intramuscular cocktail of ketamine hydrochloride (30 mg/kg; Imalgene 1000, Merial, Milan, Italy) and xylazine (4 mg/kg; Sedaxylan 2%, Dechra Veterinary Products Srl, Barcelona, Spain) and maintained with isoflurane (1-3%; Isoflurane Vet, Merial, Milan, Italy) in oxygen by a face mask. The marginal ear vein was catheterized, and animals were hydrated with sterile solution. In the postoperative pain control, hydrochloride buprenorphine (0.03 mg/kg; Buprenodale, Dechra Srl, Turin, Italy) was intravenously injected. Other postoperative treatments included subcutaneous administrations of flunixin meglumine (1 mg/kg; Finadyne, MSD Animal Health Srl, Segrate, Italy) and parenteral administrations of marbofloxacin (2 mg/kg, Marbocyl, Vetoquinol Italia Srl, Bertinoro, Italy) for 5 days. After 12 weeks of follow-up, animals were anesthetized as aforementioned, then euthanized with an

overdose of pentobarbital-sodium (90 mg/kg, Pentothal Sodium, Intervet Productions Srl, Aprilia, Italy) in order to proceed with the ex vivo analyses.

2.4. Bone Marrow Harvest and rbBMSC Culture.

Rabbits included in the TEG group underwent a bone marrow harvest to retrieve autologous rbBMSCs. Briefly, under general anaesthesia, animals were placed in ventral recumbency with the hind limbs flexed underneath. The dorsal area was shaved and disinfected for the procedure. The iliac crest was identified, a small skin incision was performed, and a bone marrow aspiration needle (Jamshidi biopsy needle 7 cm; 18 G; Byopsibell, Modena, Italy) was introduced through the marrow cavity by clockwise and counterclockwise rotations. Then, the needle stylus was removed and a 10 ml syringe containing 5000 UI/ml sodium heparin (Pharepa, PharmaTex Italia, Milan, Italy) was connected to the luer-lock. After the heparin injection, about 5 ml of bone marrow was immediately aspirated and mixed gently, the syringe was capped, and the samples were stored at 4°C to be processed within few hours.

The skin incision was closed with monofilament nylon sutures (Monosof 3-0, Medtronic, Milan, Italy) and rabbits were recovered from anaesthesia. Following, rbBMSCs were isolated by centrifuging the bone marrow samples at 400 xg for 5 min, removing the supernatant, collecting the buffy layer of mononuclear cells, and washing twice in phosphate-buffered saline (PBS, Gibco). Subsequently, the obtained pellet was suspended in a complete medium (CM) composed of a high glucose Dulbecco's modified Eagle's medium containing 4.5 g/l glucose (DMEM-HG) (Gibco), 10% foetal bovine serum (FBS, HyClone), 100 U/ml penicillin-streptomycin, 2 mM L-glutamine, 1% sodium pyruvate, 1% HEPES (all from Gibco), and 10 ng/ml of basic fibroblast growth factor (bFGF, Invitrogen, Milan, Italy) and plated in cell culture flasks. Rabbit BMSCs were selected by plastic adherence [16] and further expanded by seeding cells at a density of 6000 cells/cm^2 at 37°C, 5% CO_2) in CM. Fresh medium was changed twice a week, and cells were subcultured after reaching 90% of confluence after about 12 days, as described elsewhere [12]. Second-passage cells were frozen until use.

2.5. Cell Reseeding of Decellularized Xenografts and Dynamic Culture in a Bioreactor.

Xenografts obtained by the decellularization of equine superficial digital flexor tendons were measured for the DNA content (17.95 ng/mg ± 7.87 SD dry weight) to assess the efficiency of cell removal, and then, they were terminally sterilized as widely described in our previous studies [8, 17]. Autologous rbBMSCs were thawed at the second passage, expanded, and seeded onto and into the decellularized xenografts at the third passage. The decellularized xenografts were sized at 0.5 cm width × 4 cm length × 0.3 cm thickness, and their surfaces seeded with 50,000 cells/cm^2 resuspended in 30 μl of CM and incubated for 2 h to allow the cell attachment. Moreover, twelve injections of 20,000 rbBMSCs/20 μl were performed perpendicular to the decellularized matrix fibres throughout their length. Afterwards, the CM was added to completely cover the constructs, and rbBMSCs were cultured on the surface of decellularized xenografts in static conditions for 72 h. Then, the cell-seeded decellularized xenografts were mounted in the culture chamber of a custom-made bioreactor and dynamically cultured for 7 days based on our previous study [13]. Finally, the tissue-engineered xenografts were implanted as tendon substitutes, after verifying the viability of reseeded cells through the Live&Dead assay (data not shown).

2.6. Surgical Procedure to Implant Tendon Grafts.

Under general anaesthesia and in ventral recumbency, one hind limb of each subject was shaved and disinfected as standard. The Achilles tendon complex was exposed by a midline skin, subcutis, and the fascia incision at 0.5 cm distal to the gastrocnemius muscle and 0.5 cm above the calcaneus (Figure 1(a)). A 2 cm long segmental resection was created in the midsubstance of the Achilles tendon, including the medial and lateral gastrocnemius. The segmental resected tendons were used as reversed autografts in the AG group. Then, immediately after tenotomy, and according to the experimental group, the tendon defect was bridged end-to-end with AG (Figure 1(b)), DG, or TEG constructs—shaped to fit in the defects—with a 4-0 absorbable material (Polysorb, Medtronic) using the modified Kessler technique that connected the stumps of the native tendon and the specific implanted graft (Figure 1(c)). The edges of the tendon were also sutured by running epitendinous stitches with the same suture material, based on the technique described elsewhere [18, 19]. The plantaris tendon, also known as flexor digitorum superficialis (FD), was left intact as an internal splint. The paratenon was closed with a 5-0 absorbable material (Polysorb, Medtronic) (Figure 1(d)), and the skin sutured as standard with a nonabsorbable suture (Monosof 3-0, Medtronic, Milan, Italy). After suturing the paratenon, the TEG group also received a local injection of autologous rbBMSCs (1×10^6 cells/kg b.w.) with the purpose to ameliorate the tissue healing and to modulate the host response to the xenograft after implantation (Figure 1(e)). After surgery, an antimicrobial ointment (Hyalosilver, Fidia Pharmaceutics, Abano Terme (PD), Italy) was sprayed on the wound and the treated leg was wrapped up with a soft padded bandage before putting in a plaster cast (X-Lite, A3-MED, Zola Predosa, Italy). The cast extending up to the ankle joint was applied for 10 days at 150° flexion to prevent overloading (Figure 1(f)) [20]. Animals were free to move within the cage without restrictions. After 10 days, the plaster cast was removed, and under general anaesthesia, high frequency ultrasounds were performed in longitudinal planes with a linear probe of 18 MHz (MyLab™One, Esaote S.p.A., Genoa, Italy) to monitor the status of the tendon replacement in all animals. The contralateral healthy tendon was evaluated as controls (NT). In particular, the attachments of the grafts to the proximal and distal ends of the tendon were assessed. Then, a soft cast (Vetrap, 3M, Pioltello, Italy) was worn for 2 weeks and then definitively removed. After 12 weeks, animals were sacrificed and tendon specimens were harvested from the calcaneus to the muscle aponeurosis junction. In particular, for each experimental group, six explants were processed for histological
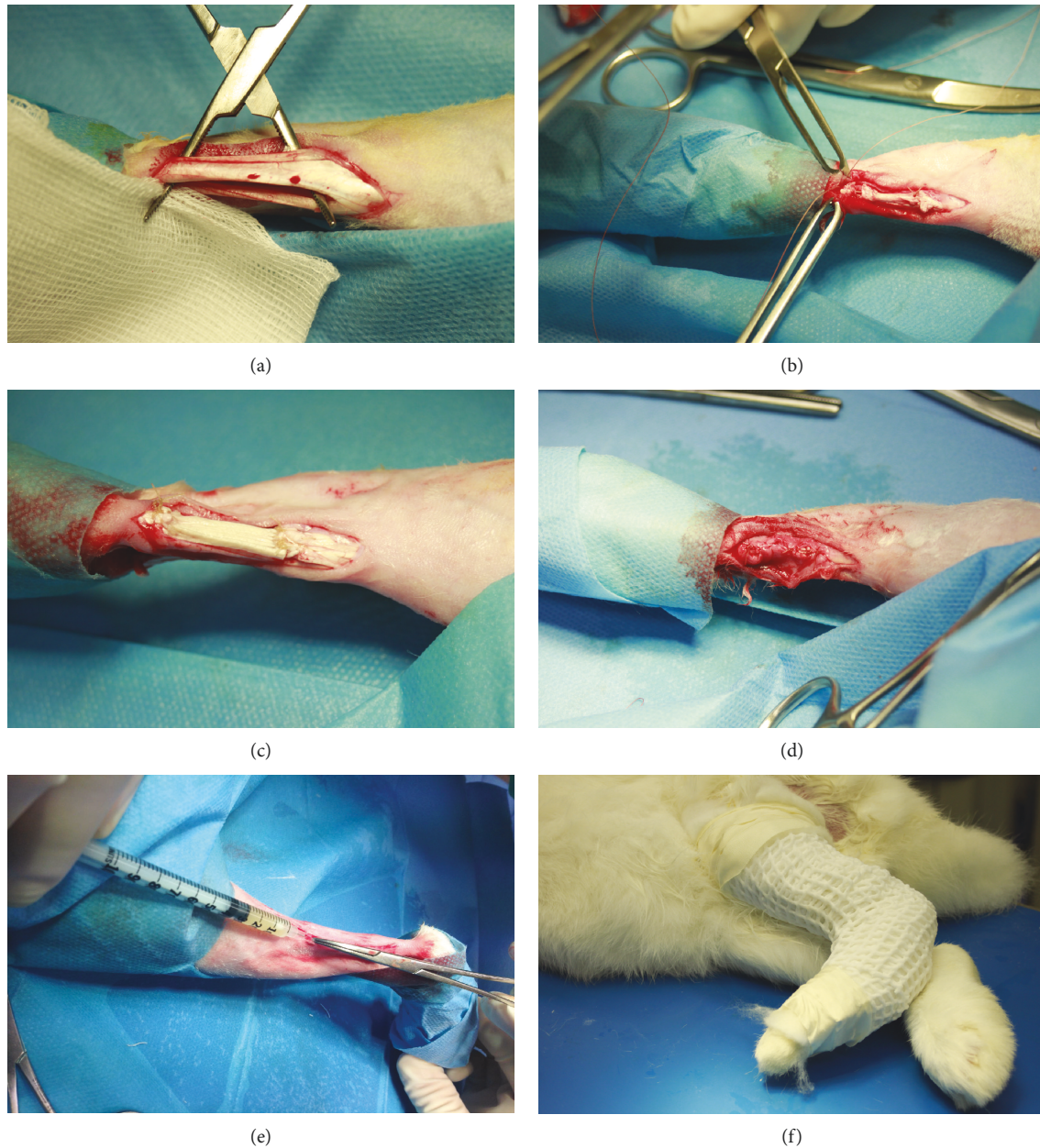
(a)

(b)

(c)

(d)

(e)

(f)

FIGURE 1: Surgical approach. (a) Achilles tendon complex exposure (NT). (b) Tenotomy bridged with an autograft (AG). (c) Implantation of the decellularized graft (DG). (d) A representative picture of the tendon sheath closure. (e) Injection of autologous rbBMSCs within the tissue-engineered graft (TEG). (f) Application of the plaster cast at 150° flexion.

analyses (except for the AG group $n = 5$) and six explants were dry-stored at -80°C for both biochemical and biomechanical tests.

2.7. Biochemical Analysis for Glycosaminoglycan Quantification. Small segments of tendon explants were weighted, minced, and digested in 2 mg/ml proteinase K (pH 7.6) (Sigma-Aldrich, Milan, Italy) at 56°C for 16 h under agitation. Digested samples were centrifuged at 10000 xg for 10 min at RT, and the supernatant was collected for analyses. The quantification of glycosaminoglycans (sGAG) was performed using the 1,9-dimethylmethylene blue (DMMB) dye-binding assay (Sigma-Aldrich, Milan, Italy). Briefly, samples were

incubated in 40 mM glycin/NaCl (pH 3.0) with 16 mg/ml DMMB at RT. The sGAG concentration was determined by reading the absorbance at 500 nm (Perkin Elmer Victor X3 microplate reader) and comparing the results to a standard curve of chondroitin sulphate (Blyscan, Biocolor, Magenta, Italy). Data from the sGAG content analysis were normalized on the sample dry weights.

2.8. Histological Analysis. Being explanted tendons very long, before fixation and inclusion, each sample was divided for the entire width at its middle thirds into a proximal and a distal portion, representing the areas of transition between the native tendons and the grafts. Then, the specimens were fixed

in 10% neutral buffered formalin for 24 h and dehydrated in alcohol scale before embedding in paraffin and cutting into 4 μm longitudinal sections. The slides were stained with Alcian Blue (AB). Photomicrographs of the tissue were captured through an Olympus IX71 light microscope and an Olympus XC10 camera (Japan). Three independent, blinded examiners assessed the tendon histopathology according to a modified semiquantitative grading score, as proposed by others [20, 21]. In particular, the following parameters were evaluated: organization of the extracellular matrix (0-2), cellularity (0-2), cell alignment (0-2) and distribution (0-1), the morphology of the cell nuclei (0-2), organization of repair tissue of the tendon callus (0-2), transition from defect to normal tissue (0-2), vascularization (0-1), degenerative changes (0-3), inflammation (score 0-1), and proteoglycan content (0-1). The maximum score (19) represented the best outcome in terms of tendon tissue integrity, and the minimum value (0) represented the worst condition.

2.9. Immunohistochemistry for Type I and III Collagen Detection.
To evaluate the distribution of type I and III collagen, immunohistochemistry was performed on deparaffinised sections. The sections were incubated with monoclonal primary antibodies for anticollagen type I (1 : 200 dilution) and type III (1 : 2000 dilution) (Sigma-Aldrich Corporation, Saint Louis, MO) for 1 h at RT. Then, sections were exposed to a biotinylated anti-mouse secondary antibody (1 : 200 dilution; Vinci Biochem, Vinci, Florence, Italy) for 30 minutes. The signal was detected by means of the streptavidin-biotin method coupled with the 3′-Diaminobenzidine (DAB) chromogen system (Vinci Biochem). Sections were counterstained with haematoxylin, microscopically analysed. Negative control was carried out by omitting the primary antibodies. Positive control staining was obtained from rabbit ear tissues.

2.10. Histomorphometric Analysis by Means of Stereological Method.
The presence of sulphate proteoglycans was assessed in AB-stained sections by means of histomorphometry. In particular, the histological quantification was performed using the ImageJ 1.45 software (open source: http://rsbweb.nih.gov/ij), as described elsewhere [22]. Specifically, the area occupied by proteoglycans within the region of interest (ROI) was analysed after removing both the white and the collagen matrix areas by means of a colour threshold. Data are reported as the percentage of the total ROI of the tissue.

2.11. Gelatin Zymography.
The proteolytic activity of matrix metalloproteinase 2 (MMP-2) and 9 (MMP-9) was evaluated through gelatine zymography. Proteins were extracted from tendon specimens as previously described [23, 24]. Briefly, 50 mg of tendon was minced and incubated with 500 ml of extraction buffer composed of 10 mM cacodylic acid (pH 5.0), 0.15 M NaCl, 1 μM ZnCl$_2$, 20 mM CaCl$_2$, 1.5 mM NaN$_3$, and 0.01% Triton X-100 (all from Sigma-Aldrich) at 4°C for 24 h. Then, the extraction buffer was collected and refreshed, and samples were treated for further 24 h. Before protein separation, the pH of the collected extraction buffer was raised to 7.5 by adding a 1 M solution of Tris (pH 8.0,

Sigma-Aldrich) and the extracted proteins were quantified using the Pierce™ BCA Protein Assay Kit (Thermo Fisher Scientific). After that, 0.12% gelatine precasted gels (Novex™, Life Technologies) were loaded with 20 μg of proteins and run at 125 V until the dye front ran off the gel. Gels were then removed from the cassettes and incubated first in renaturing buffer (Novex™, Life Technologies) for 30 min with gentle agitation and then similarly in developing buffer for 30 min. Subsequently, the developing buffer was decanted and refreshed, and gels were incubated overnight at 37°C for maximum sensitivity. Prior to staining, gels were rinsed three times with dH$_2$O to remove any remaining of sodium dodecyl sulphate (SDS) and immersed in Coomassie blue staining solution (SimplyBlue™ SafeStain, Life Technologies) for 15 min. Metalloproteinases activity was visualized as clear bands in the blue gel. Images of the gels were acquired by means of the ChemiDoc™ Imaging System (Bio-Rad), and band intensity was measured using ImageJ software (https://imagej.nih.gov/ij/). Data are reported as peak area values normalized on positive controls (FBS, HyClone).

2.12. Biomechanical Analysis.
At 12 weeks postsurgery, the specimens were harvested proximally from the muscle tendinous aponeurosis to distally to the calcaneus bone insertion and then stored at -80°C until processing. Biomechanical tests were performed at room temperature on the explants using an electromechanic testing machine (MTS Synergie, Eden Prairie, MN, USA), equipped with a load cell of 1 kN. Briefly, after thawing, to prevent the slippage of the samples, the calcaneal insertion and muscle-tendon transition were wrapped in sheets of sandpaper, glued with cyanoacrylate, and clamped between the grips. During the biomechanical test, the samples were continuously irrigated with PBS to prevent dehydration. Six preconditioning cycles till 10% of initial length were applied to every sample before the tests. Then, specimens were ultimately loaded to failure at a uniaxial tension at 1%/s strain rate following the protocols of our previous studies [8, 17]. The elastic modulus at high strains (EM, MPa), evaluated as the slope of the final linear portion of the stress-strain curve, and the failure stress (MPa) of the tendon hyperelastic response were derived from the failure tests. The dataset was analysed by normalizing the obtained results on the cross-sectional area of each specimen.

2.13. Statistical Analysis.
Statistical analyses were performed with GraphPad Prism 5 software (GraphPad Software Inc., La Jolla, USA). The Shapiro-Wilk test was used to assess the normal distribution of data.

Data obtained for normal distributed values were analysed with one-way analysis of variance (ANOVA) and coupled with Bonferroni's post hoc test; for nonparametric data, Kruskal-Wallis test coupled with Dunns' post hoc was performed. Values of $p < 0.05$ were considered statistically significant. Data are expressed as mean ± standard error (SE). For the in vivo study, the sample size was calculated by power analysis assuming the 80% power to detect differences in the presence or in the absence of transplanted xenograft integration within the native tissue, using a two-sided t-test with an α error = 0.05 (G*Power 3.1 software,

Düsseldorf, Germany). The interrater reliability of the examiners' scores for histopathological evaluations was calculated with intraclass correlation coefficient (ICC): ICC = 1, perfect reliability; ICC > 0.75, excellent reliability [25].

3. Results

3.1. Clinical Examination, Ultrasound Imaging, and Gross Appearance. Three weeks after surgery, one rabbit of the AG group was suppressed following a trauma occurred in the cage that compromised the animal mobility and determined the development of severe bedsores. Therefore, this subject was excluded from the study. None of the other animals included in any group died or had clinical evidence of local or systemic infection, such as local inflammation (hyperaemia or exudation), diarrhoea, and behavioural alterations.

All wounds healed well and completely 10 days after surgery. At that time, all animals were able to ambulate with a full range of motion after the cast removal.

At the ultrasound examination along the longitudinal plane (Figure 2), all treated groups showed an enhanced echogenicity in their midthird section. The DG group showed a greater hyperechogenicity compared to the AG and TEG. Moreover, in the DG group, the elongated, linear shape of the tendon was lost and a great presence of reactive tissue together with hypoechogenic granulation tissue was found in the transition zones. Again, in the DG group, the heterogeneity of greyscale ultrasound revealed the presence of swollen tissue within and around the implanted graft, as well as unordered fibre structure. Finally, the presence of adhesions between the implanted graft and the superficial plane of the skin was evident in the DG group. Despite both the detection of suture material and hypoechogenic areas next to the repair site were recognizable, the implanted zones were homogeneous in their slightly enhanced echogenicity in AG and TEG. More importantly, the ultrasound analysis identified an enlargement of the treated area in all groups that was more detectable in the TEG group compared to both the DG and the AG.

At 12 weeks postrepair, the treated tendons appeared longer compared to the NT on gross examination (data not shown). DG and TEG groups exhibited relatively enlargement in the middle third of the flexor tendon complex compared to both AG and NT. In particular, the measurement of the explanted specimens demonstrated greater enlargement of the TEG compared to both the DG and NT groups, as shown in Table 1, thus confirming data recorded by the ultrasonography.

3.2. Glycosaminoglycan Content. A greater amount of sulphated glycosaminoglycans was found in all the treated groups. In particular, the AG group had higher sGAG content compared to the NT and TEG groups for $p < 0.01$ and 0.05, respectively. No significant differences were found between DG or TEG and the NT (Figure 3).

3.3. Qualitative and Semiquantitative Histopathological Evaluations and Immunohistochemical Analysis. The qualitative histology and immunohistochemistry for type I and III collagen are depicted in Figure 4.

In all the samples of the NT group, parallel wavy bundles of dense type I collagen fibres and absence of type III collagen were detected. Uniaxial and homogenous distribution of elongated tenocytes was found as well as no abnormalities in terms of degenerative tissue, vascularization, or inflammatory reaction were present.

In the AG group, the recognizable transition zone presented a heterogeneous appearance of compact and mildly disorganized collagen fibres mainly consisting in type III collagen. The AB staining highlighted the presence of slightly enhanced proteoglycans and a moderate increase cell density, where rounded cells, irregularly arranged, were interposed between elongated cells. The neoangiogenesis was a little increased and associated with few lymphocytes along with the presence of a moderate formation of oedema.

In the DG group, the evident transition zone presented granulation tissue intermingled with proteoglycans and newly formed fibrocartilage tissue (Figure 4, small box). A huge amount of inflammatory cells was present (Figure 5); in particular, foreign body giant cells were detectable along with a significantly increased cell number, which showed a disorganized pattern. Areas of graft destruction were present with noticeable necrotic changes, correlating with the ultrasound examination. The entire tissue structure was lost and the matrix depicted a barely present type I collagen and a poor amount of type III collagen deposed in small areas within the inflammatory reaction (Figure 4). Moreover, an increased number of small and large capillaries was detected in this group (Figure 5).

In the TEG group, despite the presence of a mild proteoglycan deposition and some degenerative changes, such as fat infiltrating tissue and a hypervascularization, the transition zone presented a variation between crimped and disorganized collagen fibres. Some sparse inflammatory cells were present, thus potentially altering the deposition of type I collagen. However, type III collagen was identifiable as a response to resident cell deposition of newly formed matrix. Indeed, after 12 weeks of healing process (second proliferation stage), tendon fibroblasts from the epitenon and the synovial sheath and intrinsic tenocytes from the endotenon are recruited to the injury site to produce collagen type III and ECM components (e.g., proteoglycans) to create an initially unorganized ECM. Then, the production of collagen type III begins to be further replaced by stronger collagen type I over time.

The interrater reliability of the histological score performed by three blinded observers was excellent with an ICC 0.93 (95% CI "0.8865 to 0.9599"). Table 2 reported the mean values of each single parameter of the modified Stoll's score evaluated by the three blinded observers for the treated groups AG ($n = 5$), DG ($n = 6$), and TEG ($n = 6$).

The overall sum of the histopathological score showed a significant difference between DG and AG or TEG for $p < 0.05$ and $p < 0.01$, respectively. No differences were found between AG and TEG. As expected, all the treated groups had a score significantly different compared to the native tendon ($p < 0.001$) (Figure 6).
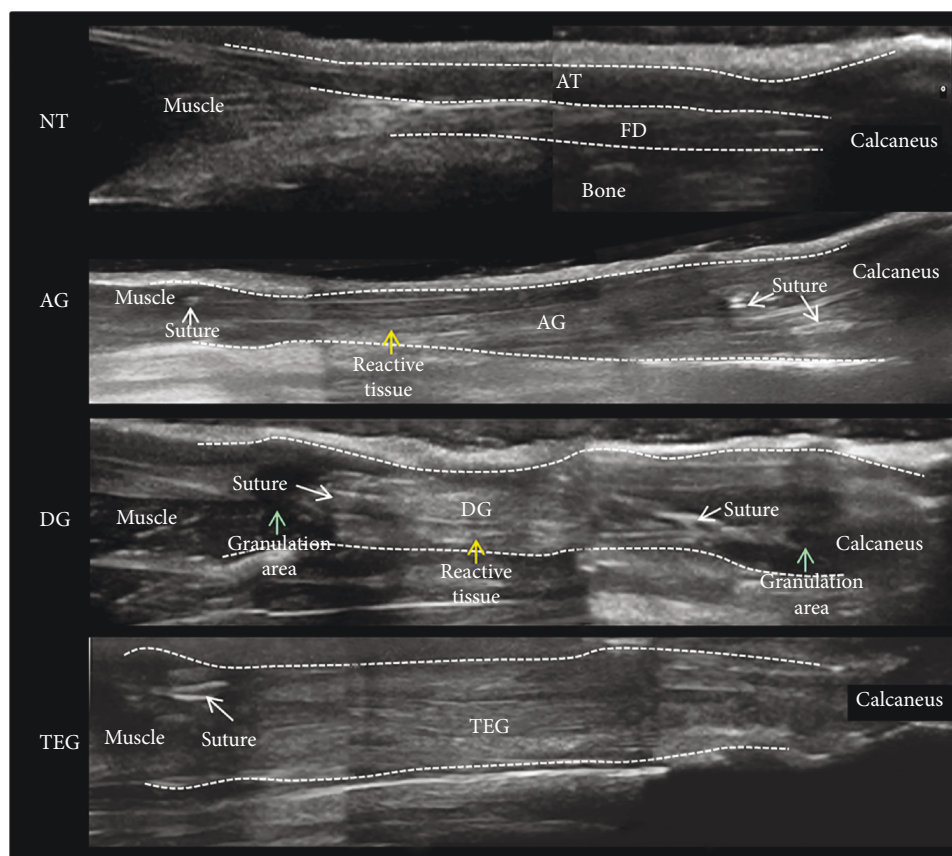
FIGURE 2: High-frequency ultrasound images of the longitudinal plane of rabbit Achilles tendon complex (AT) and flexor digitorum superficialis (FD) at proximal, mid-, and distal section of the native tendon (NT) and treated groups (AG, DG, and TEG).

TABLE 1: Measurements of width, thickness (mm), and cross-sectional area (mm^2) of the experimental groups. Data are reported as mean ± standard deviation (SD). A significant difference was found between TEG and DG or NT for width ($p < 0.05$), thickness ($p < 0.001$), and cross-sectional area ($p < 0.001$); a difference was also found between TEG and AG for thickness ([a]$p < 0.01$) and cross-sectional area ([b]$p < 0.05$).

	Width (mm)	Thickness (mm)	Cross-sectional area (mm^2)
NT	6.74 ± 0.9	5.15 ± 0.6	27.32 ± 5.4
AG	7.41 ± 1.0	5.71 ± 0.6[a]	33.56 ± 7.7[b]
DG	6.41 ± 0.5	4.81 ± 0.4	24.64 ± 7.7
TEG	8.05 ± 0.5*	7.14±0.4***	45.20±5.2***

3.4. Quantitative Assessment of Sulphate Proteoglycans.

The histomorphometric analysis of the proteoglycan content showed an increased amount in all the treated groups compared to the native tendons. Particularly, the presence of proteoglycans in the AG group was different from NT for $p < 0.05$, and both DG and TEG depicted a higher increase compared to NT ($p < 0.001$). More importantly, no significant differences were found for the proteoglycan content between AG and TEG, while a significant increase of these mucoproteins was present in the DG group compared to both AG and TEG ($p < 0.001$) (Figure 7).
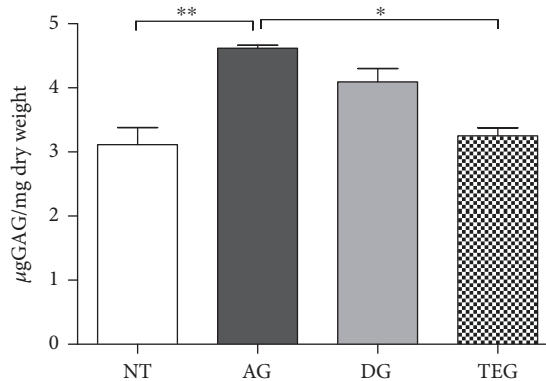

FIGURE 3: Glycosaminoglycan content of the experimental groups (μg GAGs/mg dry weight). Data are reported as mean ± SE. Nonparametric one-way ANOVA with Dunn's correction showed a significant difference between AG and TEG or NT $p < 0.05$ and $p < 0.01$, respectively. No differences were found between DG or TEG and NT.

3.5. Matrix Metalloproteinase Detection.

The zymography method allowed the identification of protease enzymes with gelatinolytic activity depicted in the bands reported in Figure 8. The 72 kD band represents the latent form of MMP-2 (Pro-MMP-2), while the migrating 62 kD band represents the activated form of the MMP-2 enzyme. There were
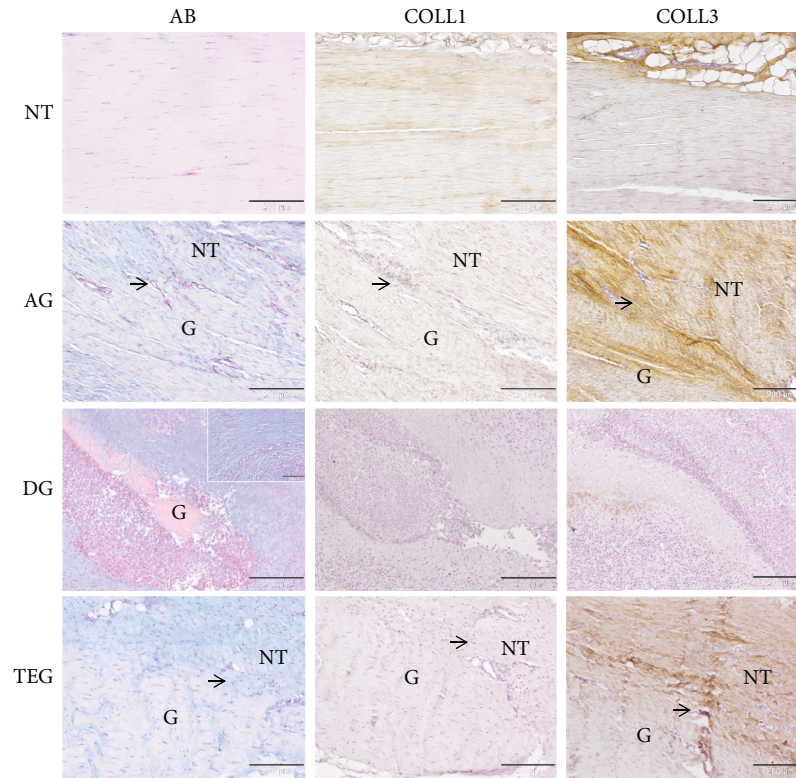
FIGURE 4: Representative histological and immunohistochemical microphotographs of the native tendon (NT) and treated groups (AG, DG, and TEG) at 12 weeks. The panel reports the Alcian Blue staining (AB) and immunohistochemistry for type I and III collagen (COLL1, COLL3). The black arrows show the transition zones between the native tendon (NT) and the grafts (G). In the DG group, the granulation tissue and inflammatory tissue impede the identification of the transition zone; G letter identifies a portion of the transplanted graft. Magnification 100x, scale bar 200 μm. Detailed box, magnification 200x, scale bar 100 μm.
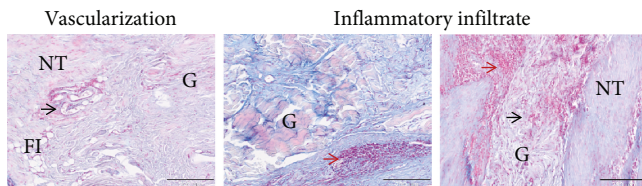

FIGURE 5: Representative histological panel of the increased vascularization and inflammatory infiltrated found in the DG group at 12 weeks. The panel reports the Alcian Blue staining (AB). The black arrows show the enlargement and increasing small and large capillary vessels in the transition zone and within the implanted graft (G). The red arrows show the huge inflammatory infiltration both near the vessels and in the transition zone between the native tissue (NT) and the graft (G). The fatty infiltrate (FI) is also detectable. Magnification 100x, scale bar 200 μm.

no significant changes in the intensity of Pro-MMP-2 bands among the treated tendons and between treated tendons and NT. Differently, the activated form of MMP-2 showed a significantly higher activity in DG and TEG compared to NT for $p < 0.01$ (a) and $p < 0.001$ (b). A significantly higher activity was also detected between DG and TEG compared to AG ($p < 0.05$). No results were obtained for MMP-9 due to the poor quality of barely visible bands in the gels.

3.6. *Biomechanical Testing.* The results of uniaxial tensile tests conducted till failure on NT and tendon substitutes (AG, DG, and TEG) are reported in Figure 9. Figure 9(a) shows the elastic modulus (EM) at high strains computed in the linear region of each stress-strain curve before the explant failure. The tendons treated with autologous grafts or DG and TEG showed no differences among groups, while a significant decrease of EM existed between the treated tendons and the NT group as expected. Although in the absence of significant differences, an improvement of EM was found in the TEG group compared to both AG and DG. The failure stress is shown in Figure 8(b). No differences were found between AG and NT, while DG and TEG showed a lower failure stress compared to NT for $p < 0.001$ and $p < 0.01$, respectively. Despite no differences were found between TEG and DG, the last one had a significant lower failure stress compared to AG ($p < 0.01$), while no differences were found between AG and TEG.

4. Discussion

Tendon ruptures and large defects are great burdens in clinics that always require challenging surgical and grafting procedures. Viable graft materials, as substitutes for tendon repair, have been explored in orthopaedics, and novel biological grafts have been proposed for clinical use. Among

TABLE 2: Mean values of each single parameter of the modified Stoll's score evaluated by the three blinded observers for the treated groups AG ($n = 5$), DG ($n = 6$), and TEG ($n = 6$). Statistical analysis by the Kruskal-Wallis test corrected with Dunn's post hoc: [*]$p < 0.05$ between DG and both other groups; [a]$p < 0.05$ between DG and AG; [b]$p < 0.05$ between DG and TEG.

(a)

	ECM organization (0-2)	Cellularity (0-2)	Cell alignment (0-2)	Cell distrib. (0-1)	Cell nuclei morphol. (0-2)	Proteoglycans (0-1)
AG	1.07	0.88	1.00[a]	0.58	0.77	0.25
DG	0.56[*]	0.32[*]	0.25[a]	0.14[*]	0.33	0.22[b]
TEG	1.06	0.86	0.72	0.56	0.89	0.50[b]

(b)

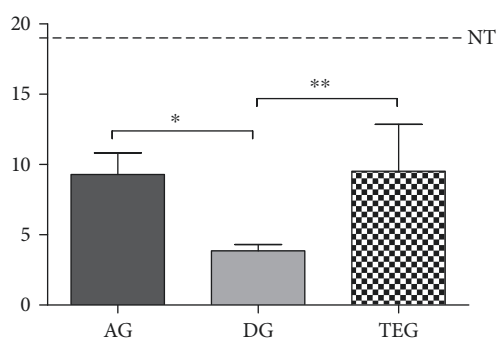|	Degenerative changes (0-3)	Vascularization (0-1)	Inflammation (0-1)	Org. tissue repair (0-2)	Transition zone (0-2)
AG	2.03	0.58	0.62	1.02	1.30
DG	1.10	0.06[*]	0.08[*]	0.46	0.33[*]
TEG	1.75	0.51	0.49	0.97	1.17

FIGURE 6: Histopathological score of the treated groups at 12 weeks. No differences were found between AG and TEG, while a significant increase was measured in AG and TEG compared to AG for $p < 0.05$ and $p < 0.01$, respectively.
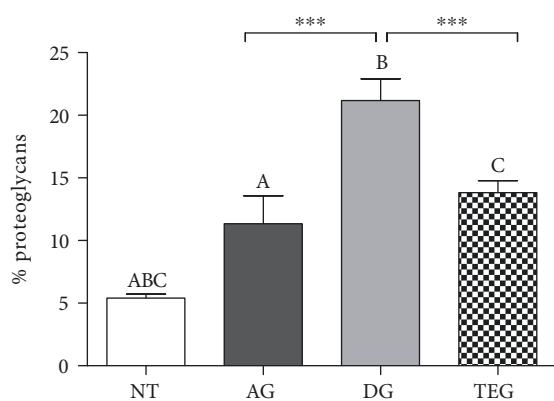

FIGURE 7: Histomorphometric analysis of proteoglycan content at 12 weeks. No differences were found between AG and TEG, while a significant increase was measured in DG compared to both AG and TEG for $p < 0.001$.
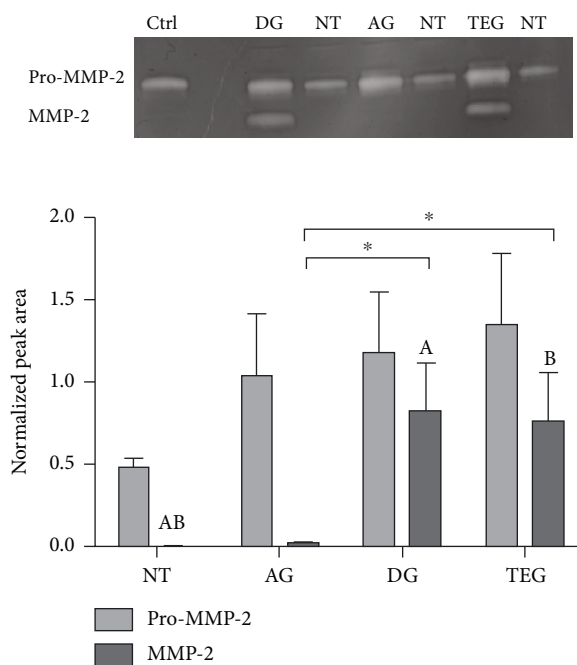

FIGURE 8: Expression and enzymatic activity of MMP-2. Bands at 72 and 62 kD represent the latent (Pro) and the active form of MMP-2, respectively. The values of the normalized peak areas on the reference control (Ctrl) are reported as the mean ± SEM ($n = 6$). There was no significant change in 72 kD bands among the treated tendons and between treated tendons and NT. In 62 kD bands, the activity was significantly higher in DG and TEG compared to NT for $p < 0.01$ (A) and $p < 0.001$ (B). A significantly higher activity was detected between DG and TEG compared to AG ($p < 0.05$).

biological scaffolds, the use of decellularized tendon-derived matrices represents a promising approach to treat tendon ruptures [7, 8]. In the present study, the efficacy for tendon regeneration of decellularized tendon xenografts enriched or not with autologous bone marrow mesenchymal stem cells
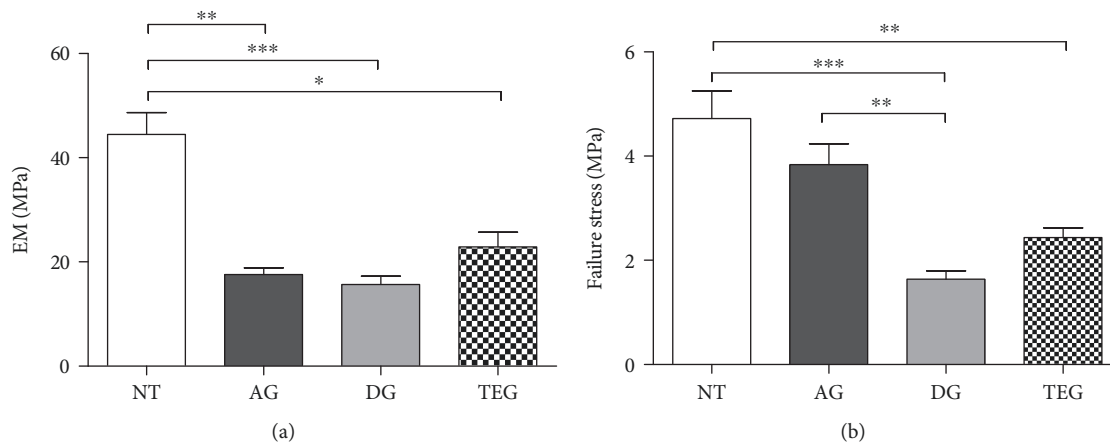
FIGURE 9: Biomechanical results on the explants at 12 weeks. (a) Elastic modulus of treated samples is significantly lower in NT compared to AG ($p < 0.01$), DG ($p < 0.001$), and TEG ($p < 0.05$); no differences exist between treated tendons. (b) Failure stress is lower between NT and DG or TEG for $p < 0.001$ and $p < 0.01$, respectively; no differences exist between NT and AG; DG has also a lower failure stress compared to AG ($p < 0.01$).

via a dynamic culture in bioreactor has been assessed in a rabbit model of full tendon transection and compared to autograft as the gold standard. The rabbit has been chosen as the model of Achilles tendon transection because of its widespread use for tendon engineering purposes due to the appropriate tendon size that allows intravital evaluations (e.g., ultrasounds), the presence of an intrasynovial component and biomechanics similar to flexor tendons of the human hand [8, 20, 26]. The high clinical translatability of this model permitted the evaluation of a regenerative strategy involving the use of decellularized xenografts. Indeed, the ultimate goal was to generate a scaffold free of donor cellular components, while maintaining its biocompatibility. In this context, a cell-based approach for the development of biological vital scaffolds has been extensively demonstrated as an effective strategy [27]. The use of autologous BMSCs was considered because of the well-known capability of these undifferentiated cells in proliferating and differentiating towards tendon-like cells [28], especially when cultured under dynamic stretch and perfusion conditions within the tendon matrix [13]. Indeed, our group has previously demonstrated that the dynamic culture of undifferentiated rbBMSCs injected within the decellularized tendon graft produced a mature and aligned collagen matrix in vitro [13]. This evidence was also supported by others who used different scaffold materials [29–31]. More importantly, the regenerative and immunomodulatory potential of BMSCs has been widely reported in the literature, as well as the capability of BMSCs to secrete growth factors and cytokines for the activation of tissue-resident cells, stimulation of neoangiogenesis, and inhibition of inflammation [32]. Based on these premises, the employed animal model was fundamental to examine the effects on both the integration within the native tissue and the host response of decellularized tendon xenografts enriched with autologous BMSCs specifically cultured in a customized bioreactor. The obtained results demonstrated the beneficial role of undifferentiated BMSCs when loaded within the decellularized xenografts undergoing a

stretch-perfusion culture as an immunomodulatory weapon, reducing the inflammatory process commonly associated with nonself, biological implants. An essential role in the evaluation of the host response following the xenograft implantation is played by histological analysis, which permits to investigate not only the morphological changes of the tissue structure but also the inflammatory status and the healing process determined by the treatment. Regarding the recovery and regeneration processes, the modified Stoll's score was able to picture a good assessment of the healing status of implanted grafts 12 weeks after surgery. No significant differences were found between AG and TEG groups that showed a clearly superior tissue healing compared to the DG group. Specifically, the histological results indicate an increased concentration of collagen fibres in both AG and TEG groups, considered as an index of the healing process [33]. Similarly, the presence of a mild inflammatory pattern in these groups represents the basis for the healing process [34]. Indeed, an overlapping between the later stage of inflammation and the proliferation stage in which fibroblasts stat synthesize collagen type III could be possible, then followed by the tardive remodelling phase [35]. These findings were also described by other authors who demonstrated that the inflammatory reaction ameliorates the fibroblastic response, controlling the cell behaviour and the matrix production [3]. In general, AG and TEG showed a similar response in terms of newly formed collagen fibres, mostly type III collagen. Despite type III collagen retains poor biomechanical properties, the early mobilization of the rabbit limbs could convert type III into functional type I collagen over time, as also supported by others [18]. It could also be possible that TEG took the advantage of the effect of both the seeded cells onto the decellularized tendon matrix and the locally injected autologous rbBMSCs, thus resulting in a greater production of collagen compared to unseeded DG [36]. Despite the collagen protein localization and distribution has been assessed in the present study, a quantitative analysis of the collagen gene expression lacks to corroborate

this immunohistochemical finding. Morphologically, the cell density increased in all treated tendons as expected, showing both a more physiologically cell distribution and elongated cell morphology in AG compared to TEG. However, although with longer follow-up, the TEG group would probably exert a similar healing process and cell alignment compared to the AG group. Indeed, the migration of resident cells to the repairing site not only comes from the tendon stumps but also comes from the epitenon, thus needing a longer time to reach the injured area [2]. Overall, the higher amount of cells and newly formed collagen fibres could be the reason for larger and thicker tendon structure in the TEG group, as diagnosed by means of ultrasounds and measured on the explants. The increased cellularity in terms of cells able to synthesize tendon-specific ECM is reflected also in the greater level of proteoglycans and glycosaminoglycans detected in AG and TEG groups [37–39], as well as of inflammatory cells in the DG group, thus inducing a common increased swelling. In fact, the DG group demonstrated a massive inflammatory and giant cell response associated with graft destruction and necrosis, as similarly found by others following the implant of extracellular matrix scaffolds [40–42]. This could be due to the use of xenogeneic biological material that in the absence of autologous, immunomodulatory BMSCs determined an adverse immune response of the host. More importantly, the greater level of proteoglycans detected in the DG group compared to the AG and TEG may also be the result of altered mechanical loads that might increase the local levels of growth factor and cytokines, thus affecting also the activation of MMPs and consequently the disorganization of the tendon ECM [38]. Indeed, under physiological conditions, low levels of the latent form of MMPs are present within the matrix and MMPs are activated only during the tissue turnover [24]. Differently, during pathological events, there is an imbalance between the synthesis and degradation of the matrix components (i.e., collagen, glycoprotein, and sGAG) led by the expression and activation of MMPs. In this context, an increase in MMP activity is likely to indicate the matrix degradation, as part of the remodelling process in tissue healing [43]. In particular, MMP-9 commonly participates in collagen degradation, whereas MMP-2 participates in both collagen degradation and remodelling [44, 45]. Despite no differences were found in MMP-2 levels between DG and TEG, it can be hypothesized that in the severely compromised DG group in terms of inflammation and necrosis, MMP-2 could have had a stronger effect in denaturing both collagen types I and III, thus supporting the immunohistochemical results, i.e., absence of both types of collagen. This phenomenon is particularly true when the analyses are performed in the late time point until the remodelling process occurs [46]. In this context, it would have been helpful to evaluate also the levels of MMP-9, to have a deeper insight into the mechanism driving the collagen degradation process. Notoriously, cells are poorly present in tendons and decellularized tendons are even less populated tissues. Nonetheless, MMPs are difficult to extract being tightly bonded to ECM [47]. For these reasons, the extraction of proteins from the explanted specimens resulted in a demanding process and in a scarce yield, thus representing a limitation of the

MMP analysis through gelatine zymography reported in the present study. Indeed, the final concentration of the extracted proteins was certainly sufficient to detect the activity of MMP-2, but not enough to appreciate the levels of MMP-9, as also suggested by Monteiro and colleagues, who loaded only 8 μg of protein to detect MMP-2 and 50 μg to detect MMP-9 with scarce results [48]. Regarding biomechanics, all treated groups had inferior biomechanical properties compared to NT due to the presence of sutures used for the widely employed Kessler's tenorrhaphy [33] that could affect the elasticity of the entire implant, as expected. Moreover, the great presence of collagen type III in AG and TEG, commonly deposited during the tendon healing process, had surely affected the tendon biomechanics [49]. Nevertheless, AG showed a failure stress very similar to the NT. It was also expected that DG and TEG treated tendons depicted a weaker behaviour compared to AG, confirming data reported by others [50, 51]. However, 12 weeks after implantation, we found an increased EM and failure stress in the TEG group compared to the DG, supporting data obtained with all the other analyses. The presence of autologous BMSCs and of a more mature construct obtained from the dynamic culture in OPBS may be responsible for ameliorating the elasticity and resistance of the reimplanted tissue, as also demonstrated elsewhere [52]. Moreover, the absence of a proper amount of both collagen types I and III and of a higher amount of proteoglycans and inflammatory cells in the DG group could have affected the unfavourable biomechanical response in this group, in particular when compared to the cell-reseeded TEG group. Indeed, the presence of a severe local inflammatory response and focal necrosis, together with the great amount of proteoglycans and MMP-2 in the DG group, compromised the collagen deposition with a significant effect not only on the construct structure (histology) but also mainly in the biomechanical properties [53]. Our results are consistent with those of Chong et al. [18] in which intratendinous BMSC therapy improved histological and biomechanical parameters in the early tendon healing of defect models. Otherwise, our findings are in contrast with the study of Zhang et al. [51], in which reseeded decellularized tendon grafts showed similar results of unseeded grafts. The good results obtained in the present study could be explained by utilizing the OPBS to precondition cell-seeded xenografts. Even though this study is limited to the analysis of efficacy at one time point (12 weeks), the use of ultrasound permitted to monitor the implanted grafts also at an early stage of healing (10 days) with a good specificity for lesions and tissue changes, as also supported by others [26]. More importantly, this technique avoided to include a greater sample size and to avoid useless animal sacrifice in order to evaluate the progression of the tendon healing process, thus respecting the 3R's principles. Again, the lack of an internal control for the TEG group—eventually represented by reseeded, engineered grafts without the local injection of BMSCs—did not permit to discriminate the effect of seeded or locally injected cells in terms of both healing and immunomodulatory effect. Finally, further analyses should also monitor the modulation of tissue inhibitors of metalloproteinases (TIMPs) according to MMP levels expressed in

the different region of the tendon by means of the reverse zymography method.

Indeed, the evaluation of the balance between MMP and TIMP expression would have been helpful to have a complete picture of the tendon remodelling process driven by the tested regenerative strategies.

5. Conclusions

This tissue-engineering-based approach consisting of decellularized tendon xenografts loaded with autologous BMSCs and cultured in a customized stretch-perfusion bioreactor can represent a valid alternative to autografts to repair tendon full defects. Indeed, the results of this study suggest that TEG constructs support the side-to-side tendon repair with the formation of new collagen fibres and biomechanical features similar to the autografts used as controls. Overall, the present study identified an alternative treatment, here represented by the TEG, to the standard use of autograft (AG). Based on the obtained results, TEG could be a valid option in the case of severe tendon ruptures in the presence of tissue loss, showing similar histopathological outcomes both for the TEG and for the AG with respect to the DG group. According to this, TEG could be a suitable graft material as a substitute for tendon reconstruction, bypassing the limited availability of autografts for dimensions and sites of harvest, as well as the consequent donor site morbidity and prolonged surgical time. Conversely, unexpected results occurred in the DG group—in terms of granulation tissue and inflammatory pattern—open new ways to further investigations to ameliorate the decellularization processes and to reduce the abnormal host response to apparently inert decellularized grafts.

Data Availability

The data used to support the findings of this study are available from the corresponding author upon request.

Conflicts of Interest

The authors declare that there is no conflict of interest regarding the publication of this paper.

Authors' Contributions

Marta Bottagisio and Daniele D'Arrigo contributed equally to this work.

Acknowledgments

References

[1] P. Sharma and N. Maffulli, "Basic biology of tendon injury and healing," *The Surgeon*, vol. 3, no. 5, pp. 309–316, 2005.

[2] P. Sharma and N. Maffulli, "Biology of tendon injury: healing, modeling and remodeling," *Journal of Musculoskeletal & Neuronal Interactions*, vol. 6, no. 2, pp. 181–190, 2006.

[3] A. Moshiri and A. Oryan, "Tendon and ligament tissue engineering, healing and regenerative medicine," *Journal of Sports Medicine & Doping Studies*, vol. 3, p. 126, 2013.

[4] C. Legnani, A. Ventura, C. Terzaghi, E. Borgo, and W. Albisetti, "Anterior cruciate ligament reconstruction with synthetic grafts. A review of literature," *International Orthopaedics*, vol. 34, no. 4, pp. 465–471, 2010.

[5] U. G. Longo, A. Lamberti, S. Petrillo, N. Maffulli, and V. Denaro, "Scaffolds in tendon tissue engineering," *Stem Cells International*, vol. 2012, Article ID 517165, 8 pages, 2012.

[6] A. Ratcliffe, D. L. Butler, N. A. Dyment et al., "Scaffolds for tendon and ligament repair and regeneration," *Annals of Biomedical Engineering*, vol. 43, no. 3, pp. 819–831, 2015.

[7] A. B. Lovati, M. Bottagisio, and M. Moretti, "Decellularized and engineered tendons as biological substitutes: a critical review," *Stem Cells International*, vol. 2016, Article ID 7276150, 24 pages, 2016.

[8] M. Bottagisio, A. Pellegata, F. Boschetti, M. Ferroni, M. Moretti, and A. B. Lovati, "A new strategy for the decellularisation of large equine tendons as biocompatible tendon substitutes," *European Cells and Materials*, vol. 32, pp. 58–73, 2016.

[9] L. Liu, J. Hindieh, D. J. Leong, and H. B. Sun, "Advances of stem cell based-therapeutic approaches for tendon repair," *Journal of Orthopaedic Translation*, vol. 9, pp. 69–75, 2017.

[10] G. S. Kryger, A. K. S. Chong, M. Costa, H. Pham, S. J. Bates, and J. Chang, "A comparison of tenocytes and mesenchymal stem cells for use in flexor tendon tissue engineering," *The Journal of Hand Surgery*, vol. 32, no. 5, pp. 597–605, 2007.

[11] H. Omae, Y. L. Sun, K. N. An, P. C. Amadio, and C. Zhao, "Engineered tendon with decellularized xenotendon slices and bone marrow stromal cells: an in vivo animal study," *Journal of Tissue Engineering and Regenerative Medicine*, vol. 6, no. 3, pp. 238–244, 2012.

[12] M. Bottagisio, S. Lopa, V. Granata et al., "Different combinations of growth factors for the tenogenic differentiation of bone marrow mesenchymal stem cells in monolayer culture and in fibrin-based three-dimensional constructs," *Differentiation*, vol. 95, pp. 44–53, 2017.

[13] G. Talò, D. D'Arrigo, S. Lorenzi, M. Moretti, and A. B. Lovati, "Independent, controllable stretch-perfusion bioreactor chambers to functionalize cell-seeded decellularized tendons," *Annals of Biomedical Engineering*, pp. 1–15, 2019.

[14] M. Bottagisio and A. B. Lovati, "A review on animal models and treatments for the reconstruction of Achilles and flexor tendons," *Journal of Materials Science: Materials in Medicine*, vol. 28, no. 3, p. 45, 2017.

[15] G. P. Doherty, Y. Koike, H. K. Uhthoff, M. Lecompte, and G. Trudel, "Comparative anatomy of rabbit and human Achilles tendons with magnetic resonance and ultrasound imaging," *Comparative Medicine*, vol. 56, no. 1, pp. 68–74, 2006.

[16] D. J. Prockop, "Marrow stromal cells as stem cells for nonhematopoietic tissues," *Science*, vol. 276, no. 5309, pp. 71–74, 1997.

[17] A. F. Pellegata, M. Bottagisio, F. Boschetti et al., "Terminal sterilization of equine-derived decellularized tendons for clinical use," *Materials Science and Engineering: C*, vol. 75, pp. 43–49, 2017.

[18] A. K. S. Chong, A. D. Ang, J. C. H. Goh et al., "Bone marrow-derived mesenchymal stem cells influence early tendon-healing in a rabbit Achilles tendon model," *The Journal of Bone & Joint Surgery*, vol. 89, no. 1, pp. 74–81, 2007.

[19] A. Oryan, A. Moshiri, and A. H. Meimandi-Parizi, "Short and long terms healing of the experimentally transverse sectioned tendon in rabbits," *Sports Medicine, Arthroscopy, Rehabilitation, Therapy & Technology*, vol. 4, no. 1, p. 14, 2012.

[20] G. M. Bürgisser, M. Calcagni, E. Bachmann et al., "Rabbit Achilles tendon full transection model - wound healing, adhesion formation and biomechanics at 3, 6 and 12 weeks post-surgery," *Biology Open*, vol. 5, no. 9, pp. 1324–1333, 2016.

[21] C. Stoll, T. John, C. Conrad et al., "Healing parameters in a rabbit partial tendon defect following tenocyte/biomaterial implantation," *Biomaterials*, vol. 32, no. 21, pp. 4806–4815, 2011.

[22] D. D'Arrigo, M. Bottagisio, S. Lopa, M. Moretti, and A. B. Lovati, "Tissue engineering approaches to develop decellularized tendon matrices functionalized with progenitor cells cultured under undifferentiated and tenogenic conditions," *AIMS Bioengineering*, vol. 4, no. 4, pp. 431–445, 2017.

[23] J. P. M. Cleutjens, J. C. Kandala, E. Guarda, R. V. Guntaka, and K. T. Weber, "Regulation of collagen degradation in the rat myocardium after infarction," *Journal of Molecular and Cellular Cardiology*, vol. 27, no. 6, pp. 1281–1292, 1995.

[24] R. C. Marqueti, J. Prestes, M. Paschoal et al., "Matrix metallopeptidase 2 activity in tendon regions: effects of mechanical loading exercise associated to anabolic-androgenic steroids," *European Journal of Applied Physiology*, vol. 104, no. 6, pp. 1087–1093, 2008.

[25] J. L. Fleiss, *Statistical Methods for Rates and Proportions*, John Wiley & Sons, New York, NY, USA, 1981.

[26] J. Buschmann, G. Puippe, G. M. Bürgisser, E. Bonavoglia, P. Giovanoli, and M. Calcagni, "Correspondence of high-frequency ultrasound and histomorphometry of healing rabbit Achilles tendon tissue," *Connective Tissue Research*, vol. 55, no. 2, pp. 123–131, 2014.

[27] E. Shapiro, D. Grande, and M. Drakos, "Biologics in Achilles tendon healing and repair: a review," *Current Reviews in Musculoskeletal Medicine*, vol. 8, no. 1, pp. 9–17, 2015.

[28] A. B. Lovati, B. Corradetti, F. Cremonesi, D. Bizzaro, and A. L. Consiglio, "Tenogenic differentiation of equine mesenchymal progenitor cells under indirect co-culture," *The International Journal of Artificial Organs*, vol. 35, no. 11, pp. 996–1005, 2012.

[29] R. G. Young, D. L. Butler, W. Weber, A. I. Caplan, S. L. Gordon, and D. J. Fink, "Use of mesenchymal stem cells in a collagen matrix for Achilles tendon repair," *Journal of Orthopaedic Research*, vol. 16, no. 4, pp. 406–413, 1998.

[30] H. A. Awad, D. L. Butler, G. P. Boivin et al., "Autologous mesenchymal stem cell-mediated repair of tendon," *Tissue Engineering*, vol. 5, no. 3, pp. 267–277, 1999.

[31] B. Wang, W. Liu, Y. Zhang et al., "Engineering of extensor tendon complex by an ex vivo approach," *Biomaterials*, vol. 29, no. 20, pp. 2954–2961, 2008.

[32] B. A. Bunnell, A. M. Betancourt, and D. E. Sullivan, "New concepts on the immune modulation mediated by mesenchymal stem cells," *Stem Cell Research & Therapy*, vol. 1, no. 5, p. 34, 2010.

[33] R. Arenhart, A. L. Severo, P. E. C. Maia, D. A. Silveira, R. R. Lopez, and D. Bocaccio, "Thermographic and histological analysis of rabbit different tenorrhaphies techniques (4 and 6 strands) after early active mobilization," *Fisioterapia em Movimento*, vol. 27, no. 4, pp. 611–619, 2014.

[34] S. A. Fenwick, B. L. Hazleman, and G. P. Riley, "The vasculature and its role in the damaged and healing tendon," *Arthritis Research*, vol. 4, no. 4, pp. 252–260, 2002.

[35] D. Docheva, S. A. Müller, M. Majewski, and C. H. Evans, "Biologics for tendon repair," *Advanced Drug Delivery Reviews*, vol. 84, pp. 222–239, 2015.

[36] H. W. Ouyang, J. C. H. Goh, A. Thambyah, S. H. Teoh, and E. H. Lee, "Knitted poly-lactide-co-glycolide scaffold loaded with bone marrow stromal cells in repair and regeneration of rabbit Achilles tendon," *Tissue Engineering*, vol. 9, no. 3, pp. 431–439, 2003.

[37] M. de Mos, B. van el, J. DeGroot et al., "Achilles tendinosis: changes in biochemical composition and collagen turnover rate," *The American Journal of Sports Medicine*, vol. 35, no. 9, pp. 1549–1556, 2007.

[38] J. Parkinson, T. Samiric, M. Z. Ilic, J. Cook, and C. J. Handley, "Involvement of proteoglycans in tendinopathy," *Journal of Musculoskeletal & Neuronal Interactions*, vol. 11, no. 2, pp. 86–93, 2011.

[39] C. N. M. Ryan, A. Sorushanova, A. J. Lomas, A. M. Mullen, A. Pandit, and D. I. Zeugolis, "Glycosaminoglycans in tendon physiology, pathophysiology, and therapy," *Bioconjugate Chemistry*, vol. 26, no. 7, pp. 1237–1251, 2015.

[40] J. E. Valentin, J. S. Badylak, G. P. McCabe, and S. F. Badylak, "Extracellular matrix bioscaffolds for orthopaedic applications. A comparative histologic study," *The Journal of Bone & Joint Surgery*, vol. 88, no. 12, pp. 2673–2686, 2006.

[41] S. F. Badylak and T. W. Gilbert, "Immune response to biologic scaffold materials," *Seminars in Immunology*, vol. 20, no. 2, pp. 109–116, 2008.

[42] T. Tischer, S. Aryee, G. Wexel et al., "Tissue engineering of the anterior cruciate ligament-sodium dodecyl sulfate-acellularized and revitalized tendons are inferior to native tendons," *Tissue Engineering Part A*, vol. 16, no. 3, pp. 1031–1040, 2010.

[43] G. P. Riley, V. Curry, J. DeGroot et al., "Matrix metalloproteinase activities and their relationship with collagen remodelling in tendon pathology," *Matrix Biology*, vol. 21, no. 2, pp. 185–195, 2002.

[44] H. R. Choi, S. Kondo, K. Hirose, N. Ishiguro, Y. Hasegawa, and H. Iwata, "Expression and enzymatic activity of MMP-2 during healing process of the acute supraspinatus tendon tear in rabbits," *Journal of Orthopaedic Research*, vol. 20, no. 5, pp. 927–933, 2002.

[45] D. Sbardella, G. Tundo, G. Fasciglione et al., "Role of metalloproteinases in tendon pathophysiology," *Mini Reviews in Medicinal Chemistry*, vol. 14, no. 12, pp. 978–987, 2014.

[46] S. Minkwitz, A. Schmock, A. Kurtoglu et al., "Time-dependent alterations of MMPs, TIMPs and tendon structure in human Achilles tendons after acute rupture," *International Journal of Molecular Sciences*, vol. 18, no. 10, article 2199, 2017.

[47] P. A. M. Snoek-van Beurden and J. W. Von den Hoff, "Zymographic techniques for the analysis of matrix metalloproteinases and their inhibitors," *BioTechniques*, vol. 38, no. 1, pp. 73–83, 2005.

[48] J. C. Monteiro, M. L. Gomes, T. C. Tomiosso et al., "More resistant tendons obtained from the association of Heteropterys aphrodisiaca and endurance training," *BMC Complementary and Alternative Medicine*, vol. 11, no. 1, p. 51, 2011.

[49] A. Inui, T. Kokubu, H. Fujioka et al., "Application of layered poly (L-lactic acid) cell free scaffold in a rabbit rotator cuff defect model," *Sports Medicine, Arthroscopy, Rehabilitation, Therapy & Technology*, vol. 3, no. 1, p. 29, 2011.

[50] Y. Cao, Y. Liu, W. Liu, Q. Shan, S. D. Buonocore, and L. Cui, "Bridging tendon defects using autologous tenocyte engineered tendon in a hen model," *Plastic and Reconstructive Surgery*, vol. 110, no. 5, pp. 1280–1289, 2002.

[51] A. Y. Zhang, J. Thorfinn, S. Saber et al., "Tissue engineered intrasynovial tendons: in vivo graft survival and tensile strength," *European Journal of Plastic Surgery*, vol. 33, no. 5, pp. 283–289, 2010.

[52] J. Thorfinn, S. Saber, I. K. Angelidis et al., "Flexor tendon tissue engineering: temporal distribution of donor tenocytes versus recipient cells," *Plastic and Reconstructive Surgery*, vol. 124, no. 6, pp. 2019–2026, 2009.

[53] J. J. Yang, E. C. Jang, and J. S. Lee, "The effect of amniotic membrane transplantation on tendon-healing in a rabbit Achilles tendon model," *Tissue Engineering and Regenerative Medicine*, vol. 7, pp. 323–329, 2010.